THE GEOLOGY, GEOCHEMISTRY AND PETROLOGY OF THE METAGABBRO UNITS OF THE TATI NI-CU SULPHIDE MINES AND DEPOSITS AND ASSOCIATED PGEs MINERALISATION

Kabelo Thabiso Thari

A Dissertation submitted to the Faculty of Science, University of the Witwatersrand, Johannesburg in fulfilment of the requirements for the degree of Master of Science

February 2019

DECLARATION

I declare that this dissertation is my own unaided work and any data sourced somewhere has been accordingly referenced and acknowledged. It is being submitted for the degree of Master of Science (MSc) at the University of the Witwatersrand, Johannesburg. It has not been submitted before for any other degree or examination at any other university**.**

…………………………………….

(Signature of candidate)

FEBRUARY 2019

ABSTRACT

Various metagabbro bodies host sulphide mineralisation in the Tati Sulphide Mines and Deposits Complex located in the Tati greenstone belt, southwestern margin of the Zimbabwe craton. The Tati Sulphide Mines and Deposits Complex, referred to here as the TSMDC, is a major metallogenic zone in east Botswana. This study focuses on gaining insight into the geology, whole-rock geochemistry and petrology of the Ni-Cu-PGE-mineralised gabbro units and contact lithologies in order to develop effective exploration targets for the TSMDC.

The TSMDC mainly comprises three types of gabbroic units-melanogabbro, mesogabbro and leucogabbro-in contact with a wide range of magmatic rocks that include, granodiorite, porphyritic granodiorite, quartz diorite, tonalite, amphibolite, basalt, dolerite and pegmatites. The gabbro units occur near metasedimentary units that include dolomite, Banded Iron Formation (BIF) and quartzite.

Some of the gabbro units host sulphide mineralisation comprising mainly pyrrhotite, pentlandite, chalcopyrite and pyrite, whereas some gabbro units are barren. The gabbro units are generally medium grained and composed mainly of variable propositions of the primary minerals pyroxene (20-30%), plagioclase (30-35%) and quartz (2-7%) and minor secondary minerals that include, chlorite (~2%) and epidote (~1%). The major and trace elements data indicate a suite of variably magmatically evolved gabbro units, which show a wide compositional range in MgO (4-17 wt. %), FeOt (5-20 wt. %), SiO_2 (45-52 wt. %), Al_2O_3 (10-17 wt. %) and CaO (5-15 wt. %). Based on the positive correlations between MgO and FeO_{total}, CaO and MgO and Y and Zr, the gabbro units are interpreted as having been generated through a fractional crystallisation process, where pyroxene and plagioclase were the dominant rock-forming minerals. Fractional crystallisation is also evidenced by positive correlation between SiO_2 and Na_2O, + K_2O, and resulted in the formation of an enriched quartz mineralogy in granitoid units of the TSMDC.

Generally, gabbro units show chondrite-normalised plots with slight enrichment of LREE relative to depletion of HREE. There is a weak positive Eu anomaly, which suggests plagioclase in combination with pyroxene and sphene controlled the fractionation of the partial melts in the upper crust.

The gabbro units and contact lithologies were emplaced in a continental margin environment prior to and following several deformation events. Three deformation events, D_1, D_2 and D_3 were identified in TSMDC. D_1 is ductile-brittle in nature and is characterised by folding (fo_1), foliation S_1, and NE-SW and NNE-SSW trending faults (F_1). D_2 resulted in the formation of the Phoenix, Selkirk and Rooikoppie shear zones associated with a regional foliation (S_2), lineation (L_2) and en echelon quartz veins (V_2). The third deformation event, D_3, is associated with formation of fracture cleavage and joints that dominate most of the study area.

On a regional scale, the N-S and NE-SW trends of crustal lineaments controlled the geometry of the Phoenix, Selkirk mines, Tekwane and Rooikoppie deposits. On a local scale, the structural factors controlling the current position of the Phoenix, Selkirk mines, Tekwane and Rooikoppie deposits are a network of proximal fractures to the crustal lineaments, which provided transport and settling of differentiated magma during interaction with sulphide minerals in the formation of the Ni-Cu-PGEs mineralisation.

The integration of the geology, whole rock geochemistry and petrology suggests that various gabbro units host Ni-Cu-PGEs mineralisation and are affected by structural lineaments, which include shear zones in TSMDC. The shear zones acted as conduits for the propagation of Ni-Cu-PGEs mineralisation and hydrothermal fluids. The geometry of the Phoenix, Selkirk mines, Tekwane and Tekwane deposits is coincident with NE and NW trends of the shear zones.

ACKNOWLEDGEMENTS

I would like to express my utmost gratitude to Tati Nickel Mining Company (TNMC) for a lifetime opportunity to study at the University of the Witwatersrand, Johannesburg. I wish to thank Mr. Koketso Gabriel Botepe and Mr. Kebalemogile Tau for their recognition of my studies, allowing me time out of my daily duties and provision of funds for the geochemical analyses. My appreciations are in order to former TNMC Managing Director, Mr. Ditiro Lentswe and his executive management team for providing company resources. I appreciate the firm support of former TNMC employees especially Gabadire Ngakane, Isaiah Emang, Bee Kgati, Davison Singeni, Terry Motsemeng, Kagiso Mahika and Kind Nthokwa. Special thanks for guidance of Mr. Puso Akanyang

I would also like to thank Prof. Kim Hein for her guidance and mentorship in turning me into a better geologist. Special thanks are due to Dr. Asinne Tshibubudze for his dedication and mentorship despite the demands of his doctoral studies during my first journey of this study. My salutes are in order to the WITS School of Geosciences technical staff, Musa Cebekulu, for his assistance with polished thin sections, Mr. Caiphas. Majola and Joe Aphane for ensuring access to prepare samples for geochemical analyses and Marlin Patchappa for assistance with XRF and ICPMS analyses at the EarthLab.

The Department of Geology at University of Botswana deserves special honour for use of their microscopic facilities and granting Dr. Zibisani Bagai to join my supervisory team. Special thanks are due to Prof. Read Brown Mapeo for his fruitful discussions and encouragement. Trillion thanks to Dr. Zibisani Bagai for supervision of the petrography and geochemistry components. I thank Prof. Proyer for assistance during the petrographic analyses. Mr. Maatla Letsholo thanks for the invaluable discussions on ore petrology. Great thanks are due to Mr. Charles Byron and Mr. Vince Atkinson and their exploration crew led by Swikani and Refilwe Vince at Mupane mine.

Special thanks to Mr. Kealeboga “Soccer” Mogotsi for his input in my research ambitions. I would also like to appreciate the never-ending support of my sisters and former work colleagues, Ndix “MmaTekwane” Tawana, Tsholo Malatji, Lemo Pelaelo, Tinae Etani, Irene Mokobi and Ruth Mogolwane for the dearly efforts to proof read my manuscripts. My time in Johannesburg was always great due to the bold hospitality of my great guys-Sifiso Siwela and Themba Mabundza - trillion thanks. Special thanks for unwavering support from my parents and family. Thanks to my wife-Florence and sons, Nthabie-Tinashe and Boithabiso Tinotenda Makanaka Thari, for providing the utmost motivation and being pillar of strength.

SPECIAL DEDICATIONS

This dissertation is bestowed with great memory to Professor Henri Kampunzu, Gotsilemang "Gee" Josiah and her husband, Richard.

My special memories to my guardian and sister-Didimalang Moanei and special brother-Rex-you contributed greatly to my upbringing-Thank you very much.

God, May their souls rest in long lasting peace.

There is nothing impossible with God

God motivates for lifetime

TABLE OF CONTENTS

CONTENTS **PAGE**

LIST OF FIGURES

LIST OF TABLES

CHAPTER 1.0: INTRODUCTION

1.1. Location of Study Area

The Phoenix, Selkirk mines and Tekwane, Rooikoppie deposits occur as a cluster in the Tati greenstone belt, southwestern margin of the Zimbabwe craton. Collectively, Phoenix, Selkirk mines, Tekwane and Rooikoppie deposits are referred to as Tati Sulphide Mines and Deposits Complex (TSMDC) in this study and are located between 35-40 kilometres east of city of Francistown, Botswana (Figure 1.1).

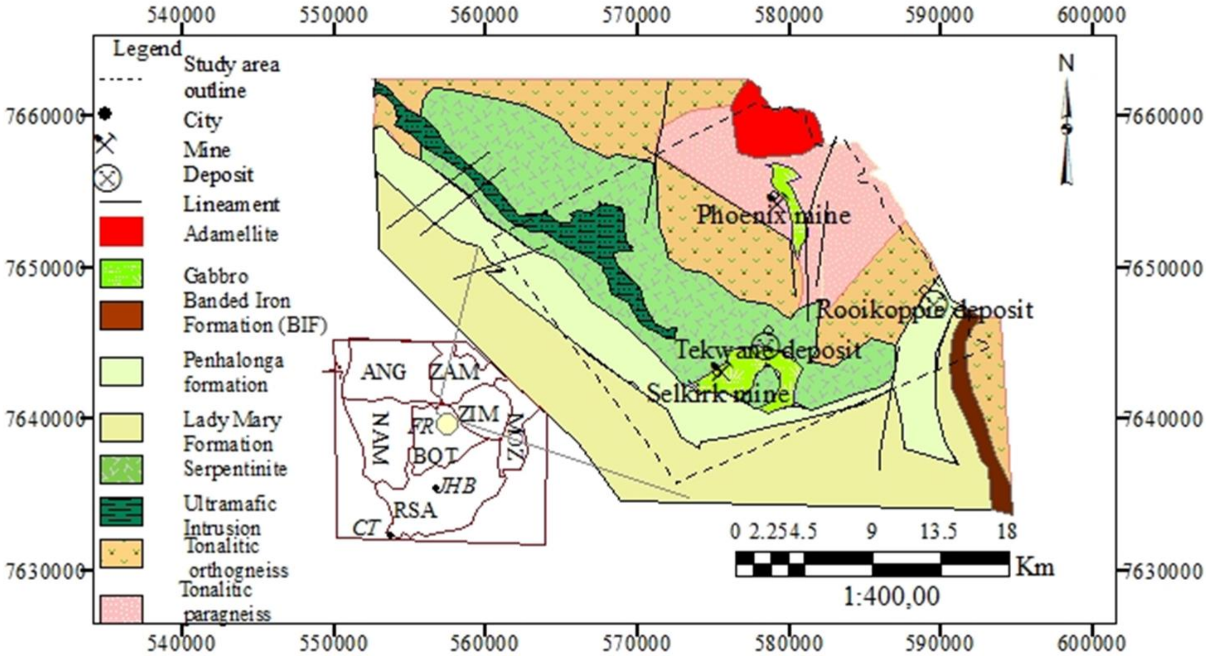

Figure 1.1: The map of the study area indicates the location of Phoenix, Selkirk mines, Tekwane and Rooikoppie deposits east of City of Francistown. The Phoenix, Selkirk mines, Tekwane and Rooikoppie deposits constitute the Tati mines and deposits complex (TSMDC) FR (Francistown), JHB (Johannesburg), CT (Cape Town), BOT (Botswana), RSA (Republic of South Africa), ZIM (Zimbabwe), ZAM (Zambia), NAM (Namibia), ANG (Angola) and MOZ (Mozambique) (Modified after Key (1976) and Maier et al. (2007).

1.2. Existing Knowledge

The geology, structure and geochemistry of the Phoenix, Selkirk mines and Tekwane, Rooikoppie deposits has been studied by Key (1976), Tombale (1992), Carney et al. (1994), Kampunzu et al. (1993), McCourt et al. (2004), Dirks (2004, 2005), Van Geffen (2005), Døssing et al. (2009) and Fiorentini et al. (2012). The TSMDC comprises of orthogneiss, tonalitic paragenesis, metagabbro, granites, granodiorite and tonalite (Key, 1976; Tombale, 1992). Likewise, the study of Carney et al. (1994) showed that different gabbro units occur in proximity to amphibolite, tonalite, monzonite, banded ironstones, quartzite and limestone. Dirks (2004, 2005) presented that various gabbro units, which are in contact with granodiorite, tonalite, quartz diorite and dolerite, host the Ni-Cu-PGEs mineralisation in the Phoenix and Selkirk mines.

The regional faults and shear zones form contacts of lithological units in TSMDC (Key, 1976: Tombale, 1992). Hunt and Dirks (2006) pointed that the architectural distribution of the metagabbro units in the Phoenix and Selkirk mines is due to the displacement by faults during its post emplacement period and resulted in the conduit geometry of the Phoenix mine. Different deformation events affected these gabbro and granodiorite units, which had implications in the current stratigraphy, local and regional controls on the Ni-Cu-PGEs mineralisation in the TSMDC. The Phoenix mine has both northwesterly and southwesterly trending foliations, attributed to change in accommodation of deformation (McCourt et al., 2004; Dirks, 2004; 2005; Hunt and Dirks, 2006). Regionally, the Phoenix, Selkirk mines and Tekwane deposit trend north northeasterly whereas the Tekwane trend northeasterly, demonstrating different structural orientations in these closely spaced mines and deposits (Van Vureen, 2005; Dirks and Hunt, 2006).

The whole rock geochemical features of the gabbro and mafic units of TSMDC show wide-ranging composition of MgO (2-16 wt. %) and FeO total (4-16 wt. %), which correlate positively in the major element variation diagrams (Tombale, 1992; Kampunzu et al., 2003). The granitoids show high Na_2O/K_2O reflective of tonalite trondjenite granite (TTG) suite (Bagai, 2008). The gabbro and granodiorite show enrichment of both heavy rare earth elements (HREE) and light rare earth elements (LREE) (Kampunzu et al., 2003; Bagai, 2008).

The source magmas of gabbro and contact granodiorite generated from partial melting of mafic slab, followed by fractional crystallisation in back arc convergent margin environment produced by northward subduction of mafic slab of Limpopo Orogenic belt beneath continental crust of Zimbabwe craton (Kampunzu et al., 2003; Bagai, 2008). Studies by Maier et al. (2007) indicated that MgO and FeO contents of various gabbro units correlate positively and contributed to sulphide saturation, which experienced significant crustal contamination in the Phoenix and Selkirk mines. Maier et al. (2007) pointed that the parental magma of the gabbro units resulted from partial melt formed in divergent setting subsequent to the subduction of the mafic slab of the Limpopo Orogenic belt under the felsic crust of the Zimbabwe craton.

1.3. Knowledge gaps

The studies of Key (1976), Tombale (1992), Carney et al. (1994) and Dirks (2004, 2005) indicate potential relationship between the geology of different gabbro units, contact lithologies and sulphide mineralisation. Nevertheless, it is difficult to explain the local geological features of the lithologies adequately as the studies by Key (1976), Tombale (1992) and Carney et al. (1994) were mainly on regional basis without thorough consideration of local geology of the mines and deposits. The studies conducted by Dirks (2004, 2005) managed to present petrographic classifications of Phoenix and Selkirk mines metagabbro but failed to shed understanding in geology of their contact lithologies adequately. Moreover, Dirks (2004, 2005) did not study the geology of gabbro and their contact lithologies of the Tekwane and Rooikoppie deposits. The studies of Key (1976) and Tombale (1992) indicate possible influence of the faults and shear zones in the geometry and mineralisation trends of TSMDC. The study by McCourt et al. (2004) showed that the regional kinematics in the TSMDC resulted from NE-SW shortening direction, which resulted in NW trending and steep foliation. However, it is not clear from the studies by Key (1976), Tombale (1992) and McCourt et al. (2004) on how the coexistence of the faults, shear zones, mines and deposits relate to regional and local controls of the PGE mineralisation including its exploration potential of the TSMDC. The study by Hunt and Dirks (2006) showed that the NE and NW trending shear zones accommodated the displacement of blocks in the Phoenix and Selkirk mines. Nevertheless, their interpretation remain limited as it failed to account for the structural framework of the Tekwane and Rooikoppie deposits, which possibly play important role in understanding the exploration potential of the Ni-Cu-PGEs mineralisation in TSMDC.

The studies by Maier et al. (2007) and Bagai (2008) show that the parent magmas of gabbro and contact lithologies were either formed in divergent or convergent margin settings due to subduction of mafic slab of Limpopo orogenic belt beneath continental crust of Zimbabwe craton. Thus, these contrasting views make proper recognition of the petrogenetic characteristics of the gabbro and contact lithologies unclear. In addition, these differing views on the tectonic setting of the metagabbro units create a great challenge in understanding the favourable environment for the formation of the Ni-Cu-PGE mineralisation, critical factor in generating targets for exploration. Thus, considering the problematic issues regarding the geology, geochemical and petrogenetic features of metagabbro and contact lithologies, it is utmost important to be guided by the following aims and objectives in this study.

1.4. Aims and Objectives

The following aims and objectives are addressed in order to understand the geology, geochemistry and petrogenetic framework of the Phoenix, Selkirk mines, Tekwane and Rooikoppie sulphide deposits. They include:

- Determination of the regional geology of Phoenix, Selkirk mines, Tekwane and Rooikoppie sulphide deposits by discussing the petrogenesis of the gabbro units and contact lithologies.
- Determine the processes associated with modal composition and textural heterogeneity of the gabbro units and their contact lithologies. This was done by constraining the whole-rock geochemistry of the gabbro units and contact lithologies.
- Establish the role of faults and shear zones in the geometry of the deposits and their styles of sulphide mineralisation.
- Develop exploration criterion through integration of the petrogenesis, whole-rock geochemistry and structural geology as an input in the improvement of current geological and genetic models of the deposits.

1.5. Exploration and Mining History

The east of Botswana has been a focus for gold and Ni-Cu massive sulphide bodies exploration and mining for decades. The artisanal mining of base metals deposits resulted in developments of shafts and adits in and around the city of Francistown in the Tati greenstone belt. Tati Territory Exploration Company undertook exploration for base metal deposits in 1964 after identification of gossan outcrops at both Phoenix and Selkirk mines (Key, 1976) The Anglo-American Corporation (AAC) undertook preliminary studies of both Phoenix and Selkirk deposits and drilled approximately 60 000 metres of drillcores in 1971.

The Bamangwato Concessions Limited (BCL) in partnership with Anglo American acquired Tati Nickel Mining Company (TNMC) and commenced the trial mining of Phoenix deposit from February 1992 until December 1992. Phoenix deposit feasibility study was completed in 1993. It showed that the Phoenix deposit contains 42 890 tonnes of ore reserves at 0.37% Ni and 0.21% Cu. The Phoenix deposit mining resumed on a large scale from December 1994 until its closure in October 2016. The mining of the Selkirk deposit was by underground operation between June 1988 and December 2001. The crushing of massive sulphides happened at small crushing plant at Selkirk and later ferried to Selibe Phikwe for smelting. Lion Ore Pty Ltd took over the operations at both Phoenix and suspended Selkirk mine operations in 2002.

Further exploration by Lion Ore Pty Ltd of Selkirk through soil sampling, gravity, magnetic and induced polarisation (IP) surveys was followed by drilling of targets from 2004 until 2007. A total of 259 boreholes were achieved, totalling over 103 600 metres. The Selkirk mine measured resource amounts to 40.7 million tonnes at 0.20% Nickel cut-off grade (Geldenhuys, 2008) and was remodelled to 88, 875, 71 tonnes at 0.23% Ni cut-off grade (Gipronickel, 2012). The Selkirk mine was planned to be re-opened using open pit method in the future. Currently, the Phoenix mine is mined out and is under care and maintenance.

Gallery Gold Pty Ltd began exploration of Tekwane deposit in 2002 until 2004 when IAMGOLD Pty Ltd acquired the exploration rights. No major exploration programmes were initiated other than few trenches opened before they relinquished the license.

1.6. Dissertation Organisation

This dissertation is organised into eight chapters including Introduction as Chapter 1.0 and the remaining chapters are as follows:

Chapter 2.0 provides a review of the regional and local geological setting of the Tati sulphide deposits. In addition, the previous work on the geochemistry and structural geology framework of the deposits is reported.

Chapter 3.0 provides detailed description of the methodologies used. It includes fieldwork techniques, laboratory processes, data interpretation and data analyses. The processes, which include surface and pit geological mapping, geochemical analyses, and the use of Co-Plot®, Microsoft® Excel 2013 and Micromine®, ArcGIS™ are outlined.

Chapter 4.0 covers the petrography of the lithological units in the study area.

Chapter 5.0 provides for major oxide and minor elements whole geochemistry. It mainly includes the characterization of both major oxide, minor and rare earth elements.

Chapter 6.0 covers the general overview of the structural framework of the Phoenix, Selkirk mines, Tekwane and Rooikoppie deposits.

Chapter 7.0 presents the Discussion.

Chapter 8.0 presents the Conclusions and provides Recommendations.

1.7. Abbreviations and Acronyms

PGEs	Platinum Group Elements
TNMC	Tati Nickel Mining Company
ºC	Degree Celsius
UTM	Universal Transverse Mercator
WGS 84	World Geodetic System 1984
Ga	Billion years
Ma	Million years
U-Pb	Uranium-Lead
ICP-MS	Inductively coupled plasma–mass spectrometry
U-Pb SHRIMP II	Uranium-Lead Sensitive High-Resolution Ion Micro Probe
XRF	X-Ray Diffraction
TSMDC	Tati Sulphide Mines and Deposits Complex
D_1	First deformation event
D_2	Second deformation event
D_3	Third deformation event
S_0	Initial bedding orientation
S_1	First tectonic foliation
S_2	Second tectonic foliation
V_1	First vein set
V_2	Second vein set
Fo_1	First Fold set
F_1	First Fault
mN	Metres to the North
mE	Metres to the East
GPS	Global Positioning System
ca.	Circa

CHAPTER 2.0: REGIONAL GEOLOGY

2.1. Tectono-magmatic stratigraphy of Zimbabwe Craton

The different gabbro units generally host sulphide mineralisation in the Tati Sulphide Mines and Deposits Complex (TSMDC), which occurs within Tati greenstone belt in the southeastern margin of Zimbabwe craton. The crustal growth of the Zimbabwe craton is approximately 3.5 Ga old based on the Sm-Nd (tDM) geochronological work undertaken in the Tokwe granitoid segment (Taylor et al., 1991). The crustal formation was followed by tectonic regimes and metamorphism, which resulted in widespread magmatism and deformations between 2.7 and 2.6 Ga (Kusky, 1998; Johnson et al., 2005; Fedo and Eriksson, 1996; Fedo et al., 1996; Tingjie et al., 2008). It is during this period when greenstone belts were formed across the Zimbabwe craton (Dirks et al., 2002; Hansen et al., 2009; Flowers and Schoene, 2010).

The studies undertaken in the twenty-six greenstone belts of the Zimbabwe craton demonstrate presence of volcano-sedimentary sequences of ultramafic-mafic units and tonalite-trondhjemite-granodiorite (TTG) bodies (Figure 2.1, Bickle et al., 1975; Compston and McElhinny, 1975; Saggerson and Turner, 1976; Moorbaths et al., 1977; Snowden and Snowden, 1981; Wilson, 1990; Shackleton, 1995; De Wit, 1998; Kusky, 1998; Kusky and Polat, 1999; Hofmann et al., 2001; Vinyu et al.,2001; Bohr et al.,2002 and Oberthür et al., 2002). According to de Wit and Ashwal (1997), the granite-greenstone belts form the margins and interiors of the Zimbabwe Craton. The calc-alkaline enriched magmatism generated various suites of tonalite-trondhjemite-granodiorites (TTGs) in the greenstone belts of Zimbabwe craton (Dirks and Van Der Merwe, 1997; Hoffmann et al., 2002; James et al., 2003; Johnson et al., 2005; Zhai et al., 2005; Ranganai et al., 2008; Yingjie et al., 2008). Basaltic and komatiite units are part of the greenstone belt geology (Wilson et al, 1995; Zhou, 1994). These units were generated from the eruption of mafic and ultramafic magmas (Hofmann and Kusky, 2004; Shimizu et al., 2005), which are associated with the formation of sulphide deposits (Markwitz et al., 2010).

The Tati greenstone belt is one of the many greenstone belts, which are part of the Zimbabwe craton (Kusky, 1998; Johnson et al., 2005; Tingjie et al., 2008; Hansen et al., 2009; Flowers and Schoene, 2010). The Tati greenstone belt borders the northern margin of the Limpopo Orogenic belt (Van Reenen et al., 1992). It bears economic implications due to its magmatic and structural features, which has spatial association with sulphide mineralisation.

2.2. Structural lineaments of the Zimbabwe Craton

Ranganai et al. (2008) presented that major sets of faults, fractures and shear zones dominate the Zimbabwe Craton as interpreted from satellite images, aeromagnetic and gravity studies (Figure 2.2). The northeast-southwest trending faults and shear zones are widely distributed in the southern part of the Zimbabwe Craton (Roering et al., 1992; Kamber et al., 1995; Jelsma and Van Der Beek, 1993; Dirks and Jelsma, 1998). This probably also resulted into northwest trending fold systems along the suture zones (Aldiss, 1991; McCourt and Vearncombe, 1992; McCourt et al., 2004).

Shear zones, folds and faults characterize the Tati sulphide mines and deposits complex (TSMDC) (Key, 1976; Hunt and Dirks, 2005). In summary, northerly trending faults and shear zones define contacts between the gabbroic and granitic units (Key, 1973). The foliation within metagabbroic units of Phoenix mine and Rooikoppie deposits generally strikes northeasterly with steep dips of between 70º and 80º to the southeast (Tombale, 1992).

The prominent structural lineaments were presented by Tombale (1992) and generally define NNE-SSW, NE-SW and NW-SE orientations in TSMDC (Figure 2.3). Tombale (1992) reported that deformation events are recognised in and around the deposits and include;

(1) D_1 characterized by northeast verging folding and SW directed thrusting. The Matsiloje, Mphoeng and Signal hill thrust zones formed during this event and is associated with formation of gold mineralization at Mupane mine (Figure 2.3) (Tombale, 1992).

(2) D_2 is marked by northwest trending shear zones associated with foliation (S_2) and southwest plunging mineral lineation (L_2) (McCourt et al., 2004)

(3) D_3 is reported to be associated with the development of NE trending crenulation cleavage (S_3) (Dirks, 2005) and northeast verging folds (Tombale, 1992).

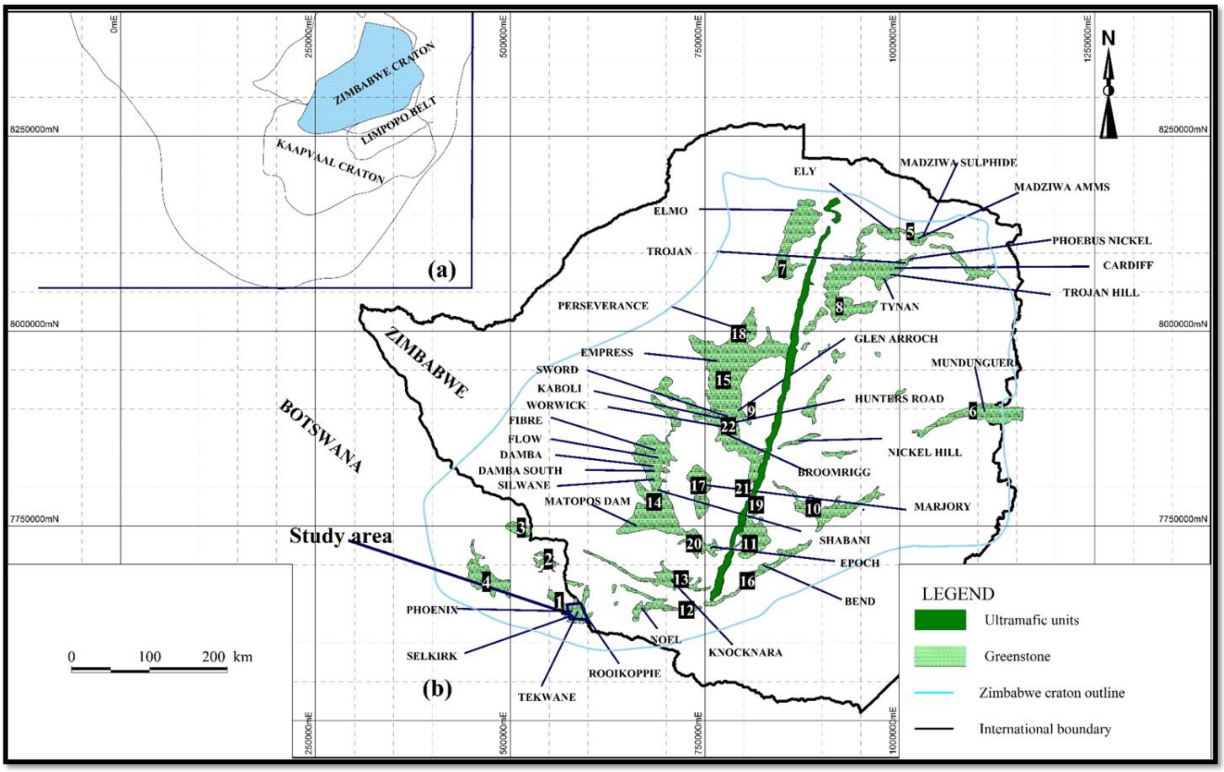

Figure 2.1: Location of Nickel-Copper-Platinum Group Elements (Ni-Cu-PGEs) (Ni-Cu-PGEs) sulphide deposits in greenstones belts of Zimbabwe Craton. (a) The main geological cratons of the southern Africa. (b) The distribution of greenstone belts across the Zimbabwe craton which includes; (1) Tati, (2) Vumba, (3) Maitengwe, (4) Matsitama, (5) Mount Darwin, (6) Mutare, (7) Kadoma, (8) Harare-Bindura-Shamva, (9) Kwekwe, (10) Mashava-Masvingo, (11) Belingwe, (12) Antelope, (13) Gwanda, (14) Bubi-Bulawayo, (15) Midlands, (16) Buhwa, (17) Shangani, (18) Chegutu, (19) Shurugwi, (20) Filabusi, (21) Gweru-Mvuma, (22) Fort Rixon, (Modified after Kusky, (1998), Jelsma and Dirks (2000), Hofmann et al. (2002), Dirks, (2004), Markwitz et al. (2010). The Tati Sulphide Mines and Deposits Complex occur in the Tati greenstone belt.

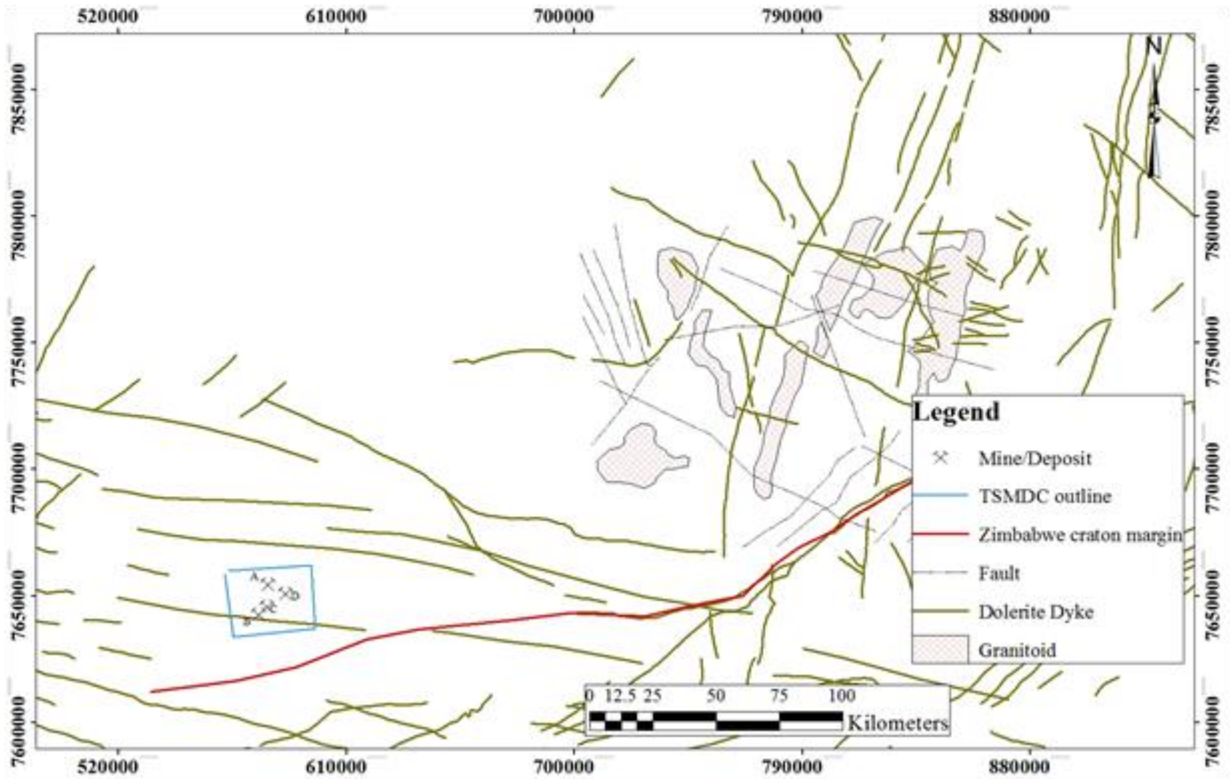

Figure 2.2: The distribution of prominent lineaments associated with faults and dolerite dykes with respect to the study area, TSMDC in the Zimbabwe craton. There is a cluster of faults in the southeast and central parts of Zimbabwe craton, which show general NE trend, coincident with the TSMDC (modified from Ranganai et al. (2008). Please note the following denotations as A (Phoenix mine) B (Selkirk mine) C (Tekwane deposit) and D (Rooikoppie deposit).

The interpretations made on the geological models of the Phoenix and Selkirk mines assumed that faults define contacts between gabbroic units (Dirks, 2005). Thus, it is important to present kinematic information of the shear zones and faults to improve interpretations on the Phoenix and Selkirk mines. Hunt and Dirks (2005) established that the faults and shear zones were pathways for the generation of sulphide mineralisation in the Phoenix and Selkirk deposits based on occurrence of massive bodies in and round the faults and shear zones. However, the extent to which, the faults and shear zones contributed to the sulphide mineralization in the deposits is not fully established.

2.3. Mineral deposits of the Zimbabwe Craton

The Zimbabwe craton hosts various mineral occurrences, which include Coal, Diamonds, Chromite, Iron, Gold, Asbestos, Antimony, Limestone, Rare Earth Elements (REE) and Ni-Cu-PGEs sulphide deposits. Gold deposits occur along a network of quartz veins within shear zones (Carney et al., 1992; Blenkinsop et al., 2000). Gold deposits occurrences are associated with hydrothermal fluids transported along fracture zones associated with shears (Tombale, 1992). Diamonds occur in Karoo basins as alluvial type in Marange, and exploited by artisanal mining in East Zimbabwe (Moore et al., 2009). Prendergast (2013) reported occurrence of nickel laterite mineralisation in the northern Great Dyke. Markwitz et al. (2010) recognised that some of the Ni-Cu-PGEs deposits in Zimbabwe craton include; Madziwa, Epoch, Zinca, Mimosa, Selukwe, Damba, Noel, Hills Prospect, Hunters Road and Trojan (Figure 2.1). The platinum group minerals and chrome are dominant in layered mafic intrusions of the Great Dyke of Zimbabwe (Wilson et al., 2011).

2.4. Local geological setting of the east Botswana mines and deposits

The east Botswana mines and deposits occur in the margin of the Zimbabwe Craton and Northern Margin Zone of Limpopo Belt. The stratigraphy of the east Botswana mines and deposits consists of major meta-volcanic and sedimentary groups. The Phoenix, Selkirk, Tekwane and Rooikoppie Ni-Cu-PGEs sulphide deposits are located in the Tati granite-greenstone belt of the Zimbabwe craton (Key, 1976). The Tati greenstone comprises of the Tati volcanic group, which consist of intrusive, extrusive lithologies and metasedimentary units classified under different formations. These include Kgarimacheng, Lady Mary, Penhalonga, and Selkirk Formations (Key, 1976; Tombale, 1992). The Kgarimacheng Formation consists of ultramafic-mafic intrusive units, which include serpentinites and pyroxenites that have been metamorphosed under amphibolite facies (Carney et al., 1994). In addition, the Kgarimacheng Formation comprise of banded iron formation, which formed in depositional basins at approximately 2.7 Ga based on Pb isotopes ages (Døssing et al., 2009). The basaltic and metasedimentary units, which include conglomerate and quartzite, make up the Lady Mary formation (Carney et al., 1994). The Penhalonga Formation consists of metamorphosed andesitic and dacitic units that intruded the serpentinites and pyroxenites. The emplacement of granodiorite occurred at ca. 2.5 Ga based on U-Pb zircon crystallisation ages as result of the back arc subduction of the mafic slab of Limpopo belt unto the felsic crust of Zimbabwe craton (Bagai, 2008). The metagabbro and granodiorite units were metamorphosed under greenschist facies and form part of Selkirk Formation. The rest of the Tati Volcanic Group stratigraphy is composed of old Tati, Kgarimacheng, Lady Mary and Penhalonga, formations. The intrusion of Okavango dolerite dykes is interpreted to be approximately 179 ± 1.1 Ma based on $^{40}Ar/^{39}Ar$ of plagioclase, which marks one of the youngest unit in the Zimbabwe Craton (Le Gall et al., 2002).

2.5. Sulphide Deposits

The Ni-Cu-PGEs sulphide deposits occur in cratons and orogenic belts worldwide (Arndt et al., 2005). Sulphide deposits are broadly classified into two types, that is, hydrothermal (González-Álvarez et al., 2013; Hofmann et al., 2014) and magmatic (Song et al., 2014). Laterites are another form of nickel bearing deposits (Hoatson et al., 2006; Thorne et al., 2012). The laterite deposits occur as result of weathering of ultramafic units in temperate climates; for example, in Australia, Brazil, Turkey and West Africa (Barros de Oliveira et al., 1992; Eliopoulosa et al., 2012).

2.5.1. Hydrothermal sulphide deposits

Mafic, ultramafic and sedimentary units, which include carbonate, graphite, shale, and siliciclastic units host hydrothermal deposits (Guilbert and Park Jr, 1986; Xu et al., 2013). The sulphides were concentrated in hot fluids and transported in pathways within felsic, mafic, ultramafic and sedimentary rocks to form hydrothermal sulphide deposits (Scott et al., 2002). The pathways consist of faults, shear zones and folds. Examples of these deposits include Avebury in Tasmania, Mt Martin in Australia and Epoch in Zimbabwe (Pirajno and Gonalez-Alvarez, 2013). The ore minerals occur as massive, disseminated, veined and stringered bodies within these magmatic and hydrothermal deposits (Hoatson et al., 2006). The ore minerals include pentlandite, chalcopyrite, pyrrhotite, pyrite and millerite, and host PGEs, mainly platinum and palladium (Johnson, 1986; Naldrett, 1997).

2.5.2. Magmatic sulphide deposits

Magmatic sulphide deposits are hosted by mafic and ultramafic units i.e., komatiite, gabbro, gabbronorite, dunite, peridotite, pyroxenite, boninitic and picritic rocks (Hoatson et al., 2006). Fundamental parameters for the formation of magmatic sulphide deposits includes the ability of the mantle melt enriched in chalcophile elements (i.e., Ni, Cu and PGEs) to interact with sulphur, usually sourced from mantle and reaching sulphide saturation through progressive fractionation, or externally from sulphur rich contact wall rocks such as sediments (Barnes and Maier, 1999; Li et al., 2001, 2010). The placement localities such as faults and basins concentrate the sulphide enriched melts, which result in different geometries such as tabular and massive magmatic sulphide bodies. The magmatic sulphide deposits are the most dominant Ni-Cu-PGEs type, which include; Kabanga in Tanzania, Norilsk Talnakh in Russia, Pechanga in China, Voisey`s Bay in Canada, Mount Keith in Western Australia, Bushveld Complex in South Africa, Great Dyke in Zimbabwe and Selebi Phikwe in Botswana (Barnes and Lightfoot, 2005; Evans et al., 2009).

Gabbroic-hosted sulphide deposits often occur in close proximity to one another, forming clusters. Examples of these include; Pechanga in China, Voisey`s Bay in Canada, Duluth in United States of America (Eckstrand, 1996), and Tati in Botswana (Figure 1.1). The metagabbro units of the Tati sulphide deposits complex are of particular interest in this research because it is important to understand their sulphide mineralisation. The understanding of the local and regional controls in the Ni-Cu-PGEs sulphide mineralisation would improve targeting for sulphide mineralisation in exploration models. It is, therefore important to establish the whole rock geochemistry of the host metagabbro units and the influence of crosscutting faults and shear zones.

2.6. Tati Sulphide Mines and Deposits Complex (TSMDC)

The Tati sulphide mines and deposits complex (TSMDC) is composed of the Phoenix, Selkirk mines, Tekwane and Rooikoppie sulphide deposits (Table 2.1) and is located in the east of Botswana close to the international triple borders of Botswana, Zimbabwe and South Africa (Figure 1.1). The deposits are located approximately 40km southeast of city of Francistown. The Rooikoppie deposit lies close to the border of Zimbabwe and Botswana.

Table 2.1: The GPS coordinates of the Phoenix, Selkirk mines, Tekwane and Rooikoppie sulphide deposits in east Botswana.

LOCALITY	COORDINATE SYSTEM	mE	mN
Phoenix mine	UTM (WGS 1984)	579017	7654716
Selkirk mine	UTM (WGS 1984)	575333	7642993
Tekwane deposit	UTM (WGS 1984)	578660	7645774
Rooikoppie deposit	UTM (WGS 1984)	585927	7651232

Phoenix, Selkirk mines and Tekwane deposit are the largest Ni-Cu-PGEs discovery of east Botswana since 1964. They have been subject of various economic mining optimisations by Tati Territory Exploration Company, Anglo American, Morex, Bamangwato Concessions Limited, Falconbridge, Gallery Gold, IAMGOLD, Galane and Tati Nickel Mining Company (TNMC). The Phoenix deposit was the only active operation at the time this project started. The Phoenix mine contains 76 million tonnes at 0.27% Ni and 0.25% Cu when the resource model was updated in 2009 (Geldenhuys, 2009). The Selkirk deposit was underground mining operation from June 1988 to December 2001 and was later suspended pending the development of an open pit mine. The Selkirk deposit contains 135.3 million tonnes at 0.23 Nickel (Geldenhuys, 2008). The Selkirk deposit was remodelled to 133.53 million tonnes at 0.21% Ni and 0.17% Cu (Gipronickel, 2013). Since 2010, Tati Nickel Mining Company (TNMC) and Galane Gold have been exploring the Tekwane deposit, and they are focused on

Ni-Cu-PGEs and gold. The Rooikoppie deposit is still under evaluation with limited preliminary studies done by TNMC between 2010 and 2012.

2.6.1. Phoenix mine

The Phoenix mine is located north of Selkirk mine (Figure 1.1). The Phoenix mine consists of north trending metagabbroic body, which extends approximately five kilometres in length. The Phoenix mine contains the best exposure of metagabbro units, their geology, geochemistry and petrology forms part of the current research. Dirks (2004, 2005) described and discussed the geology of the Phoenix mine, which provided motivation to undertake this research. Dirks (2004, 2005) classified the Phoenix mine metagabbro units into three types. These include melanocratic, marginal leucocratic and mesocratic megabbro (Table 2.2).

There are three types of mineralisation styles recognised within the Phoenix mine. These include fine and blebby disseminations, vein and stringer ore (Dirks, 2005; Maier et al., 2007). The veined sulphide mineralisation occurs as massive bodies within the Phoenix mine.

Table 2.2: The proposed classification nomenclature of metagabbro units in the Phoenix mine (Dirks, 2005).

GABBRO FACIES	CHARACTERISTICS
• Melanocratic metagabbro (MG_a	• more than 75% mafic minerals with minor plagioclases,
• Marginal leucocratic (MG_aP),	• more than 55% mafic minerals with minor plagioclases
• Mesocratic metagabbro (MG_Pa	• more than 55% plagioclases with minor mafic minerals
• Leucocratic metagabbro (MG_P),	• more than 75% plagioclases with minor mafic minerals

2.6.2. Selkirk mine

The Selkirk mine occurs south of Tekwane deposit and Phoenix mine (Figure 1.1). The Selkirk orebody plunges at 20° to the south with gossan outcropping at surface above the underground mine stope. The geology of the Selkirk mine has been described and discussed by Hunt and Dirks (2005) who stated that the orebody is hosted by two types of metagabbro units, namely, taxitic and leucocratic porphyritic metagabbro (Maier et al., 2007). The taxitic metagabbro is characterised by sulphide mineralisation of low to high grade, whereas the leucocratic porphyritic gabbro is barren (Carney et al., 1994). Northwest trending Karoo-age dolerite dykes, and south trending feldspar porphyries (FP) crosscut these metagabbro units. Alteration assemblages consist of epidote-chlorite, fuchsite and saussurite (Dirks, 2004, 2005). The pentlandite, pyrrhotite, chalcopyrite and pyrite contain the Ni-Cu-PGEs mineralisation (Johnson, 1986). Pentlandite is hosts PGEs mineralisation.

2.6.3. Tekwane deposit

Rogers (2002) described the geology of Tekwane deposit as part of exploration programme. In summary, gabbroic units occur in contact with granodiorite and contain Ni-Cu-PGEs mineralisation in the Tekwane deposit. The Tekwane deposit is the northern extension of Selkirk deposit and pinches into granodiorite (Key, 1973). The mineralisation is in the form of disseminated pyrrhotite, pentlandite, chalcopyrite and pyrite (Maier et al., 2007).

2.6.4. Rooikoppie Deposit

The Rooikoppie deposit consists of meta-volcanic and meta-sedimentary sequences (Key, 1976; Tombale, 1992). Karimacheng Formation, Lady Mary Formation and Penhalonga Formation define the Rooikoppie Deposit (Carney et al., 1994). It consists of the granodiorite units, which intruded the amphibolite approximately 2.7 Ga based on U-Pb crystallisation ages (Zhai et al., 2006). Tombale (1992) studied the geology of East Botswana and pointed out that Rooikoppie deposit is bounded by east dipping Mphoeng and Matsiloje thrust zones that are NE trending (Figure 2.3). Perry (1977) established that the gossan outcrops within Rooikoppie deposit form extension of the Mphoeng thrust zone in east Botswana.

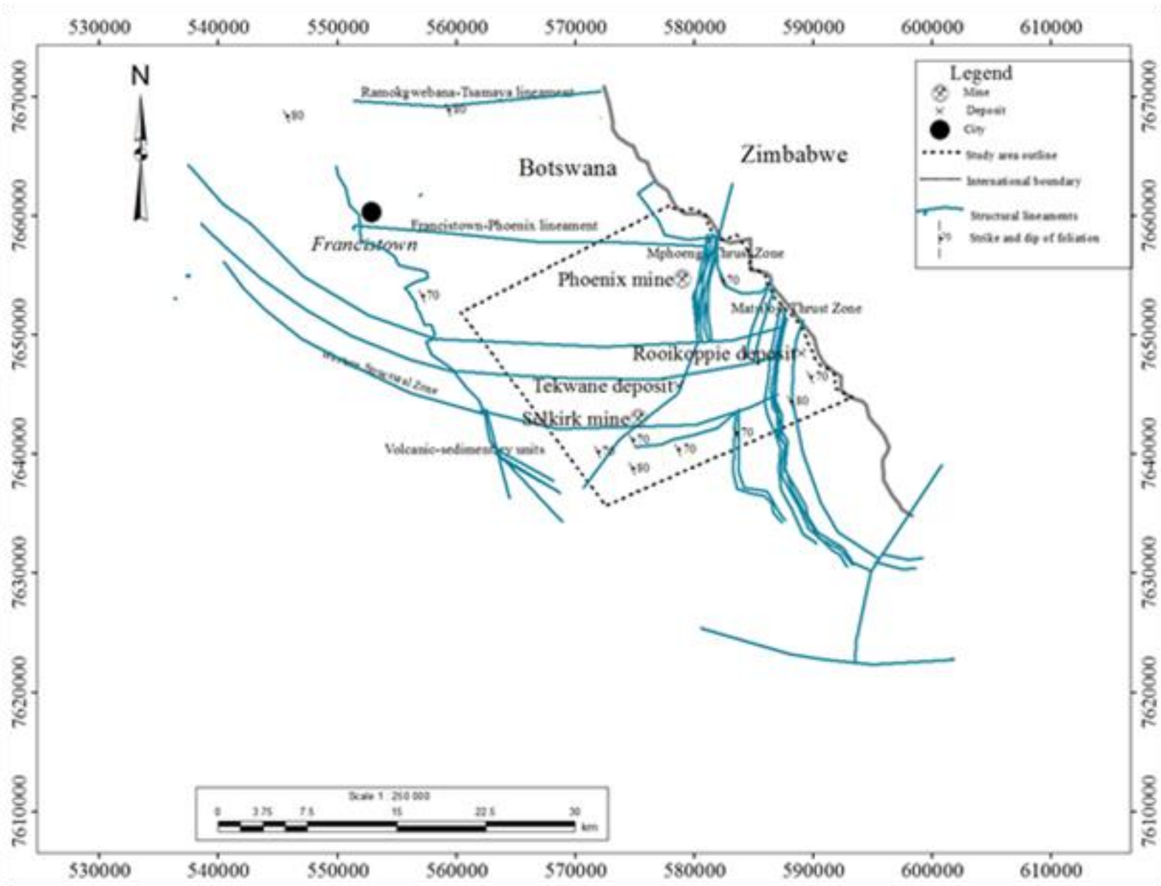

Figure 2.3: The lineament patterns associated with thrust zones that bound the Rooikoppie deposit in the southwest part of the Zimbabwe craton (modified from Tombale (1992), McCourt et al. (2004) and van Geffen (2005).

2.7. Whole rock geochemistry of metagabbroic units

Major element oxides composition of the granitic and gabbroic units of the Tati sulphide mines and deposits complex (TSMDC) are described by Tombale (1992), Kampunzu et al. (2003), Maier et al. (2007) and Bagai (2008). In summary, they demonstrated that the gabbroic units are characterised by moderate content of SiO_2 of between 42 wt. (%) and 50 wt. (%). The gabbroic units have moderate to high MgO content of between 3 wt. (%) and 16 wt. (%) indicative of poorly fractionated primitive mantle source rocks. The CaO content of the gabbroic units ranges from 2 wt. (%) to 6 wt. (%). The geochemistry of the gabbroic units resolves positive correlations between MgO and CaO contents.

The FeO content of the gabbroic units ranges from 4 wt. (%) to 9 wt. (%) (Tombale, 1992). The gabbroic units are characterised by enriched light rare earth elements (LREE) and depleted heavy rare earth elements (HREE). Kampunzu et al. (2003) and Bagai (2008) reported that the gabbroic units and their contact lithologies formed in a continental margin environment, subsequent to subduction of the Limpopo belt oceanic slab beneath the Zimbabwe Craton continental crust. However, Maier et al. (2007) argued that the gabbroic units formed in oceanic arc environment.

CHAPTER 3.0: METHODOLOGY

Three methods of data collection used to complete the research are field studies, laboratory analysis and data manipulation. Data manipulation involved data processing into a form that can be easy to analyse and interpret. The work base was the Phoenix mine exploration office in Botswana, where drill cores from Phoenix and Selkirk mines are kept and office workstations are based.

3.1. Field Studies

Field studies in and around the Phoenix, Selkirk mines and Tekwane, Rooikoppie deposits were completed through detailed geological mapping and core logging. Detailed geological mapping was completed in July-October 2013 and March-July 2014 to document different lithological units, contacts and structural elements relationships. Geological mapping of the Phoenix pit was undertaken where access to the pit benches was safe. Gabbroic units, granodiorite and dolerite and their contacts, and geological structures, such as shear zones, foliation and mineral lineation were observed and recorded. The structural data in the form of strike, dip, dip direction, trend (azimuth) and plunge were measured using Silva® Ranger model 15 and Brunton® geological compasses and are presented in Appendix B;Table B1. The compass clinometer was corrected for magnetic declination of 11º west as appropriate for east Botswana. In addition, Sirovision® (version 5.2) of 2014 was used to capture pit wall images and derive strike and dip of fault planes of inaccessible pit faces especially risky high walls. It provided 3D images at accuracy of ±5º for strike and dip angles, and ±2 cm for every 100 metres of camera position away from the pit wall. Surface geological mapping within Phoenix and Selkirk mine leases and Tekwane and Rooikoppie deposits was conducted along east-west traverses. The positions of observed rock types and structures were recorded as UTM coordinates based on WGS 84 (Zone 35K) system and presented in Appendix B: Tables B2 and B3).

3.1.1. Surface geological mapping

Surface geological mapping was undertaken to obtain as much information from in-situ outcrops. The steps, which were followed during geological mapping are as follows:

A desktop study of the area to be mapped was undertaken through interpretation of the Landsat 7 Enhanced Thematic Mapper (ETM) Red, Green, Blue (RGB) of band ratio 7, 3, 1 for accessibility routes and streams. The reconnaissance study was undertaken to determine the general geology of the area.

The lithological units' descriptions as observed and structural elements measurements from outcrops were noted. The representative samples were collected at selected outcrops for petrographic and whole-rock geochemistry analysis. The coordinates of localities of observed outcrops, sampled and photographed points were noted in the field notebook. The photographs were captured using Sony® Cyber-shot 14.1 mega pixels camera. The coordinates were provided by hand held GARMIN® GPSmap 62 (Accuracy ±3m) based on World Geodetic System (WGS) 84 /Universal Transverse Mercator (UTM) (Zone 35K).

The recorded locality positions, rock types and structural measurements were captured into Micromine® (2014) and ArcGIS™ plotted to generate outcrop maps of the deposits (Figure 3.1).

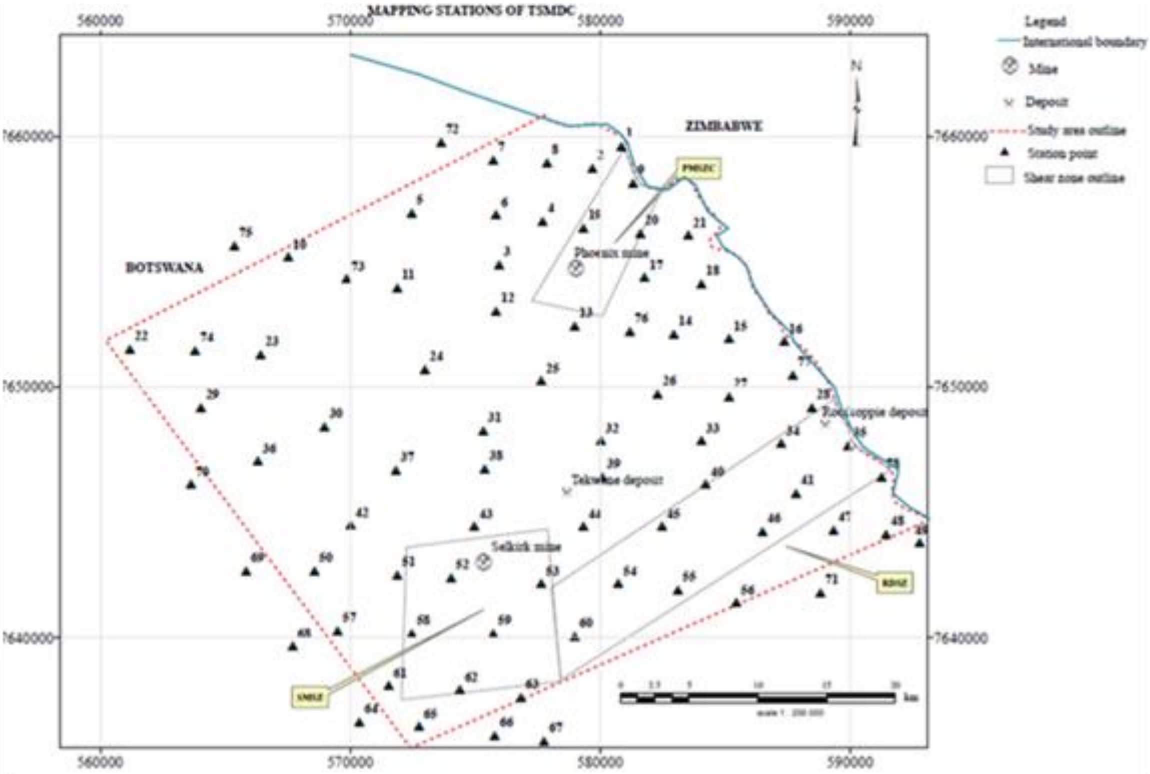

Figure 3.1: The location of regional studies mapping station points in which geological data was obtained around TSMDC excluding mine and deposit scale studies station points.

The outcrop map was enhanced into a 2-dimensional geological map by addition of petrological and structural data (Figure 3.2). Structural data is plotted as lines and planes in the equal area stereonet using Stereonet® 8 version software. The stereonet plots are generated for analysis and interpretation of the orientation of the foliation.

3.1.2. Pit mapping of the Phoenix mine

Mapping of the Phoenix mine was achieved along the ramp, benches, and faces where it was safe to do so, and to ensure compliance with mine safety standards. The procedure on pit mapping is outlined below,

The measuring tape was laid at the foot of the face to be mapped for positioning of the notable features, which include lithological contacts and structural elements, rock types, and mineralization types were noted and recorded in the mapping sheet. The start and end of the mapped faces, lithological contacts, and structural elements were marked using red spray for easy identification on the face. The marked points were surveyed using Trimble® R8 Rover-TSC 2 differential GPS (Accuracy ±1mm) based on the Cape Clarke 1880 LO 27 coordinates, which were later converted to WGS 84 UTM system. The recorded data were downloaded into ArcGIS™ and strings generated for the lithological domains. Thus, the geological map was created for Phoenix mine (Figure 3.3). The manual geological mapping was also undertaken in the Selkirk mine and Rooikoppie deposit and geological maps were created (Figures 3.4, 3.5).

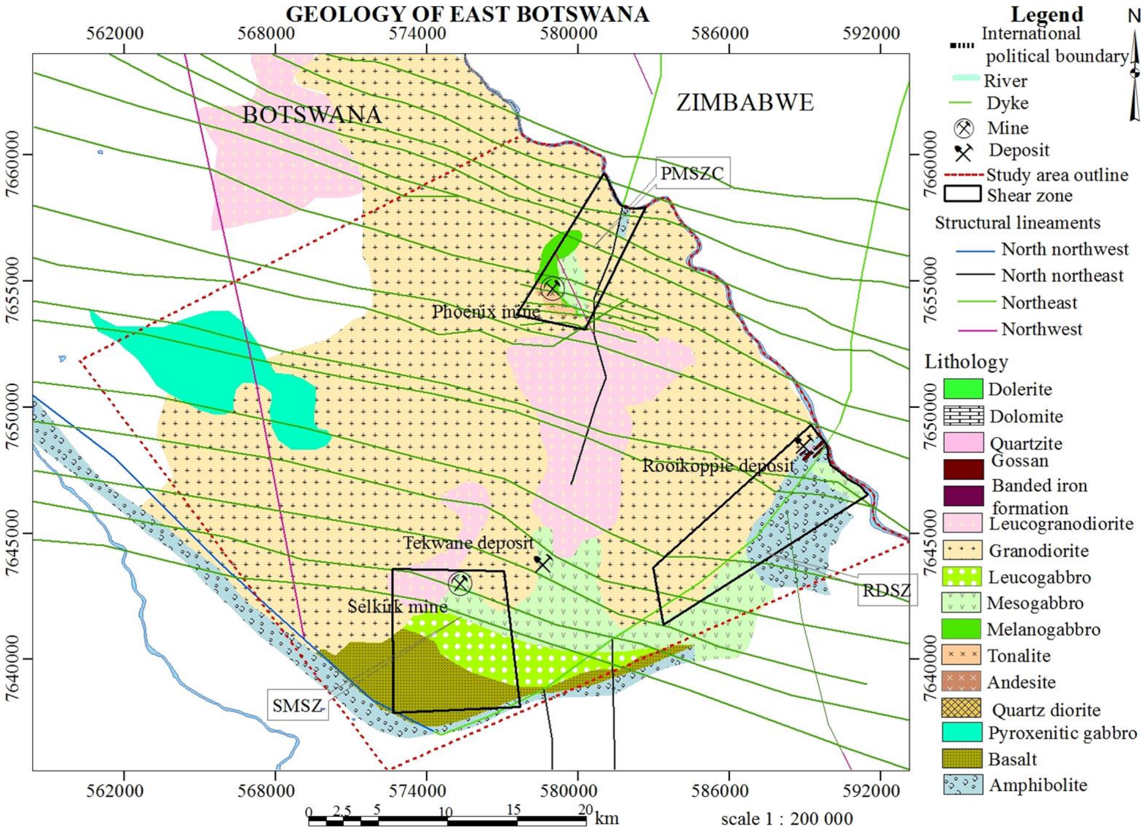

Figure 3.2: The geological map of the east Botswana mines and deposits, which shows major rock units and the shear zones of Phoenix Mine Shear Zone Complex (PMSZC), Selkirk Mine Shear Zone (SMSZ) and Rooikoppie Deposit Shear Zone (RDSZ).

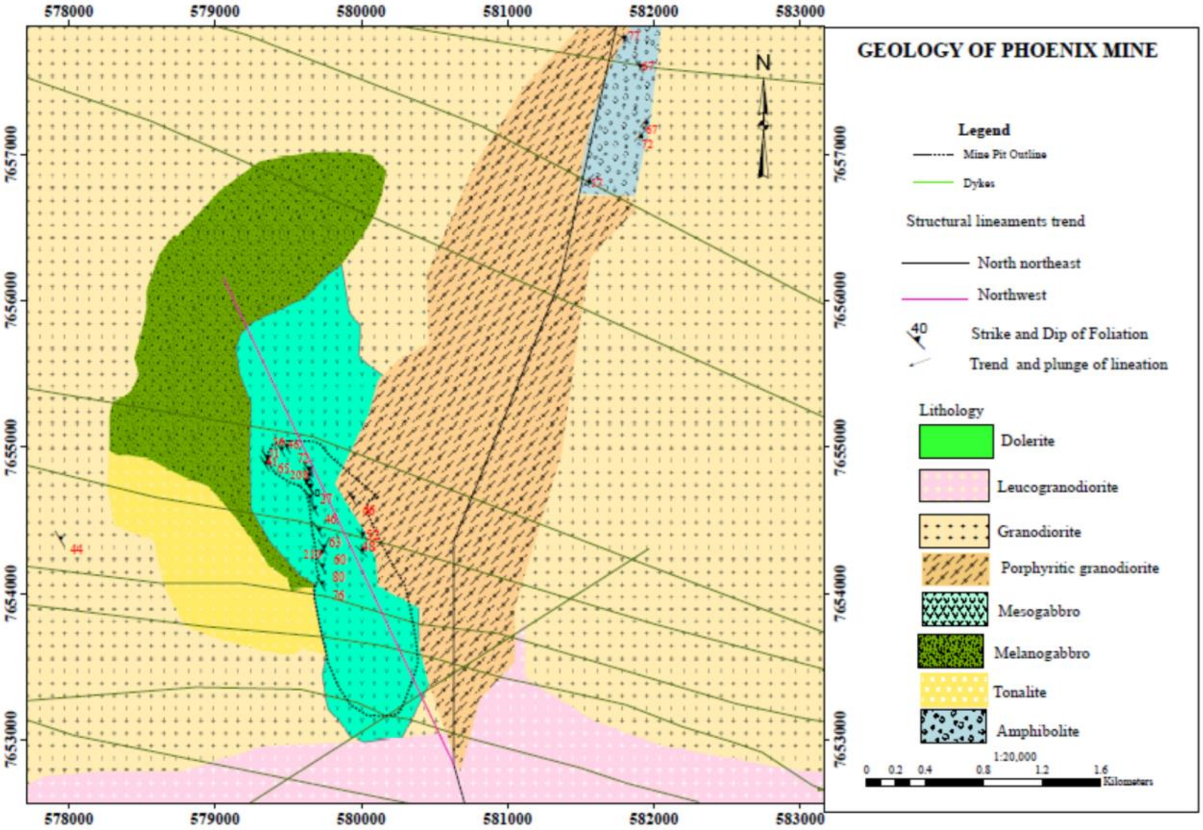

Figure 3.3: The geological map of Phoenix mine showing NNE-SSW and NW-SE trending lineaments that occurs along the zones where structural data were collected during fieldwork.

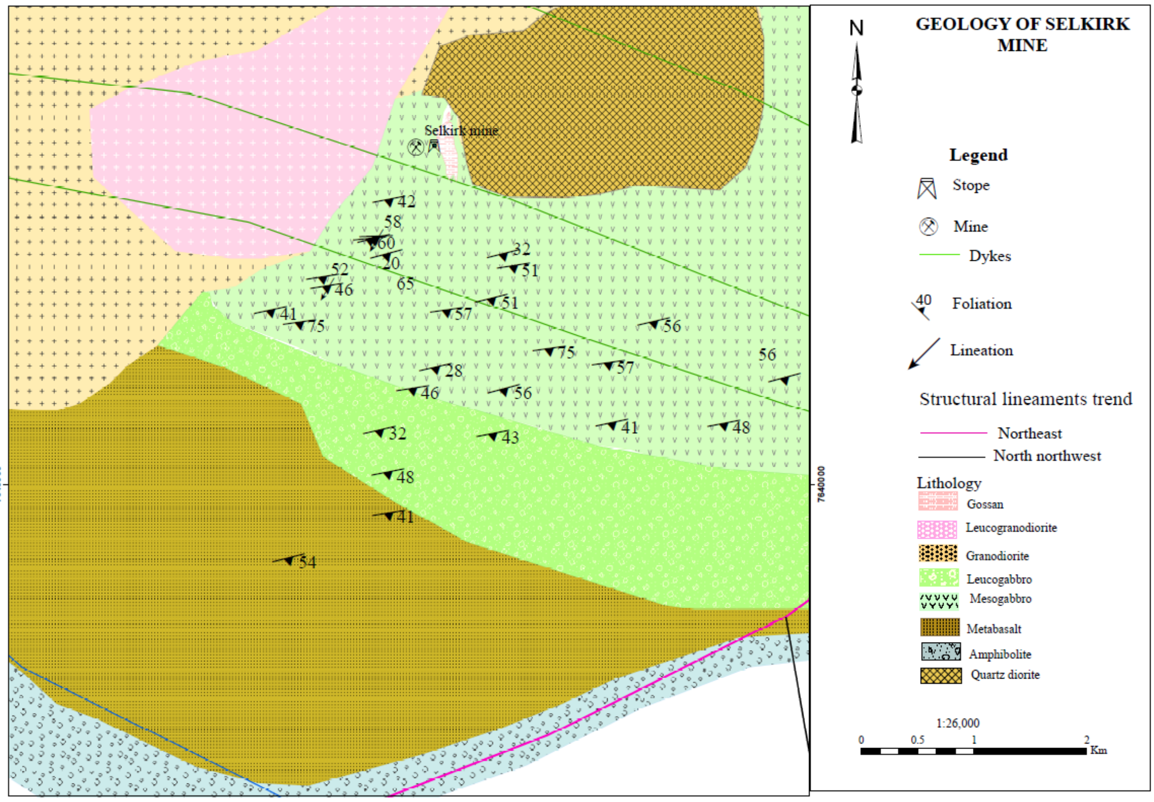

Figure 3.4: The geological map of the Selkirk mine, which shows the location of the gossan outcrops, mesogabbro, leucogabbro units, quartz diorite, basalt and amphibolite to the south. The Selkirk Mine Shear Zone (SMSZ) crosscuts the mesogabbro, leucogabbro units and basalt.

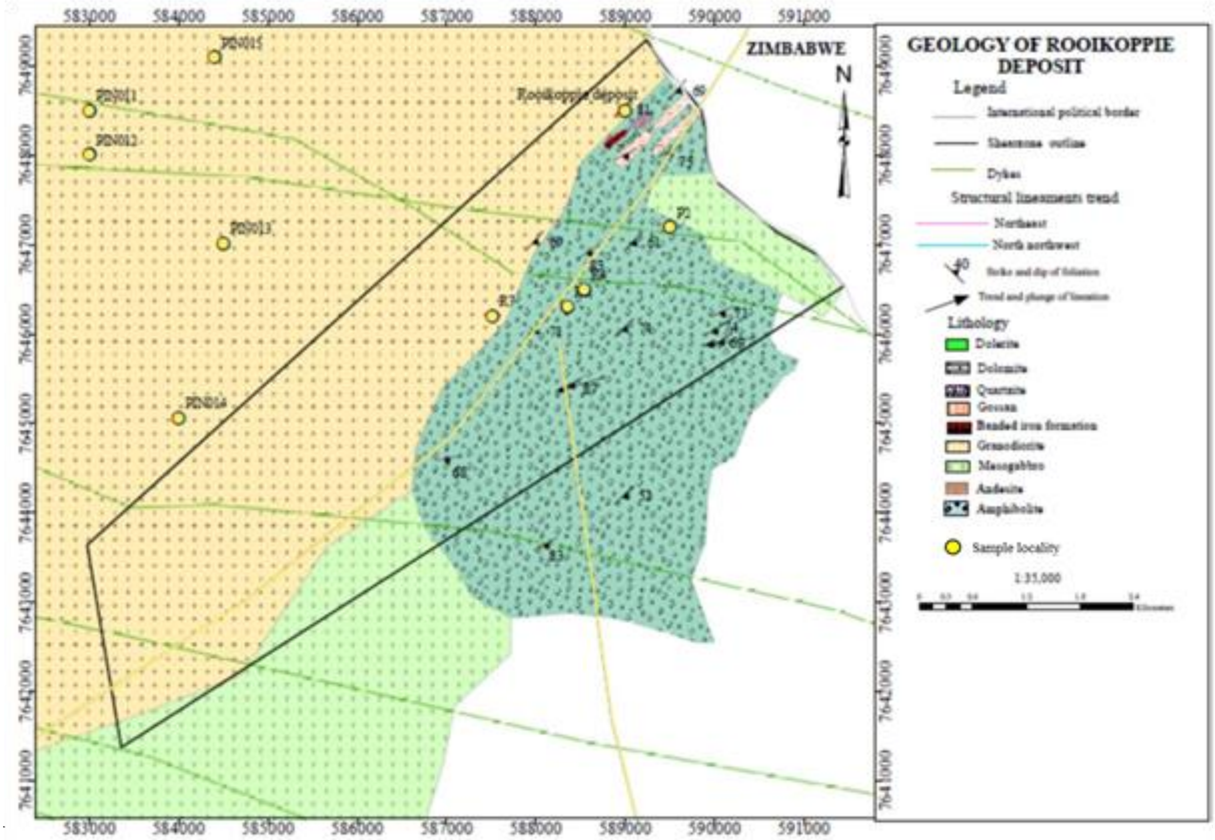

amphibolite, mesogabbro, gossan and dolomite. The andesite occurs sporadically near banded iron formation (BIF) and quartzite outcrops in the Rooikoppie deposit.

3.2. Core Logging and Sampling

Core logging was conducted on nineteen (19) diamond boreholes from Phoenix and Selkirk mines and Tekwane and Rooikoppie deposits with observations recorded on logging sheets. These include boreholes DSLK233, DSLK133, DSLK245, DSLK251, and DSLK181 from the Selkirk deposit. Boreholes PN001, PN010, PS486, PS467, and PS138 from the Phoenix deposit. Boreholes TW08, TW19, TW25, and TW27 from the Tekwane deposit. Boreholes; DRKP001, DRKP002, DRKP003, DRKP004 and DRKP005 from Rooikoppie deposit.

These boreholes were selected because they represented different domains within the mines and deposits. Logging data was captured into Field Marshal® software and downloaded into Micromine® for processing. Fist-sized field samples and 160 mm long core samples were collected for petrographic and geochemical analyses. Samples were collected during core logging and geological mapping for petrographic and whole rock geochemical analyses (Appendix B: Table B2 and B2).

3.3. Petrology

The petrology of Phoenix and Selkirk mines, and Tekwane and Rooikoppie sulphide deposits is studied from representative samples of different rock units. These samples were obtained from outcrops in the Phoenix, Selkirk mine leases and Tekwane and Rooikoppie prospect areas. The samples are also obtained from the Phoenix mine pit faces. The petrology is studied from normal thin sections and polished thin sections. Normal and polished thin sections were generated at the rock-cutting laboratory at the School of Geosciences, University of the Witwatersrand, Johannesburg. The normal thin sections and polished thin sections were prepared from forty-one (41) oriented rock samples obtained from logged boreholes, mapped pit faces and outcrops.

3.4. Laboratory analysis

Thirty-five (35) samples were analysed for both major oxide elements and trace elements using X-Ray fluorescence (XRF) at the Earthlab, University of the Witwatersrand Johannesburg. The representative samples were analysed to understand their formation processes and the geotectonic settings. The powdered samples were turned into pellets, which were formed from pressed ignited mixture in a fused disk. The mixtures were generated from the powdered samples and flux. The powdered samples had been ignited for 40 minutes to determine their loss of ignition (LOI). The standards were also analysed after every five rounds of samples analysis for monitoring the accuracy of results, which is a critical component of the quality assurance and quality control (QAQC). These standards include NIM-P, NIM-D, W2, NIM-S, GSP-2, NIM-N, NIM-G, PCC1, BHVO2, AGV-2, G2 and DTS-1. The background standards used included; 100% SiO_2, 60% CaO with 40% SiO_2 and 40% Fe_2O_3 with 60%SiO_2.

The trace elements analysis in the XRF machine were undertaken on pellets generated from pressed mixture of 6 grams of each powdered sample and polyvinyl alcohol. The polyvinyl alcohol was added to the powdered sample to make the particles stick or bind together when being compressed into disc shaped pellets. The pellets formed in aluminium cups for stability and easy labelling using a marker for sample labels. The pellets were left to dry for 24 hours before being analysed. The standards were inserted after every round of five samples analysis for trace elements, which includes NIM-D, NIM-S, BHVO2, NIM-N, AGV-2 and GSP-2.

Twelve (12) samples were selected for rare earth elements analysis using inductively coupled plasma mass spectrometry (ICPMS) at Earthlab, University of the Witwatersrand, Johannesburg. The selected samples were analysed based on having low levels of Copper (Cu) because the ions interference was kept at minimal, protecting the ICPMS machine from blowing up. The samples analysed by XRF and ICPMS had been crushed and pulverized into powders. The samples were broken into manageable pieces before being crushed by Dickie and Stockler (Pty) Ltd oscillatory jaw crusher at Earthlab laboratory and milling laboratory at the School of Geosciences building at University of the Witwatersrand, Johannesburg. The samples were cleaned by removal of the iron-weathered coating using a hammer to obtain fresh sample. The jaw crusher parts, i.e. the bucket, hammer and the support panel were cleaned using clean tap water to avoid any form of contamination. The bucket was wiped off and placed at the bottom of jaw crusher each time before crushing.

The crushed samples were kept in correctly labelled sample bags to avoid any form of sample confusion. The crushed samples were pulverised in a tightly clamped basin of the Dickie & Stockler TS 250 mill machines at Earthlab laboratory and milling laboratory. The suction duct was always switched on to allow for removal of contaminant dust. The milling basin, hammer, lid and ring were cleaned using clean water and acetone before every round of milling. Quartz crystals were milled prior to milling of each crushed samples to control any form of contamination. The samples were milled for one (1) minute and then the powder was put in small sample bags, clearly labelled and sealed.

3.5. Geochemical data analysis

The major element oxides, trace elements data, and rare-earth element data was provided as Microsoft Excel® files by the Earthlab, University of Witwatersrand, Johannesburg. The data were copied into the CoPlot® clipboard and saved as datafile with preferred title as CoStat (*. dt) format in the right folder destination. The data was also plotted into Microsoft Excel®. The datafile formed part of the dataset in which Harker-variation, chondrite-normalized multi-element and ternary tectonic discrimination diagrams were created. The diagrams were copied and edited in the Microsoft PowerPoint®. The edited diagrams were copied into Microsoft Word® 2013 for analysis and interpretation.

CHAPTER 4.0: GEOLOGY

Various rock units, which include melanogabbro, mesogabbro, leucogabbro, porphyritic granodiorite, granodiorite, leucogranodiorite, quartz diorite, amphibolite, basalt, andesite, tonalite, dolerite, Banded Iron Formation (BIF), quartzite, dolomite and pegmatite constitute the Phoenix and Selkirk mines, Tekwane and Rooikoppie deposits (Figure 3.2). This chapter presents the petrographic descriptions of some of the rock types mentioned above. The samples selected generally demonstrate petrographic compositions, which experienced low effects of secondary processes such as alteration, metasomatism, metamorphism and deformation.

4.1. Lithological descriptions

The Phoenix and Selkirk mines, Tekwane and Rooikoppie deposits have different degrees of exposure of magmatic and sedimentary lithologies. The Phoenix mine has good exposure of lithologies on pit walls though observation during mapping was hampered by mining operations dust. The pit lithologies are mapped well during the rainy seasons, when there is periodic wash of the dust from the pit walls. Selkirk mine generally comprises of good outcrops although there is vast coverage of black cotton soils in some places with no outcrops. Tekwane deposit is composed of sporadic and low-lying outcrops. There are good outcrops though limited to an areal extent of less than two kilometres in the Rooikoppie deposit. Since the mapped lithological units are all metamorphosed, their nomenclature will exclude the prefix meta for simplicity in this research.

4.1.1. Magmatic units

The different gabbro units occur throughout the Phoenix and Selkirk mines, Tekwane and Rooikoppie deposits (Figure 3.2). The gabbro units include leucogabbro, mesogabbro and melanogabbro in this dissertation.

4.1.1.1. Melanogabbro

The melanogabbro covers an area of approximately 2 kilometres by 2 kilometres to the west and northwest of Phoenix mine. The melanogabbro is in contact with the Ni-Cu-PGEs sulphide mineralised mesogabbro in the Phoenix mine. The melanogabbro does not contain sulphide mineralisation in the Phoenix mine. Nevertheless, the melanogabbro contains sulphide mineralisation and occurs sporadically in Selkirk mine and Tekwane deposit. Thus, the petrographic study of the melanogabbro is vital for understanding its possible influence in the sulphide mineralisation in contact with the mesogabbro and leucogabbro units in Phoenix mine. In addition, the gradational contact relationship between melanogabbro and other gabbro units has potential to influence sulphide mineralisation in Selkirk mine and Tekwane deposit. The melanogabbro was studied from eight samples (W2, NW1, W8, SL1A, SL1B, TEK7, TEK8 and TEK9) (Figures 3.2, 3.3 and Appendix C).The melanogabbro preserves green to greyish green appearance, phaneritic and defined by primary minerals, mainly plagioclase, pyroxene, hornblende and biotite ranging from approximately 500 µm to 950 µm in size (Figure 4.1).

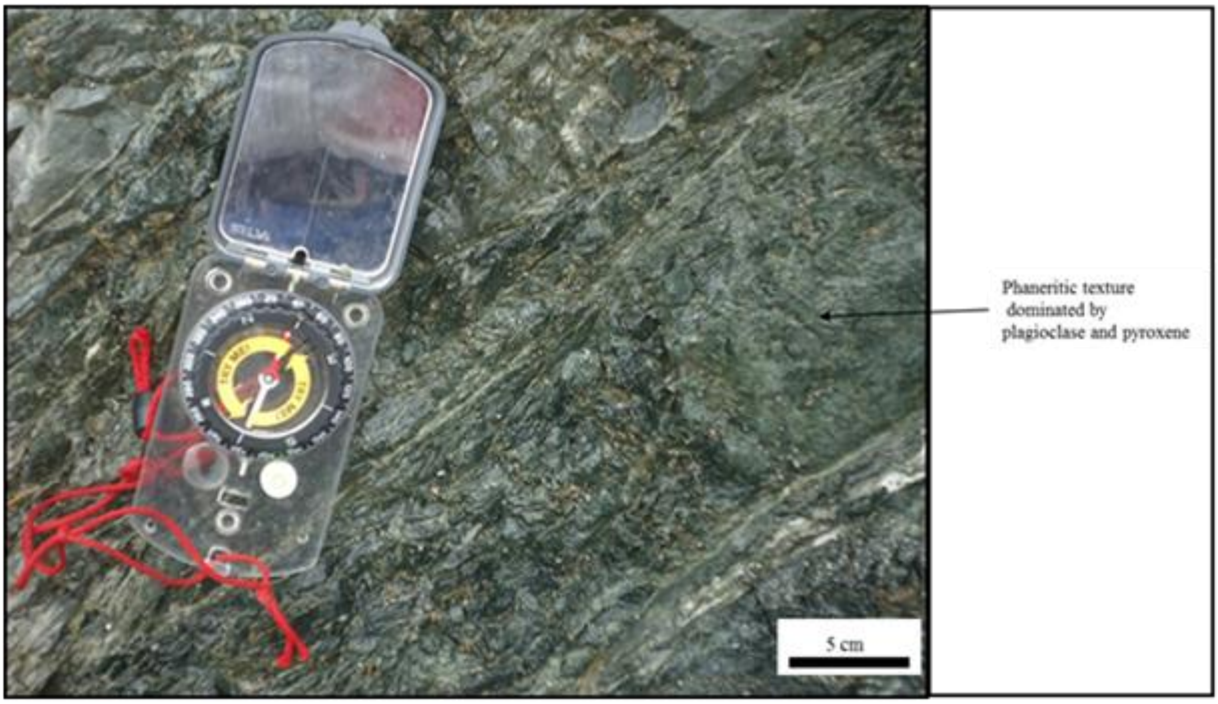

Figure 4.1: The melanogabbro is generally green, homogenous with mineralogy dominated by plagioclase and pyroxene to the west of the Phoenix mine (UTM 35K, 0579715 mE, 7654067 mN).

It forms a sharp contact with the tonalite in the western part of the Phoenix mine (Figure 4.2). It forms gradational contact with the mesogabbro and leucogabbro as demonstrated by intersections in the Phoenix mine historic drill holes.

Figure 4.2: The melanogabbro and tonalite form a sharp contact in the southwest part of the Phoenix mine (UTM 35K, 0579712 mE, 7654045 mN).

The Phoenix mine melanogabbro is crusscut by shear zones, quartz-carbonate veins, dolerite dykes and dykelets (Figure 4.3). Microscopically, the melanogabbro is green and medium grained (~500 -950 µm).

Figure 4.3: The Phoenix melanogabbro is crosscut by shear zone, which hosts quartz-carbonate veins, which resulted from precipitation of hydrothermal fluids. It is crosscut by dolerite dykelet, which suggests the dolerite intrusion postdate the formation of the shear zone in the Phoenix mine (UTM 35K, 0579749 mE, 7654318 mN).

The melanogabbro contains primary mineralogy of hornblende (~35%), plagioclase (~25%), clinopyroxene (~20%), biotite (~6%) and olivine (~8%) (Figure 4.4). Titanite (~4%) and apatite (~2%) makes up the accessory mineralogy of the melanogabbro. The plagioclase forms grains with strong polysynthetic twinning whereas biotite is brown and characteristic of strong pleochroism when viewed under the microscope. The hornblende displays strong greenish pleochroic shades.

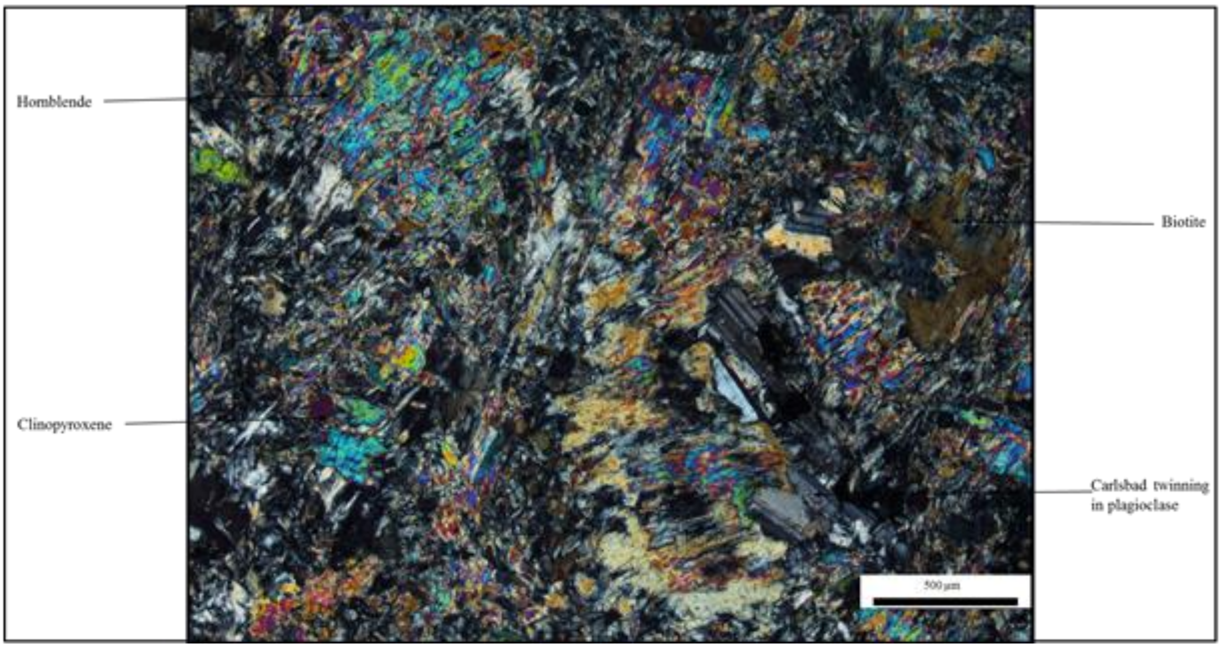

Figure 4.4: Photomicrograph of sample W8 (crossed polar) obtained from melanogabbro showing subhedral hornblende and plagioclase grains, with simple twins. The plagioclase, clinopyroxene and hornblende exhibit similar size (~300 μm).

4.1.1.2. Mesogabbro

The mesogabbro covers an area of approximately 3 by 2 kilometres in Phoenix mine. The mesogabbro occurs dominantly in Selkirk mine and Tekwane deposit, covering area approximately 4 by 4 kilometres. It outcrops abundantly, covering approximately 1 by 2 kilometres in the Rooikoppie deposit. It is considered vital to study the mesogabbro given its abundance and its relationship with sulphide mineralisation in TSMDC. The mesogabbro was studied in the field with its detailed petrography studied microscopically from eight samples obtained from Phoenix, Selkirk mines, Tekwane and Rooikoppie deposits (N1, S10, SL5, SL07, TEK3, TEK4, R11 and R012) (Figures 3.2, 3.4 and Appendix C). The contact between the Phoenix mine mesogabbro, melanogabbro and tonalite is not well established. The contact between the Phoenix mine mesogabbro and tonalite is difficult to constrain, possibly due to the area that has been mined out and turned into a ramp. The Phoenix mine mesogabbro hosts mafic enclaves (Figure 4.5).

Figure 4.5: The Phoenix mine mesogabbro hosts mafic enclave possibly derived from the melanogabbro, which suggests mesogabbro postdate the melanogabbro unit (UTM 35K, 0579662 mE, 76546156 mN).

It also hosts sulphide mineralisation in the form of disseminations and massive sulphide veins (Figure 4.6). It is intruded by dolerite dykes and porphyritic granodiorite, which occur extensively in the northern part of Selkirk mine. Furthermore, it is in proper order to consider the petrography of mesogabbro on basis of its important role as host to sulphide mineralisation in TSMDC. Thin shear zones associated with Phoenix Mine Shear Zone Complex (PMSZC), Selkirk mine Shear Zone (SMSZ) and Rooikoppie Deposit Shear Zone (RDSZ) crosscut the mesogabbro and would be explained in detail in chapter 6.

Figure 4.6: The Phoenix mine mesogabbro also hosts massive sulphide veins ranging from 10 cm to 50 cm thickness. The massive sulphide veins consist of pentlandite, pyrrhotite and chalcopyrite, (UTM 35K 0579871 mE, 7653922 mN).

Voluminous buck quartz veins intrude the mesogabbro in some localities in Selkirk mine (Figure 4.7). The Rooikoppie deposit mesogabbro is composed of plagioclase phenocrysts in a groundmass of plagioclase, hornblende and quartz (Figure 4.8). The Rooikoppie deposit mesogabbro have phenocrystic texture. Thus, it has a different texture to the Phoenix, Selkirk mines and Tekwane deposit mesogabbro.

Figure 4.7: The Selkirk mine mesogabbro outcrops is crosscut by buck quartz veins, which suggests precipitation of hydrothermal fluids transported along fractures was extensive in contact with mesogabbro units, (UTM 35K 0580270 mE, 7654112 mN).

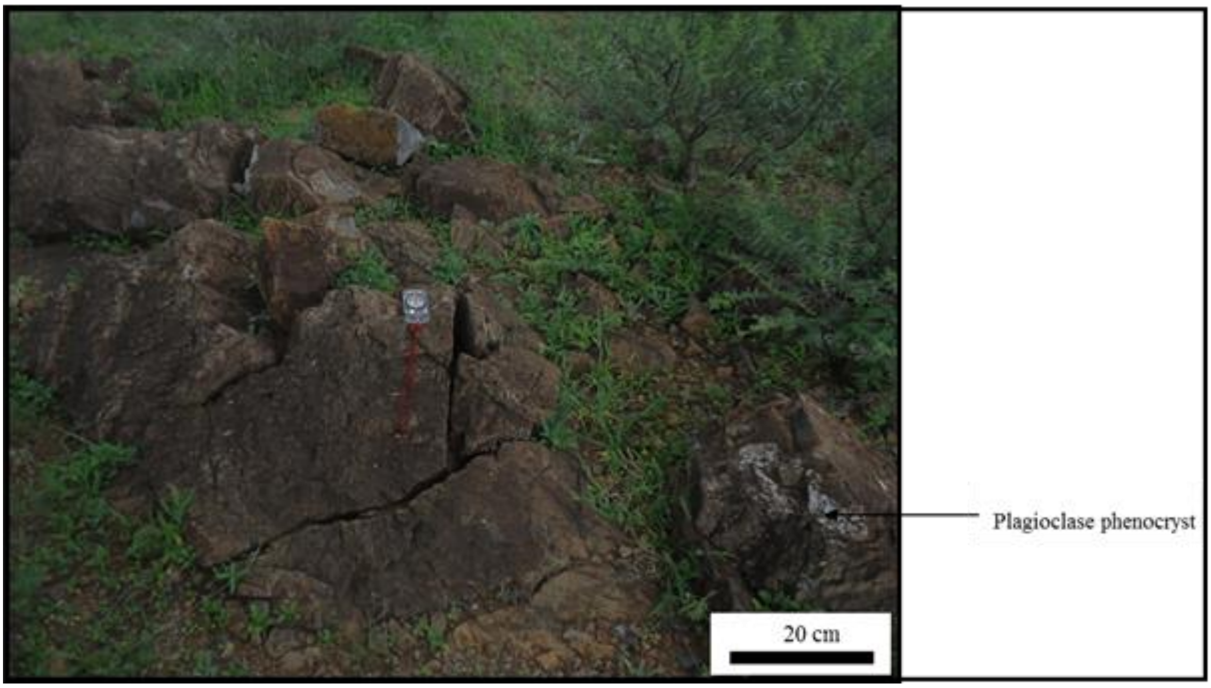

Figure 4.8: The Rooikoppie deposit mesogabbro outcrops is characterised by brown weathered surfaces (UTM 35K, 0580270 mE, 7654112 mN). The Rooikoppie mesogabbro is composed of plagioclase phenocrysts in groundmass of interstitial quartz, plagioclase and hornblende.

The mesogabbro is olive-green and medium grained (~300-400µm). The mesogabbro is composed of primary mineralogy of hornblende (~30%), plagioclase (~35%), clinopyroxene (~20%), biotite (~5%) and olivine (~5%) (Figure 4.9). The accessory minerals include apatite (2%) and titanite (3%).

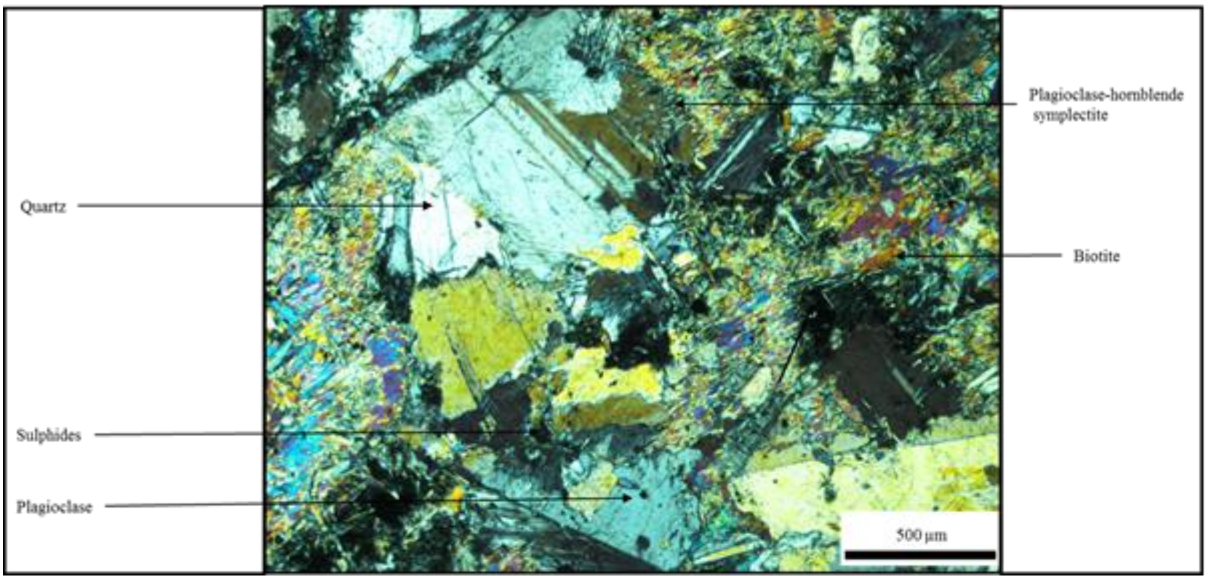

Figure 4.9: The photomicrograph (crossed polars) of sample TE07 obtained from Tekwane mesogabbro, which shows granoblastic texture, dominated by plagioclase with simple and polysynthetic twinning and hornblende, drillhole TW07, (UTM 35K, 0580451 mE, 7643963 mN). The symplectite borders plagioclase, typical of replacement of plagioclase by hornblende in the Tekwane deposit.

4.1.1.3. Leucogabbro

The leucogabbro outcrops abundantly in the southern part of Selkirk mine, covering areal extent of 2 by 2 kilometres. On the contrary, the leucogabbro is not exposed at surface except through intersections in Phoenix mine and Tekwane deposit drill holes. The Selkirk mine leucogabbro does not contain sulphide mineralisation. On the contradictory, the Phoenix mine and Tekwane deposit leucogabbro contain sulphide mineralisation. Thus, the study of leucogabbro is of significance as it bears features, which could possibly explain differing aspects associated with its sulphide mineralisation contents. The study of leucogabbro was undertaken in the field and at microscopic level based on representative samples obtained from Phoenix and Selkirk mines (S1 and SL09) (Figures 3.2, 3.4 and Appendix C). The Selkirk mine leucogabbro is texturally distinct and comprises of sub-rounded to rounded plagioclase phenocrysts (Figure 4.10). The Selkirk mine phenocrystic leucogabbro contains traces of pyrrhotite and chalcopyrite of less than 0.1 %. Thus, it is poorly mineralised and is regarded as an unmineralised leucogabbro in this study. Microscopically, the plagioclase occurs as poorly oriented and twinned euhedral crystals.

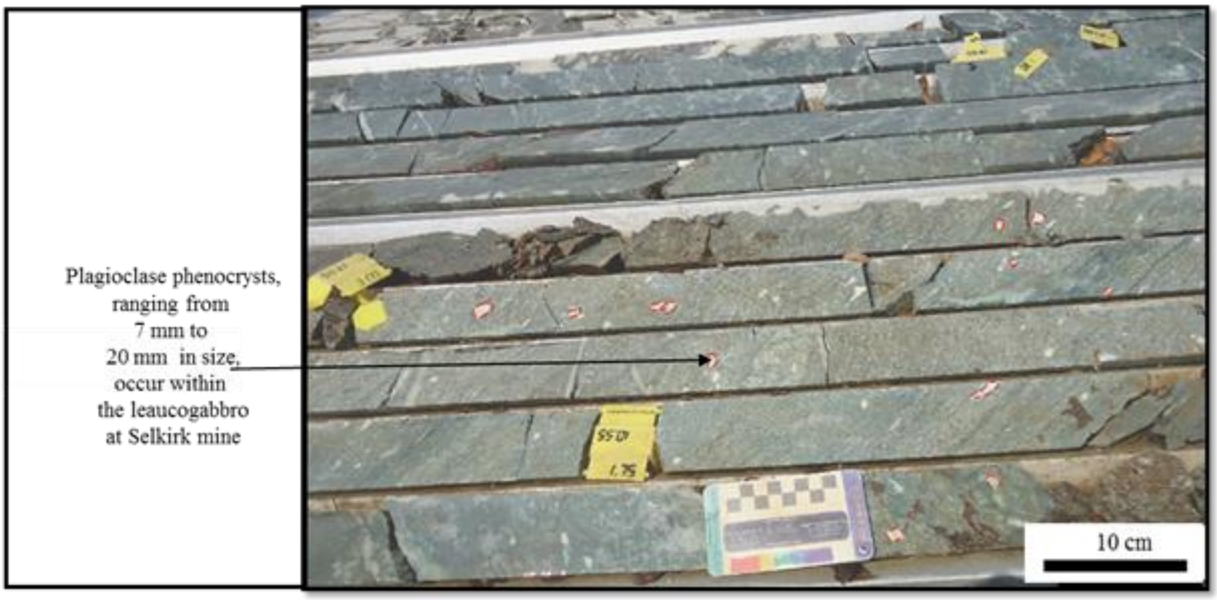

Figure 4.10: The Selkirk mine leucogabbro consists of sub rounded and rounded phenocrysts of plagioclase, drill hole, DSLK145 (UTM 35K, 0575196 mE, 7642227 mN).

The leucogabbro is grayish-green and medium grained (~ 400µm in diameter). The leucogabbro contains primary mineralogy, which comprises of hornblende (25%), plagioclase (55%), clinopyroxene (12%), biotite (3%) and olivine (3%) (Figure 4.11). Apatite (2%) makes up the accessory mineralogy of the leucogabbro.

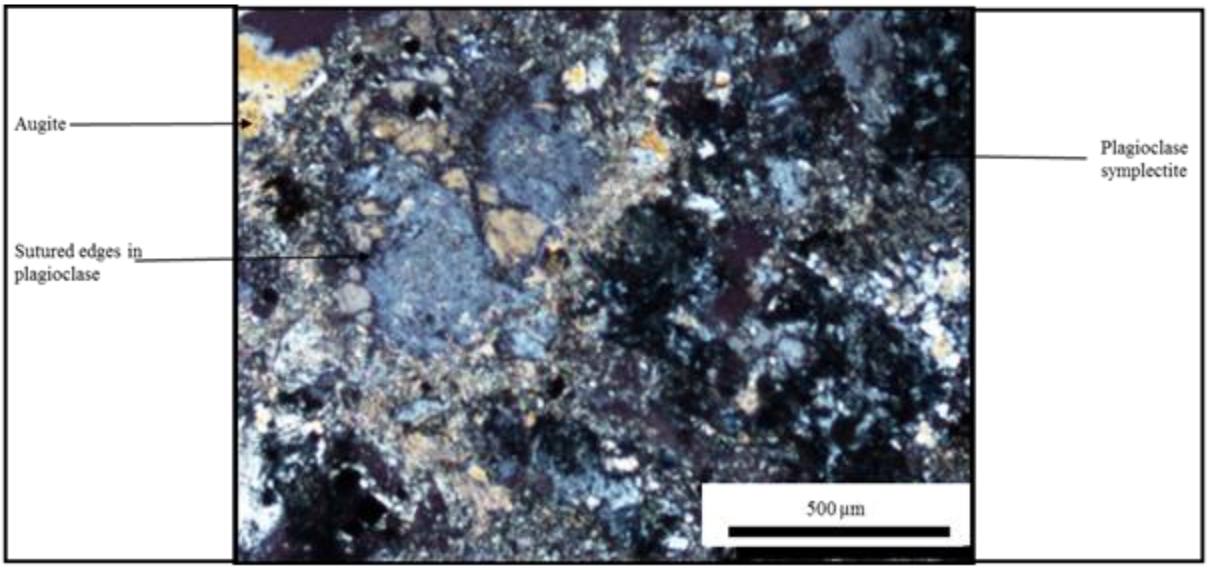

Figure 4.11: The photomicrograph (crossed polar) of sample SL09 obtained from Selkirk mine leucogabbro shows plagioclase grains characterised by poor twinning and opaque minerals possibly sulphides, drill hole, DSLK145 (UTM 35K, 0575196 mE, 7642227 mN).

4.1.1.4. Tonalite

The tonalite outcrops sporadically to the west of Phoenix mine, covering area of approximately one square kilometre. However, the tonalite is well exposed in the western walls of the Phoenix mine. The occurrence of tonalite is limited to the Phoenix mine. The contact between tonalite and melanogabbro is sharp. Nevertheless, the contact between tonalite and mineralised mesogabbro is not clearly defined in the field. The tonalite forms sharp contact with mineralised mesogabbro as observed in the Phoenix mine historic drill cores. It is vital to study the tonalite for its significance in unravelling its relationship with unmineralised melanogabbro and mineralised mesogabbro in the Phoenix mine. The tonalite was studied in the field and microscopically from representative samples (W1 and W9) (Figures 3.2, 3.3 and Appendix C). The tonalite hosts mafic enclaves, possibly derived from melanogabbro and pre-existing ultramafic units (Figure 4.12).

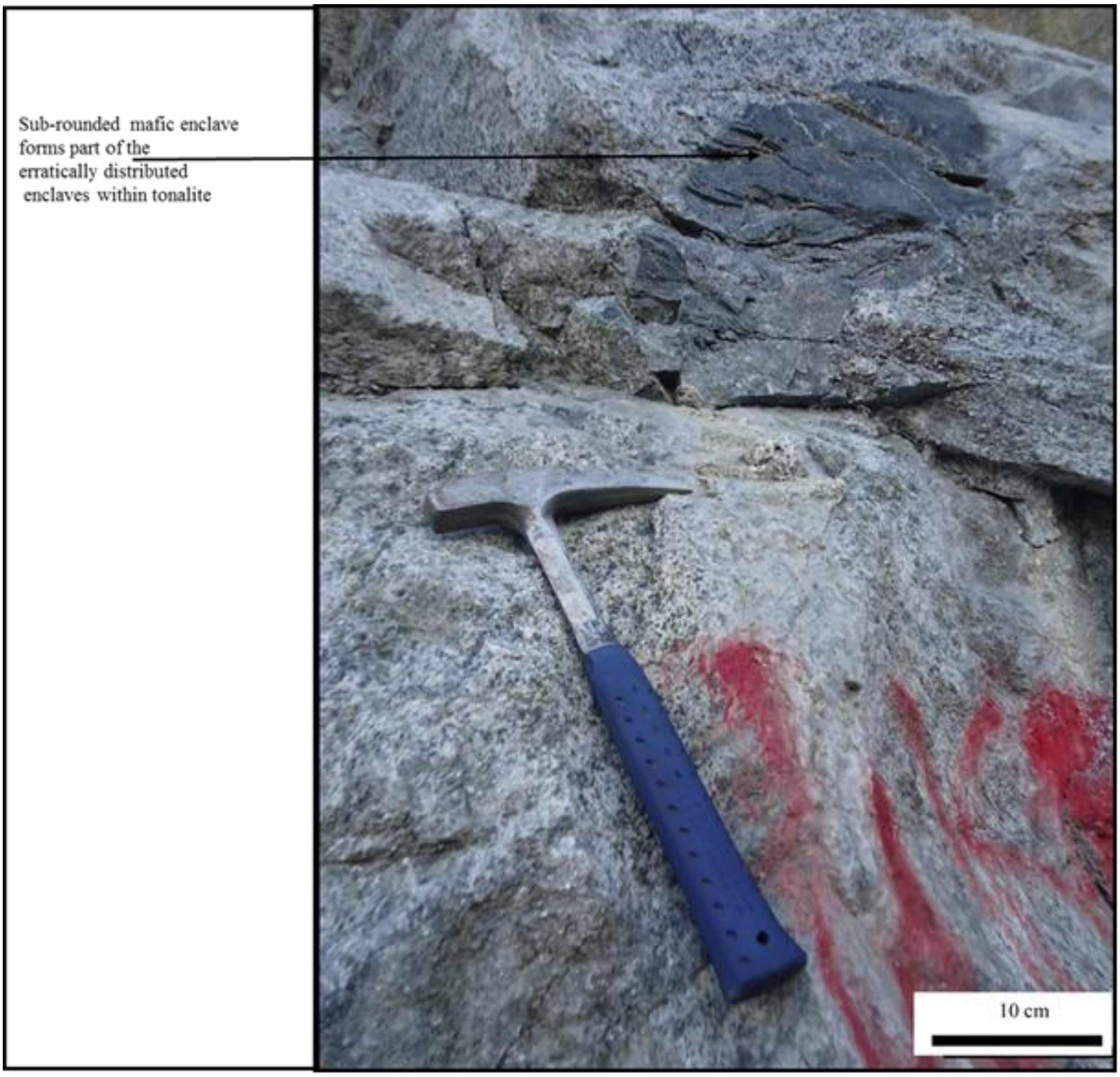

Figure 4.12: The tonalite hosts elliptical mafic enclaves, which are distributed in similar orientation akin to the magmatic foliation (UTM 35 K, 0579705 mE, 7654048 mN).

The tonalite is greyish, phaneritic textured and is composed, on average of plagioclase (70%), quartz (22%) and hornblende (6%). It also contains approximately 2% apatite. The quartz grains are anhedral and show undulose extinction (Figure 4.13).

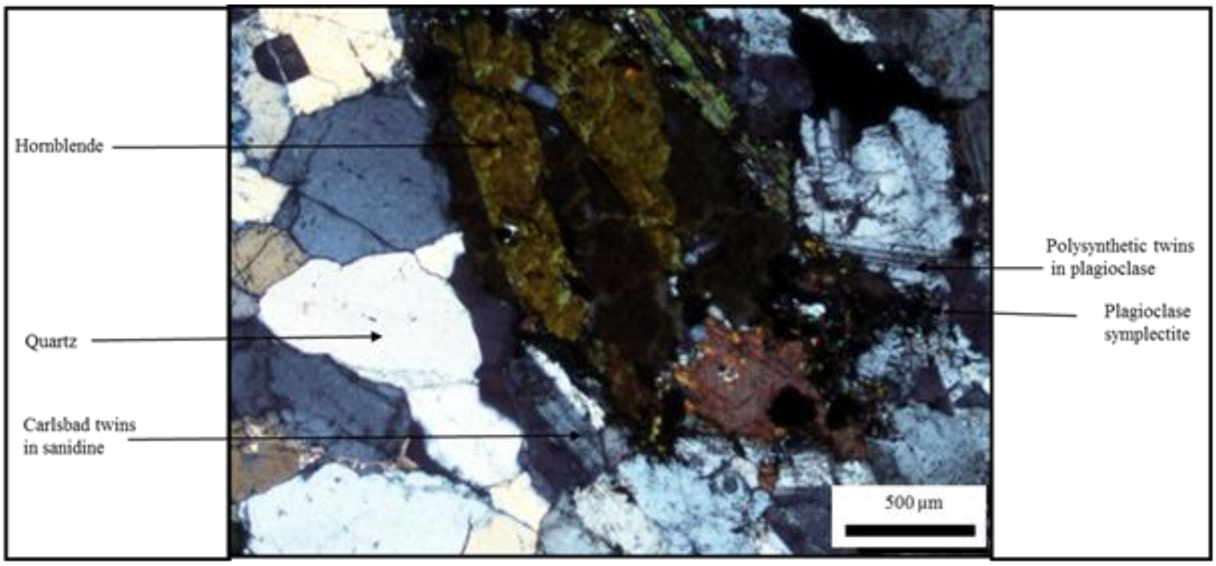

Figure 4.13: The photomicrograph (crossed polars) of sample, W1 obtained from tonalite, which shows granoblastic texture and consists of quartz, plagioclase and hornblende. The plagioclase exhibits simple twinning (UTM 35 K, 0579705 mE, 7654048 mN).

4.1.1.5. Quartz diorite

The quartz diorite outcrops in and around Selkirk mine, Tekwane and Rooikoppie deposits. It covers approximately 20 square kilometres. It forms a gradational contact with the mesogabbro in the Selkirk mine and Tekwane deposit. The contact between quartz diorite and mesogabbro is not well exposed, partly due to poor outcropping levels in eastern part of Rooikoppie deposit. It is generally barren of sulphide mineralisation though it hosts massive sulphide veins in the Selkirk mine and Rooikoppie deposit (Figures 4.14). Thus, it is of significance to study the quartz diorite for its association with sulphide mineralisation including its contact relationship with different types of gabbroic units in Selkirk mine, Tekwane and Rooikoppie deposits. The study of quartz diorite was undertaken in the field and at microscopic level based on two representative samples (TEK5, R7) obtained from Tekwane and Rooikoppie deposits. The Rooikoppie deposit quartz diorite consists of array of quartz veins and is characterised by potassic alteration (Figure 4.15).

Figure 4.14: The quartz diorite hosts massive sulphide veins dominated by pyrrhotite and chalcopyrite in the Selkirk mine, drillhole DSLK130, (UTM 35K, 0575230 mE, 7642363 mN).

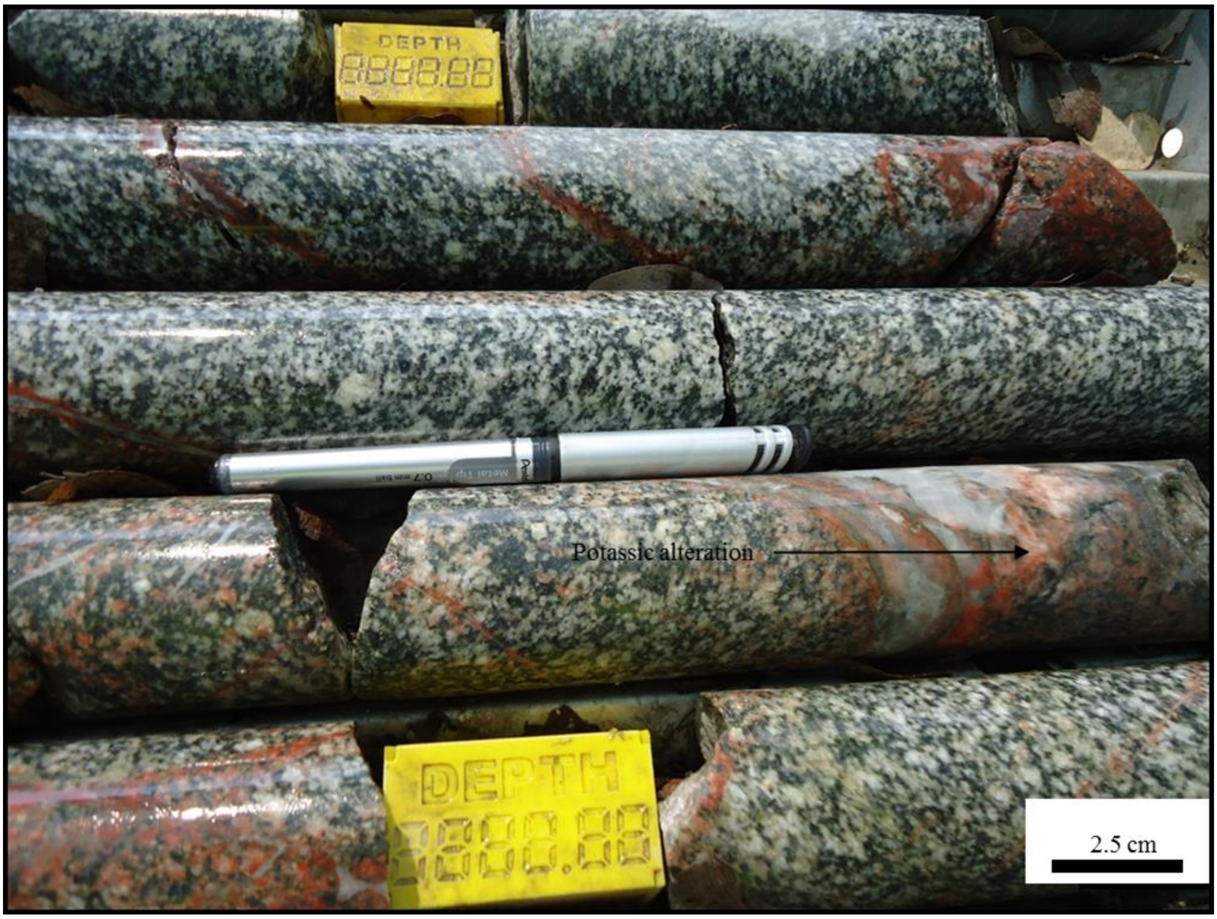

Figure 4.15: The Rooikoppie deposit quartz diorite is composed of quartz veins and pervasive potassic alteration, which suggests replacement of K-feldspar by biotite due to increase in temperature conditions as result of hydrothermal fluids, drill hole, DRKP04, (UTM 35K, 0589099 mE, 7648651 mN).

The quartz diorite is greyish green and phaneritic textured. It consists of plagioclase (~45%), hornblende (~25%), quartz (~15%) and K-feldspar (~10%) (Figure 4.16). The accessory minerals of quartz diorite include titanite and apatite, which mark up 3% and 2% of respectively. Quartz occurs as subhedral phenocrysts. The quartz grains are characterised by different stages of undulose extinction.

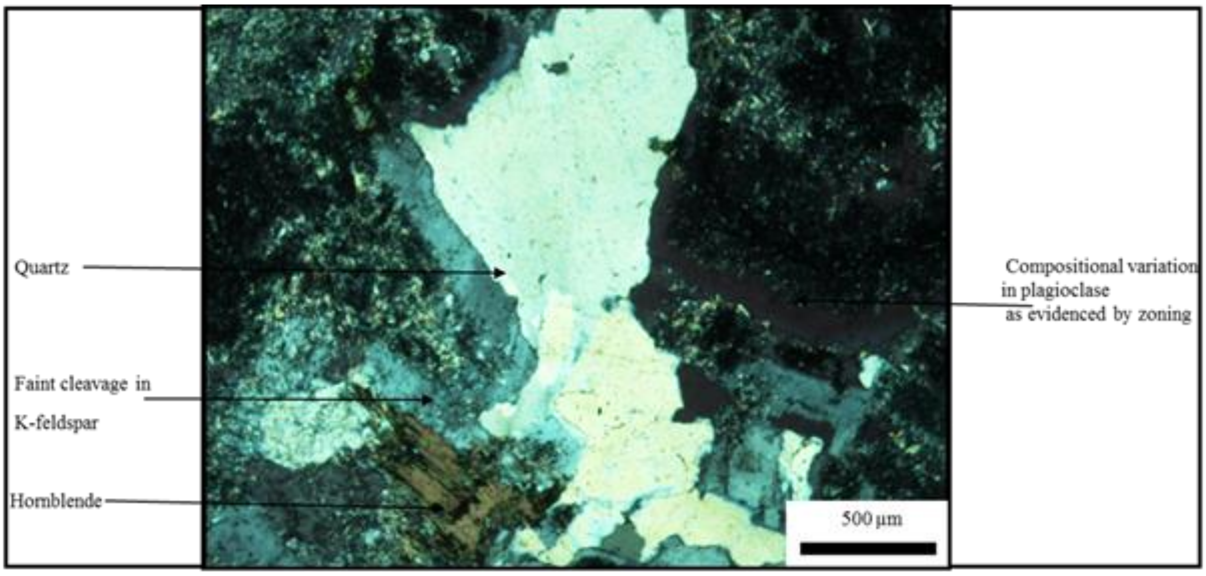

Figure 4.16: The photomicrograph of quartz diorite of the Tekwane deposit showing quartz, hornblende and plagioclase, drillhole TW29, (UTM 35K, 0580110 mE, 7643280 mN).

4.1.1.6. Granodiorite

The granodiorite outcrops extensively in and around Selkirk mine, Tekwane and Rooikoppie deposits. The granodiorite covers approximately 15 square kilometres. The petrographic description of granodiorite was studied in the field and on the microscopic analysis of five samples (P2, PIN011, PIN012, PIN013, and PIN015). The significance of the study on the granodiorite is based on its chilled contact relationships with mineralised and unmineralised gabbro units in TSMDC. Thus, it has potential to influence the form of the sulphide mineralisation. The granodiorite is generally undeformed. Stringers of sulphide mineralisation in some localities crosscut the granodiorite. The granodiorite occurs as dykes in the Phoenix mine. The contact between the granodiorite and dolerite is characterised by chilled margins. The granodiorite contains the rounded mafic enclaves in the Rooikoppie deposit, where it outcrops abundantly (Figure 4.17).

The granodiorite is grey and fine to medium-grained (~800 µm on average). It is composed of approximately 25% quartz, 5% hornblende, 25% K-feldspar, 40% plagioclase. The accessory mineralogy is made up of apatite (3%) and titanite (2%) (Figure 4.18). The granodiorite is characterised by oscillatory-zoned plagioclase.

Figure 4.17: Granodiorite hosts mafic enclaves, which range variably from ~10 to 500 mm in diameter (UTM 35K, 0585344 mE, 7653548 mN).

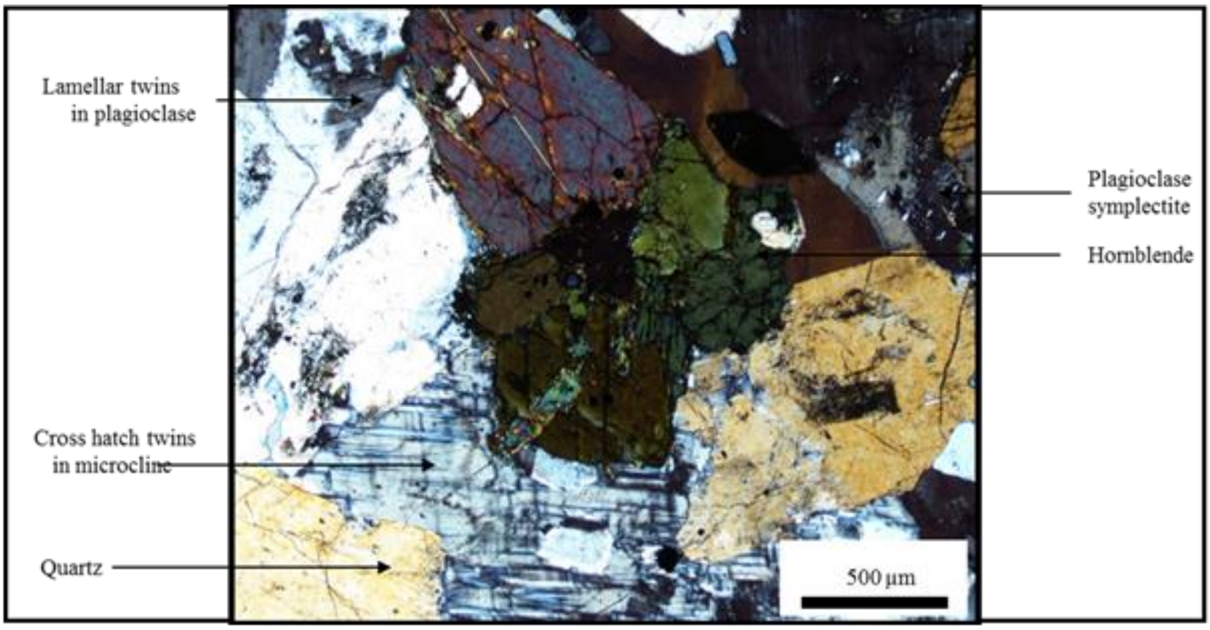

Figure 4.18: The photomicrograph of granodiorite of the Tekwane deposit showing quartz, hornblende and plagioclase, drill hole TW29, (UTM 35K, 0580110 mE, 7643280 mN).

4.1.1.7. Porphyritic granodiorite

The porphyritic granodiorite occurs extensively in the northeastern part of Phoenix mine where it crosscuts the mesogabbro as evidenced by chilled margins at contacts. The porphyritic granodiorite covers approximately 10 square kilometres between Phoenix mine and the international border between Republics of Botswana and Zimbabwe. It trends parallel to the north-northeast trending shear zones associated with the Phoenix Mine Shear Zone Complex (PMSZC) (Figure 3.2). It is medium grained and displays elongated plagioclase phenocrysts (Figure 4.19). The study of the porphyritic granodiorite is significant as it bears potential relationship with lineaments in TSMDC. In addition, it has crosscutting relationship with mineralised mesogabbro in both Phoenix and Selkirk mines. The porphyritic granodiorite was studied in the field with microscopic evidence obtained from three representative samples (W3, SL06, and SL08). It is crosscut by the north-northeast trending shear zone in the Phoenix mine and to the northeast of Phoenix mine.

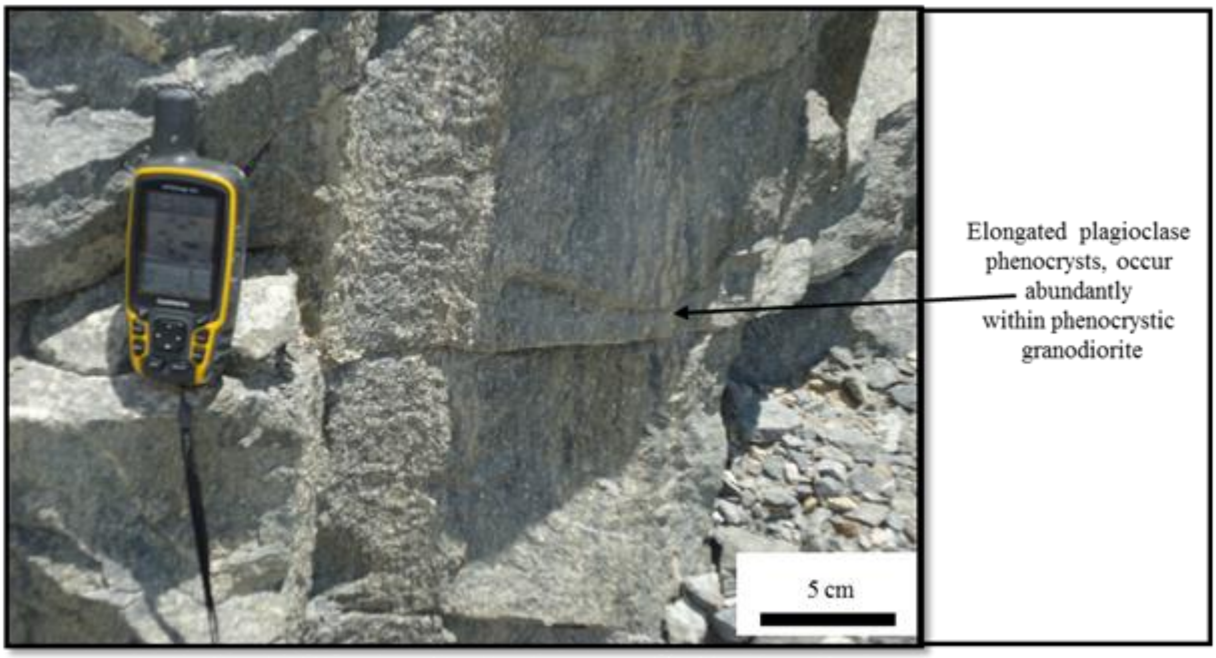

Figure 4.19: The porphyritic granodiorite is characterised by elongated plagioclase phenocrysts on a groundmass of K-feldspar, quartz and hornblende.

The porphyritic granodiorite consists of mineral assemblages of, plagioclase (55%), K-feldspar (15%), microcline (10%) and quartz (18 %) (Figure 4.20). The apatite (2%) makes up the accessory mineralogy of the porphyritic granodiorite.

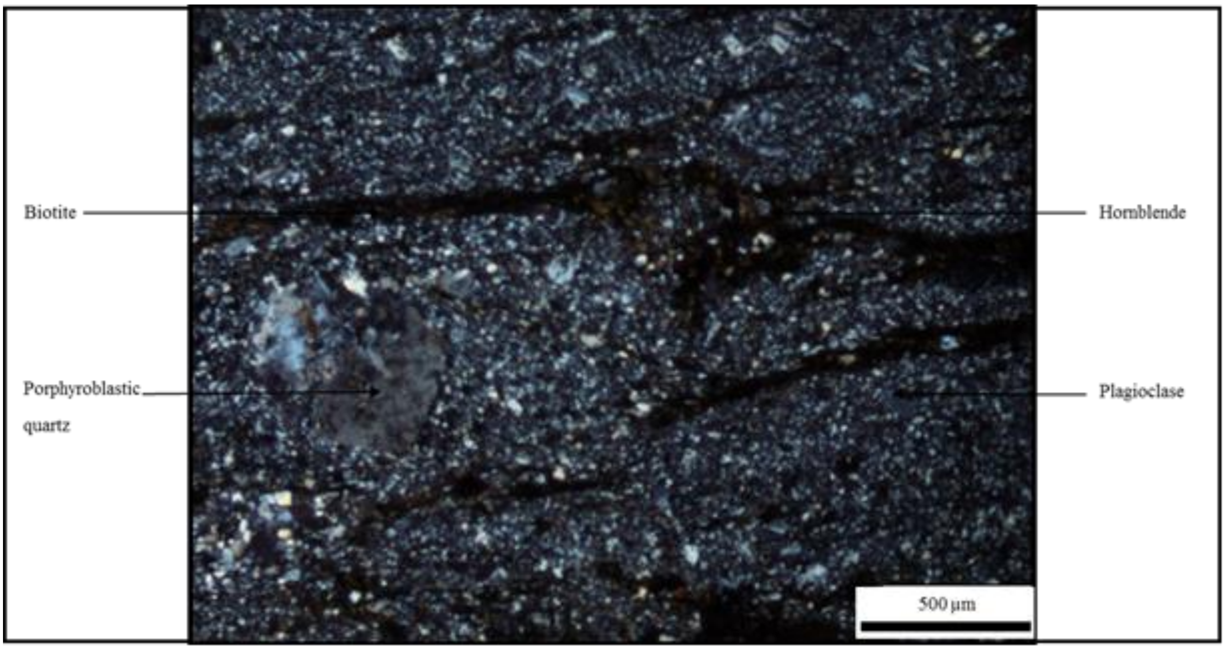

Figure 4.20: The photomicrograph (crossed polar) of sample, W3 obtained from Phoenix mine porphyritic granodiorite, which shows plagioclase phenocrysts embedded in matrix of biotite and recrystallised quartz grains (UTM 35K, 0579482 mE, 7654974 mN).

4.1.1.8. Leucogranodiorite

The leucogranodiorite occurs extensively east and south of the Phoenix mine. The leucogranodiorite covers approximately six square kilometres. It forms chilled margin contacts with mesogabbro and dolerite (Figure 4.21). It forms transitional contact with granodiorite to the west and north of the Selkirk mine and Tekwane deposit. It is vital to study the leucogranodiorite as it bears potential link with its contact mineralised mesogabbro units. The leucogranodiorite was studied in the field and microscopically, from samples (TEK2, P14). It is greyish-white, phaneritic textured and contains approximately, 30% plagioclase, 20% quartz, 20% hornblende and 25% K-feldspar (Figure 4.22). In addition, the leucogranodiorite contains accessory minerals, which include apatite and titanite making 3% and 2% respectively.

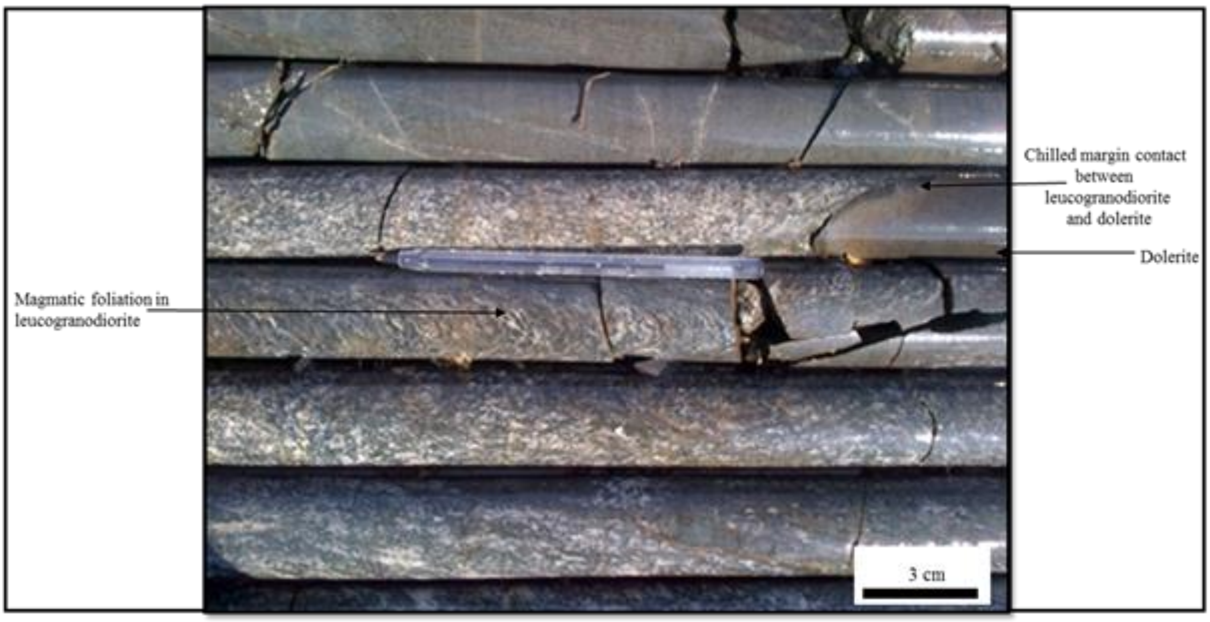

Figure 4.21: The Tekwane deposit leucogranodiorite forms a chilled margin contact with dolerite, which suggests the intrusion of the dolerite postdate the emplacement of the granodiorite, drill hole, TW27 (UTM 35K, 0580910 mE, 7645590 mN).

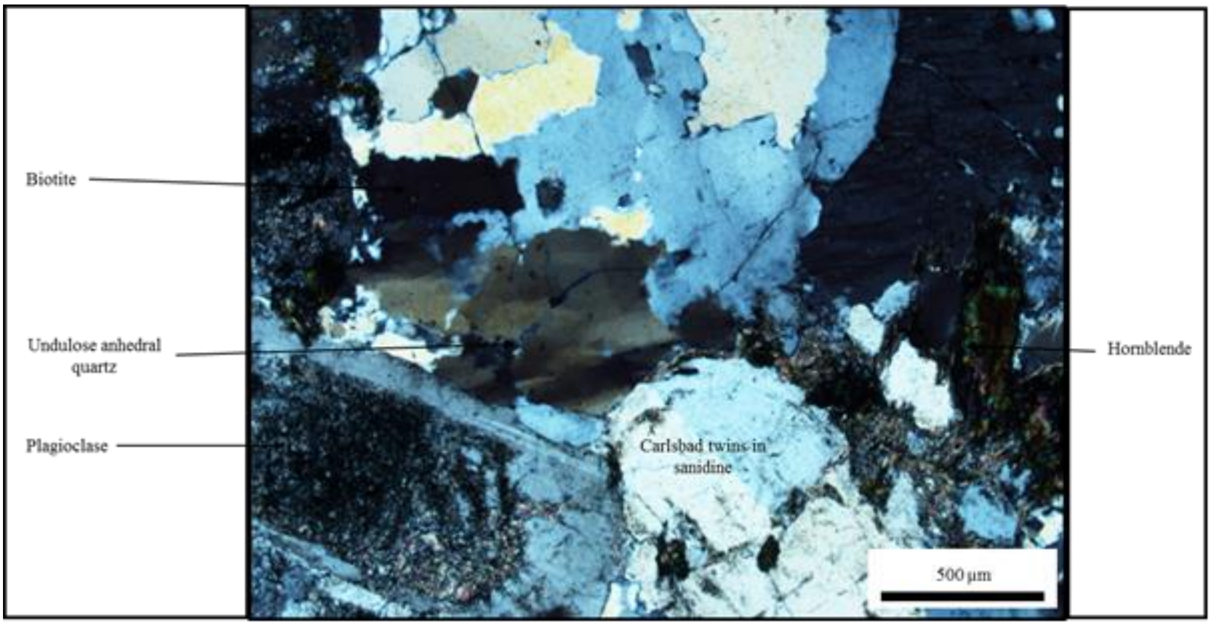

Figure 4.22: The photomicrograph (crossed polar) of sample TEK2, obtained from leucogranodiorite of the Tekwane deposit, shows quartz, hornblende and oscillatory-zoned plagioclase. The presence of zoned plagioclase indicates compositional changes due to temperature variations during magma ascent (UTM 35K, 0580910 mE, 7645590 mN).

4.1.1.9. Amphibolite

The amphibolite outcrops linearly in Rooikoppie deposit and intermittently to the northeast of the Phoenix mine. The amphibolite is medium grained and is crosscut by cherty pegmatite veins. It occurs in contact with mesogabbro in the Rooikoppie deposit though exposure is very poor, possibly due to very low outcropping levels coincident with their contacts. It is crosscut by a foliation associated with the Rooikoppie Deposit Shear Zone (RDSZ) in most localities in the Rooikoppie deposit (Figure 4.23). The amphibolite was mainly studied in the field and comprises of, on average, hornblende (75%), plagioclase (20%), quartz (5%), biotite (2%) and magnetite (3%).

Figure 4.23: The amphibolite is crosscut by a shear zone, which consists of foliation that is steeply dipping to the southeast in the Rooikoppie deposit (UTM 35K, 0589327 mE, 7648817 mN).

4.1.1.10. Dolerite

The dolerite occurs extensively as dykes and dykelets in some localities across the study area especially in the Phoenix mine where pit faces clearly show the thickness and geometry of dolerite (Figure 4.24). The dolerite dykes show thickness of between 3 metres and 50 metres. The dolerite dykes and dykelets intruded the mineralised, barren gabbro units, granodiorite units and tonalite in TSMDC. The dolerite was studied at macroscopic level in the field whereas samples (R2 and P4) provided microscopic evidence.

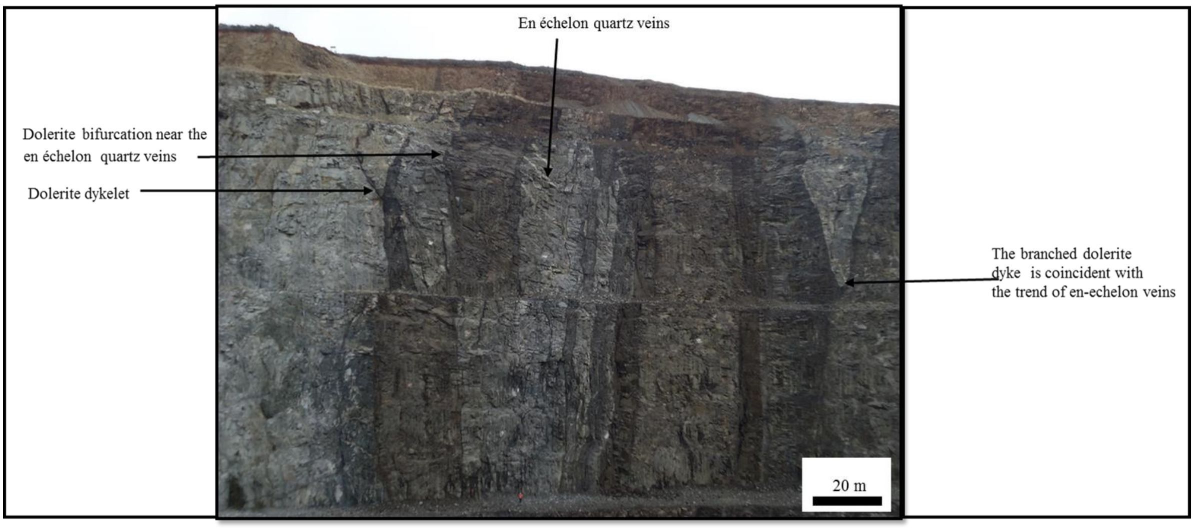

Figure 4.24: The dolerite dykes and dykelets are branched in some localities in the Phoenix mine.

Microscopically, the dolerite consists of fine groundmass made up of clinopyroxene laths and polysynthetic twinned plagioclase (Figure 4.25). It consists of, on average, 60% plagioclase, 25% clinopyroxene, 7% olivine and 8% biotite.

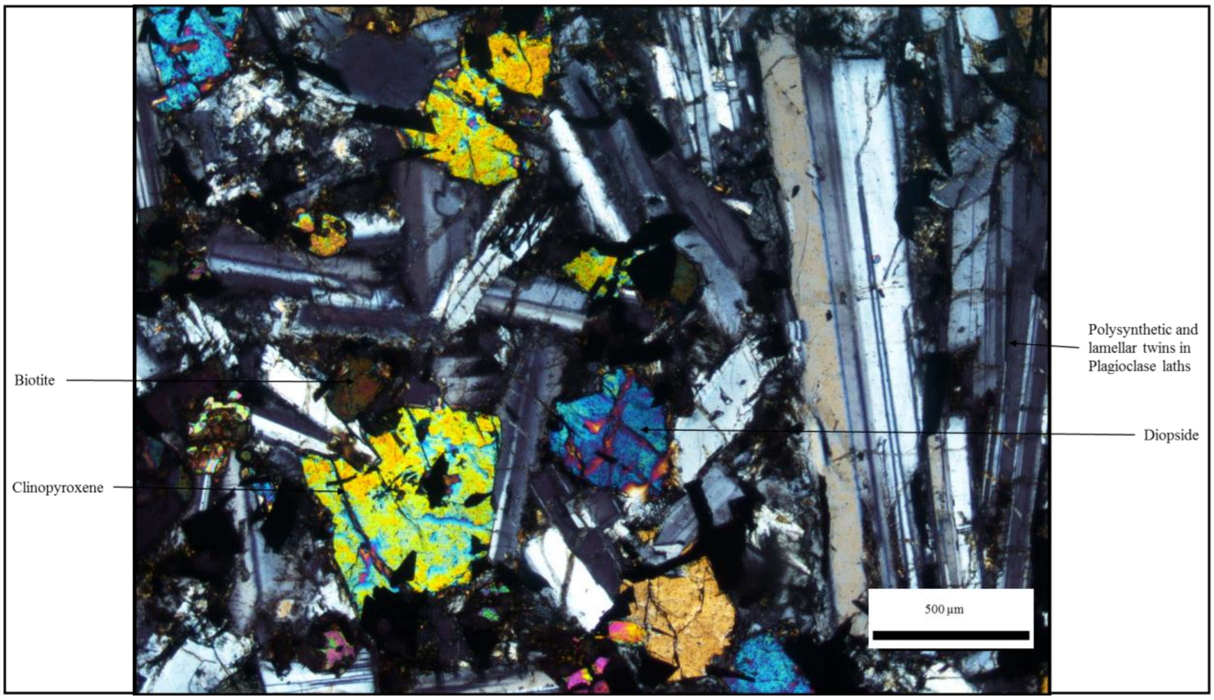

Figure 4.25: The photomicrograph of the sample R2 obtained from Rooikoppie deposit dolerite, drill hole DRKP02 shows random orientation of plagioclase, diopside and olivine. The plagioclase crystals exhibit polysynthetic albite-type twins (UTM 35K, 0589337 mE 7648811 mN).

4.1.1.11. Andesite

The andesite unit is greyish brown, medium grained and composed of porphyritic plagioclase crystals on a groundmass of hornblende, plagioclase and quartz. The andesite consists of, on average, 66% plagioclase, 6% quartz, 15% K-feldspar, 10% hornblende and 3% biotite. It occurs as isolated linear outcrops in the Rooikoppie deposit (Figure 4.26). The andesite occurs in proximity to the mesogabbro in the Rooikoppie deposit. Thus, the andesite was studied in the field and considered important as it might have contact relationship with the mesogabbro in the Rooikoppie deposit.

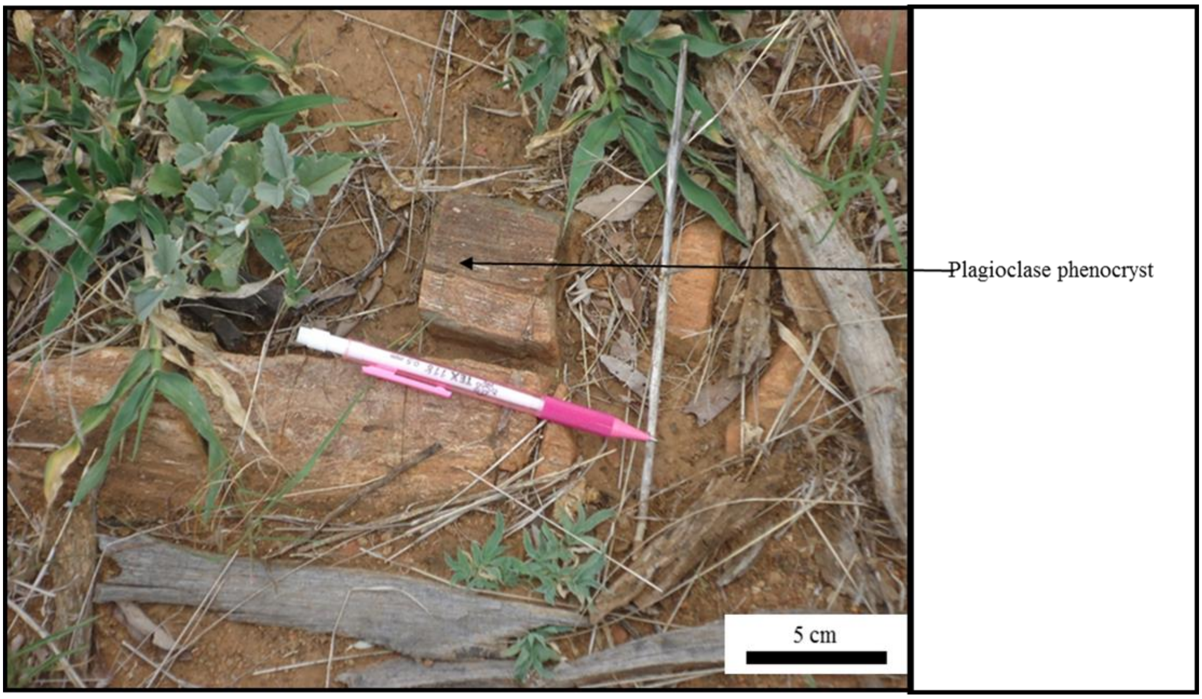

Figure 4.26: Andesite occurs as isolated and flat lying outcrops in the Rooikoppie deposit. The andesite unit is composed of plagioclase phenocryst, which trend parallel to the foliation within the Rooikoppie Deposit Shear Zone (RDSZ) (UTM 35K, 0580270 (mE), 7654112 (mN).

4.1.1.12. Basalt

The basalt occurs dominantly to the south of the Selkirk mine. It occurs sporadically as very small, randomly positioned low-lying outcrops in the Tekwane and Rooikoppie deposit. It is generally intersected in some drill holes in the Rooikoppie deposit. The basalt was studied in the field and from samples, P3 and P14. It is composed of fine-grained groundmass defined by plagioclase, clinopyroxene, orthopyroxene and quartz. The basalt exhibits aphanitic texture, with groundmass dominated by plagioclase and clinopyroxene (Figure 4.27). Microscopically, the basalt is grey-green, aphanitic textured and contains approximately 40% plagioclase, 30% clinopyroxene, 15% clinopyroxene, 10% Olivine and 5% quartz (Figure 4.28).

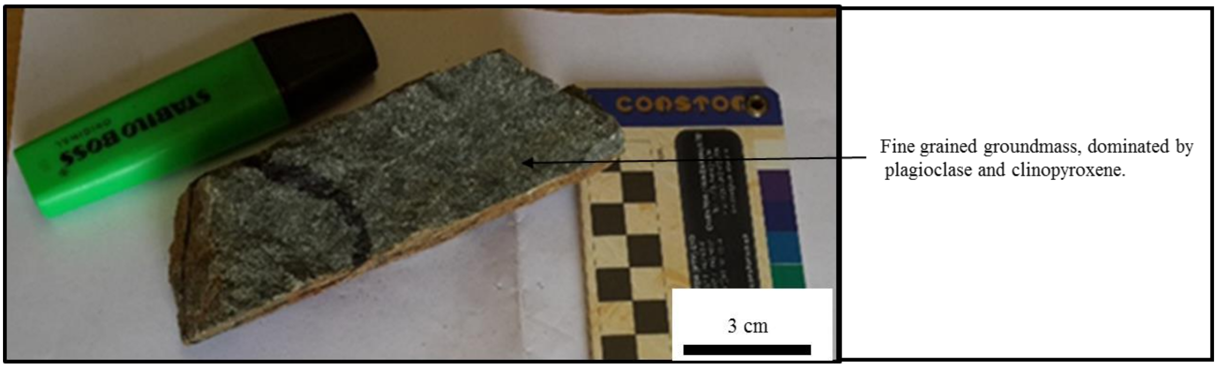

Figure 4.27: The basalt hand specimen exhibits aphanitic texture in, which, plagioclase and clinopyroxene are identifiable (UTM 35K, 0585312 (mE), 7653256 (mN).

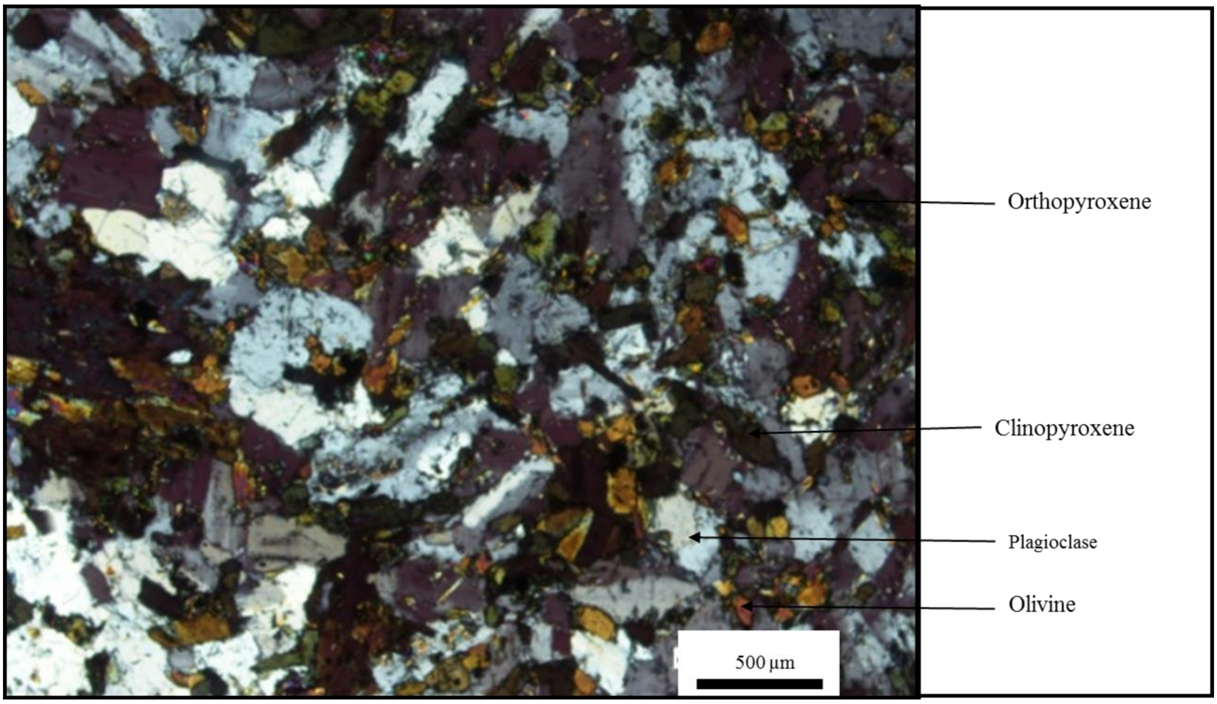

Figure 4.28: The photomicrograph of basalt (sample P3) obtained from Rooikoppie deposit showing plagioclase laths in a matrix, which composes of orthopyroxene, clinopyroxene, olivine and interstitial quartz (UTM 35K, 0585312 (mE), 7653256 (mN).

4.1.2. Metasedimentary units

The mappable metasedimentary units occur as part of the stratigraphic succession of the Rooikoppie deposit. There are few metasedimentary units recognised. These include; banded iron formation (BIF) quartzite and dolomite.

4.1.2.1. Banded Iron Formation (BIF)

The Banded Iron Formation (BIF) is reddish brown and is defined by magnetite and chert (silica rich layers) layers (Figure 4.26). The chert layers are predominantly coated with iron coloration. It occurs as isolated beds, which are aligned to the trend of the amphibolite and Rooikoppie Deposit Shear Zone. It is composed of approximately 55% quartz, 30% magnetite and 15% hematite.

Figure 4.29: The Banded Iron Formation (BIF) is composed of ironstone and quartz bands in the Rooikoppie deposit. The Banded Iron Formation beds dip steeply at an average of 82° to northeast (UTM 35K, 0589390 mE, 7648902 mN).

4.1.2.2. Quartzite

The quartzite is characterised by isolated beds, steeply dipping with an average dip of 74° to the northwest. The quartzite beds range from 200 mm up to 400mm in width (Figure 4.27). It is generally outcropping in the northwest part of the Rooikoppie deposit. It is greyish-brown and consists of well-sorted siliceous matrix with approximately 80% quartz, 15% alkali feldspar and 5% muscovite.

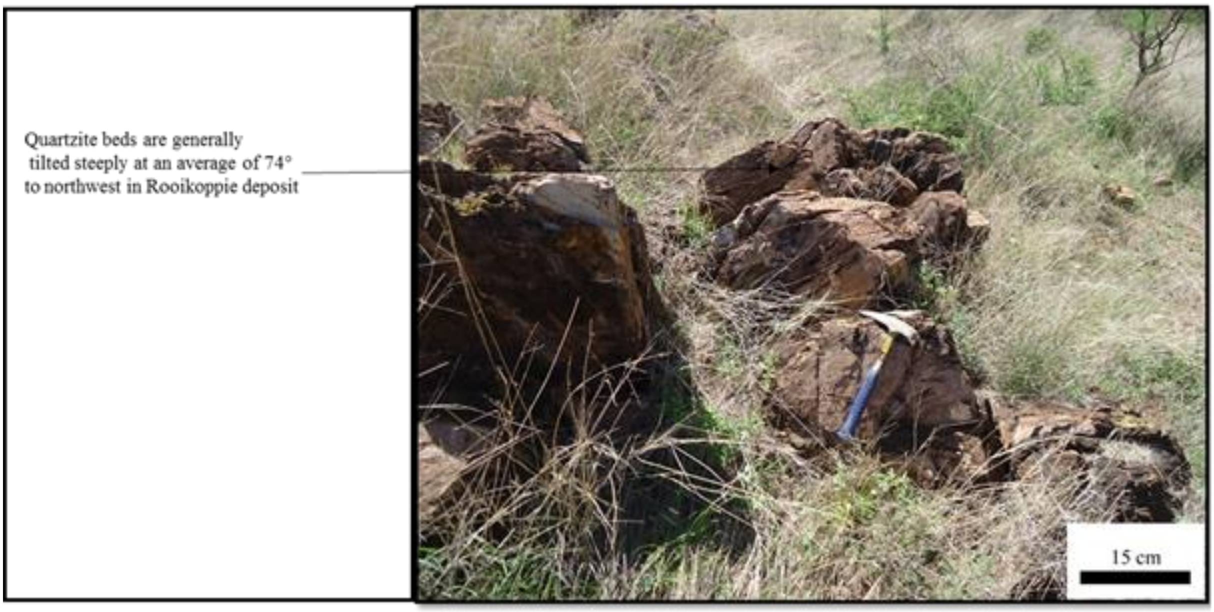

Figure 4.30: The Rooikoppie deposit is composed of quartzite outcrops, steeply dipping at an average of 74° to northwest (UTM 35K, 0588899 mE, 7648275 mN).

4.1.2.3. Dolomite

The dolomite outcrops sporadically around the Rooikoppie deposit area (Figure 4.28). It overlies the amphibolite and has a thickness of about 12 metres in drill cores. It is grey and generally characterised by thin beds. It is composed of approximately 90% calcite and 10% quartz. The calcite grains are well sorted and cemented.

Figure 4.31: The Rooikoppie deposit consists of isolated and shallow dipping dolomite outcrops, with shallow dips ranging from 24° to 27° to northeast (UTM 35K, 0588914 mE, 7648257 mN).

4.2. Sulphide mineralisation

A total of 16 samples from TSMDC were collected to study the sulphide ore geology. Different metagabbroic units host the Ni-Cu-PGEs sulphide mineralisation in TSMDC. Petrographically, the Ni-Cu-PGEs sulphide mineralisation is concentrated as blebby disseminations and veins in mesogabbro and leucogabbro in the Phoenix mine. Locally, remobilised sulphide mineralisation occurs in the granodiorite intrusive contact with the mesogabbro and leucogabbro in the Phoenix mine. The Phoenix mine melanogabbro does not consists of sulphide mineralisation. However, it is difficult to explain the deficiency in sulphide mineralisation in the melanogabbro, possibly due to lack of petrographic evidence.

The sulphide mineralisation is hosted by mesogabbro and melanogabbro in the Selkirk mine and Tekwane deposit. The Selkirk mine leucogabbro does not contain sulphide mineralisation. The pyrrhotite, pentlandite, chalcopyrite and pyrite are the most common ore assemblages. The pentlandite, $(Fe, Ni)_9S_8$ occurs in massive blebs of approximately 700 µm. and consists of randomly oriented flakes in the Phoenix mine mesogabbro (Figure 4.29a). The pyrrhotite (Fe_1-xS) occurs throughout the ore assemblage of the mineralised metagabbroic units in the Phoenix, Selkirk mines, Tekwane and Rooikoppie deposits. It occurs as brownish fine, medium and coarse-grained blebs and globules in the Selkirk mine mesogabbro (Figure 4.29b). The pyrrhotite is highly distributed in the ore mineralogy contained within Tekwane deposit melanogabbro (Figure 4.30a). The chalcopyrite ($CuFeS_2$) is yellow and occurs in massive and stringers form in the Phoenix and Selkirk mine sulphide ores. It occurs in stringer form in the massive sulphide ores of Rooikoppie deposit. Pyrite (FeS_2) occurs as euhedral blebs. It occurs abundantly interstitial with galena in the Rooikoppie deposit sulphide mineralisation. Goethite (FeO (OH)) occurs sporadically and show grey–blue aggregates (Figure 4.30b). Bornite (Cu_5FeS_4) occurs as small inclusions of less 10 µm in diameter.

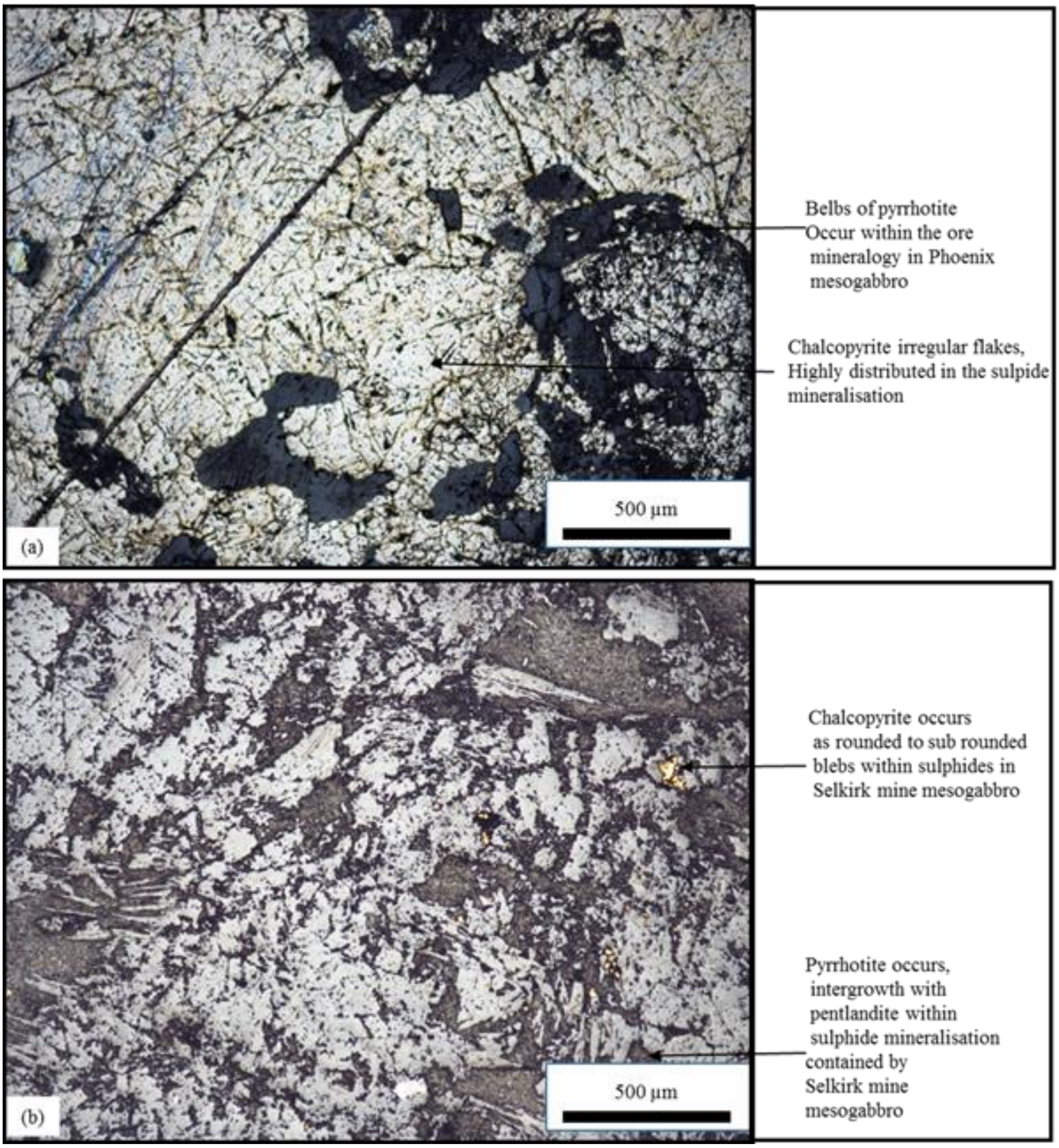

Figure 4.32: Photomicrographs of sulphides contained in (a). Phoenix mine mesogabbro, (b) Selkirk mine mine mesogabbro. Pyrrhotite and chalcopyrite dominate the ore assemblages in Phoenix mine mesogabbro. There are intergrowths of pyrrhotite and chalcopyrite within sulphide mineralisation within Selkirk mine mesogabbro.

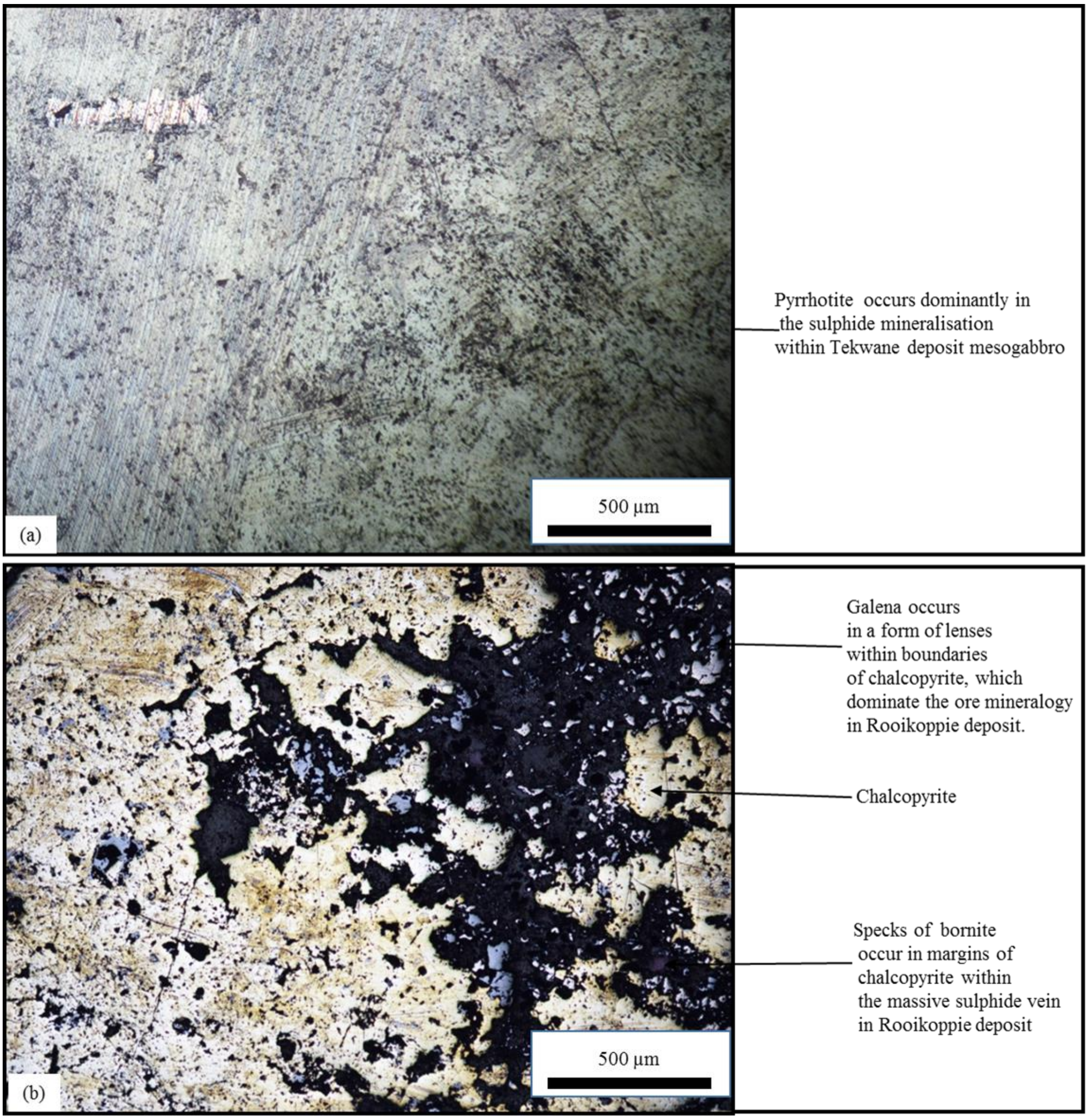

Figure 4.33: Photomicrographs of sulphides contained in (a). Tekwane deposit melanogabbro, (b) Rooikoppie deposit massive sulphide vein. Pyrrhotite occurs abundantly within the sulphide mineralisation contained in Tekwane deposit melanogabbro whereas abundant inclusions of goethite and bornite appear on the margins of the pyrrhotite and chalcopyrite in the Rooikoppie deposit massive sulphide ore. Galena occurs as grey-blue aggregates in the Rooikoppie massive sulphide ore.

CHAPTER 5.0: WHOLE-ROCK GEOCHEMISTRY

5.1. Introduction

Thirty-five (35) representative samples were selected from Phoenix, Selkirk mines and Tekwane, Rooikoppie sulphide deposits magmatic and sedimentary units. The representative samples were analysed for both major and trace elements composition. It is important to have obtained unaltered samples to have true reflection of the major and trace elements contents. Irrespective of these secondary processes mentioned above, steps were taken for consideration when selecting the samples. Though some samples still show high loss on ignition (LOI), which exceed 5 wt. % and this may be indicative of hydrothermal alteration effects. This is consistent with conspicuous chloritisation of amphibole in some sampled gabbro units. The sampled units are classified based on the ferromagnesian mineral contents and geographic locations. This chapter presents the major, minor and rare earth elements geochemical characteristics and classification of the gabbro units, granitoids and metasedimentary units. It is vital to determine geochemical processes, which influenced sulphide mineralisation content in the host gabbro units.

5.2. Major Elements Characterisation and statistical distribution

The analysed samples contain major elements of different concentrations, which illustrate different geochemical characteristics. The major elements include SiO_2, Al_2O_3, Fe_2O_3, FeO, MnO, MgO, CaO, Na_2O, K_2O, TiO_2, P_2O_5, Cr_2O_3, NiO. Table 5.1 contains the analytical data explained below. With reference to Table 5.1, the mineralised leucogabbro (sample S1) and mesogabbro (samples, S10 and N1) units in the Phoenix mine exhibit low MgO contents, which range from 0.49 wt. % to 4.38 wt. % (Table 5.1). Contrary, the unmineralised melanogabbro units (samples, NW1 and W8) are characterised by variable MgO content, which ranges from 4.26 wt. % to 17.63 wt. % (Table 5.1).

Table 5.1: Major element oxides composition of gabbro units in the Phoenix, Selkirk mines, and Tekwane sulphide deposits in east Botswana. The Selkirk mine consists of leucogabbro and mesogabbro, which display MgO contents ranging slightly from 4.83 % to 11.81%.

Major element.wt. (%)	PHOENIX MINE							SELKIRK MINE		
	Mesogabbro (N1)	Melanogabbro (NW1)	Mesogabbro (S10)	Tonalite (W1)	Melanogabbro (W8)	Porphyritic granodiorite (W3)	Mesogabbro (S1)	Mesogabbro (S5)	leucogabbro (SL09)	Granodiorite (SL06)
	N1	NW1	S10	W1	W8	W3	S1	SL 5	SL09	SL06
SiO_2	47.29	46.27	27.06	64.37	61.60	68.74	45.75	46.70	46.64	61.67
Al_2O_3	20.00	16.73	11.05	17.58	16.77	17.03	20.74	18.28	26.00	15.06
Fe_2O_3	1.24	0.94	4.98	0.48	0.62	0.29	0.79	0.88	0.59	0.62
FeO	10.03	7.64	40.33	3.88	5.04	2.35	6.39	7.11	4.80	5.04
MnO	0.03	0.13	0.10	0.06	0.09	0.04	0.11	0.13	0.09	0.07
MgO	0.49	17.63	4.38	1.42	4.26	1.3	12.79	11.81	4.83	3.92
CaO	6.85	9.88	2.53	6.03	7.40	3.88	11.21	11.98	14.32	8.21
Na_2O	4.62	1.01	1.90	4.26	3.31	5.03	1.39	1.10	1.53	3.27
K_2O	0.87	0.11	0.55	0.81	0.78	1	0.17	0.12	0.03	0.18
TiO_2	0.30	0.18	0.19	0.7285	0.60	0.3567	0.1697	0.24	0.31	1.10
P_2O_5	0.02	0.03	0.09	0.18	0.12	0.1	0.02	0.03	0.03	0.37
Cr_2O_3	0.00	0.08	0.05	0.0071	0.02	0.0067	0.0498	0.17	1.04	0.03
NiO	0.59	0.09	6.06	0.0022	0.01	0.0023	0.2526	0.22	0.03	0.01
TOTAL	92.32	100.72	99.28	99.81	100.62	100.13	99.83	98.76	100.25	99.56
LOI	4.71	4.06	10.07	1.06	1.28	1.45	4.18	6.50	4.65	3.91

The mineralised leucogabbro (sample S1) and mesogabbro units (samples, S10 and N1) in the Phoenix mine show moderate compositional content of Al_2O_3 (11.05 wt. % - 20.00 wt. %) and CaO (2.5 wt. % -9.88 wt. %), while the unmineralised melanogabbro units (samples, NW1 and W8) show restricted compositional variation of Al_2O_3 (16.73 wt. % - 16.77 wt. %) and CaO (7.40 wt. % - 9.88 wt. %). The FeO_{total} content in the mineralised leucogabbro (sample S1) and mesogabbro units (samples, S10 and N1) varies considerably from 10.03 wt.% to 40.33 wt. % while it only displays narrow variation in the unmineralised melanogabbro units (5.04 to 7.64 wt. %) in the Phoenix mine. In terms of the NiO content, there is no distinctive variation between the mineralised and unmineralised melanogabbro and mesogabbro units. The unmineralised and mineralised melanogabbro and mesogabbro units show overlapping NiO concentrations of between 0.01 wt. % and 6.06 wt. % in the Phoenix mine. The mineralised mesogabbro (samples, N1 and S10) in Phoenix mine shows low to medium SiO_2 content ranging from 27.06 wt. % to 47.29 wt.%. Despite the compositional differences between the mineralised leucogabbro and unmineralised melanogabbro highlighted above, their SiO_2 contents are similar and both vary narrowly between 46.27 wt. % and 47.29 wt. %.

In Selkirk mine, the mineralised mesogabbro (sample SL 5) is characterised by high MgO content (11.81 wt. %) in contrast to the unmineralised leucogabbro (sample SL 09), which contains low MgO content (4.83 wt. %). In terms of the Al_2O_3 content, both mineralised and unmineralised mesogabbro units exhibit high overlapping values that range between 18.28 and 26.00 wt. %. The CaO content ranges narrowly from 11.98 wt. % to 14.32 wt. % for both mineralised and unmineralised mesogabbro units. The mineralised mesogabbro unit (sample SL5) in the Selkirk mine is characterised by higher FeO content (7.11 wt. %) than unmineralised leucogabbro unit (4.80 wt. %) (Sample SL09). Additionally, the mineralised mesogabbro recorded higher NiO content 0.22 wt. % than the unmineralised leucogabbro. The SiO_2 content of both mineralised and unmineralised mesogabbro units is invariable in the Selkirk mine.

The relationship between K_2O and Na_2O is positive for Phoenix, Selkirk and Tekwane gabbro units, which is mostly associated with the sodic field (Figure 5.1a). The relationship between SiO_2 and MgO is defined by negative trend, which indicates that increase in SiO_2 correlates to decrease in MgO content (Figure 5.1b). The plot between Na_2O and MgO shows negative trend, typical of inverse relationship of the contents of Na_2O and MgO in gabbro and mafic units in TSMDC (Figure 5.1c).

The Phoenix, Selkirk mines and Rooikoppie deposit gabbro units plot in the tholeiitic field in the FeO_{total}-Na_2O+K_2O-MgO ternary diagram (Figure 5.2). In contrary, the Tekwane deposit mesogabbro and melanogabbro straddle the tholeiitic-calc-alkaline boundary. The unmineralised mesogabbro (sample R012) in the Rooikoppie deposit shows slightly higher MgO content (5.35 wt. %) (Table 5.2) than unmineralised leucogabbro (4.83 wt. %) (Sample SL09) in the Selkirk mine (Table 5.1). The massive sulphide bodies represented by samples, R1 and R4 in the Rooikoppie deposit are characteristic of high FeO content (58 wt. % to 63 wt. %) (Table 5.2).

The unmineralised mesogabbro unit (sample R012) in the Rooikoppie deposit exhibit NiO content similar to the unmineralised leucogabbro of the Selkirk mine. The unmineralised mesogabbro unit (sample R012) in the Rooikoppie deposit display wide MgO compositional range (3.52 to 10.42 wt. %; Table 5.2). The correlation between FeO_{total} and MgO is positive for both mineralised mesogabbro and unmineralised melanogabbro units of Phoenix mine

(Figure 5.3a). The mineralised mesogabbro units in the Tekwane deposit display moderate correlation between MgO and FeO_{total} (Figure 5.3a).

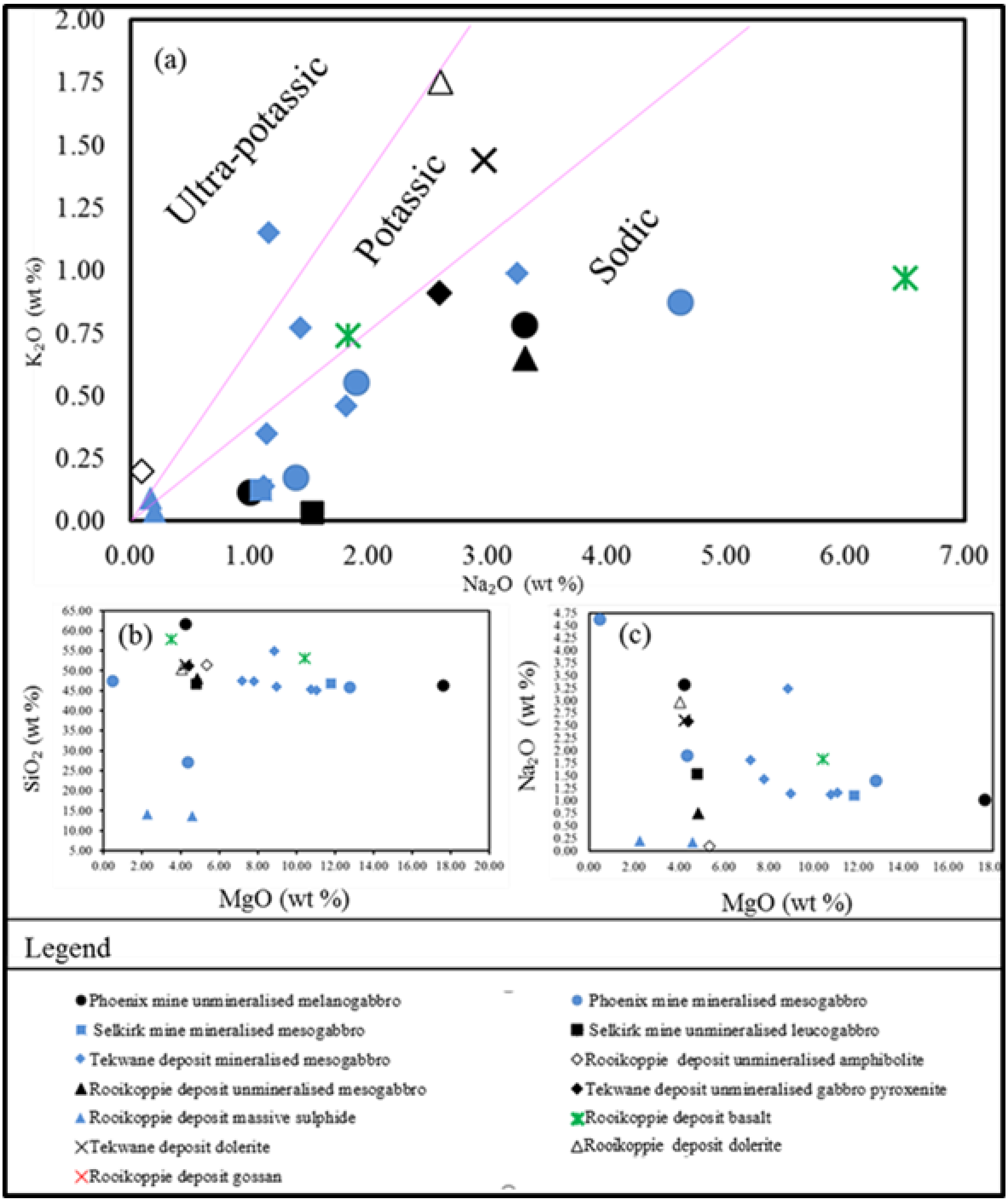

Figure 5.1: (a) The bi-variant plots for K_2O against Na_2O, (b) SiO_2 against MgO and (c) Na_2O against MgO for mineralised, unmineralised leucogabbro, mesogabbro, melanogabbro

and dolerite units in the Phoenix, Selkirk mines, Tekwane and Rooikoppie deposits. The gabbro units in the Phoenix and Selkirk mines belong to sodic field whereas the mineralised, unmineralised gabbro and dolerite units in the Tekwane and Rooikoppie deposits belong to both potassic and sodic fields.

The mineralised mesogabbro (sample SL 5) and unmineralised leucogabbro (sample SL 09) units in the Selkirk mine are characterised by positive correlation between FeO_{total} and MgO (Figure 5.3a). Similarly, the mineralised mesogabbro units (samples, S10 and N1) in the Phoenix mine, a positive correlation exists between MgO and Cr_2O_3 for mineralised and unmineralised leucogabbro and mesogabbro units in the Selkirk mine (Figure 5.3b).

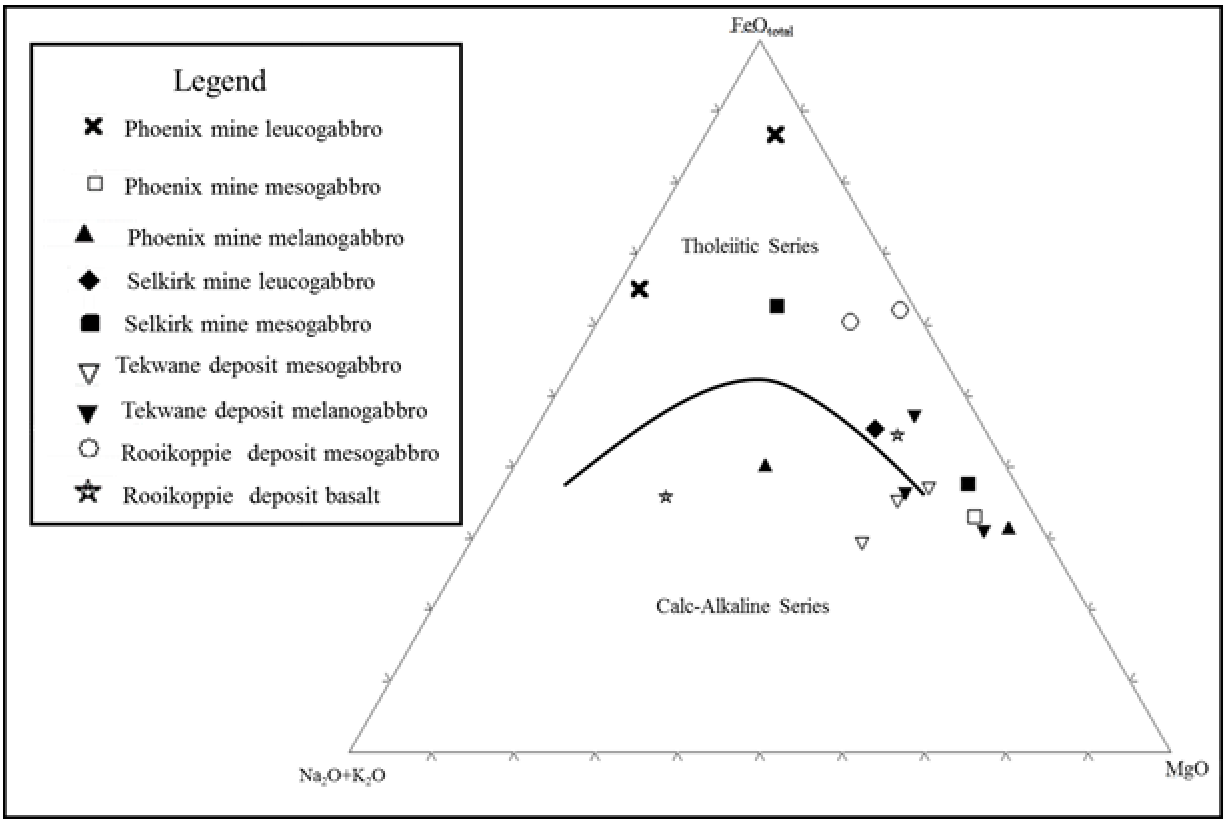

Figure 5.2: The ternary plot of FeO_{total}-Na2O+K2O-MgO (after Irvine and Baragar, 1971) shows Phoenix mine melanogabbro belong to the tholeiitic series. The Tekwane deposit melanogabbro and mesogabbro are generally clustered though showing affinity to both tholeiitic and calc-alkaline fields.

In the Tekwane deposit, both the mineralised mesogabbro units display closely distributed data with a positive correlation between MgO and Cr_2O_3 contents (Figure 5.3b). A positive correlation is noticeable between MgO and CaO for both mineralised mesogabbro and unmineralised melanogabbro units in the Phoenix mine (Figure 5.3c).

Table 5.2: Major elements oxides composition of gabbro, dolerite, basalt units and massive sulphides in the Rooikoppie deposit in east Botswana. The Rooikoppie deposit comprises of gossan, which exhibits high content of FeO (76.03 wt. %) as represented by sample R9.

	ROOIKOPPIE DEPOSIT									
Major element.wt. (%)	Basalt (P3)	Dolerite (P4)	Pyroxenite gabbro (P12)	Basalt (PIN014)	Massive sulphide (R 1)	Dolerite (R 2)	Massive sulphide (R 4)	Gossan (R9)	Mesogabbro (R11)	Mesogabbro (R012)
SiO_2	53.13	51.46	51.14	57.85	14.14	50.36	13.71	10.73	51.46	48.06
Al_2O_3	12.29	15.2	13.86	17.37	0.58	17.01	2.14	0.78	12.54	16.10
Fe_2O_3	1.16	1.25	1.48	0.68	7.22	1.18	7.82	9.39	1.03	1.06
FeO total	9.39	10.15	11.97	5.51	58.44	9.55	63.3	76.03	8.32	8.60
MnO	0.18	0.15	0.19	0.11	1.34	0.15	2.4	0.13	0.36	0.26
MgO	10.42	4.24	4.4	3.52	2.26	4.05	4.6	0.06	5.35	4.86
CaO	10.25	9.27	9.33	6.35	11.37	9.48	4.09	0.20	19.38	18.80
Na_2O	1.83	2.6	2.59	6.50	-0.2	2.97	0.17	0.22	0.09	0.75
K_2O	0.74	1.75	0.91	0.97	0.04	1.44	0.09	0.03	0.20	0.65
TiO_2	0.80	3.33	3.69	0.81	0.0449	3.47	0.099	0.08	0.63	0.72
P_2O_5	0.06	0.60	0.46	0.42	0.03	0.54	0.03	0.09	0.07	0.10
Cr_2O_3	0.10	0.02	0.02	0.01	0.0231	0.02	0.0266	0.03	0.10	0.06
NiO	0.03	0.01	0.01	0.01	0.0247	0.01	0.0201	0.02	0.03	0.02
TOTAL	100.38	100.03	100.05	100.12	95.31	100.23	98.15	97.34	99.55	100.04
LOI	2.09	1.73	1.35	1.00	11.3	1.32	11.49	12.69	2.05	2.01

Furthermore, both the mineralised mesogabbro and unmineralised melanogabbro units of Phoeniix mine display positive correlation of MgO and Al_2O_3 contents similar to mesogabbro and leucogabbro units in the Selkirk mine (Figure 5.3d). Likewise, Al_2O_3 and contents within the mineralised mesogabbro units in the Tekwane deposit display positive correlation against MgO content (Figure 5.3d). Similarly, the MgO content of mineralised mesogabbro units (samples, S10 and N1), correlate positively with TiO_2 in the Phoenix mine

(Figure 5.3e). The Phoenix, Selkirk mine and Tekwane deposit mesogabbro units show positive correlation between MgO and NiO (Figure 5.3f).

The Phoenix mine tonalite (sample W1), porphyritic granodiorite (sample, W3) Selkirk mine porphyritic granodiorite (sample SL06), Rooikoppie deposit granodiorite (samples, PIN011, PIN012, PIN013 and PIN015) and Tekwane deposit leucogranodiorite and quartz diorite (samples, TEK2 and TEK5) contain SiO_2 contents, which vary widely from 45.75 wt. % to 74.37 wt. % (Table 5.3). The Tekwane deposit leucogranodiorite and quartz diorite (samples, TEK2 and TEK5) exhibit higher SiO_2 content than those of Phoenix, Selkirk mines and Rooikoppie deposit.

Table 5.3: Major element oxides composition of tonalite, granodioritic units, dolomite and quartzite in the Phoenix, Selkirk mines, Tekwane deposit. The Tekwane deposit leucogranodiorite (sample TEK2) contains high content of SiO_2 of 74.37 %.

	PHOENIX MINE		SELKIRK MINE	TEKWANE DEPOSIT	
Major oxides (wt. (%)	Tonalite (W1)	Porphyritic granodiorite (W3)	Porphyritic granodiorite (SL06)	Leucogranodiorite (TEK2)	Quartz diorite (TEK5)
SiO_2	64.37	68.74	61.67	74.37	69.75
Al_2O_3	17.58	17.03	15.06	14.28	15.80
Fe_2O_3	0.48	0.29	0.62	0.15	0.28
FeO total	3.88	2.35	5.04	1.20	2.30
MnO	0.06	0.04	0.07	0.02	0.04
MgO	1.42	1.3	3.92	0.51	1.08
CaO	6.03	3.88	8.21	2.04	3.33
Na_2O	4.26	5.03	3.27	4.06	4.62
K_2O	0.81	1	0.18	2.84	2.03
TiO_2	0.7285	0.3567	1.10	0.17	0.36
P_2O_5	0.18	0.1	0.37	0.05	0.10
Cr_2O_3	0.0071	0.0067	0.03	0.00	0.00
NiO	0.0022	0.0023	0.01	0.02	0.00
TOTAL	99.81	100.13	99.56	99.73	99.69
LOI	1.06	1.45	3.91	0.80	1.47

The Al_2O_3 contents of the tonalite (sample W1), granodiorite (samples, PIN011, PIN012, PIN013 and PIN015), leucogranodiorite (PIN2, TEK2, TEK5) and porphyritic granodiorite (W3, SL06) within the Phoenix, Selkirk mines, Tekwane and Rooikoppie deposits vary between 14 and 20.5 wt.%. The FeO and MgO contents in the same units vary from 1.28 wt. % to 6.39 wt. % and 9.50 wt. % to 1.42 wt. %, respectively.

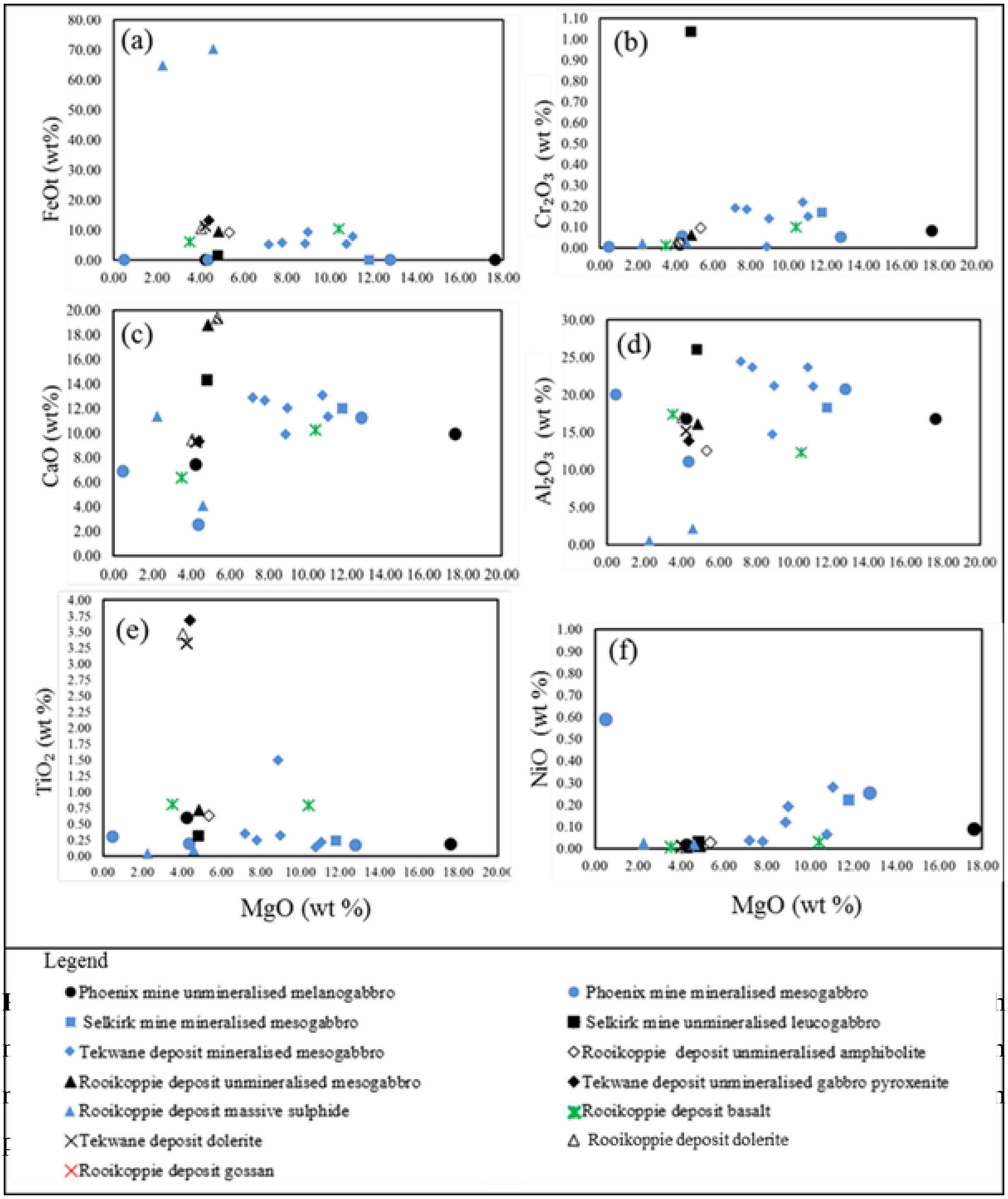

The granodiorite and tonalite units are characterised by negative correlation between MgO and SiO_2 contents in all the five areas (Phoenix, Selkirk mines, Tekwane, and

Rooikoppie deposits) (Figure 5.4a). MgO, FeO and CaO contents of the granodiorite and tonalite units in all the areas display a significant negative correlation with increasing SiO_2 content. Na_2O content of the granitoids display a good positive correlation versus the SiO_2 content. The FeO_{total} and CaO contents of the granodiorite exhibit negative trend with increasing SiO_2 content (Figure 5.4b and 5.4c). The relationship between Al_2O_3 and SiO_2 contents in granodiorite units is generally erratic with no well-defined trend in TSMDC (Figure 5.4d). The Na_2O and K_2O contents display positive correlation against SiO_2 (Figure 5.4e and 5.4f).

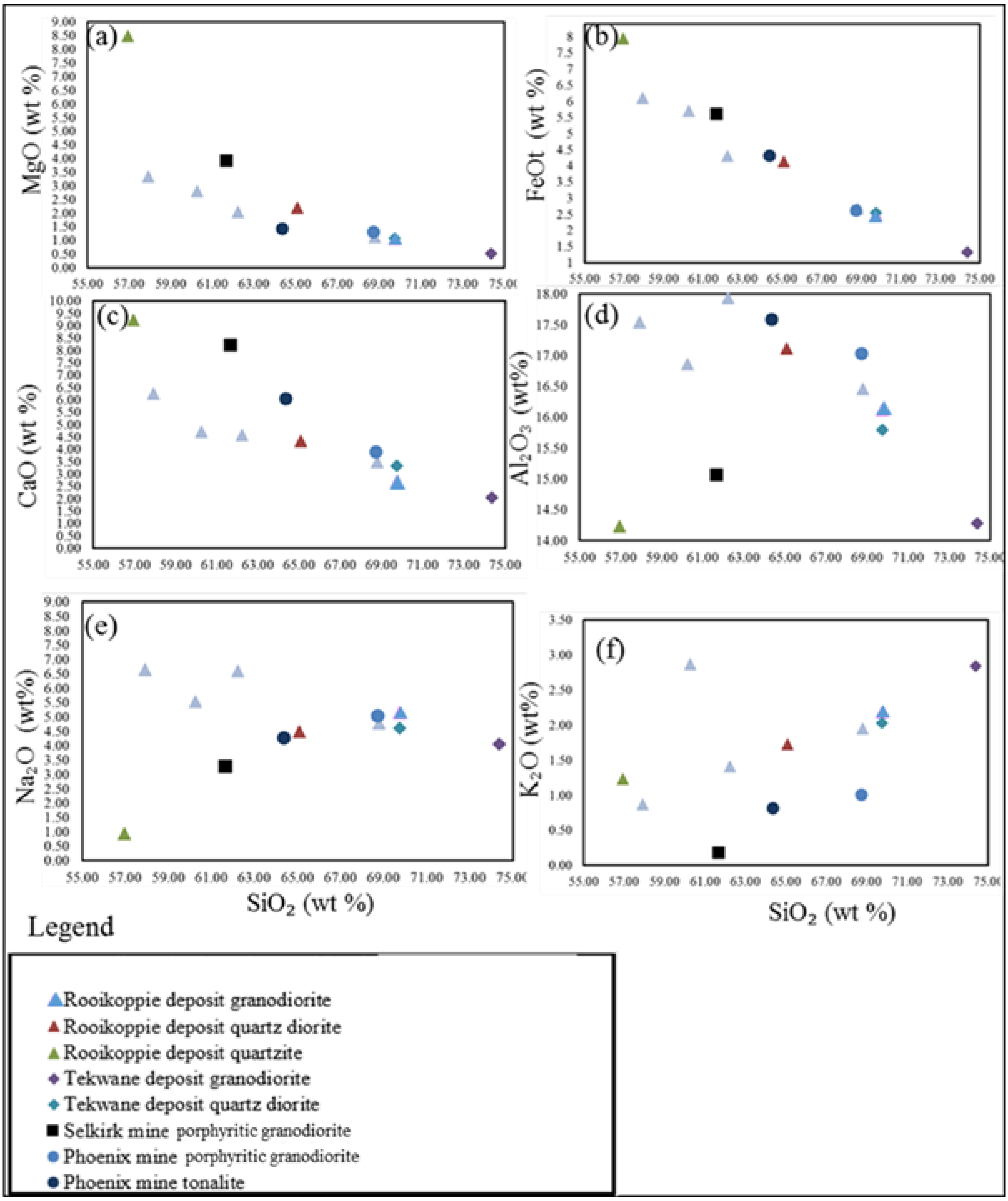

Figure: 5.4: The Harker variation diagrams plots showing inverse relationship between the differentiation index, SiO_2 against (a), (a) MgO, (b) Fe_2O_3, (c) CaO, (d) Al_2O_3 contents in Phoenix, Selkirk mines, Tekwane, Rooikoppie deposits granodioritic units. The SiO_2 content correlates positively with Na_2O (e) and K_2O (f) indicative of both increase in SiO_2 and Na_2O.

However, Na_2O against SiO_2 plot shows inverse relationship between Rooikoppie and Tekwane deposit granodiorite.The quartz diorite (sample R7) exhibits CaO content that vary slightly as compared to the granodiorite (samples, PIN011, PIN012, PIN013, PIN015) in the Rooikoppie deposit (Table 5.4).

Table 5.4: The major elements oxide contents of the Rooikoppie deposit granodiorite, dolomite and diorite units. The SiO_2 contents of the granodiorite, dolomite and diorite units vary from 57.92 wt. (%) to 69.75 wt. (%) in the Rooikoppie deposit.

	ROOIKOPPIE DEPOSIT						
Major oxides (wt. %)	Granodiorite (P2)	Granodiorite (PIN011)	Granodiorite (PIN012)	Granodiorite (PIN013)	Granodiorite (PIN015)	Quartzite (R011)	Quartz diorite (R7)
SiO_2	69.75	62.23	60.25	57.92	68.79	56.94	65.08
Al_2O_3	16.12	17.94	16.86	17.54	16.46	14.23	17.12
Fe_2O_3	0.28	0.48	0.63	0.68	0.30	0.88	0.46
FeO total	2.24	3.87	5.13	5.49	2.41	7.16	3.72
MnO	0.05	0.11	0.10	0.11	0.04	0.21	0.08
MgO	1.04	2.04	2.81	3.34	1.13	8.49	2.19
CaO	2.68	4.57	4.72	6.25	3.50	9.23	4.34
Na_2O	5.16	6.60	5.54	6.66	4.78	0.94	4.49
K_2O	2.18	1.41	2.87	0.87	1.95	1.23	1.73
TiO_2	0.34	0.53	0.69	0.82	0.38	0.69	0.57
P_2O_5	0.14	0.24	0.33	0.42	0.13	0.16	0.17
Cr_2O_3	0.00	0.00	0.01	0.01	0.00	0.07	0.01
NiO	0.00	0.01	0.00	0.01	0.01	0.04	0.00
TOTAL	99.98	100.03	99.96	100.12	99.88	100.27	99.96
LOI	1.65	1.08	0.81	0.91	0.97	1.63	1.62

The granodiorite (samples, PIN011, PIN012, PIN013 and PIN015) in the Rooikoppie deposit show CaO contents that vary slightly similarly to the Phoenix mine tonalite (sample W1) and porphyritic granodiorite (sample W3). The dolomite (sample R12) within the Rooikoppie deposit exhibits highest CaO content of 9.53 wt. %.

5.3. Trace Elements Characterisation and statistical distribution

The Phoenix mine mineralised mesogabbro units (samples, S10 and N1) contain high Ni concentration, which varies widely from 5,919.79 ppm to 46,336.58 ppm (Table 5.5). In contrast, to the mineralised mesogabbro units (Samples, S10, N1 and SL 5) and the unmineralised melanogabbro units (Samples, NW1 and W8) from Phoenix and Selkirk mines contain low Ni concentration, which ranges from 87.09 ppm to 661.74 ppm. Moreover, the mineralised mesogabbro units exhibit wide variation in Cu concentration, which ranges from 1,068 ppm to 56,607.49 ppm.

Table 5.5: The XRF analysis show high Ni contents, which range from 87.09 ppm to 46 336.58 ppm in melanogabbro, mesogabbro and leucogabbro units in the Phoenix, Selkirk mines and Tekwane deposit.

Trace element (ppm)	PHOENIX DEPOSIT				SELKIRK DEPOSIT		TEKWANE DEPOSIT					
	Mesogabbro (N1)	Melanogabbro (NW1)	Mesogabbro (S10)	Melanogabbro (W8)	Mesogabbro (SL 5)	Leucogabbro (SL09)	Mesogabbro (TEK1)	Mesogabbro (TEK3)	Mesogabbro (TEK4)	Mesogabbro (TEK7)	Mesogabbro (TEK8)	Mesogabbro (TEK9)
Sc	11.18	19.27	12.74	18.68	16.61	17.77	41.62	20.65	19.78	26.33	15.03	17.22
V	2.20	63.18	70.01	106.61	72.44	153.85	290.58	70.09	116.56	118.96	92.85	57.85
Cr	9.18	420.15	424.84	60.34	1,141.43	7,133.95	3.54	929.09	1211.68	885.85	1122.66	1274.98
Co	148.52	78.92	1,176.50	21.42	74.45	25.19	43.08	81.5	34.47	107.72	40.85	46.96
Ni	5,919.79	661.74	46,336.58	87.09	1,447.14	220.88	925.07	2104.78	270.49	1317.4	256.63	460.1
Cu	56,607.49	49.17	1,068.48	31.85	1,043.01	32.24	46.66	1670.42	0,00	1085.87	11.51	14.82
Zn	110.66	53.83	60.41	54.66	79.35	49.50	55.88	83.54	54.11	65.43	52.26	48.83
Ga	15.68	10.52	27.63	16.36	9.39	15.73	20.32	11.89	13.83	13.81	14.34	13.17
Rb	29.30	4.76	31.32	28.05	3.46	2.12	38.06	52.49	19.58	15.85	41.69	7.95
Sr	173.37	57.82	50.77	199.27	101.15	122.58	172.12	123.99	139.46	94.52	144.27	94.3
Y	13.83	5.58	1.58	15.56	4.46	7.36	16.58	5.77	6.37	7.13	6.19	2.9
Zr	136.63	7.80	22.66	107.78	10.06	11.57	185.64	13.7	15.48	12.34	11.57	8.1
Nb	10.51	1.31	32.06	5.16	0.00	0.92	6.68	1.85	2.14	1.12	2.74	1.69
Mo	1.77	0.00	17.52	1.76	0.00	0.00	0.37	0.68	26.32	0.46	1.33	6.89
Ba	118.58	5.50	51.68	240.78	27.22	4.07	127.68	130.57	35.55	19.24	35.14	3.62
Pb	22.14	3.60	7.25	11.02	8.13	13.37	10.34	5.91	4.51	5.27	5.96	0.91
Th	46.70	5.34	0.00	3.73	0.00	0.00	0.00	0.00	0.00	0.00	1.5	2.64
U	11.82	0.00	0.00	0.00	0.00	0.00	0.00	0.00	0.00	0.00	0.00	0.00

The mineralised mesogabbro contains higher Ni concentration (1,447.14 ppm) than the unmineralised phenocrystic leucogabbro (220.88 ppm) in the Selkirk mine. In addition, the mineralised mesogabbro in the Selkirk mine contains relatively low Cu concentration (1043.01 ppm) when compared to the mineralised mesogabbro units in the Phoenix mine, which has high abundance of Cu (1068 ppm). The mineralised leucogabbro and mesogabbro units in the Phoenix mine are characterised by positive correlation between Ni and Cu concentrations (Figures 5.4 and 5.5). The mesogabbro units in the Tekwane deposit (samples, TEK1, TEK3, TEK6, TEK7 and TEK8) are characterised by high and variable abundances of Ni that range from 256.63 ppm to 2104.80 ppm (Table 5.5). However, they exhibit lower Cu concentration than the mesogabbro units in the Phoenix mine. Co concentration of the mesogabbro units in the Tekwane deposit is lower than that of the mesogabbro units in the Phoenix mine.

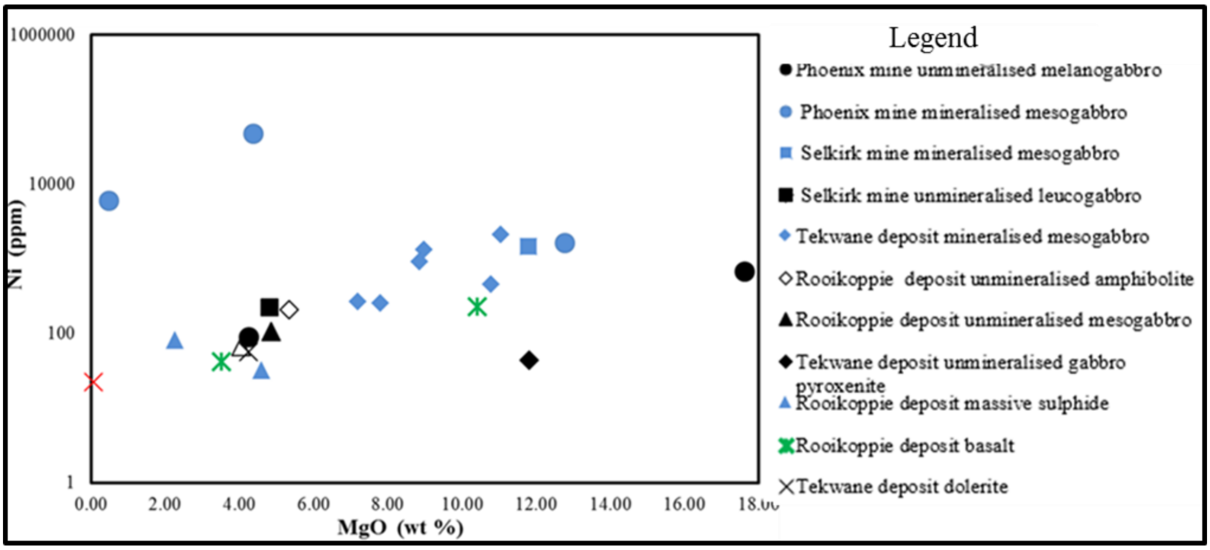

Figure 5.5: The plot of Ni against MgO shows linear positive relationship that indicates an increase in both MgO and Ni.

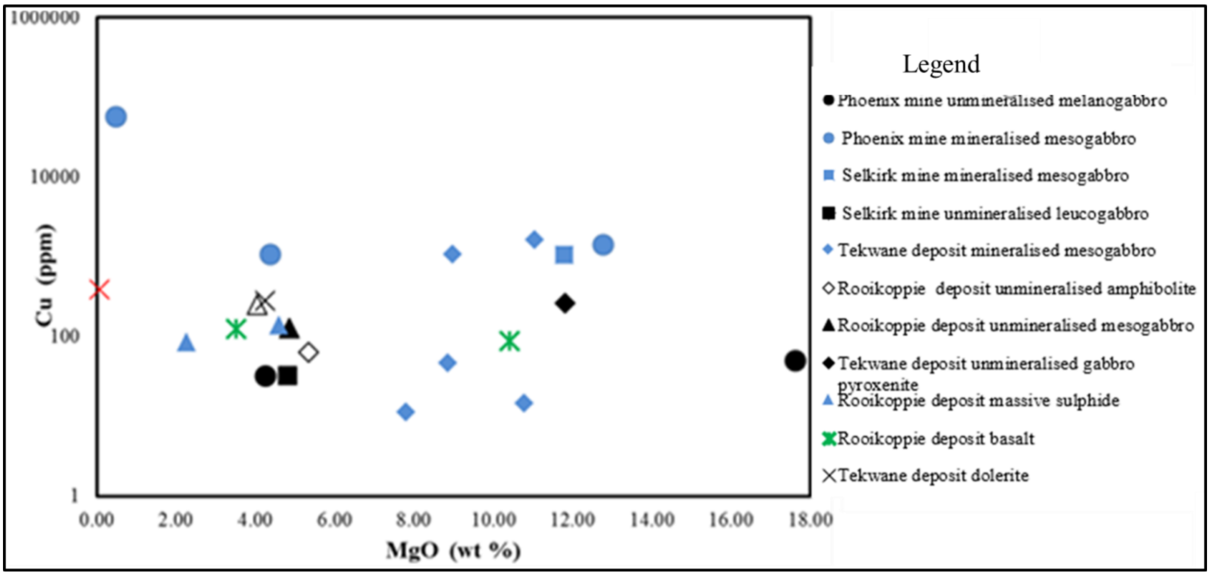

Figure 5.6: The plot of Cu against MgO shows linear positive relationship that indicates an increase in both MgO and Cu.

Both the mineralised and unmineralised melanogabbro and mesogabbro units show Sr concentration, which varies from 50.77 ppm to 199.27 ppm. The Zn content in the mineralised mesogabbro units ranges from 60.41 ppm to 110.66 ppm while in the unmineralised melanogabbro units is 54.66 ppm. The mineralised mesogabbro units contain moderate abundance of Ba, which ranges from 51.68 ppm to 118.58 ppm in the Phoenix mine.

The mesogabbro (sample R012) in the Rooikoppie deposit exhibits low Ni abundance (205.55 ppm) similar to unmineralised leucogabbro unit in the Selkirk mine (Table 5.6). It also displays higher Cu concentration than the mesogabbro units in the Phoenix, Selkirk mines and Tekwane deposit.

Table 5.6: The XRF trace elements concentrations of Rooikoppie deposit mesogabbro, massive sulphide, basalt and dolerite units, which exhibit Ni contents ranging from 22.33 ppm to 229.04 ppm with Sc values of between 0.92 ppm and 43.03 ppm.

	ROOIKOPPIE DEPOSIT									
Trace element (ppm)	Basalt (P3)	Dolerite (P4)	Pyroxenite gabbro (P12)	Massive sulphide (R1)	Dolerite (R2)	Massive sulphide (R4)	Basalt (PIN014)	Meso Gabbro (R11)	Mesogabbro (R012)	Gossan (R9)
Sc	43.03	22.51	27.84	8.23	17.51	1.23	14.70	39.69	41.09	0.92
V	267.30	254.04	382.45	5.99	207.80	51.95	107.15	235.93	222.75	138.22
Cr	623.42	58.05	48.94	3.15	65.22	22.09	57.85	543.74	292.21	14.70
Co	45.97	28.31	38.70	0.00	37.93	0.00	26.12	38.27	42.27	0.00
Ni	229.04	55.88	43.32	81.01	67.07	32.52	41.99	205.55	105.96	22.33
Cu	87.67	281.60	263.91	87.25	248.55	140.11	124.62	63.16	126.81	387.30
Zn	74.26	119.52	138.93	37.34	110.81	97.65	98.05	67.41	67.95	23.59
Ga	13.30	28.47	25.94	0.00	30.55	5.91	21.09	15.69	20.81	1.03
Rb	33.04	42.02	27.56	5.30	29.13	8.39	17.92	7.38	23.51	4.65
Sr	99.63	770.53	555.54	20.89	871.16	14.97	787.26	135.11	158.21	19.83
Y	18.50	40.83	40.01	10.90	35.52	10.19	15.24	14.83	17.26	0.00
Zr	53.74	444.69	318.57	6.60	382.23	15.47	135.83	45.81	73.09	11.31
Nb	3.58	40.99	22.93	2.45	32.38	2.18	7.27	2.89	3.70	4.40
Mo	0.00	3.53	2.49	3.18	2.37	0.00	0.25	1.01	1.54	4.43
Ba	117.60	925.63	527.87	9.82	585.18	10.61	257.74	18.03	168.18	47.48
Pb	4.06	8.57	7.65	9.28	3.50	10.22	14.45	5.98	9.10	4.51
Th	5.61	16.65	0.00	0.00	2.95	0.00	4.30	1.34	0.00	0.00
U	0.00	0.00	0.00	0.00	0.00	0.00	0.00	0.00	0.00	0.00

The mesogabbro in the Rooikoppie deposit exhibits Ni concentration ranging from 105.96 ppm to 205.55 ppm when compared to the unmineralised mesogabbro units at the Phoenix mine (Table 5.6). Similarly, to unmineralised phenocrystic leucogabbro in the Selkirk mine, the mesogabbro in Rooikoppie deposit has low Co abundance (26.12 ppm). It has higher Sr concentration (787.26 ppm) than the mineralised and unmineralised melanogabbro and mesogabbro units in the Phoenix, Selkirk mines and Tekwane deposit.

Sc and Y contents of the mineralised and unmineralised leucogabbro, mesogabbro and melanogabbro units in the Phoenix mine display positive correlation against MgO content (Figures 5.7a and 5.7b). The Tekwane deposit mesogabbro units display positive correlation between Y (Yttrium) against MgO (Figure 5.7b). V (Vanadium) content in the mesogabbro (samples, S10 and N1) and melanogabbro units (samples, NW1 and W8) display positive correlation with MgO in Phoenix mine similar to mesogabbro units in the Tekwane deposit (Figure 5.7c). The relationship between Zr (Zirconium) and MgO is characterised by negative and positive trend for gabbro units in the Phoenix mine (Figure 5.7d). In contrary, positive correlation exists between Co (Cobalt) and MgO for melanogabbro units in the Phoenix mine.

The mineralised and unmineralised phenocrystic leucogabbro and mesogabbro units in Selkirk mine and Tekwane deposit display negative and gentle to moderate correlation between Cr (Chromium) and MgO, and Nb (Niobium) against MgO similarly to unmineralised melanogabbro units in the Phoenix mine (Figures 5.7e and 5.7f). The relationship between Co and MgO is positive for mineralised and unmineralised gabbro units in the Phoenix, Selkirk mines, Tekwane and Rooikoppie deposits (Figure 5.7g). Both mineralised and unmineralised leucogabbro, mesogabbro and melanogabbro units in Selkirk mine and Tekwane deposit display negative correlation between Pb (Lead) and MgO (Figure 5.7h).

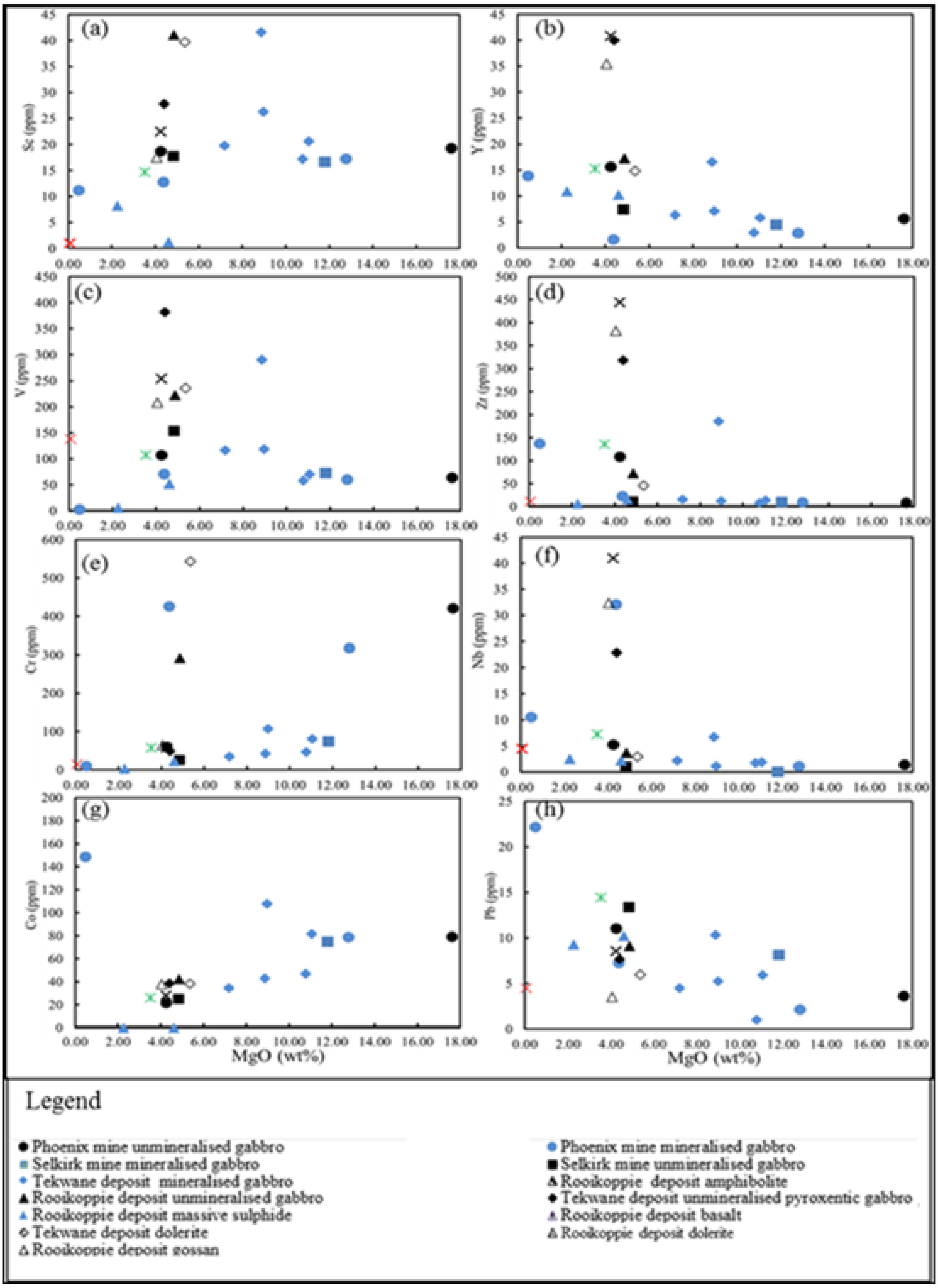

Figure 5.7: The Harker diagrams plots indicating positive relationship between the differentiation index, MgO against (a) Sc, (b) Y, (c) V, (d) Zr, (e) Cr (f) Nb, (g) Co and (h) Pb

in the gabbro units. The MgO content correlates negatively with (b) Y, (d) Zr, (f) Nb and (h) Pb. The plot between MgO and Co shows both inverse and positive trends. The Sc concentrations of Phoenix and Selkirk mines porphyritic granodiorite units are low, ranging from 5.42 ppm to 12.88 ppm (Table 5.7). Furthermore, the Phoenix mine tonalite and porphyritic granodiorite contain moderate concentrations of 311.4 ppm and 354.6 ppm respectively. The Tekwane and Rooikoppie deposits quartz diorite range narrowly from 360 ppm to 456.5 ppm. The Rooikoppie deposit granodiorite units show moderate concentration of Sr, ranging widely from 327ppm to 801.1ppm (Table 5.7).

Table 5.7: The XRF analysed trace elements concentrations of Phoenix, Selkirk mines, Tekwane and Rooikoppie sulphide deposits intermediate and felsic units, which show high Sr content of between 114.37 ppm and 801.13 ppm.

Trace element (ppm)	PHOENIX MINE		SELKIRK MINE	TEKWANE DEPOSIT		ROOIKOPPIE DEPOSIT						
	Tonalite (W1)	Porphyritic granodiorite (W3)	Porphyritic granodiorite (SL06)	Leucogranodiorite (TEK2)	Quartz diorite (TEK5)	Quartz diorite (R7)	Quartzite (R011)	Granodiorite (P2)	Granodiorite (PIN011)	Granodiorite (PIN012)	Granodiorite (PIN013)	Granodiorite PIN015)
Sc	10.15	5.42	12.18	0.11	4.34	6.96	28.5	3.05	9.35	9.65	15.96	6.77
V	82.4	36.66	87.39	16.24	35.7	65.78	133	31.8	66.82	90.72	101.7	36.05
Cr	9.57	15.47	143.62	2.71	13.9	28.21	429	4.51	26.15	40.48	40.24	5.53
Co	12.21	9.02	14.07	8.64	7.73	16	38.1	10.4	16.6	19.76	23.61	6.43
Ni	18.16	17.56	76.94	131	9.46	13.8	256	16.9	23.7	29.29	33.73	8.88
Cu	40.5	25.2	49.67	10.87	8.47	8.87	59.7	8.19	15.06	24.24	105.1	9.66
Zn	53.57	47.8	42.5	39.3	48.5	80.42	79.1	43.8	77.54	103.18	95.16	53.78
Ga	18.78	19.45	18.78	15.51	18.4	20.63	17.4	19.3	20.59	22.01	19.21	19.39
Rb	27.15	32.94	11.05	58.16	48	47.04	91.1	65.4	34.72	61.98	13.86	57.46
Sr	311.4	356.1	114.37	237.1	360	456.5	249	327	763.77	789.66	801.1	532.06
Y	15.67	6.07	26.16	3.53	6.18	6.72	15.4	8.17	21.34	10.11	15.85	3.63
Zr	264.3	119.6	242.63	55.33	107	100.5	131	104	200.21	204.39	144.5	111.51
Nb	6.73	2.33	10.07	2.02	3.78	1.98	5.74	2.78	12.17	8.64	7.48	2.95
Mo	1.23	0.4	1.76	0.83	0.5	0.24	0.32	0.27	0.68	0.43	0.44	0.35
Ba	199.5	340.8	34.57	470	484	635.4	606	535	475.41	985.49	226.6	516.18
Pb	8.16	12.12	15.79	20.5	16.2	21.81	8.61	7.62	17.35	21.43	13.41	19.67
Th	5.61	7.07	8.26	7.78	8.56	2.14	3.8	10	16.46	10.71	5.53	6.75
U	0.00	0.00	0.00	0.00	0.00	0.00	0.00	0.33	0.00	0.00	0.00	0.00

The plot between Sc and SiO_2 defines a positive relationship exists between the two elements (Figure 5.8a). Meanwhile, the plot between Ni and SiO_2 displays a negative correlation (Figure 5.8b). The relation between Sr (Strontium) and SiO_2 is positive for granodiorite units in the Phoenix, Selkirk mines and Rooikoppie deposits (Figure 5.8c). There is a scattered distribution though with general negative correlation between Zr (Zirconium) and SiO_2 in the Tekwane and Rooikoppie deposits (Figures 5.8d, 5.8e and 5.8f).

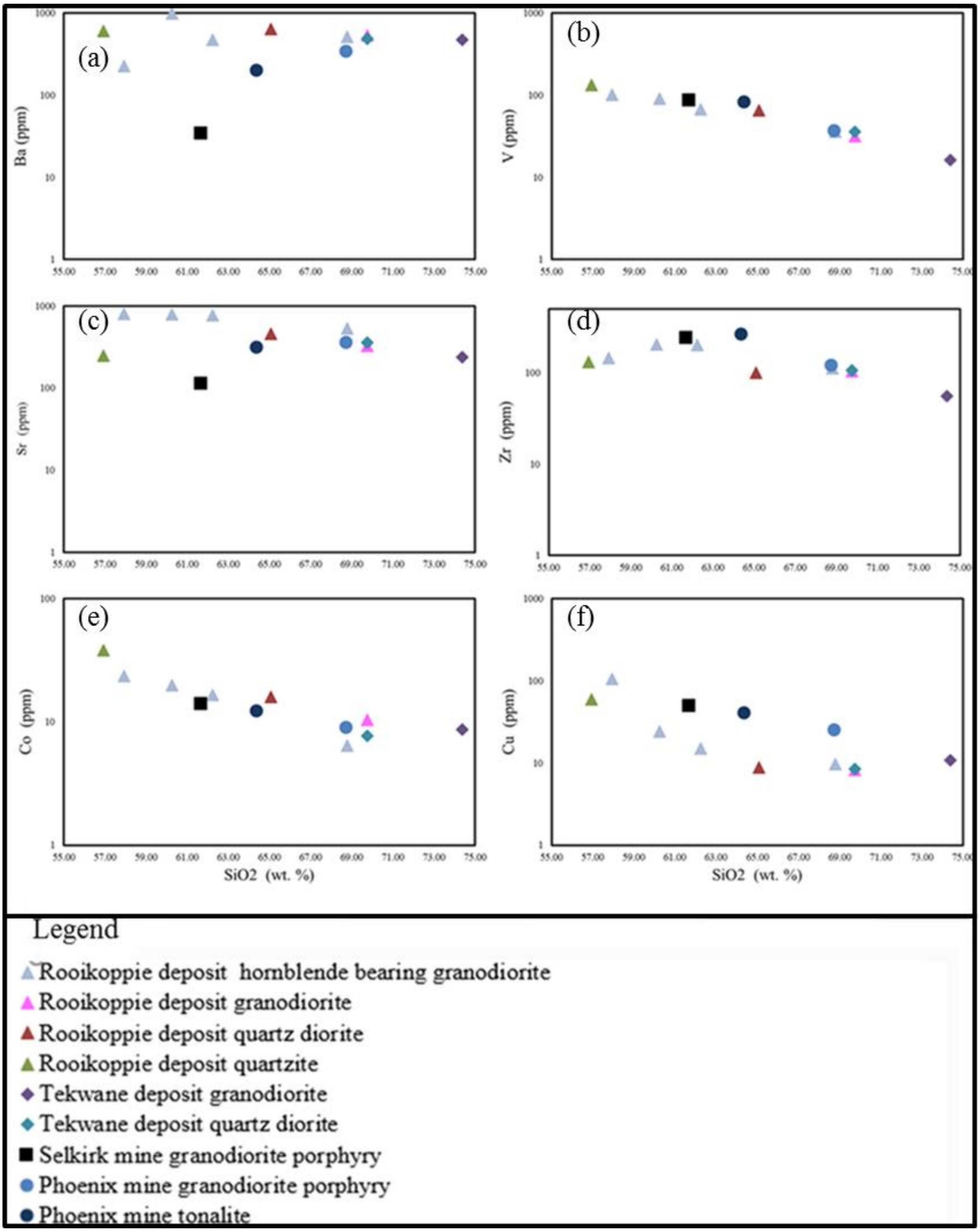

Figure 5.8: The Harker variation plots for SiO_2 against trace elements, (a) Ba, (b) V, (c) Sr, (d) Zr, (e) Co and (f) Cu compositions in tonalite, granodiorite and metasedimentary units in the Phoenix, Selkirk mines, Tekwane and Rooikoppie deposits. The plots display positive

trends between SiO_2, Ba, and Sr, which reflect positive correspondence in concentration of these elements. However, there is decrease in Cu, Co and V concentration corresponds with increase in SiO_2 content.

5.4. Rare Earth Elements (RRE) patterns

The rare earth elements play important role in variety of magmatic processes and tectonic settings associated with the gabbroic units and contact lithologies in TSMDC. There is a positive correlation between the concentration of Ce in relation to Pb content for felsic and mafic units of TSMDC (Figure 5.9a). The Phoenix and Selkirk mines gabbroic units illustrate positive correlations to the granitoids especially Phoenix mine tonalite and Tekwane deposit quartz diorite. A negative correlation is illustrated for both La and Rb concentrations in the mafic and felsic units of TSMDC (Figure 5.9b). The Phoenix and Selkirk mine porphyritic granodiorite and Rooikoppie deposit granodiorite contain La and Rb characteristed by negative relationships. The La\Nb plot show positive relationship for La and Nb concentrations for both mafic and felsic units in TSMDC (Figure 5.9c).

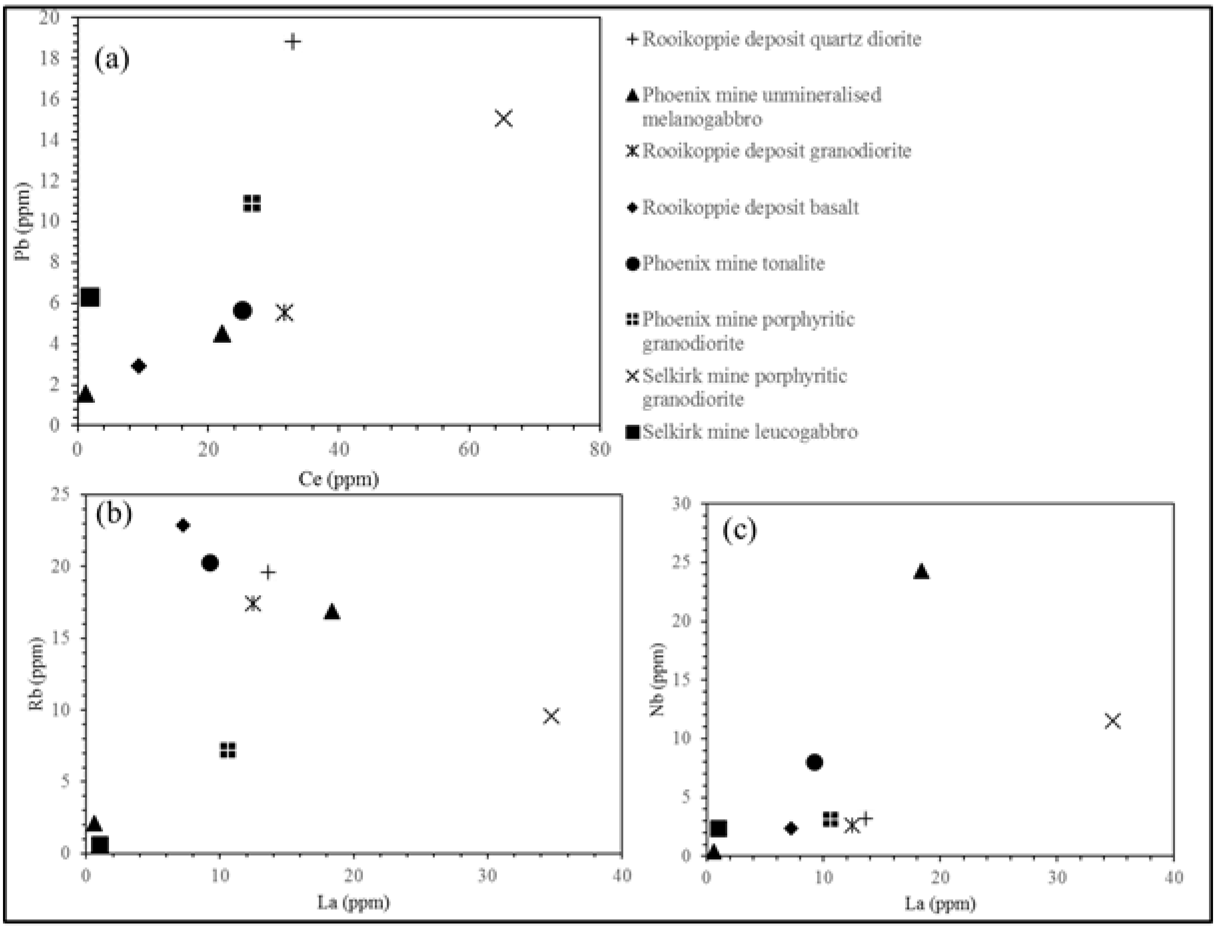

Figure 5.9: The bivariate diagrams showing the distribution of selected elements. Pb against Ce (b), Rb against La and (c) Nb plotted against La.

The normalised concentrations of rare earth elements (REE) in mesogabbro, tonalite, diorite, dolerite and granodiorite units in the Phoenix, Selkirk mines, Tekwane and Rooikoppie deposits were normalized based on Bonyton (1984) chondrite abundance values, with the normalized values are presented in Table 5.8.

Table 5.8: ICP-MS trace elements concentrations of melanogabbro, granodiorite, diorite and dolerite units in Phoenix and Selkirk mines and Tekwane and Rooikoppie sulphide deposits. Chondrite normalizing values of Bonyton (1984) were applied in the data

	PHOENIX DEPOSIT				SELKIRK DEPOSIT		ROOIKOPPIE DEPOSIT					
Trace element (ppm)	Tonalite (W1)	Porphyritic granodiorite (W3)	Melanogabbro (W8)	Melanogabbro (NW1)	Porphyritic granodiorite (SL06)	Leucogabbro (SL09)	Dolerite (R1)	Dolerite (R4)	Quartz diorite (R7)	Meso Gabbro (R11)	Leucogranodiorite (P2)	Basalt (P3)
Li	19.52	26.70	10.03	27.83	5.38	6.68	1.06	7.33	31.69	4.74	21.84	12.98
P	759.97	407.45	461.44	79.22	1582.19	74.37	50.53	53.95	710.80	282.83	545.70	249.67
Sc	6.18	3.02	13.91	12.89	16.58	10.12	1.18	0.89	6.57	29.22	2.25	34.67
Ti	3995.93	1968.92	2511.63	953.21	6352.76	988.25	132.27	379.73	2970.98	3416.65	1887.90	4412.53
V	81.70	34.82	100.25	64.23	108.61	124.52	8.91	37.09	60.04	200.93	29.60	228.38
Cr	14.64	21.42	41.44	488.04	154.68	3805.95	10.58	10.66	24.85	565.28	12.10	638.92
Co	11.66	7.82	15.38	76.45	14.94	18.71	37.83	45.55	12.36	46.70	9.04	48.59
Ni	24.50	30.12	67.49	584.45	89.34	107.36	74.59	39.22	26.65	191.52	25.74	207.79
Cu	29.11	33.20	28.12	49.26	45.29	22.65	54.79	70.34	20.05	45.68	12.32	61.96
Zn	85.46	79.77	69.13	77.82	81.15	59.09	56.18	80.97	84.81	77.71	136.35	157.61
Ga	17.36	18.64	9.55	8.40	19.73	8.34	2.24	4.87	19.62	13.67	18.46	13.27
As	0.20	0.23	0.24	0.27	0.46	1.72	8.53	1.95	0.48	3.34	0.20	0.27
Rb	20.29	7.20	16.87	2.10	9.59	0.65	1.12	2.62	19.60	4.93	17.42	22.87
Sr	232.70	213.09	144.10	46.62	121.24	81.32	19.45	10.93	364.35	123.32	177.96	92.49
Y	8.70	3.63	12.78	3.25	27.45	4.32	14.42	11.78	5.65	14.60	4.71	15.19
Zr	128.68	107.58	138.42	8.08	233.22	6.57	4.99	13.99	117.09	39.79	105.21	51.42
Nb	8.02	3.11	24.27	0.41	11.49	2.39	0.49	1.52	3.21	3.39	2.61	2.36
Ba	132.40	164.28	164.91	9.02	26.41	5.32	3.11	13.49	652.45	21.92	287.16	110.36
Sn	1.32	1.32	2.25	0.26	1.82	0.27	0.74	0.69	0.87	1.22	0.71	0.77
Cs	1.71	2.20	1.30	0.26	2.09	0.13	0.74	0.45	0.95	0.08	0.46	0.22
La	9.21	10.58	18.40	0.61	34.77	0.98	8.40	6.96	13.62	5.94	12.47	7.24
Ce	25.19	26.75	22.10	1.21	65.32	1.90	12.11	12.34	32.93	11.99	31.66	9.42
Pr	2.27	2.19	3.48	0.18	8.10	0.29	1.43	1.37	3.70	1.68	2.87	1.62
Nd	9.01	8.00	13.05	0.94	31.23	1.46	5.55	4.97	14.79	7.43	10.66	7.09
Sm	1.98	1.41	2.58	0.30	5.64	0.44	1.06	0.90	3.21	1.95	1.87	1.92
Eu	0.65	0.45	0.73	0.15	1.60	0.23	0.67	0.66	1.15	0.90	0.62	0.65
Gd	2.06	1.45	2.56	0.40	6.16	0.54	1.38	1.18	2.44	2.34	1.70	2.19
Tb	0.27	0.15	0.37	0.08	0.85	0.11	0.21	0.16	0.28	0.41	0.17	0.39
Dy	1.53	0.71	2.13	0.54	4.67	0.75	1.42	1.02	1.28	2.73	0.79	2.55
Ho	0.29	0.12	0.43	0.12	0.92	0.17	0.34	0.24	0.22	0.57	0.13	0.54
Er	0.77	0.33	1.20	0.33	2.54	0.46	1.02	0.70	0.59	1.54	0.37	1.46
Tm	0.11	0.04	0.18	0.05	0.37	0.08	0.16	0.11	0.08	0.23	0.05	0.23
Yb	0.67	0.28	1.22	0.35	2.41	0.49	1.02	0.69	0.47	1.45	0.30	1.45
Lu	0.10	0.04	0.18	0.05	0.35	0.07	0.17	0.11	0.07	0.21	0.04	0.21
Hf	2.93	2.76	3.39	0.23	5.12	0.20	0.14	0.47	2.97	1.18	2.76	1.42
Ta	0.52	0.23	1.55	0.02	0.76	0.10	0.05	0.13	0.17	0.85	0.19	0.16
W	0.31	0.57	0.53	0.31	0.36	0.15	2.01	2.43	0.46	0.71	0.12	0.24
Pb	5.66	10.89	4.52	1.58	15.07	6.33	4.71	7.20	18.85	6.27	5.56	2.91
Th	1.60	3.28	4.30	0.05	6.33	0.05	0.34	0.99	2.15	1.33	2.66	1.41
U	0.80	1.08	1.03	0.02	1.81	0.12	0.36	0.71	0.94	0.56	1.49	0.38

The plotted chondrite normalized values of the Phoenix, Selkirk mines, Tekwane, and Rooikoppie deposits show similar patterns. The rare earth elements (REE) are normalised based on Bonyton (1984) as indicated by subscript, N in this study (Table 5.8). There is enrichment in light rare earth elements (La_N, Ce_N, Pr_N and Nd_N) relative to depletion in medium rare elements (Sm_N, Eu_N, Gd_N) for Selkirk mine porphyritic granodiorite as represented by sample SL06 and Rooikoppie granodiorite (representative samples, PIN011, PIN012, PIN013 and PIN015 (Figure 5.10). The unmineralised melanogabbro units (samples, NW1 and W8) are characteristic of similar negative slope. The Phoenix mine melanogabbro samples are characteristic of slightly pronounced Eu_N positive anomaly.

The Selkirk mine leucogabbro (representative sample SL 09) shows slight negative slope from light and moderate rare earth elements to heavy rare earth elements (Figure 5.10).

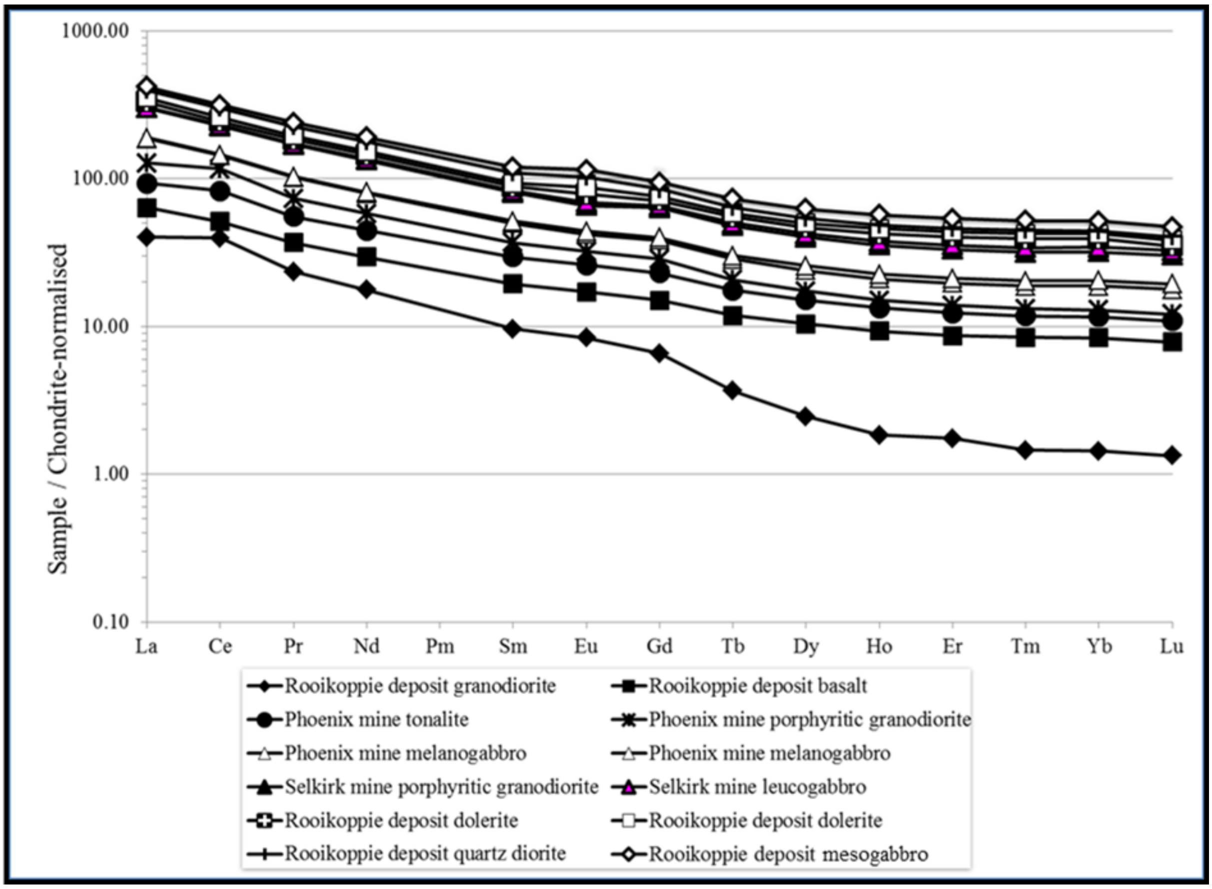

Figure 5.10: The rare earth elements (REE) chondrite normalised diagrams show enrichment of LREE relative to HREE. The light rare earth elements (La_N, $Ce_{N\,n}$, $Pr_{N\,n}$, Nd_N) show enrichment relative to medium and heavy rare elements (Sm_N, Eu_N, Gd_N, Tb_N, Dy_N, Ho_N, Er_N, Tm_N, Yb_N, Lu_N) with gentle slope. The light rare earth elements (La_N, Ce_N, Pr_N, Nd_N, Sm_N, Eu_N, Gd_N, Tb_N, Dy_N, Ho_N, Er_N, Tm_N, Yb_N and Lu_N) exhibit negative slope.

The chondrite-normalised multi-element plot generally displays similar profiles defined by enrichment of light rare earth elements (LREE) relative to heavy rare earth elements (HREE) for melanogabbro units for Phoenix and Selkirk mines (Figure 5.10). There is weak positive Eu_N anomalies for the melanogabbro and granodioritic units in TSMDC. The light rare earth elements (LREE) are characterised by slight negative anomalies of Nb_N and Ta_N in the chondrite normalized multi element diagrams (Figure 5.10). The extended chondrite-normalised REE plot shows similar patterns for light rare elements distributions in melanogabbro and granodiorite units of Phoenix mine (Figure 5.11).

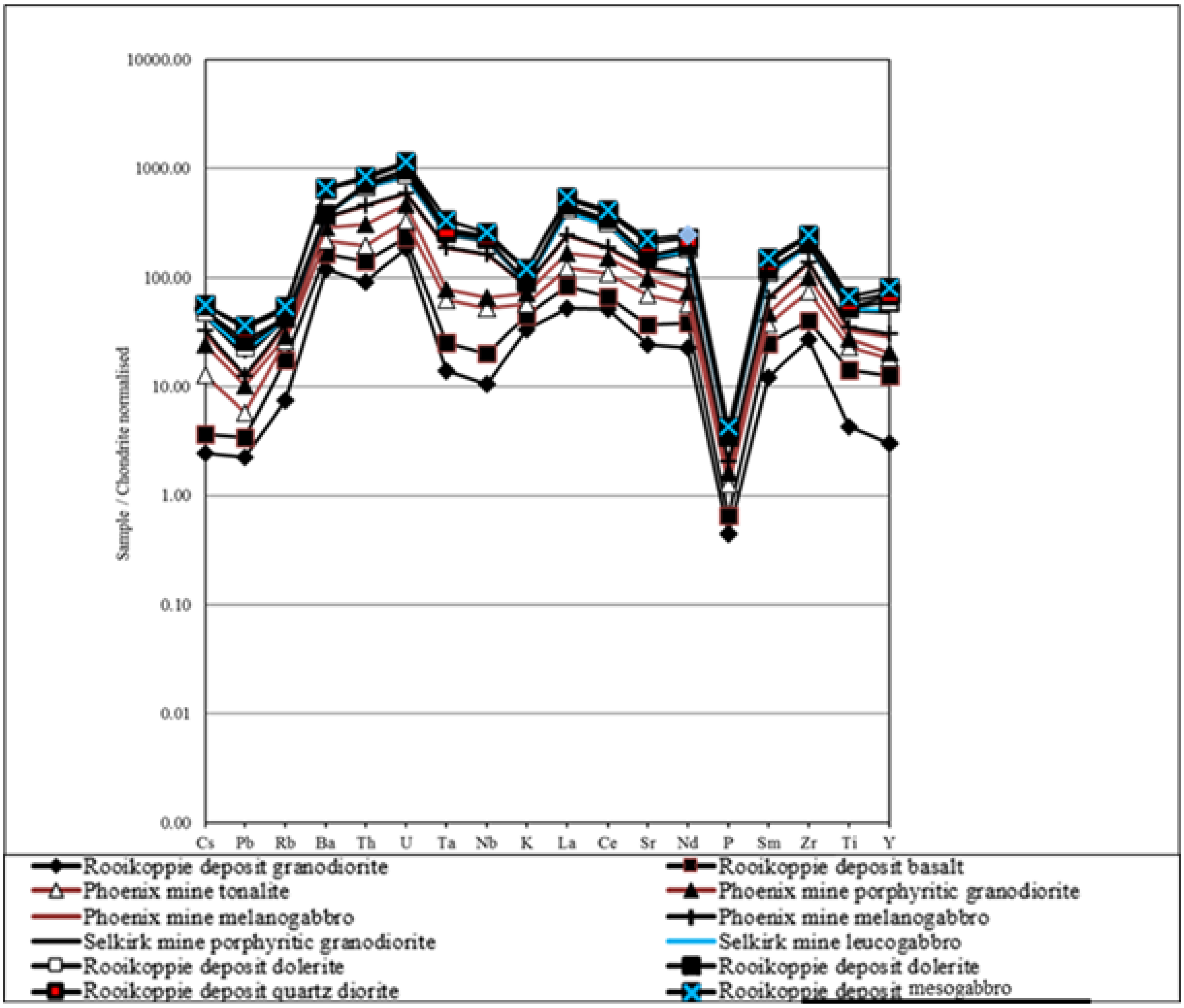

Figure 5.11: The extended REE plot showing normalized chondrite concentrations after Bonyton (1984). The multi element plot displays enrichment slight enrichment in Rb_N and depletion in Ta_N and Sr_N.

There is similar pattern for Ta_N and Nb_N in the melanogabbro and granodiorite units. In addition, there is gentle negative slope for heavy rare earth elements (HREE) for the Selkirk mine leucogabbro and Rooikoppie deposit granodiorite (Figure 5.11). The Selkirk mine porphyritic granodiorite (sample SL06), Phoenix mine unmineralised melanogabbro (samples, NW1 and W8) and Rooikoppie deposit dolerite (sample R2), quartz diorite (sample R7) and mesogabbro (sample R012) are characteristic of pronounced negative anomalies of K_N and P_N (Figure 5.11). The Sr_N values for Phoenix mine tonalite (sample, W1) and Rooikoppie deposit granodiorite (samples, PIN 011, PIN 012, PIN 013 and PIN 015) are characteristic of negative anomaly. The chondrite-normalised diagram is also characteristic of negative anomaly of Ti_N for Rooikoppie deposit dolerite (sample R1) and mesogabbro (sample R012) and Selkirk mine porphyritic granodiorite (sample SL06). Furthermore, the mafic and felsic units are characterised by negative anomalies of Ta_N and Nb_N in TSMDC.

5.5. Tectonic Setting of TSMDC rock units

Various tectonomagmatic discrimination diagrams represent the tectonic environment associated with formation of the mafic and felsic units in TSMDC (Figures, 5, 12-5.14). The magmatic units of the Phoenix, Selkirk mines, Tekwane and Rooikoppie plot mainly on the island arc basalt field (Figure 5.12).

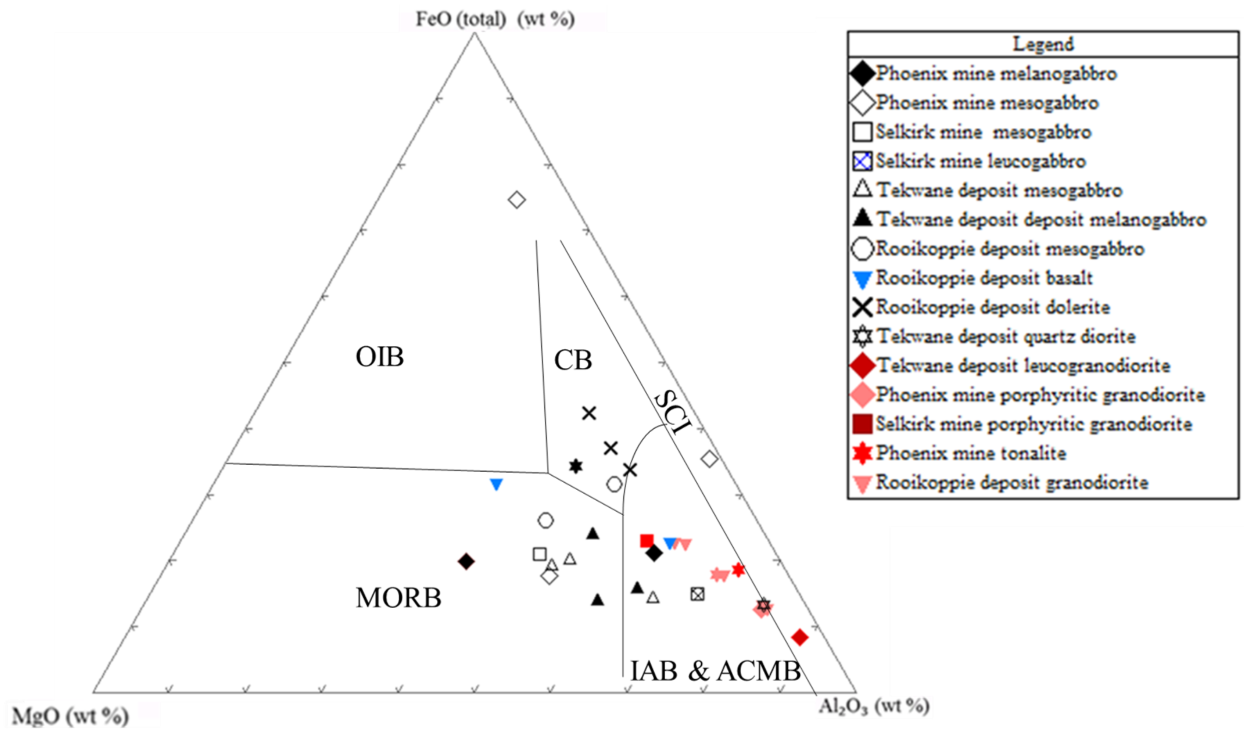

Figure 5.12: The gabbro units in the Phoenix and Selkirk mines plot within the spreading centre island (SCI), continental basalt (CB), mid oceanic ridge basalt (MORB), island arc basalt (IAB) fields.

The Phoenix mine melanogabbro and mesogabbro has strong affinity to within plate basalts (WPB) whereas Selkirk mine and Tekwane deposits gabbroic units plot in the volcanic arc basalts (VAB) field (Figure 5.13).

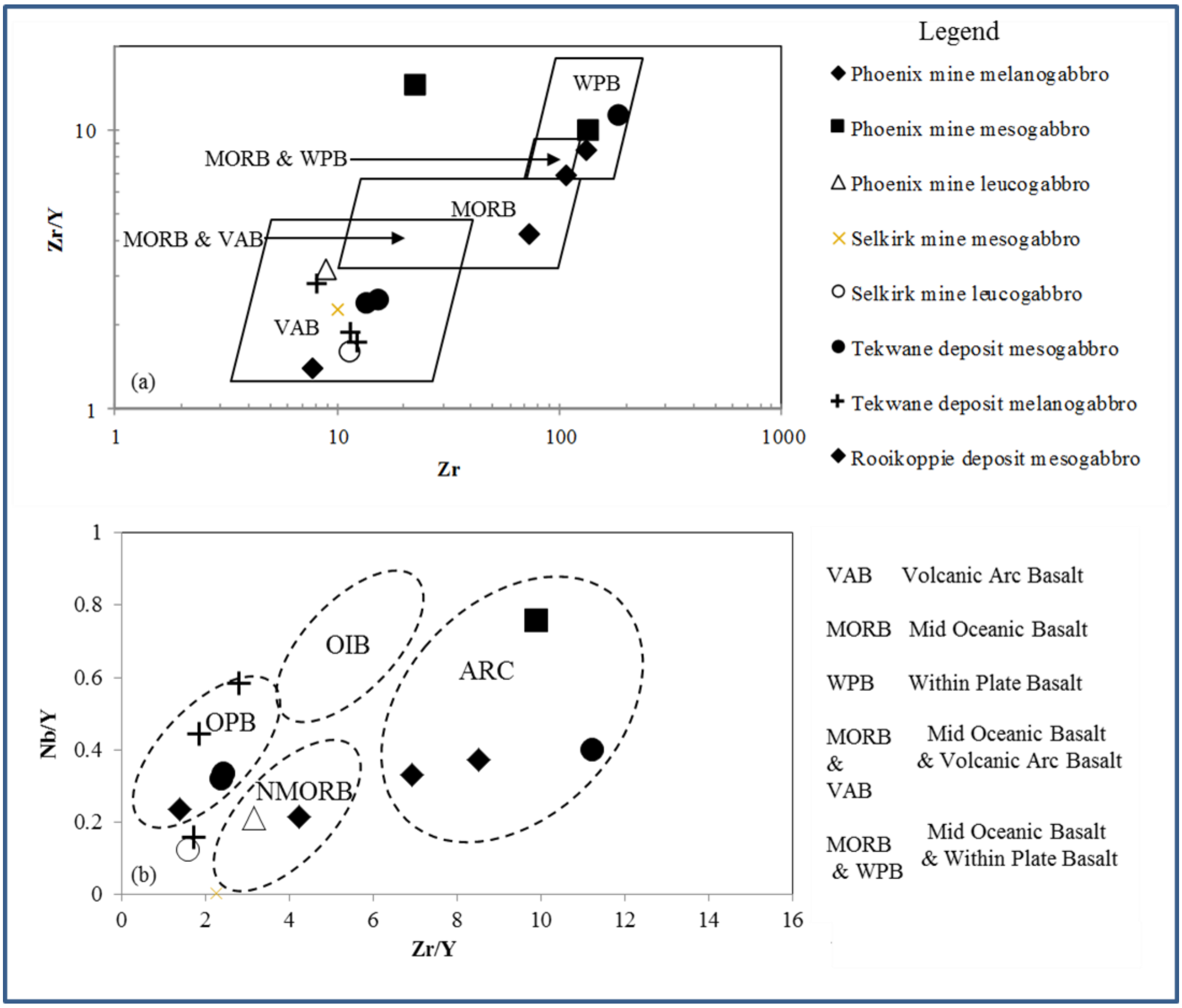

Figure 5.13: The tectonic discrimination plots of gabbroic units on: (a) Zr/Y against Zr (Pearce and Norry, 1979) and (b). Nb/Y against Zr/Y. (a). The Phoenix mine melanogabbro units plot mainly in the within plate basalt (WPB) field whereas (b). Tekwane deposit gabbroic units plot mainly in the oceanic plate basalts (OPB).

The Phoenix and Selkirk mine mafic and felsic units, notably melanogabbro, quartz diorite and porphyritic granodiorite plot mainly in the continental margin fields (Figures 5.14 a and b). The Tekwane deposit mesogabbro plots within the enriched mantle source field (Figure 5.14b).

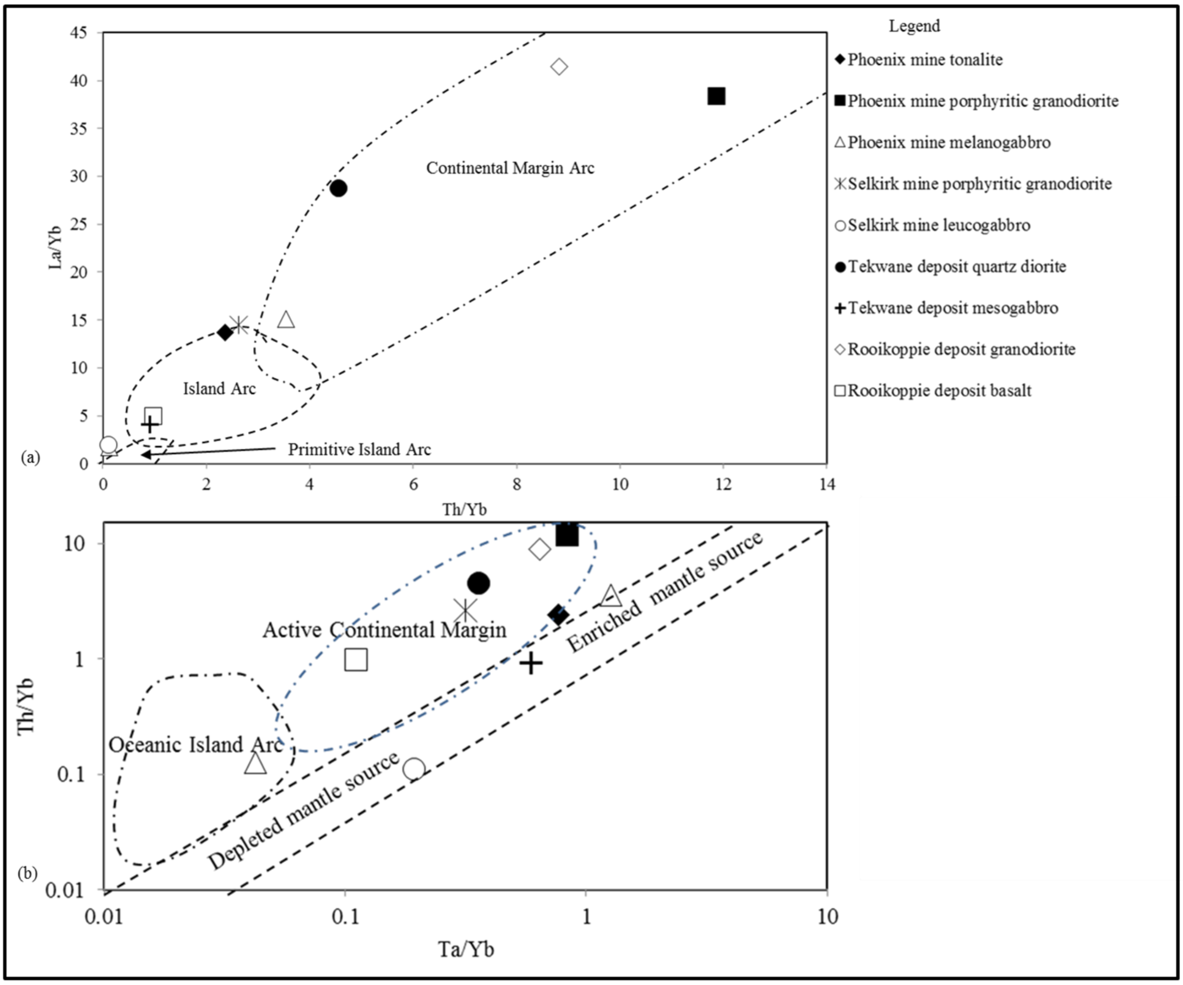

Figure 5.14: The tectonic discrimination diagram of (a). La/Yb against Th/Yb and (b). Th/Yb against Ta/Yb. The distribution of felsic and mafic units is akin to formation within island arc environment associated with continental margin.

CHAPTER 6.0: GENERAL OVERVIEW OF STRUCTURAL FRAMEWORK OF THE PHOENIX, SELKIRK MINES, TEKWANE AND ROOIKOPPIE DEPOSITS

Three deformation events, D_1, D_2 and D_3 affected the TSMDC. The first deformation event, D_1 is of brittle-ductile nature and is evidenced by the occurrence of kilometre scale fold (fo_1), faults (F_1) and shear zones, which consist of dominant regional foliations (S_1), ($S\text{-}C_1$), stretching and mineral lineation (L_1), en echelon tension gashes, and boudinaged quartz veins (V_1). D_1 is associated with NNW-SSE oriented principal stress axes. The second deformation event, D_2 is recognisable by the presence of folded and asymmetric boudinaged quartz veins (V_2) and faults (F_2) that crosscut D_1 structures. D_2 resulted from NE-SW oriented compressional principal stress and minimum principal stress, σ_3 with NW-SE orientation. The third deformation, D_3 produced the fracture, stylolitic cleavages, extensional and columnar joints, which crosscut all the D_1 and D_2 structures. The minimum principal stress, σ_3 acted NE-SW and marked the trend of the extensional regime associated with the distribution of fracture cleavages and joints. The geometry, kinematic data of structural elements associated with deformation events, D_1, D_2 and D_3, will be detailed in this section and are summarised in Table 6.1. The mapped shear zones are of great significance to this study as they consist of kinematic indicators, crucial to provide information on the control of the sulphide mineralisation in relation to the structural evolution in TSMDC. Thus, the shear zones and associated structural elements will be presented and explained accordingly with regard to D_1, D_2 and D_3.

Table 6.1: Summary of tectonic events of the TSMDC. Three deformation events are recognised and are characterised by different structural elements at different scale of exposure.

<table>
<tr><th>Deformation event</th><th>Structural element</th><th></th></tr>
<tr><td>D_1</td><td>➢ Formation of strikes-slip and normal faults (F_1), NNE, NE and NW trending shear zones, which consist of pervasive foliation, S_1 and S_1-C a as result of NNW-SSE oriented compressive forces.
➢ Development of extension, en échelon and boudinaged quartz veins (V_1)</td><td>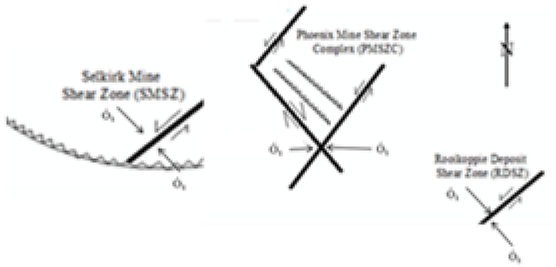
</td></tr>
<tr><td>D_2</td><td>➢ Development of folded and asymmetric boudinaged quartz veins (V_2) and strike-slip and normal faults (F_2) as result of NE-SW compressive forces.</td><td></td></tr>
<tr><td>D_3</td><td>➢ Formation of array of fracture cleavage and joints</td><td>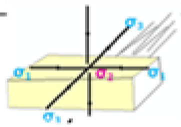</td></tr>
</table>

6.1. First Deformation event, D_1

The use of multi band high resolution Advanced Spaceborne Thermal Emission and Reflection Radiometer (ASTER) Red-Green-Blue (RGB) composition (band ratio 4:6:8) image reveals occurrence of curvilinear and anastomosing features, which were confirmed as fold and shear zones during fieldwork mapping (Figure 6.1). The ASTER image shows an array of anticline patterns throughout TSMDC. The anticline patterns are characterised by open limbs. The anticline axial traces display NNE trends. The fold (fo_1) is characterised by open anticline, which influenced the curvilinear geometry of the amphibolite and basalt in the south part of the study area. The fo_1 is defined by nearly asymmetrical axial plane with NNE trend, which resulted from NNW-SSE shortening forces.

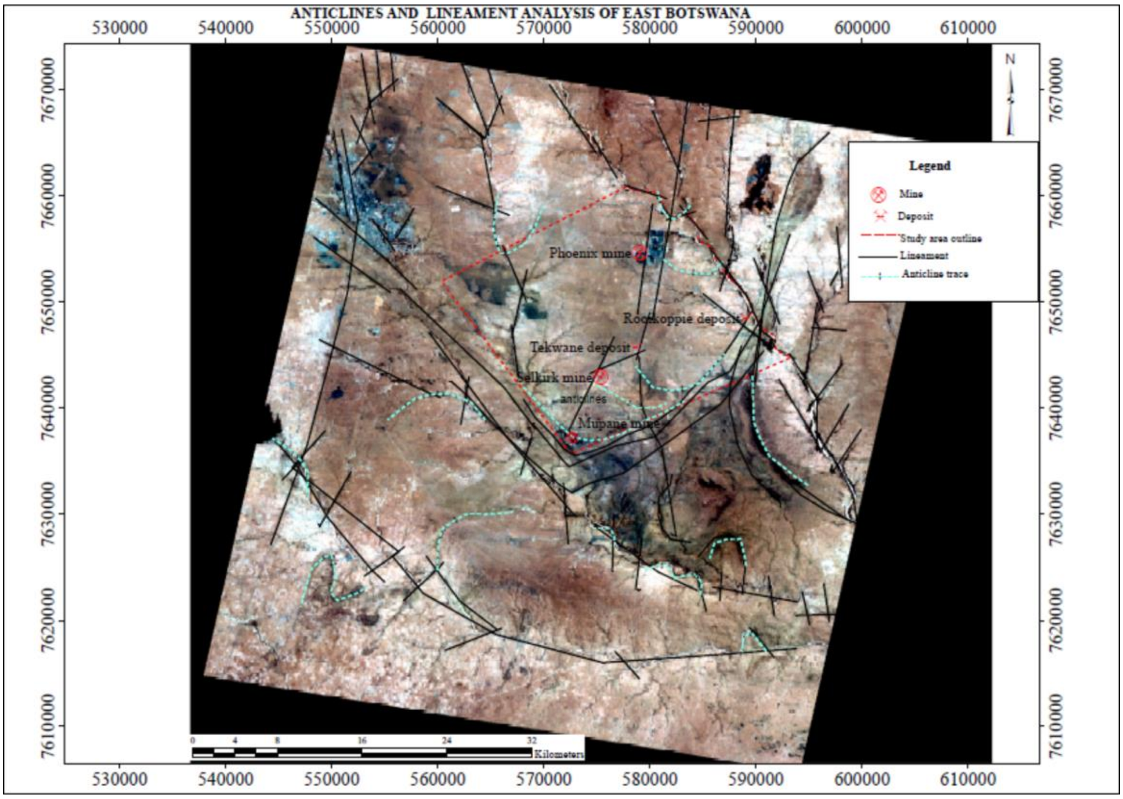

Figure 6.1: The ASTER image: Red-Green-Blue (RGB) composition (band ratio 4:6:8) of scale 1: 250 000 showing the dendritic drainage pattern, possible structural control in TSMDC and anticlinal shaped patterns, possibly pointing to occurrence of folds. The drainage network coincides with the lineaments and anticline axial trace trends in TSMDC.

A set of regional scale lineaments were identified from the ASTER band 4:6:8 image and were confirmed as NW and NE trending shear zones associated with foliation (S_1) during fieldwork mapping (Figure 6.1). The ASTER image also reveals NNE, NE, NNW and NW trending lineaments, which may represent faults (F_1). The NNE trending lineaments show offset like an en echelon patterns, which may possibly represent strike slip faults (F_1). The evidence for the existence of the faults associated with expressions within the ASTER image could not be confirmed due to poor outcropping in some localities.

The dendritic drainage pattern shows similar orientation to the NE, NNE and NW trending lineaments, which suggest strong structural control (Figures 6.1). The interpreted lineaments dominantly align to the NE, NNE, NNW and NW orientations (Figure 6.2). Similarly, the axial traces of anticlines generally trend NE and NW (Figure 6.2). In addition, the structural data recorded from outcrops consistently fall within or near the lineament expressions of the ASTER image (Figure 6.3). The general orientation of the shear zones and general geometry of the lithostratigraphy of TSMDC show compatibility with the trends of lineaments. Therefore, it is important to detail out the shear zones and ideal to characterise these shear zones as per their mines and deposits of occurrence. These include; Phoenix Mine Shear Zone Complex (PMSZC), Selkirk Mine Shear Zone (SMSZ) and Rooikoppie Deposit Shear Zone (RDSZ). The shear zones crop out where there is ongoing mining and prospecting for gold and sulphide mineralisation. Thus, the understanding of the characteristics and orientation of these shear zones may be significant if they influence the economic prospective of eastern Botswana.

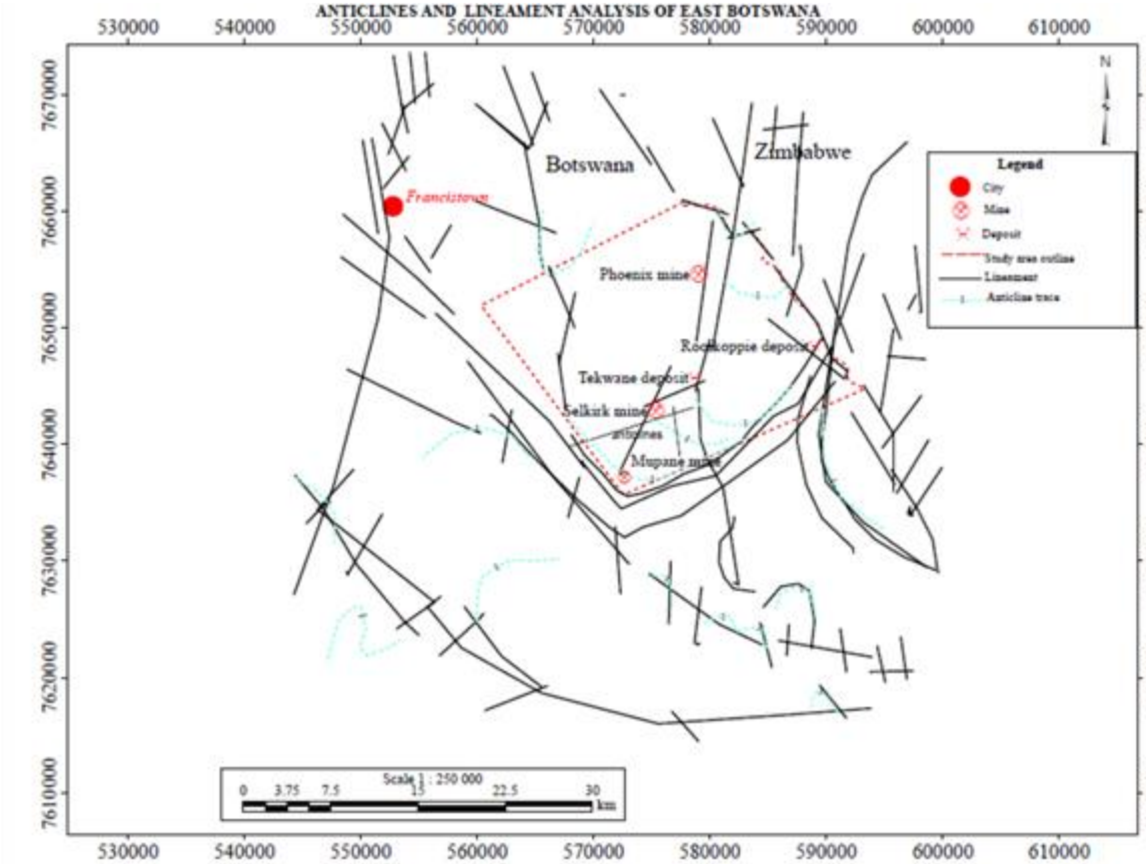

Figure 6.2: The lineament analysis map of east Botswana. The lineaments generally have NNE, NE, NNW and NW trends. The axial trace planes of the anticlines generally trend NNE.

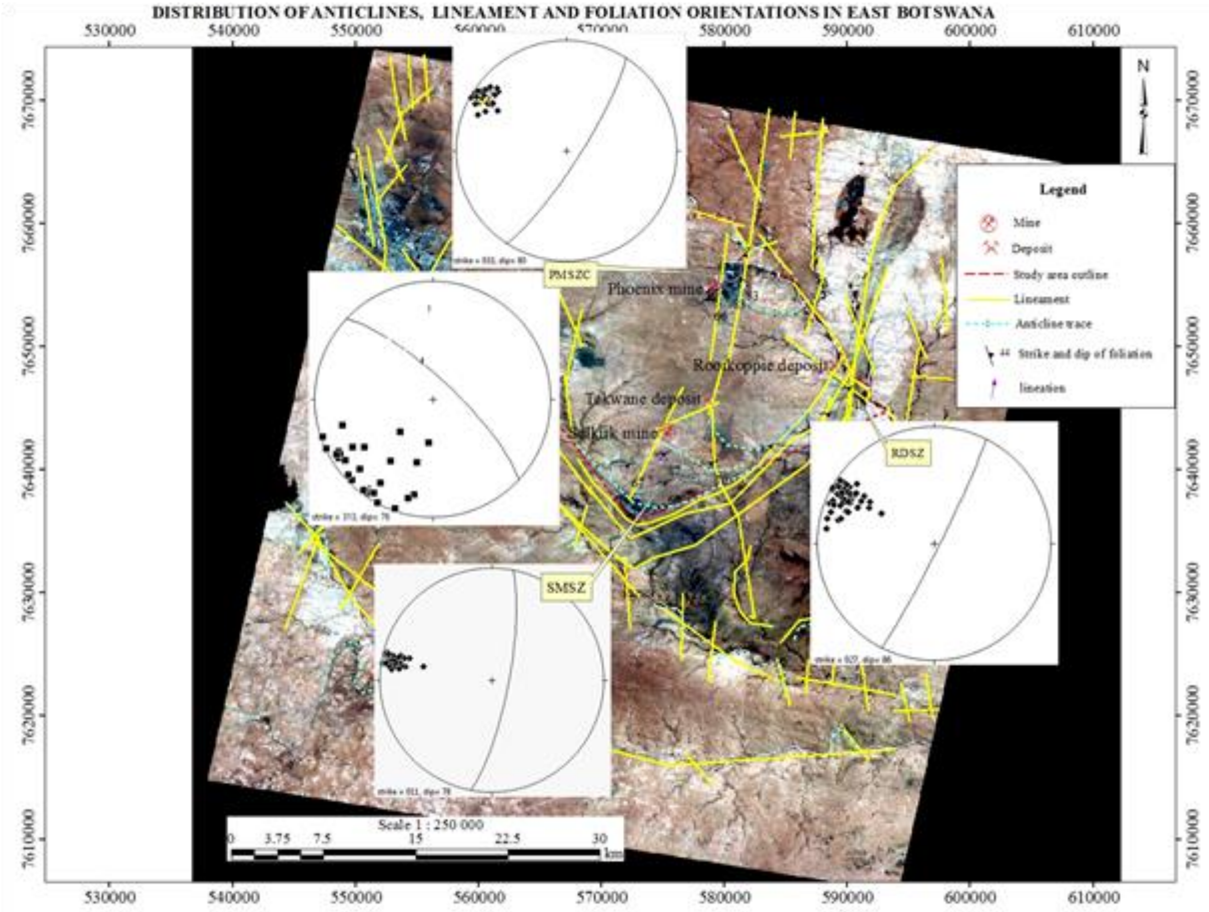

Figure 6.3: The foliation data plotted along major lineaments derived from the ASTER: Red-Green-Blue (RGB) composition (band ratio 4:6:8). The foliation data is consistent with trends observed and recorded during field mapping.

6.1.1. Phoenix Mine Shear Zone Complex (PMSZC)

The Phoenix Shear Zone Complex (PMSZC) occurs in the northeast part of the study area. The PMSZC is situated 8km west of the international border between Botswana and Zimbabwe. The PMSZC is characterised by different sets of shear zones i.e. northeast and northwest trending shear zones identified in the mine pit walls. The northwest trending shears are parallel to the Ramokgwebana seasonal river and its tributary streams, which show dendritic drainage patterns (Figure 6.3). It consists of lineation (L_1), (Figure 6.4) foliation (S_1) and kinematic indicators, which include, S_1-C foliation (Figure 6.5a and b, c and d) and en echelon quartz veins (V_1). The foliation, S_1 consists of metamorphic minerals, hornblende and biotite that suggest upper greenschist facies metamorphism affected Phoenix mine.

Figure 6.4: The mineral lineation, L_1 occurs prominently in the northeast trending shears. L_1 is defined by elengated hornblende crystals.

The kinematic analysis of the S_1-C foliation data was determined through data plotted in the lower hemisphere equal area stereonet (Figure 6.5e). The northeast trending foliation, S_1 indicates a mean strike/dip of 058°/47°SE. There is little spread of poles around the primitive circle, which demonstrates low orientation variability of the foliation in the northeast trending shear zone. The spread of the poles to S_1-C foliation data represent dextral displacement because of clockwise rotation as shown by the geometry of the S_1-C foliation. S_1 obtained from northwest trending shear zones has a mean strike/dip of 313°/75°NE in the Phoenix mine. The poles to the foliation data are closely distributed along the great circle, which suggest minor orientation variability. The spread of the poles to northwest trending foliation, S_1 exhibit anticlockwise rotation associated with dextral displacement.

The mineral lineation (L_1) associated with the northeast trending shear zone is defined by elongated hornblende. L_1 with mean orientation of 67° towards 213°. L_1 exhibits sub vertical clustered distribution in the lower hemisphere equal area stereonet (Figure 6.5f). The northwest trending shear zone crosscuts the Phoenix mine melanogabbro, mesogabbro, tonalite and leucogranodiorite. The northwest trending foliation (S_1) consists of metamorphic hornblende that suggests greenschist facies metamorphism affected the Phoenix mine.

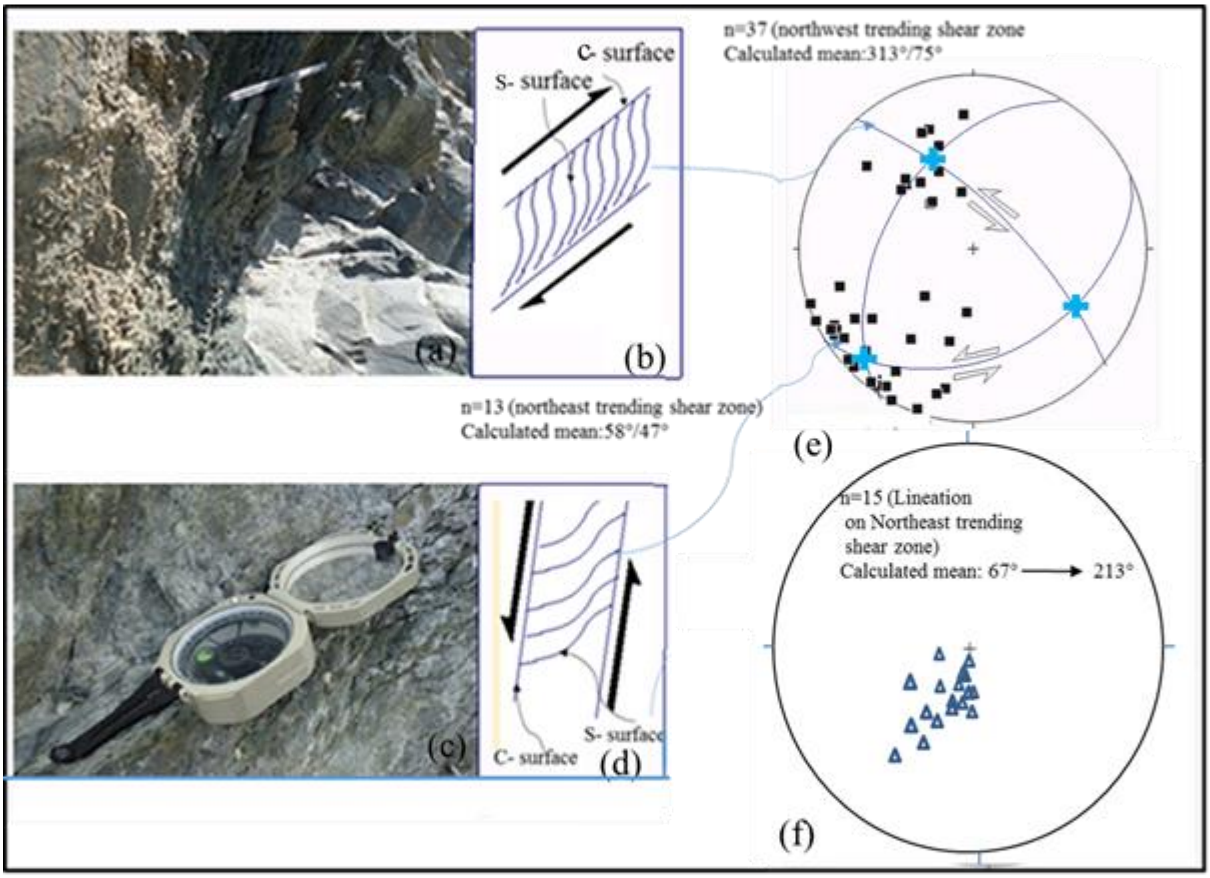

Figure 6.5: The S_1-C in both NE and NW trending shear shows different senses of displacement. (a) The S_1-C foliation shows dextral displacement (UTM 35 K 0579749 mE, 7665318 mN). (b) The diagram shows dextral displacement, associated with NE trending shears. (c) The S_1-C foliation exhibits up movement to the right (sinistral) (UTM 35K 0579655 mE, 7654735 mN). (d) The diagram depicts the NW trending shears show up movement to the right (sinistral) in the Phoenix mine. (e) The equal area stereographic projection of the poles to the S_1 foliation of the NW treading shears have calculated average strike and dip of 313°/75°NE. The equal area stereographic projection of the poles to the S_1-C foliation of the NE trending shears have mean calculated strike and dip of 058°/47°SE. (f) The L_1 plots as clustered data aligned to the southwest quadrant.

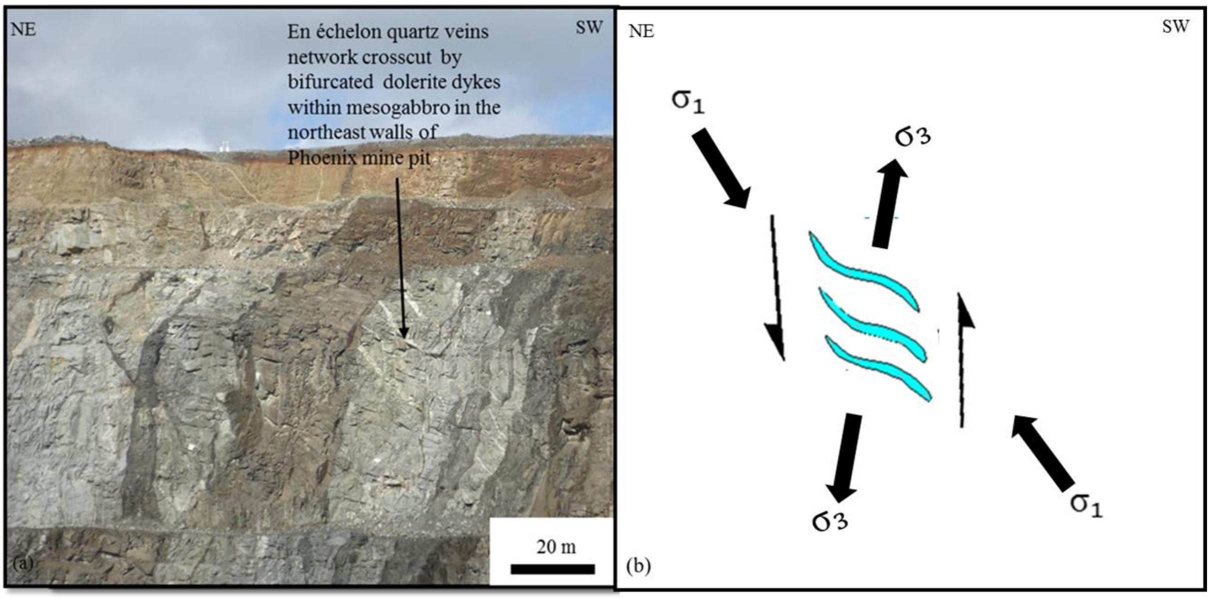

Figure 6.6: The Phoenix mine pit wall comprises of set of en echelon and tension gashes quartz veins. (a) The en echelon and tension gashes quartz veins (V_1) show thickness, which vary from approximately 1 - 3 metres and trends southwesterly. (b) The diagram illustrates the én echelon tension gashes quartz veins, which indicates down movement to the left.

The PMSZC consists of sets of en echelon tension gashes quartz veins (V_1), which were formed in fractures and acted as pathways for the propagation and accumulation of hydrothermal fluids (Figure 6.6a and b). The PMSZC hosts sulphide mineralisation, which has been actively mined since December 1994. The sulphide mineralisation consists of pyrrhotite and chalcopyrite and occurs as stringers, semi-massive and massive veins. The shears were pathways for the migration and entrapment of sulphide fluids as evidenced by the occurrence of sulphide mineralisation in massive veins in some localities (Figure 6.7a and b). The northeast trending shear zone crosscuts meta-melanogabbro, mesogabbro and leucogranodiorite in the Phoenix mine.

Figure 6.7: (a) The Phoenix Shear Zone Complex (PMSZC) hosts massive sulphide veins bounded by the foliation in some shear zones. (b) Schematic representation of the massive sulphide veins enclosed within the foliation in the PMSZC (UTM 35 K 0579716 mE, 7654055 mN).

6.1.2. Selkirk Mine Shear Zone (SMSZ)

The Selkirk Shear Zone (SMSZ) crosscuts the southern part of the study area (Figure 3.2). The SMSZ exhibits an anastomosing pattern and is approximately 2 kilometres in width. There are trenches of historic exploration and artisan mine shafts along the SMSZ.

The SMSZ crosscuts the mineralised mesogabbro and unmineralised leucogabbro units, where it is well exposed in some localities. It is bounded to the north by weakly foliated massive gossan outcrops that cap the non-operational underground stope. The SMSZ consists of foliation (S_1) (Figure 6.8). The foliation, S_1 consists of metamorphic minerals, hornblende and chlorite, which suggests greenschist facies metamorphism affected SMSZ. The S_1 is defined by average strike/dip orientation of 012°/55° to the southeast. The stretching lineation, L_1, exhibits a steep plunge and have a mean orientation of 72°towards 197° (Figures 6.9).

Figure 6.8: The metagabbro outcrops are characterised by well-defined foliation (S_1), which displays mean strike/dip of 57°/55° to the southeast and is intruded by pegmatitic quartz veins (UTM 35K 574869 mE, 7642148 mN).

The poles to foliation, S_1 are clustered close to the primitive circle, which suggests a steep dip angle for shear zone (Figure 6.10a) with a mean orientation of 011°/78°E. L_1 exhibits sub vertical distribution in the stereographic projection (Figure 6.10b) and have a mean orientation of 72° towards 197°.

Figure 6.9: The stretching lineation (L_1) shows plunge to the southwest at orientation of 72° towards 197° in the Selkirk mine (UTM 35K, 574965 mE, 7642145 mN).

The SMSZ comprises of buck quartz veins (V_1), which generally plunge 46° towards 209°. The SMSZ hosts sulphide mineralisation stringers as observed from drill-cores. The oxidised sulphide mineralisation is also identified from metagabbro units outcrops. The stringered sulphide mineralisation is dominantly made up of chalcopyrite. It can be concluded that the SMSZ acted as a conduit for remobilised sulphide mineralisation confined along fissures and stringer veins.

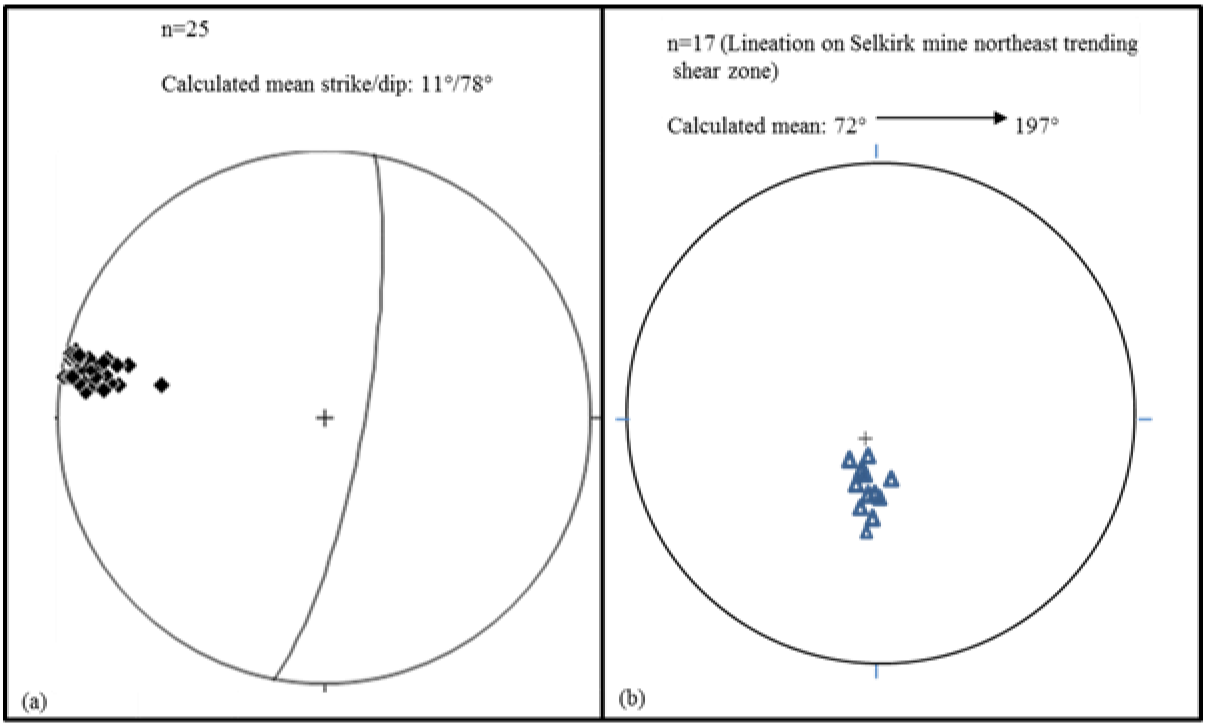

Figure 6.10: (a) Equal area stereographic projection of pole data to S_1 from the Selkirk mine. The S_1 is defined by clustered data with calculated mean strike and dip of 011°/78°SE. (b) The stereographic projection of the lineation (L_1) shows clustered distribution with subvertical lineation.

6.1.3. Rooikoppie Deposit Shear Zone (RDSZ)

The Rooikoppie Deposit Shear Zone (RDSZ) is situated in the eastern part of the study area. It is situated 2km north of Matsiloje village (Figure 3.5). It crops out approximately five kilometres on the Botswana side of the international border with Zimbabwe. Its extent beyond the international border is unknown since it has not been mapped. However, the Advanced Spaceborne Thermal Emission and Reflection Radiometer (ASTER) image produced using band combination of 4:6:8 shows that it is an anastomosing structure (Yajima and

Yamaguchi, 2013) and extends to the northeast across the international border (Figure 6.1). The RDSZ is approximately 1 kilometre wide. It crosscuts well-exposed outcrops of amphibolite. It hosts intermittent outcrops of gossan. Tati Nickel Mining Company (TNMC) has carried out the prospecting for Ni-Cu-PGEs sulphide mineralisation since 2010 with several trenches for gold prospecting.

Figure 6.11: The Rooikoppie deposit shear zone consists of foliation (S_1) and lineation (L_1). The S_1 shows northeast trending orientation. The L_1 is defined by elongated plagioclase and plunges to southeast (UTM 35K 589157 mE, 7648564 mN).

It consists of steeply dipping pervasive S_1 foliation and mineral lineation, L_1 (Figure 6.11). Metamorphic minerals that include hornblende, chlorite and epidote define S_1. L_1 is defined by elongated aggregates of plagioclase.

The analysis on S_1 data shows the calculated average strike/dip of 027°/76° dipping to the SE. The distribution of the poles to S_1 is clustered proximal to the primitive circle (Figure 6.12a). The distribution pattern of the poles to S_1 is characteristic of data obtained from C planes. Therefore, the S_1 is defined by C fabric associated with re-activation in the Rooikoppie deposit shear zone. L_1 plunges to the southwest with mean calculated plunge and azimuth of 79° towards 199° and shows sub-vertical clustered distribution (Figure 6.12b).

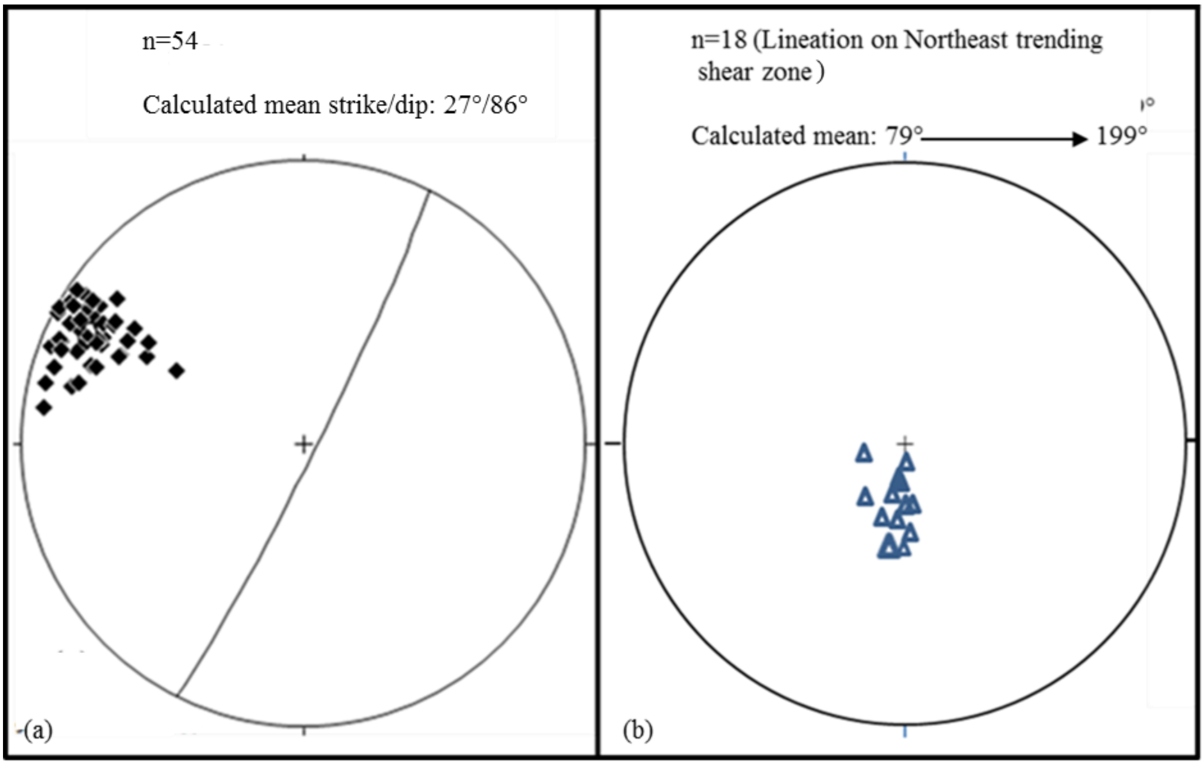

Figure 6.12: (a) Equal area stereographic projections of poles to S_1 in the RDSZ. The S_1 display a plane consistent with the calculated mean strike and dip of 027°/86°SE (b) The stereographic projection of the mineral lineation (L_1) displays clustered data in the southeast quadrant, consistent with a steep plunge.

The RDSZ continues to be of great exploration interest to TNMC. The RDSZ hosts nickel-barren massive sulphide veins that vary from approximately 1-5m in length. Barnes and Lightfoot (2005) suggested that the RDSZ provided pathway for the migration and accumulation of sulphide fluids, which formed Ni deficient pyrrhotite possibly due to incapacity to derive Ni from ultramafic, mafic, and crustal sulphur.

6.2. Second Deformation event, D_2

The second deformation event, D_2 is of brittle-ductile nature and is evident from presence of strike slip faults (F_2), foliation (S_2), folded and asymmetric boudinaged veins (V_2). The strike-slip fault, F_2 is observed in the Phoenix mine.

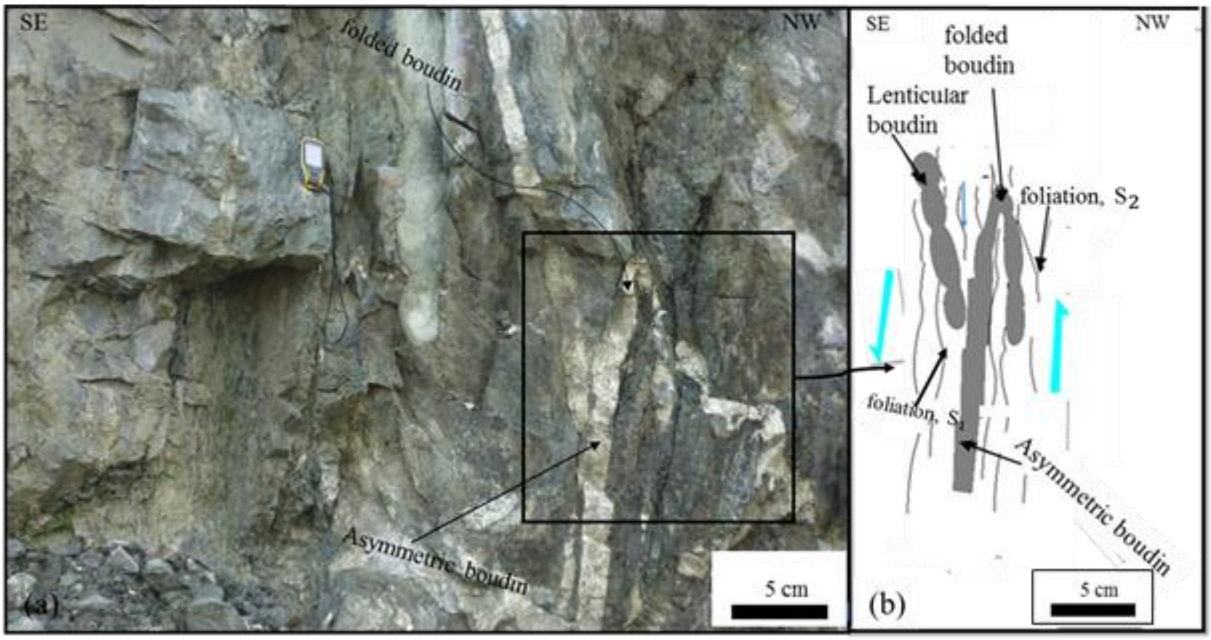

Figure 6.13: (a) The folded boudinaged quartz vein (V_2) has asymmetric or sigmoidal shaped limbs with northwesterly verging direction. The fold axis reflects re-activation of NW-SE oriented compression forces associated with second deformation event, (D_2). (b) A schematic representation of the set of folded boudinaged quartz veins. The asymmetric quartz boudinaged limbs shows down movement to the right left sense of shear i.e. dextral displacement (UTM 35 K 0579478 mE, 7654963 mN).

6.2.1. Foliation, S_2

The foliation, S_2 incorporates the asymmetrical and folded boudinaged quartz veins in the Phoenix mine. The S_2 wraps around the fold axes and trends parallel to the limbs of the asymmetric quartz boudins in the northwest part of the Phoenix mine. (Figure 6.13a and b).

6.2.2. Asymmetrical and folded boudinaged quartz boudins

The asymmetrical boudinaged quartz veins (V_2) show northwest side up component (Figure 6.13a and b). Therefore, the asymmetrical boudinaged quartz veins reflect extensional shearing in the northwest part of Phoenix mine. The V_2 indicate northwest verging direction in the Phoenix mine.

6.2.3. Faults

D_2 is also associated with normal faults (F_2), which affected the granodiorite units in the Phoenix mine. The F_2 could possibly represent extension of the lineaments network revealed in ASTER Red-Green-Blue (RGB) composition (band ratio 4:6:8) image in Figure 6.1. The exposure at Phoenix Mine pit is good and F_2 is recognisable though to a restricted extent (Figure 6.14).

Normal faults occur in the east-central and northeastern parts of the Phoenix mine. The east-central normal fault (NE-F1) is traced for approximately 30 metres i.e. between 840 metres and 870 metres levels of the Phoenix mine pit. It is characterised by displacement of extensional quartz veins downwards for approximately 30 centimetres (Figure 6.14a and b). It exhibits the deflection of en echelon quartz veins, which trend northeasterly. The deflection of the en echelon quartz veins suggests that they cut through the normal fault. The K-feldspar rich veins demonstrate displacement, which point out to crosscutting by normal fault, F_2 in the Phoenix mine (Figure 6.14c and d). The dolerite dykes are characterised by jogs, which could be effect of F_2, which suggest that the dolerite dykes intruded after the development of faulting in the Phoenix mine.

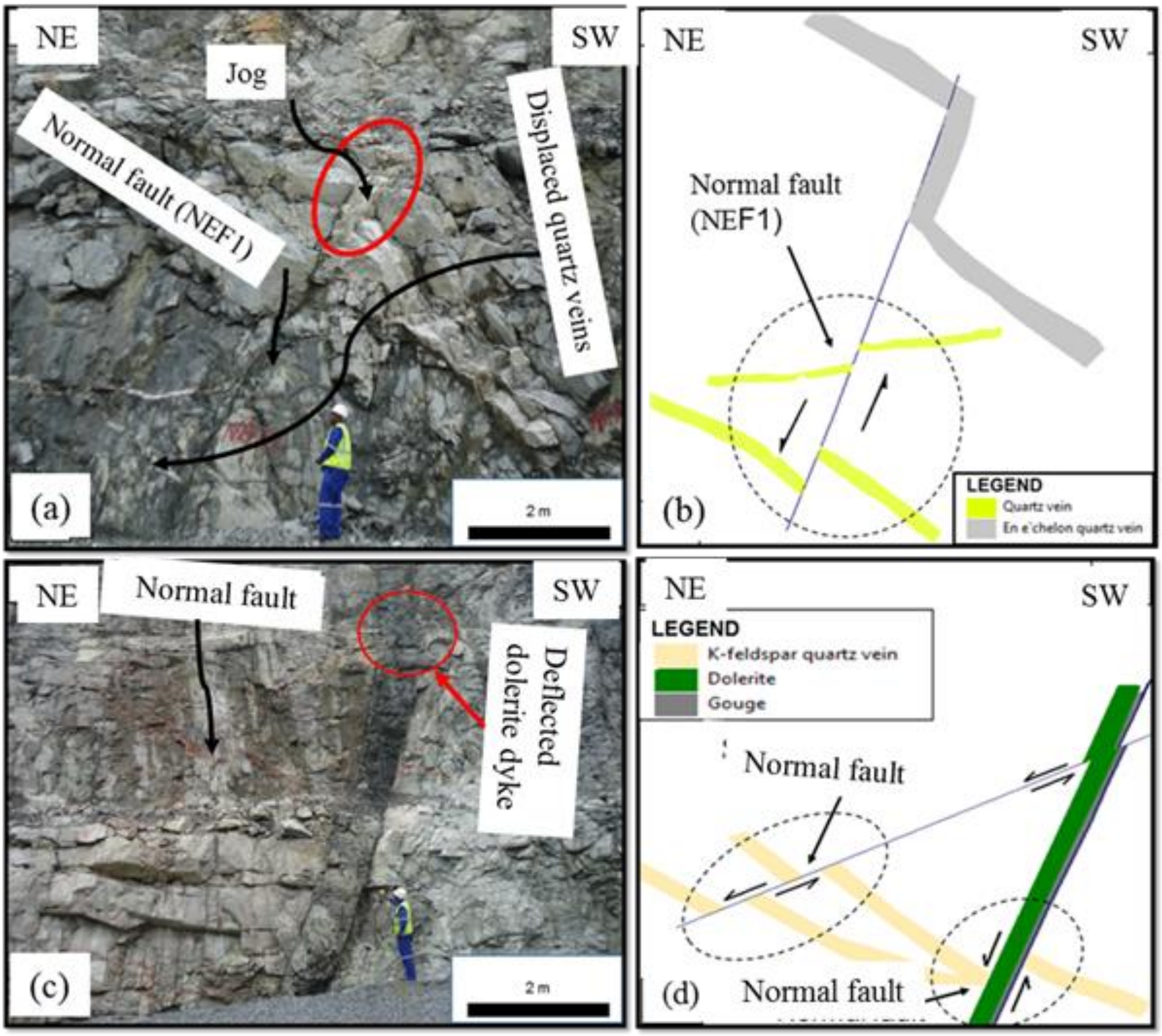

Figure 6.14: (a) The normal fault (NE-F1) is exposed in the northeastern part of the Phoenix mine. The normal fault (NE-F1) crosscuts and displaces the quartz veins downwards and resulted in formation of jog within the northeast trending quartz vein (b) The diagram depicts fault, which crosscuts quartz veins. (c) The normal fault shows the displacement of the K-feldspar rich veins. (d) The schematic diagram depicts a displacement of the K-feldspar rich veins and jog in the dolerite dyke.

6.3. Third Deformation event, D_3

The third deformation event, D_3 is a brittle regime and is characterised by the development of fracture and stylolitic cleavages, S_3. The S_3 crosscut S_1 and S_2 in TSMDC.

The stylolitic cleavage, S_3 is characterised by anastomosing fractures filled with calcite (Figure 6.15).

Figure 6.15: The amphibolite outcrops shows moderately spaced array of stylolitic cleavages (S_3). The uniform manifestation of the stylolitic cleavage marks the youngest deformation in the Rooikoppie deposit.

The S_3 is very pervasive in amphibolite outcrops in the Rooikoppie deposit. It trends in perpendicular manner to the strike of the amphibolite. Cleavage fractures and joints are common in gabbro and granodiorite units.

CHAPTER 7.0: DISCUSSION

The study of Phoenix, Selkirk mines, Tekwane and Rooikoppie Ni-Cu-PGEs deposits metagabbro units and controlling factors to the current locations of these mines and deposits provides opportunity for comparison to other Ni-Cu-PGEs mines and deposits worldwide. Given the outstanding issues, which include; limited understanding of geology and geochemical relationships between Phoenix, Selkirk mines, Tekwane and Rooikoppie Ni-Cu-PGEs deposits, petrogenesis and control factors on the current locations of these mines and deposits, it is important to present their full synthesis and exploration criteria.

7.1. Geology of TSMDC metagabbro facies

The different features of the gabbro units are of high regard considering their economic vitality in this research. Given the field relationships evidence, the tectono-magmatic sequence of TSMDC consists of different types of gabbro units. These include melanogabbro, mesogabbro and leucogabbro (Figures 4.1-4.11). This classification of the gabbro units is based on their different compositional character, which is consistent with the studies of Dirks (2004, 2005). The petrographic variations in these gabbro units are spatially associated with plagioclase contents. Generally, the melanogabbro contains ~25% plagioclase whereas mesogabbro constitutes higher content of ~35% plagioclase. The leucogabbro contains ~55% plagioclase, which reflects its distinct greyish appearance as compared to mesogabbro and melanogabbro. The significant petrographic variation in the melanogabbro, mesogabbro and leucogabbro is likely reflective of different crystallisation phases during emplacement of their source magmas. The gabbro units host sulphide mineralisation interstitial to the silicate mineralogy (Figure 4.30), which may reflect that the formation of the sulphide mineralisation occurred during emplacement of the gabbro units. There is strong relationship between the gabbro units and sulphide mineralisation in TSMDC, although some gabbros do not contain sulphide mineralisation, which might imply source magmas of these gabbro units experienced different petrogenetic influences during emplacement periods. Van Geffen (2005) recognised that the age of sulphide mineralisation of 2600 ± 200 Ma based on U/Th–Pb dating on monazite obtained in Phoenix mine mesogabbro. The sharp contact between melanogabbro and tonalite might reflect structural control, as both units resemble similar grain size and texture at their contact (Figure 4.2). Thus, the emplacement of parent magmas of melanogabbro and tonalite might have been coeval though there is no proof from geochronological study on these units. The Phoenix mine mesogabbro contains mafic enclaves, possibly derived from melanogabbro and other mafic units, which might suggest influence of lineaments. These gabbro units form different contacts with magmatic units, which include tonalite, quartz diorite, amphibolite and andesite. The occurrence of the gabbroic units in contact with other lithological units (Figure 7.1) is consistent with lithologies reported by previous workers: Key (1973), Tombale (1992), Carney et al. (1994), Maier et al. (2007) and Bagai (2008). In the context of Phoenix mine where the study recognises coincidence of the NW and NE trending shear zones with lineaments of similar orientations as interpreted from the ASTER image (Figure 6.1), there could have been migration subsequent to interaction of source magmas of mesogabbro and other mafic units. The gabbro units are crosscut by shear zones, which demonstrate that they were affected by the second deformation event, D_2 in response to the back arc subduction of the mafic slab of the Limpopo belt unto the felsic basement of the Zimbabwe craton (Kampunzu et al., 2003; McCourt et al., 2004; Bagai, 2008). There is a set of granodiorite units, which crosscut metagabbro units and occur as, dykes and small plutonic bodies in and around Phoenix, Selkirk mines and Tekwane deposits. The young granodiorite units have similarity to the granodiorite, which gave 1022 ± 16 Ma based on U-Pb SHRIMP zircon ages of Phoenix mine leucogranite (Van de Wel et al., 1998). The granodiorite and dolerite intrusions are the youngest units, which intruded the gabbro units in TSMDC.

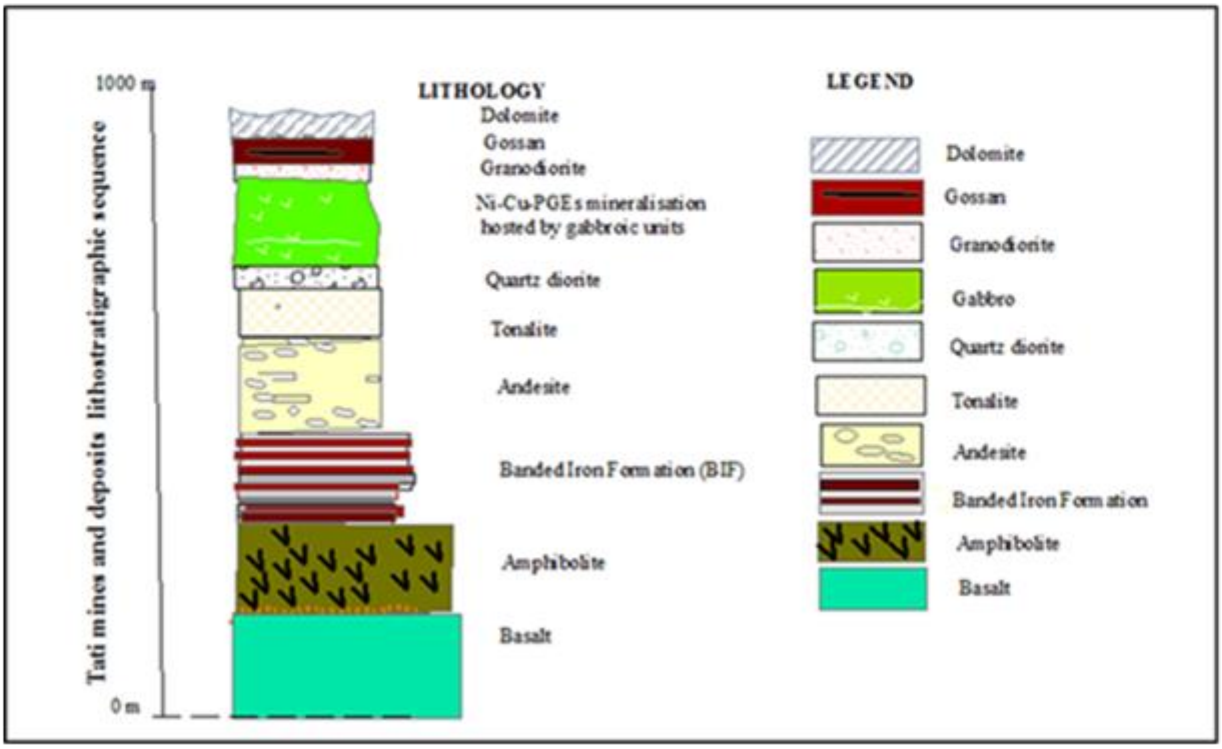

Figure 7.1: Lithostratigraphy of TSMDC, showing gabbroic units with tonalite and quartz diorite.

7.2. Local and regional structural models for the Phoenix, Selkirk mines, Tekwane and Rooikoppie deposits.

The first deformation event, D_1 is characterised by fold (fo_1), foliation, S_1 and boudinaged and extensional quartz veins (V_1). The stratigraphy of TSMDC was affected by folding, fo_1, which resulted in the steeply dipping prevalent foliation, S_1 and stretching mineral lineation, L_1. The axial plane of fo_1 trends NNE whereas the S_1 consistently strike northeasterly and L_1 plunges SW. This means, the D_1 structures noted in this study corresponds well to the observation made by Key (1973) and Tombale (1992), who recognised D_1 as composed of folding (fo_1), which occurred subsequent to the NW-SE directed compression forces.

The identification of anticline patterns from the ASTER image suggests existence of folded units in TSMDC (Figure 6.1). However, the folding is difficult to record in the field. The occurrence of folded lithological units imply vertical movement or uplift of the basal units to the gabbro units during NW directed compressive forces, which affected TSMDC. This supports the studies, which show TSMDC located in Tati greenstone belt, which is in the margin of Zimbabwe craton experienced exhumation because of the NNW-SSE directed compressive forces (Roering et al., 1992; Treloar et al., 1992; Rollison and Lowry, 1992; Van Reenen, 1992 and Laurent et al., 2014). The thickened crust was exhumed and triggered tensional stress, as result of isostatic conditions in the lithosphere, which gave rise to development of array of crustal lineaments in TSMDC, which are coincident with the regional lineaments in the Zimbabwe craton (Dirks and Jelsma, 2002). The distribution of Ni-Cu-PGEs mines and deposits was subjected to weak zones positioned during the transport and subsequent concentration of the sulphide fluids into source magmas of gabbroic units. The lineaments acted as pathways for magma and influenced its flow direction, sulphide melt segregation and rate of cooling (Naldrett, 2004; Lightfoot, 2007). The crustal lineaments generated because of gravitational and extensional collapse, which allowed for migration of source magma of gabbro and segregation of sulphide minerals from particular location to another on a regional scale within the Zimbabwe craton (Pirajno, 2000; Ernst and Jowitt, 2013). Thus, the transportation of the source magma of host gabbro units and segregated sulphide minerals might have occurred from distant locality and generated the current geometry of the mines and deposits. Thus, NNE trend of the Phoenix and Selkirk mines and Tekwane deposits is coincident with NNE trending crustal lineaments as studied by Jelsma and Dirks (2002). Therefore, the geometry of the mines and deposits fall within the regional structural trend, which is associated with the crustal lineaments in the southwest margin of Zimbabwe craton.

On a local scale, Phoenix, Selkirk mines, Tekwane and Rooikoppie deposits are characterised by development of sets of shear zones, which accommodated accretionary forces during subduction of the mafic slab of the Limpopo orogenic belt unto the felsic basement of the Zimbabwe craton consistent with the study of McCourt et al., (2004). The Phoenix mine northwest and northeast trending shear zones S-C foliations indicate that there was a change from the sinistral to dextral sense of displacement (Figure 6.5), which resulted in the back rotation or movement of block (Figure 7.2). The sinistral and dextral displacements gave rise to a space problem associated with crustal extensional collapse. The transport of the buoyant mafic and felsic magmas in the spaces created by the displaced blocks resulted in upward shift associated lineation, L_2 associated with Phoenix, Selkirk mines and Rooikoppie shear zones. Thus, the Phoenix, Selkirk mines, Tekwane and Rooikoppie are located at their current position due to the influence of the local spaces formed by the rotations or displacement of blocks.

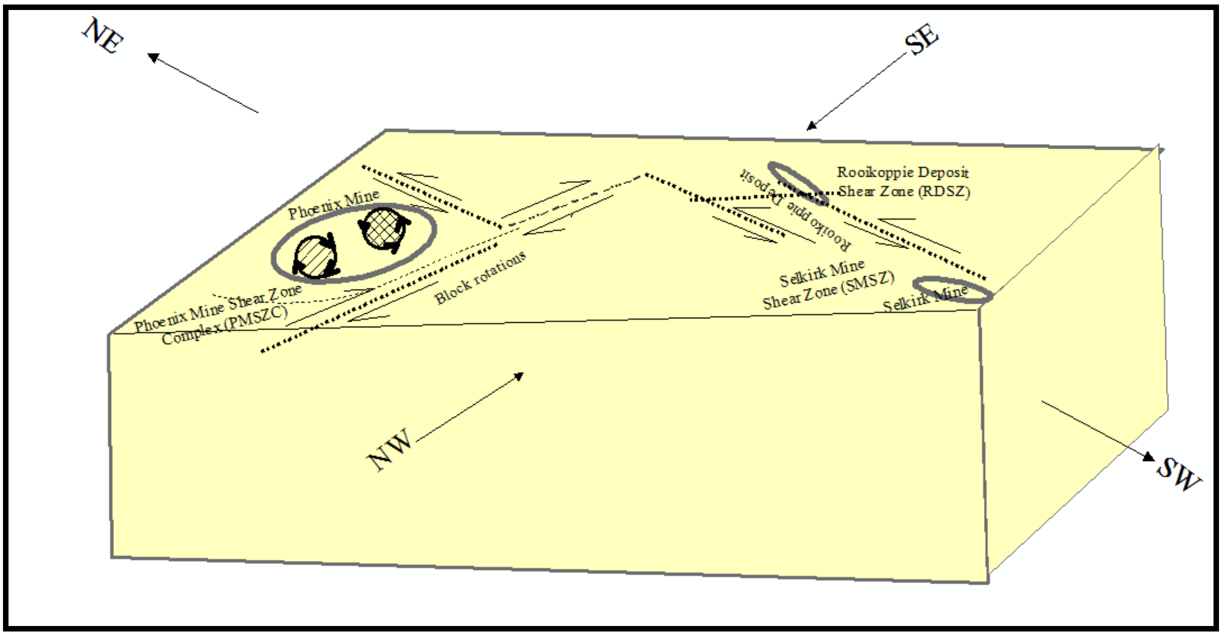

Figure 7.2: The block diagram shows the extensional shear zones generated subsequent to the NW-SE compressional forces, as result of convergence of the mafic slab of the Limpopo belt unto the felsic crust of the Zimbabwe craton. The anticlockwise and clockwise block movements within the Phoenix mine resulted in the conjugate pattern of NE and NW trending shear zones during D_2.

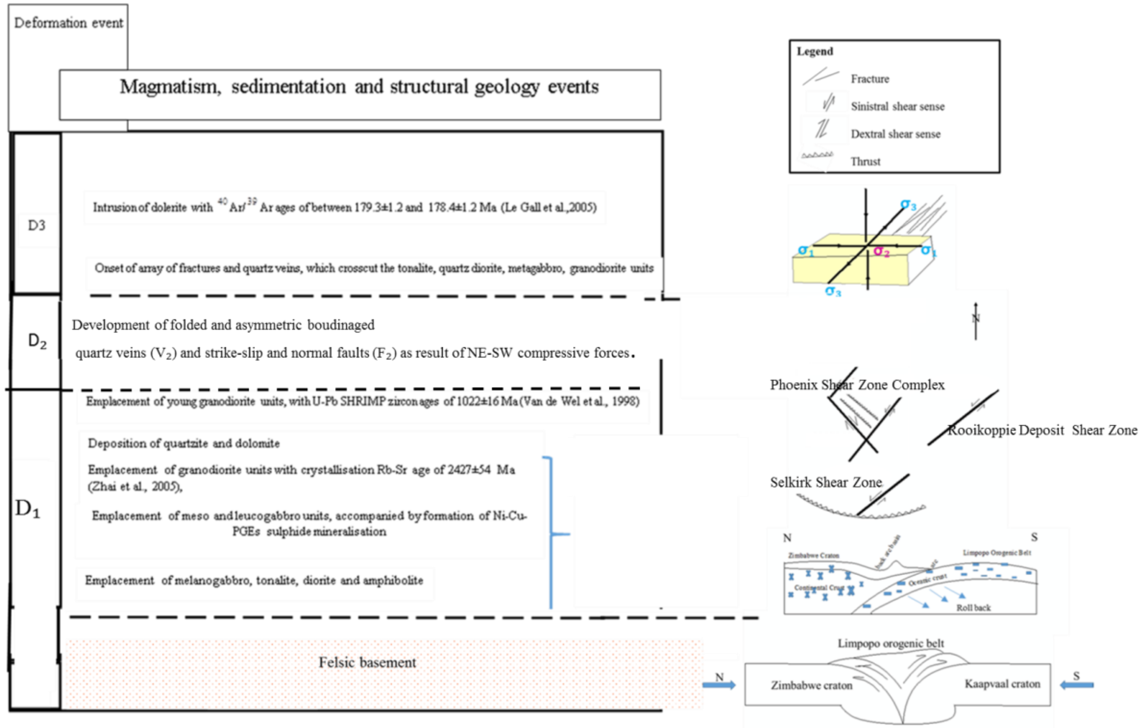

Figure 7.3: Timing relationship of deformation events, magmatism, sedimentation and structural geology of the Phoenix, Selkirk mines, Tekwane and Rooikoppie deposits. The deformation event, D_1 is defined by emplacement of the variety of gabbro units i.e. melanogabbro, mesogabbro and leucogabbro, emplaced synchronously in the Phoenix, Selkirk mines, Tekwane and Rooikoppie deposits. The deformation, D_2 is marked by development of folded and asymmetric boudinaged quartz veins where the deformation, D3 is defined by fractures and stylolitic cleavages.

7.3. Petrogenesis of gabbro units and contact lithologies of TSMDC

7.3.1. Magma source of the gabbro and contact lithologies

The gabbro units of TSMDC qualify to belong to sodic fields, which possibly suggest their source magmas are associated with alkaline composition (Figure 5.1). The TSMDC gabbro units generally plot around the tholeiitic and calc-alkaline boundary, which suggests their magmatic differentiation, is characterised by transitional from tholeiitic to calc-alkaline affinity (Figure 5.2). In the context of Phoenix mine, the magmatic source of the gabbro units is generally of tholeiitic type in agreement with studies of Bagai (2008) and Tombale (1992). The Tekwane deposit melanogabbro and mesogabbro plot within tholeiitic and calc-alkaline fields, which demonstrate transitional trend from iron enriched differentiation to calc-alkaline enriched composition. The emplacement of gabbro units in TSMDC resulted from fractional crystallisation of their parent magmas as dominated by pyroxene and plagioclase (Figure 5.3). The abundance of pyroxene and plagioclase as primary minerals of the gabbro units of TSMDC corroborate the positive correlations, which exists for MgO against FeOtotal, Cr_2O_3, CaO, Al_2O_3, TiO_2, and NiO (Figure 5.3a-f). Thus, the petrographic variations of the gabbro units in TSMDC could possibly be associated with pre and post emplacement in structurally controlled zones as influenced by D_1, D_2 and D_3. In addition, the granodiorite units formed from magmatic differentiation as evidenced by negative correlation of SiO_2, against MgO, Fe_2O_3, CaO, and Al_2O_3 (Figure 5.4a-d). Meanwhile, the positive relationship shown by SiO_2 against Na_2O and K_2O demonstrates the fractional crystallisation was dominant process, which generated quartz and K-feldspar in these granodiorite units. The contents of quartz and K-feldspar dominate the primary mineralogy of the occurred within lineaments formed after NNW-SSE shortening of the crust of Tati greenstone belt, where TSMDC is located. Consequently, the intimate occurrence of gabbro with granodiorite is possible due to migration and emplacement of their parent magmas in the same lineaments. Furthermore, a potential explanation exists for the fractionation of olivine in the primary or source magmas of gabbroic units as evidenced by the positive correlation of MgO and Ni and Cu (Figures 5.5 and 5.6). The evidence provided by the negative correlation between MgO and Sc and Y also supports the fractionation of plagioclase and pyroxene in gabbroic units within TSMDC

(Figure 5.7a and b). The positive correlation exists for MgO against V, Zr, Cr, Nb, Co and Pb, which is consistent with fractional crystallisation of plagioclase and pyroxene, as reflected in Figure 5.1a-f. The positive correlations exists between Ce and Pb and La and Nb (Figure 5.9a-b). In contrast, the La and Rb plot is characterised by negative correlation (Figure 5.9c). The inconsistent correlations as shown by Ce, Pb, La, Rb and Nb plots, suggest magma mixing between mafic and felsic units in TSMDC, possibly as influence of magma propagation through lineaments during D_1 in TSMDC.

The chondrite normalised REE plot shows different features, which suggest petrogenetic implications in TSMDC. The enrichment of light rare earth elements (LREE) relative to depletion of heavy rare elements (HREE) suggests partial melting and crystal fractionation processes, where plagioclase was involved (Figures, 5.10 and 5.11). The slight positive Eu_N anomaly is associated with accumulation of plagioclase, in addition to the crystallisation of pyroxene (Figures 5.10 and 5.11). Generally, the Phoenix mine melanogabbro, Rooikoppie deposit quartz diorite and mesogabbro display negative K_N and P_N, which suggest that these elements depleted during mobilisation of fluids associated with metasomatism. The negative anomalies of Ta_N and Nb_N indicated by mafic and felsic units of TSMDC suggest subduction setting (Rollison, 1993). The chondrite-normalised trace elements patterns for the representative granitoids and gabbros are identical, which suggest similar source magma. In the context of the regional setting of the Tati greenstone belt, the occurrence of gabbro units and voluminous granodiorite supports conclusion made by Kampuzu et al. (2003) that generated partial melts underwent high degree of fractionation, which resulted in formation of dominant silica rich lithological units. Secondly, multi elements REE diagrams show negative gentle slope to nearly flat profiles, which possibly suggests partial melt generated in shallow crustal depths of less than 40 kilometres (Rollison, 1993). The generated partial melts contributed to the mafic and felsic magmatism, which evolved through fractional crystallisation processes in TSMDC and followed by their emplacement in weak zones formed during D_1 (Figures 7.2 and 7.3).

7.3.2. Tectonic setting of the TSMDC gabbro and contact lithologies

The studied gabbros plot mainly on volcanic arc basalt (VAB) and within plate basalt (WPB) fields in Zr/Y against Zr (Figure 5.13.a). The gabbbroic units plot in the oceanic intraplate basalt (OIB) and arc basalts fields (ARC) (Figure 5.13b). Therefore, it is highly possible that the gabbroic units were formed in volcanic arc associated with oceanic plate. The absence of most of units plotting in the mid oceanic basalt affinity suggest that the gabbroic units were formed in an oceanic plate in the periphery of the continental crust. The expectation would be whenever gabbroic units show oceanic affinity, there should also be characteristic of mid oceanic ridge basalts. In this context, such a character to clearly ascribe the TSMDC gabbroic units to oceanic environment is not convincing. The formation of gabbroic units in volcanic arc environment is backed by the plotting of Phoenix mine and Tekwane deposit gabbros in the island arc and continetal margin fields (Figure 5.14a).

The formation of gabbro and contact lithologies including granodiorite occurred in volcanic arcs associated with continental margin (Figure 5.14a and b), which is in support of their current location in proximity to the Zimbabwe and Kaapvaal cratons margin. Furthermore, the felsic and mafic units plot mainly on the active continental margin fields (Figure 5.14b), which support the dominance of continental environment for the formation of gabbroic units and contact lithologies in TSMDC. The plotting of the TSMDC granitoids in the continental arc field supports subduction regime during deformation event, D_2 consistent with studies of Tombale (1992), Kampunzu et al. (2003) and Bagai (2008). Moreover, the granitoids are clustered in the post-collisional granite field, which shows strong affinity to generation in a post subduction environment (Figure 7.4 a-c).

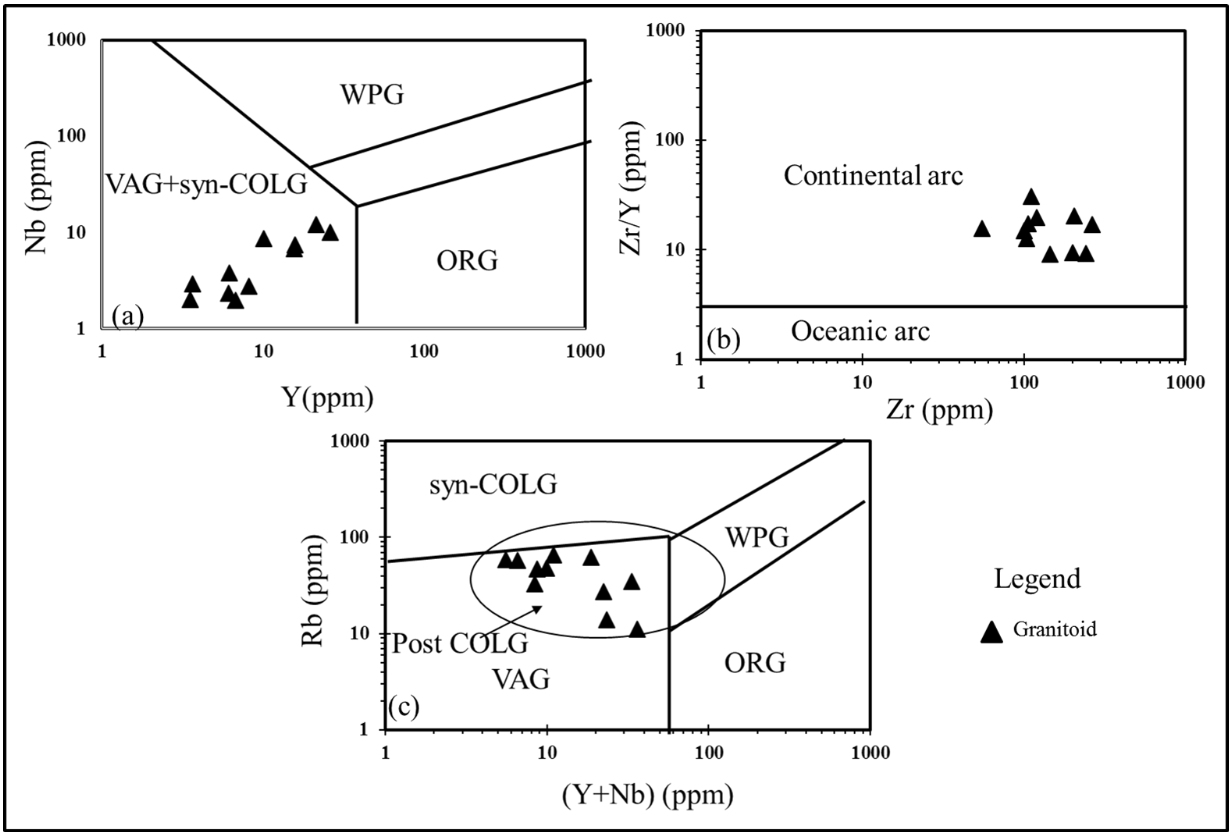

Figure 7.4: The tectonic discrimination diagrams of Pearce et al. (1984) for granitoids samples obtained from TSMDC. (a) Nb against Y, (b) Zr/Y against Zr and (c) Rb against Y+Nb. COLG (Collisional granites), WPG (Within plate granites), VAG (Volcanic Arc Granites), ORG (Oceanic Ridge).

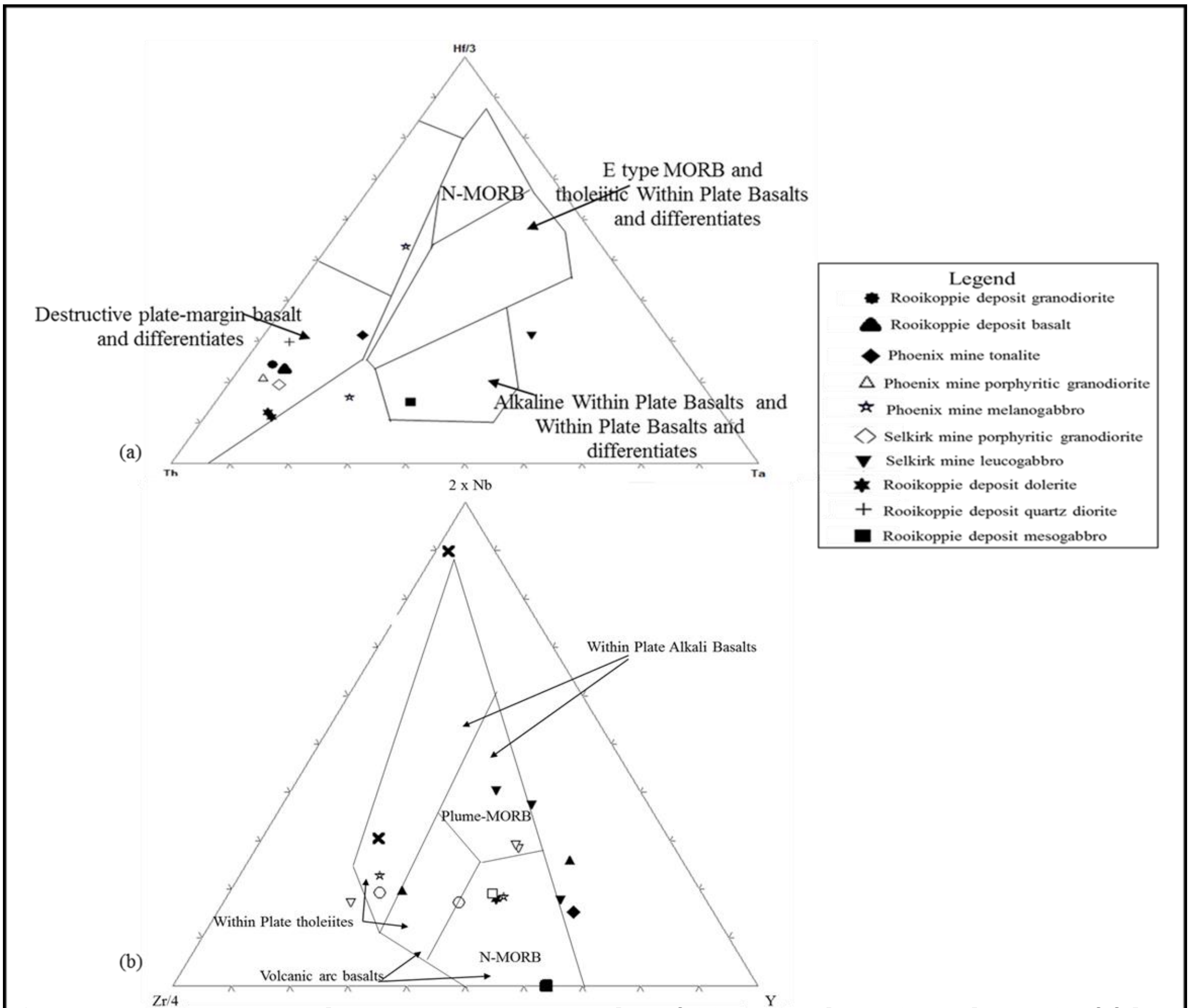

Figure 7.5: The tectonic discrimination ternary plot of (a). Hf/3-Th-Ta (Wood, 1980) of felsic and mafic units in TSMDC and (b).2xNb-Zr/4-Y ternary plot, which shows distribution of mafic and units in within plate tholeiites, plume MORB and within plate alkali basalts.

In sharp contrast, the tectonic affinity of the mafic and felsic units is defined by the clustering of the samples within destructive plate margin and differentiates fields, which signify emplacement in rift associated environment (Figure 7.5a). Therefore, source of mafic units could possibly be linked to the continental margin (Figure 5.14a-b). In essence, the plot of mafic units in the continental margin could possibly reflect their preferable distribution within adjacent rift environment. The development of mafic and felsic units in a rift imply the following possibilities; the mafic and felsic units could have formed in extensional setting, which is also supported by presence of carbonate sediments in TSMDC. The plotting of mafic units in the mid oceanic ridge basalts (MORB) field suggests that these units formed by ascent or as plumes (Figure 7.5b). Thus, the rise of plumes could possibly be attributed to presence of extensional setting environment, which would require for rift zones to allow for magma propagation or ascent of magma plumes. The volcanic arc magmatism resulted in mafic and felsic units, which were generated within oceanic plate closely associated with active continental margin in extensional setting in TSMDC.

7.4. Comparisons between the TSMDC and other Ni-Cu-PGEs mines and deposits

The TSMDC shows tectonostratigraphic sequence, which is similar to the Lusatian Block in Saxony, Germany, Duluth Ni-Cu-PGEs complex and Eagle`s Nest, Eagle Two, Blackbird, Big Daddy, AT12 and Black Thor Ni-Cu mines in many features. The Lusatian Block comprises of Ni-Cu-PGEs mineralised and unmineralised gabbro in contact with voluminous granodiorite blocks (Sandmann and Gutzmer, 2014). Several granitic and mafic dykes crosscut the gabbro units, which consist of primary mineralogy dominated by pyroxene, plagioclase and minor quartz formed under greenschist facies.

The Nokomis, Maturi, Dunka Pit, Birch Lake, Spruce Rd mines and deposits will be reported as Duluth Ni-Cu-PGEs complex. The Duluth Ni-Cu-PGEs complex consists of leucogabbro and mesogabbro units. The disseminated and massive Ni-Cu-PGEs mineralisation occurs within the mesogabbro and leucogabbro units in the Duluth Ni-Cu-PGEs complex. The Eagle`s Nest, Eagle Two, Blackbird, Big Daddy, AT12 and Black Thor Ni-Cu mines of the McFaulds Lake greenstone belt in the Superior province comprise of tonalite, gabbroic units and granodiorite, which overlay the gneissic granite basement (Mungall et al., 2010).

The TSMDC resembles structural orientation in similar way to the Okyabrysk, Taimyrsk, Gluboky, Skalisty, Zapolyamy, Medvezhi, Eastern deeps, Ovoid and Reid Brook Zone mines and deposits. The Okyabrysk, Taimyrsk, Gluboky, Skalisty, Zapolyamy, Medvezhi, Eastern deeps, Ovoid and Reid Brook Zone mines and deposits are characterised by structural features: faults, shear zones, which provide the local and regional controls of Ni-Cu-PGEs mineralisation in these mines and deposits (Naldrett, 2004; Lightfoot et al., 2012;

Lightfoot and Evans-Lamswood, 2015). The present position of Okyabrysk, Taimyrsk, Gluboky, Skalisty mines, Zapolyamy and Medvezhi deposits is associated with the localisation of fractures, which provided pathways for transportation and concentration of mineralised and unmineralised source magmas of gabbroic units (Saumur et al., 2015). On a regional scale, the Okyabrysk, Taimyrsk, Gluboky, Skalisty mines, Zapolyamy and Medvezhi deposits are aligned along N-S and NE-SE crustal lineaments. Given the geometry of these deposits, the Noril`sk-Kharaelah Fault is considered to have influenced such morphology (Zenko and Czamaske, 1994).

The structural setting of the gabbro hosted Ovoid, Eastern deeps and Reid Brook Zone deposits of the Voisey`s bay complex located in the margin of Torngat orogenic belt formed in response to the collision between the Nain and Rae provinces during early deformation event, D_1 (Van Kranedonk, 1996). The oblique subduction of the core zone of the Torngat orogenic belt under the Nain craton resulted in extensional collapse associated with extension forces, which give rise to faults and fractures during second deformation event, D_2 (Funck and Louden, 1999). The resultant block displacements provided pathways for the emplacement of gabbroic units and segregation of sulphide minerals (Lightfoot et al., 2012; Lightfoot and Evans-Lamswood, 2014). The position and trend of the Reg Dog fault and crustal lineaments controlled the regional geometry of the Ovid, Eastern deeps and Reid Brook deposits (Saumur et al., 2015). The Duluth Ni-Cu-PGEs complex is located in the oblique convergent margins of cratons as result of subduction, which resulted in generation of mafic and felsic magmas as studied by Begg et al. (2010).

7.5. Exploration criterion of Phoenix, Selkirk mines, Rooikoppie and Tekwane deposits

The key understanding of the mechanisms responsible for the formation of Phoenix, Selkirk mines, Rooikoppie and Tekwane deposits is vital for identification of Ni-Cu-PGEs exploration targets in and around these mines and deposits. Thus, this dissertation affords the opportunity to apply the current understanding as systematic guide or approach to understand ore extension zones and discover additional Ni-Cu-PGEs deposits. It is important to utilise and relate the key characteristics of Ni-Cu-PGEs with similar lithologies, structure and petrogenesis in build-up of exploration model in Phoenix, Selkirk mines, Rooikoppie and Tekwane deposits.

The geological, whole geochemistry and petrogenetic features of the gabbroic units, which host Ni-Cu-PGEs mineralisation in TSMDC point to four critical main processes for exploration model. These include; petrographic features, fractional crystallisation, tectonic setting and deformation. In the context of the variable petrographic features within gabbroic units, the Phoenix mine mesogabbro and leucogabbro units consistently consist of sulphide mineralisation. Furthermore, Selkirk mine mesogabbro hosts sulphide mineralisation. Tekwane deposit mesogabbro and melanogabbro contain sulphide mineralisation. Nevertheless, some gabbro units do not consist of Ni-Cu-PGEs mineralisation in Phoenix, Selkirk mines and Rooikoppie deposit. These include; Phoenix mine melanogabbro, Selkirk mine leucogabbro and Rooikoppie deposit mesogabbro. The inconsistency in spatial association of sulphide mineralisation and gabbroic units bring complex reckoning of these sulphides mineralisation hosts. Thus, the identification of the gabbroic units need to be thoroughly complemented by identifying the triggers for sulphide saturation. Thus, detailed geochemistry study of the gabbro units should be considered as one of the early stages in identification of exploration targets.

The gabbro units generated from partial melting as evidenced by enrichment of LREE relative to depletion of HREE (Figures 5.10 and 5.11), which gave rise to partial melts, emplaced as gabbro units in extension setting associated with the southwestern margin of Zimbabwe craton (Figure 7.7a-b). Thus, the degree of magma differentiation and interaction with craton margin environment are favourable geochemical traps for formation of Ni-Cu-PGEs mineralised gabbro deposits. Therefore, the Phoenix and Selkirk mines, Tekwane deposit mesogabbro should be highly considered as most prospective targets for Ni-Cu-PGEs mineralisation. Notwithstanding the limited outcropping of the Phoenix and Selkirk mines, Tekwane deposit mesogabbro, the identification of such gabbroic units remains challenge. Thus, to account for the identification of subsurface mesogabbro units, there is need for the use of Space borne Thermal Emission (ASTER) and Reflection Radiometer (TIR) images. The use of gravity survey would be also good approach in interpreting the spatial distribution of gabbro units, which occur as anomalous bodies. The research has also established that there is spatial association between major trends of structural lineaments mainly NW-SE and NE-

SW with known gabbro bodies in these mines and deposits. Therefore, this relationship between local and regional lineaments and gabbro bodies offers an opportunity to test the extension of such mines and deposits in the same trends. The distribution of crustal lineaments should be further identified from the magnetic, electromagnetic surveys images and geological mapping. The structural trends are considered useful exploration guides as confirmed by understanding of the ore bodies in the Okyabrysk, Taimyrsk, Gluboky, Skalisty mines, Zapolyamy and Medvezhi deposits coincident with structural features. The application of the relationship between these mines and deposits with structures opened up, for expansion and exploration in the peripheries (Makitch et al., 2014).

The database should be developed to allow for management and integration of geological, structural geology, petrogenetic, remote sensing and geophysical surveys data. The exploration targets can be successfully achieved through integration of these data, given the complex geological, petrogenetic and structural features in the Phoenix, Selkirk mines, Tekwane and Rooikoppie deposits.

CHAPTER 8.0: CONCLUSIONS AND RECOMMENDATIONS

8.1: CONCLUSIONS

The study of the geology, whole rock chemistry and petrogenesis of metagabbro and contact lithologies led to the following conclusions:

The TSMDC comprises of three types of gabbroic units: melanogabbro, mesogabbro and leucogabbro. The melanogabbro generally occurs in Phoenix mine where it is barren of Ni-Cu-PGEs mineralisation whereas the mesogabbro is the dominant gabbroic unit in TSMDC. The melanogabbro contains hornblende (~35%), plagioclase (~25%), clinopyroxene (~20%), biotite (~6%) and olivine (~8%), Titanite (~4%) and apatite (~2%). The mesogabbro is composed of hornblende (~30%), plagioclase (~35%), clinopyroxene (~20%), biotite (~5%) and olivine (~5%), apatite (2%) and titanite (3%). The leucogabbro contains hornblende (25%), plagioclase (55%), clinopyroxene (12%), biotite (3%) and olivine (3%) and apatite (2%).

The melanogabbro, mesogabbro and leucogabbro contain a wide compositional range in MgO (4-17 wt. %), FeOt (5-20 wt. %), SiO_2 (45-52 wt. %), Al_2O_3 (10-17 wt. %) and CaO (5-15 wt. %), which suggest highly magmatic evolution.

The mesogabbro is typical of Ni-Cu-PGEs sulphide mineralisation in Phoenix, Selkirk mines and Tekwane deposit. The PGEs sulphide mineralisation comprises of pyrrhotite, pentlandite, chalcopyrite and pyrite. These different gabbro units form contacts with magmatic units, which include tonalite, quartz diorite, amphibolite, porphyritic granodiorite, granodiorite, leucogranodiorite, basalt, andesite, and dolerite dykes.

The gabbro units occur where they are metasedimentary units; Banded Iron Formation, dolomite and quartzite in TSMDC. Formation of the source magmas of the gabbroic units resulted from fractional crystallisation process dominated by plagioclase and pyroxene and generated into different gabbroic units, which include melanogabbro, mesogabbro and leucogabbro. The magmatism associated with development of these gabbro units resulted in formation of different sulphide mineralisation contents. The fractional crystallisation controlled by pyroxene and plagioclase is the dominant magmatic evolution in generation of gabbro units based on the positive correlations of MgO against FeOtotal, CaO and MgO and Y and Zr. The fractional crystallisation is also dominant as evidenced by positive correlation between SiO_2 and Na_2O, and K_2O and resulted in formation of enriched quartz mineralogy associated with granitoid units of the TSMDC. The Phoenix and Selkirk mines and Tekwane deposit mesogabbro contain economic sulphide mineralisation.

Based on the structural framework of TSMDC, the propagation of the source magmas of these different types of gabbro units occurred within extensionally collapsed crust during the first deformation event, D_1 caused by NE-SW directed compression forces. The second deformation event, D_2 is associated with NW-SE compression forces during oblique subduction regime affected the gabbroic units and resulted in shear zones across TSMDC. These shear zones are recognised as Phoenix mine shear zone (PMSZ), Selkirk mine (SMZS), Rooikoppie deposit shear zone (RDSZ), which formed under lower to upper greenschist facies. The third deformation, D_3 is recognised to be is brittle in nature and is defined by stylolitic cleavages in TSMDC. Thus, three deformation events are identified to have affected TSMDC.

The source magmas of the gabbroic units were generated from partial melting within the upper crust based on enrichment of light rare earth elements (LREE) relative to depletion of high field strength elements (HFSE). Plagioclase, pyroxene and sphene played important role during fractionation of partial melts as reflected by weak positive Eu anomaly in chondrite normalised REE plots. The mafic and felsic units were formed in subduction setting as reflected by negative Ta_N and Nb_N anomalies. In addition, the granitoids belong to post-collisional granite fields, which shows strong affinity to a post subduction environment. The volcanic arc magmatism resulted in mafic and felsic units, generated within oceanic plate closely associated with active continental margin in extensional setting in TSMDC. The integration of geological, structural geology, remote sensing, geochemical and geophysical survey data is ideal for the exploration modelling to identify prime targets for Ni-Cu-PGEs sulphide mineralisation in and around Phoenix, Selkirk mines, Tekwane and Rooikoppie deposits.

8.2. RECOMMENDATIONS

The research has established tectonomagmatic framework and sulphide mineralisation potential of TSMDC. However, the research is limited in its current objectives and more considerations are need in the following aspects:

- The presence of sulphide mineralisation within TSMDC is influenced by position of gabbroic units as the host and the orientation of the regional lineaments. Therefore, it is important to generate database of mapped gabbroic units and lineaments including the shear zones.
- The exposure of gabbroic units is very poor in most localities in TSMDC, which warrant for the use of remote sensing geophysical methods especially gravity and Induced Polarisation (IP). Therefore, it is vital for remote sensing and geophysics-based exploration to delineate Ni-Cu-PGEs associated host units, which possibly are not outcropping or blanketed by felsic intrusions.
- Detailed structural mapping should be undertaken in TSMDC for through documentation and kinematic analysis of all the structures.

REFERENCES

Aerogeologia. (2012). Preliminary Report – The remote search works on copper, nickel and platinum group metals on the licensed premises of Tati Nickel Company in Botswana. Consultancy report (unpubl). Moscow, 19 pp.

Aldiss, D.T. (1991). The Motloutse Complex and the Zimbabwe Craton/Limpopo Belt transition in Botswana. Precambrian Research, **50**, 89-109.

Allsopp, H.L. Kramers, D.L. and Erlank, A.J. (1989). The age of the Umkondo Group, Eastern Zimbabwe and implications for palaeomagnetic correlations. South African Journal Geology, **92**, 11-19.

Anhaeusser, C.R. and Ryan, P.J. (1976). Barren massive sulphide deposits in the Mphoengs schist belt, Rhodesia: A case study. **104**, 36pp.

Bailie, R.H. and Reid, D.L. (2005). Ore textures and possisble sulphide partial melting at Bronken Hill, Aggeneys, South Africa 1: Petrography. South African Journal of Geology, **108**, 51-70.

Bagai, Z. (2008). Geodynamic evolution and petrogenesis of the Neoarchean Francistown granite-greenstone complex in NE Botswana, SW margin of the Zimbabwe Craton. PhD. thesis (unpubl). University of Cape Town, Cape Town, 394 pp.

Bagai, Z. Armstrong, R.A. and Kampunzu, A.B. (2002). U-Pb single zircon geochronology of granitoids in the Vumba granite-greenstone terrain (NE Botswana): implications for the evolution of the Archaean Zimbabwe craton. Precambrian Research, **118**,149–168.

Bagai, Z. (2000). Geochemical and geochronological investigations of the Vumba granite-greenstone terrain of NE Botswana. M.Phil. thesis (unpubl). Durham theses, Durham University, Durham, 207 pp.

Barnes, S.J. and Lightfoot, P.C. (2005). Formation of magmatic nickel-sulphide ore deposits and processes affecting their copper and platinum-group element contents. In: Hedenquist J.W. Thompson J.F.H. Goldfarb.R.J. and Richards J.P. (Ed.), Economic Geology. 100th Anniversary Volume, 179-213.

Barros de Oliveira, S.M., Trescases, J.J. and Jose Melfi, A. (1992). Lateritic nickel deposits of Brazil, Mineralium Deposita, **27 (2)**, 137-146.

Becker, J.K. (2000). The emplacement of the Chinamora Batholith (Zimbabwe) inferred from field observations, magnetic-and microfabrics. PhD. thesis (unpubl). University of GÖttingen, GÖttingen, 170pp.

Becker, J.K. Siegesmund, S. and Jelsma, H.A. (2000). The Chinamora batholith, Zimbabwe: structure and emplacement-related magnetic rock fabric. Journal of Structural Geology, **22**, 1837-1853.

Begg, G.C., Hronsky, J.A.M., Nicholas, A.T., William,G.L., O`Reilly, S.Y. and Hayward, N. (2010). Lithospheric, Cratonic and Geodynamic setting of Ni-Cu-PGE sulphide deposits, Economic Geology, **105**, 1057-1070.

Bickle, M.J. Martin, A. and Nisbet, E.G. (1975). Basaltic and peridotitic komatites and stromatolites above unconformity in the Belingwe greenstone belt, Rhodesia. Earth and Planetary Science Letters, **27**, 155-162.

Blenkinsop, T.G. (2010). Archean magmatic granulites, diapirism and Proterozoic reworking in the Northern Marginal Zone of the Limpopo Belt. MWR207-13, 1-23.

Blenkinsop, T.G., Oberthur, T. and Mapeto, O. (2000). Gold mineralisation in the Mazowe area, Harare-Bindura-Shamva greenstone belt, Zimbabwe: Tectonic controls on mineralization, Mineralium Deposita, **35**, 126-137.

Boggs, Jr. S. (1995). Principles of Sedimnetology and Stratigraphy (2nd edition). Prentice Hall, New Jersey, 774pp.

Bohr, R., Hofmann, A., Woodhead, J., Hergt, J. and Dirks, P. (2002). Pb and Nd-isotope systematic of stromatolitic limestones from the 2.7 Ga Ngezi Group of the Belingwe Greenstone Belt: constraints on timing of deposition and provenance. Precambrian Research, **114**, 277-294.

Brown, B.L., Gardner, J.E., Larsen, J. (2003). Amphibole reaction rims in response to decompression compared to heating; an experimental approach.EOS. American Geophysical Union Fall Meeting Supplement.

Carney, J.N., Aldiss, D.T. and Lock, N.P. (1994). The geology of Botswana. Geological Survey of the Botswana. Bulletin 37, 113p.

Compston, W. and McElhinny, M.W. (1975). The Rb-Sr Age of the Mashonaland Dolerites of Rhodesia and its significance for palaeomagnetic correlation in southern Africa. Precambrian Research, **2**, 305-315.

Cumming, B. (1999). Final report on the work completed in the prospecting licence, PL 96/93, Botswana, Bulletin No: B, 475.

Deer, W.A., Howie, R.A. and Zussman, J. (1992). An introduction to the rock-forming minerals (2nd edition). Pearson Education Limited, England, 696 pp.

De Wit, J.M. (1998). On Archaean granites, greenstones, cratons and tectonics: does the evidence demand a verdict?. Precambrian Research, **91**, 181-226.

De Wit, M.J. and Ashwal, L.D. (1997). Greenstone belts. Clarendon Press, Oxford, 809pp.

Deng, Y., Yuan, F., Zhou, T., Xu, C., Zhang, D. and Guo, X. (2013). Geochemical characteristics and tectonic setting of the Turkubantao mafic-ultramafic intrusion in West Junggar, Xinjiang, China, Geoscience Frontiers, **xxx**,1-12.

Ding, X., Ripley, E. and Chusi Li. (2011). PGE geochemistry of the Eagle Ni-Cu-PGE deposit, Upper Michigan: constraints on ore genesis in a dynamic magma conduit, Miner Deposita.

Dirks, P.H.G.M. (2005). Report on mine visit to Phoenix and Selkirk Mines, Internal Report (unpubl), Tati Nickel Mining Company, Francistown, 7pp.

Dirks, P.H.G.M. (2004). The role of structure on the distribution pattern of Ni-Sulphide mineralisation at Phoenix and Selkirk Mines, Tati Greenstone Belt, NW Botswana. Internal Report (unpubl), Tati Nickel Mining Company, Francistown, 67pp.

Dirks, P.H.G.M. and Jelsma, H. (2002). Crust-mantle decoupling and the growth of the Archaean Zimbabwe craton. Journal of African Earth Sciences, **34**, 157-166.

Dirks, P.H.G.M., Jelsma, A.H. and Hofmann, A. (2002). Thrust-related accretion of an Archaean greenstone belt in the Midlands of Zimbabwe. Journal of Structural Geology, **24**, 1707-1727.

Dirks, P.H.G.M. and Jelsma, A. (1998). Silicic Layer-Parallel Shear zones in a Zimbabwean Greenstone sequence: Horizontal Accretion Preceding Doming. Gondwana Research, **V1 (2)**, 177-193.

Dirks, P.H.G.M. and Van Der Merwe, J.A. (1997). Tectonic stacking in an Archaean greenstone sequence and its control on gold mineralisation at Dalny Mine, Zimbabwe. Journal of African Earth Sciences, **24 (4)**, 603-619.

Døssing, L.N., Frei, R., Stendai, H. and Mapeo, R.B. (2009). Characterisation of the enriched lithospheric mantle components in ~2.7 Ga banded iron formations: An example from the Tati greenstone belt, northeastern Botswana. Precambrian Research, **172**, 334-356.

Elburg, M.A. (1996). Evidence of isotopic equilibration between microgranitoid enclaves and host granodiorite, Warburton Granodiorite, Lachlan Fold Belt, Australia,Lithos, **38 (1-2)**, 1-22.

Eliopoulosa, D.G., Economou-Eliopoulosb, M., Apostolokasc, A. and Golightly, J.P. (2012). Geochemical features of nickel-laterite deposits from the Balkan Peninsula and Gordes, Turkey: The genetic and environmental significance of arsenic, Ore Geology Reviews, **48**, 413-427.

Ernest, R.E. and Jowitt, S.M. (2013). Large Igneous Provinces (LIPs) and Metallogeny, Society of Economic Geologists Special Publication, **17**, 17-51.

Evans-Lamswood, D.M., Butt, D.P., Jackson, R.S., Lee, D.V., Muggridge, M.G. and Wheeler.,R.I. (2000) Physical Controls Associated with the Distribution of Sulfides in the Voisey`s Bay Ni-Cu-Co Deposit, Labrador, Economic Geology, **95 (4)**, 749-769.

Farner, M.J., Cin-Ty, L. and Putrik.,K.D. (2014). Mafic–felsic magma mixing limited by reactive processes:A case study of biotite-rich rinds on mafic enclaves Earth and Planetary Science Letters, **393**, 49–59.

Fedo, C.M. and Eriksson, K.A. (1996). Stratigraphic framework of the ~3.0 Ga Buhwa Greenstone Belt: a unique stable-shelf succession in the Zimbabwe Archaean craton. Precambrian Research, **77**, 161-178.

Fedo, M.C., Eriksson, K.A. and Krogstad, J. (1996). Geochemistry of shales from the Archaean (~3.0 Ga) Buhwa Greenstone Belt, Zimbabwe: Implications for provenance and source area weathering. Geochimica et Cosmochimica Acta, **60 (10)**, 1751-1763.

Fiorentini, M.L., Bekker, A., Rouxel, O., Wing, B.A., Maier, W. and Rumble, D. (2012). Multiple Sulphur and Iron Isotope Composition of Magmatic Ni-Cu-(PGE) Sulfide Mineralisation from Eastern Botswana. Economic Geology, **107**, 105-116.

Flowers, R.M. and Schoene, B. (2010). (U-Th)/He thermochronometry constraints on unroofing of the eastern Kaapvaal craton and significance for uplift of the southern African Plateau, Geological Society of America, **38 (9)**, 827-830.

Funck, T. and Louden, K.E. (1999). Wide-angle seismic transect across the Torngat Orogen northern Labrador: Evidence for a Proterozoic crustal root, Journal of Geophysical Research, **104 (B4)**, 7463-7480.

Furnes, H., Dilek, Y. and de Wit, M. (2014). Precambrian greenstone sequences represent different ophiolite types. Evolution of Archean Crust and Early Life-Modern Approaches in Solid Earth Sciences, **7**, 1-22.

Geldenhuys, A. (2009). Mineral Resource Update for Phoenix Nickel Mine, Botswana, Anglo American, Johaannesburg, 56pp.

Geldenhuys, A. (2008). Mineral Resource Update for Selkirk Nickel Project, Botswana, Anglo American, Johaannesburg, 61pp.

Gipronickel Institute. (2012). Feasibility Analysis study on optimisation of open cut mining at Tati Nickel`s Phoenix and Selkirk deposits, 1 (1), Geology report book (unpubl), Gipronickel Institute, St Petersburg, 80pp.

Gore, J., James, D.E., Zengeni, T.G., Gwavava, O. (2009). Crustal structure of the Zimbabwe craton and the Limpopo belt of the southern Africa: New constraints from seismic data and implications for its evolution. South African Journal of Geology, **112**, 213-228.

Gribble, C.D, and Hall, A.J. (1992). Optical mineralogy, Principles and practise. University College London (UCL_ press, London, England, 303 pp.

Guilbert J.M., Park Jr C.F. (1986). The geology of ore deposits. W.H. Freeman and Company, New York, United States of America, 947 pp.

Hamilton, W.B. (1998). Archaean magmatism and deformation were not products of plate tectonics. Precambrian Research, **91**, 143-179.

Hansen, S.E., Nyblade, A.A. and Julia, J. (2009). Estimates of crustal and lithospheric thickness in Sub-Saharan Africa from S-wave receiver functions, South African Journal of Geology, **112**, 229-240.

Hofmann, A., Bekker, A., Dirks, P., Gueguen, B., Rumble, D. and Rouxel, O.J. (2014). Comparing orthomagmatic and hydrothermal mineralisation models for komatiite-hosted nickel deposits in Zimbabwe using multiple-sulfur, iron, and nickel isotope data, Mineralium Deposita, **49 (1)**, 75-100.

Hofmann, A., Jagoutz, O., Kroner, A., Dirks, P.H.G.M. and Jelsma, H.A. (2002). The Chirwa dome: granite emplacement during late Archaean thrusting along the northeastern margin of the Zimbabwe craton. South African Journal of Geology, **105**, 285-300.

Hofmann, A., Dirks, P.H.G.M. and Jelsma, H.A. (2001). Late Archaean foreland basin deposits, Belingwe greenstone belt, Zimbabwe. Sedimentary Geology, **141-142**,131-168.

Hortswood, M.S.A., Nesbitt, R.W., Noble, S.N. and Wilson, J.F. (2012). The Sebakwe Proto-Craton: An Extensive Early Archaean Crustal Block in Zimbabwe, A Reassessment of Craton Formation, Stabilisation and Growth: Journal of Conference Abstracts, Early Evolution of the Continental Crust, Symposium A08, 4 (1).

Hunt J.P. and Dirks, P.H.G.M. (2005). Preliminary Discussion on Lithological Characteristics and Domains and Implications for Genetic Evolution of Phoenix and Selkirk Mines. Internal Report (unpubl).Tati Nickel Mining Company, Francistown, 14 pp.

Irvine, T.N. and Baragar, W.R.A. (1971). A guide to the chemical classification of the common volcanic rocks. Canadian Journal of Earth Sciences, **8**, 523-548.

James, D.E., Niub, F. and Rokoskya, J. (2003). Crustal structure of the Kaapvaal craton and its significance for early crustal evolution. Lithos, **71**, 413-429.

Jelsma, H.A. and Dirks, P.H.G.M. (2002). Neoarchaean tectonic evolution of the Zimbabwe craton, Geological Society, Special Publications, **199**, 183-212. .

Jelsma, H, A., and Dirks, P.H.G.M. (2000) Tectonic evolution of a greenstone sequence in Northern Zimbabwe; sequential early stacking and pluton diapirism, TECTONICS, **19 (1)**, 135-152

Jelsma, H.A. and Van Der Beek, P.A. (1993). Tectonic evolution of the Bindura-Shamva greenstone belt (northern Zimbabwe): progressive deformation around diapiric batholiths. Journal of Structural Geology, **15 (2)**, 163-176.

Johnson, R.S. (1986). The Phoenix and Selkirk nickel-copper sulphide ore deposits, Tati greenstone belt, eastern Botswana, In: Anhaeusser,C.R, Maske,S. (Eds), 1986 Mineral Deposits of South Africa, Geological Society of South Africa, Johannesburg, **1**, 243-248.

Johnson, S.P., Rivers, T. and De Waele B. (2005). A review of the Mesoproterozoic to early Palaeozoic magmatic and tectonothermal history of south–central Africa: implications for Rodinia and Gondwana, Journal of the Geological Society, **162**, 433–450.

Johnson, S.P., Rivers, T. and De Waele B. (2005). A review of the Mesoproterozoic to early Palaeozoic magmatic and tectonothermal history of south–central Africa: implications for Rodinia and Gondwana, Journal of the Geological Society, London, **162**, 433–450.

Kabete, J.M., Groves, D.I., McNaughton, N.J and Mruma, A.H. (2012). A new tectonic and temporal framework for the Tanzanian Shield: Implications for gold metallogeny and undiscovered endowment. Ore Geology Reviews, 48, 88-124.

Kamber, B.S., Kramers, J.D., Napier, R., Cliff, R.A. and Rollinson, H.R. (1995). The Triangle Shear zone, Zimbabwe, revisited: new data document an important event at 2.0 Ga in the Limpopo Belt. Precambrian Research, **70** ,191-213.

Kampunzu, A.B., Tombale A.R., Zhai, M., Bagai Z., Majaule T.M. and Modisi, M. (2003). Major and trace element geochemistry of plutonic rocks from Francistown, NE Botswana: evidence for neo-Archaean continental active margin in the Zimbabwe craton. Lithos, **71**, 431–460.

Key, R.M. (1976). The geology of the area around Francistown and Phikwe, northeast and central districts, Botswana. Bulletin Geological Survey Botswana, **3**, 121pp.

Kusky, T.M. and Ramadan, T. M. (2002). Structural controls on Neoproterozoic in the South Eastern Desert, Egypt: an integrated filed, Landsat TM and SIR_C/X SAR approach, Journal of African Earth Sciences, **35**, 107-121.

Kusky, T.M. and Polat, A. (1999). Growth of granite-greenstone terranes at convergent margins and stabilisation of Archaean cratons. Tectonophysics, **305**, 43-73.

Kusky, T.M. (1998). Tectonic setting and terrane accretion of the Archaean Zimbabwe craton. Geology, **26 (2)**, 163-166.

Le Gall, B., Tshoso, G., Dyment, J., Kampunzu, A.B., Jourdan, F., Féraud, G., Bertrand, H., Aubourg, C. and Vétel, W. (2005). The Okavango giant mafic dyke swarm (NE Botswana): its structural significance within the Karoo Large Igneous Province, Journal of Structural Geology, **27**, 2234-2255.

Lightfoot, P.C. and Evans-Lamswood. (2014). Structural controls on the primary distribution of mafic–ultramafic intrusions containing Ni–Cu–Co–(PGE) sulfide mineralization in the roots of large igneous provinces, Ore Geology reviews, **64**, 354-386.

Lightfoot, P.C., Keays, R.R, Evans-Lamswood, D.E. Wheeler, R. (2012). Crustal contamination and multiple S-saturation events in Nain Plutonic Suite magmas: evidence form Voisey's Bay, Labrador, Canada. Mineralium Deposita, **47**, 23-50.

Lightfoot, P.C. (2007). Advances in Ni-Cu-PGE Sulphide Deposit Models and Implications for Exploration Technologies. In: Milkereit B. (Ed.) Proceedings of Exploration 07: Fifth Decennial International Conference on Mineral Exploration. Plenary Session: Ore Deposits and Exploration Technology Paper **44**, 629-646.

Maas, R., Nicholls, I.A. and Legg, C. (1997). Igneous and Metamorphic Enclaves in the S-type Deddick Granodiorite, Lachlan Fold Belt, SE Australia: Petrographic, Geochemical and Nd-Sr Isotopic Evidence for Crustal Melting and Magma Mixing. Journal of Petrology, **38 (7)**, 815-841.

Maier,W.D.,Smithies,R.H.,Spaggiari,C.V.,Barnes,S.J.,Kirkland,C.L.,Yang,S.,Lahaye,Y.,Kiddie,O. and MacRae,C. (2016). Petrogenesis and Ni-Cu sulphide potential of mafic-ultramafic rocks in the Mesoproterozoic Fraser Zone within Albany-Fraser Orogen, Western Australia, Precambrian, 281, 27-46.

Maier, W.D., Barnes, S. J., Chinyepi, G., Barton, J.M., Eglington, B. and Setshedi, I. (2007). The composition of magmatic Ni–Cu–(PGE) Sulfide Deposits in the Tati and Selebi-Phikwe Belts of Eastern Botswana. Mineralium Deposita, **43(1)**, 37-60.

Makitch, K., Latypoy, R, M., Badanina, I, Yu. and Sluzhenikin, S.F. (2014). Insights into ore genesis of Ni-Cu-PGE sulfide deposits of the Noril'sk Province (Russia): Evidence from copper and sulfur isotopes, Lithos, **204 (1)**, 172-187.

Markwitz, V., Maier, W.D., Gonzalez-Alvarez, I., McCuaig, T.C. and Porwal, A. (2010). Magmatic nickel sulfide mineralisation in Zimbabwe: Review of deposits and development of exploration criteria for prospectivity analysis. Ore Geology Reviews, **38**, 139-155.

McCourt, S., Kampunzu, AB., Bagai, Z. and Armstrong, R.A. (2004). The crustal architecture of Archaean terranes in northeastern Botswana, South Africa Journal of Geology, **107**,147–158.

McCourt, S. (1995). The crustal architecture of the Kaapvaal crustal block South Africa between 3.5 and 2.0 Ga, Mineral Deposita, **30**, 89-97.

McCourt, S. and Vearncombe, J.R. (1992). Shear zones of the Limpopo Belt and adjacent granitoid-greenstone terranes: implications for late Archaean collision tectonics in Southern Africa. Precambrian Research, **55**, 553-570.

McDonough, W.F. and Sun, S.S. (1995). The composition of the Earth, Chemical Geology, 120, 223-253.

Milner Jnr, J.D. and Weiblen, P.W. (1990). Anorthositic Rocks of the Duluth Complex: Examples of Rocks Formed from Plagioclase Crystal Mush, Petrology, **31(2)**, 295-339.

Geldenhuys,A (2008). Mineral Resource Update for Selkirk Project, Botswana. Consultancy report (unpubl), Anglo American Technical Division, Johannesburg, 61 pp.

Mobarhan, S.K. and Ahmadipour, H. (2010). Using Magma Mixing/Mingling Evidence for Understanding Magmatic Evolution at Mount Bidkhan Stratovolcano (South-East Iran), Journal of Sciences, Islamic Republic of Iran, **21 (2)**, 137-153.

Moorbath, S., Wilson, J.F., Goodwin. and Humm, M. (1977). Further Rb-Sr Age and Isotope data on early and late Archaean rocks from the Rhodesian Craton. Precambrian Research, **5**, 229-239.

Moore, A., Blenkinsop, T. and Cotterill (Woody), F. (2009). Southern African topography and erosion history: plumes or plate tectonics? Terra Nova, **21**, 310-315.

Moore, A.E., Cotterill (Woody), F.P.D., Broderick, T. and Plowes, D. (2009). Landscape evolution in Zimbabwe from the Permian to present, with implications for kimberlite prospecting, South Africa Journal of Geology, **112**, 65-88.

Mungall, J.E., Harvey, J.D., Balch, S.J.,Azar, B., Atkinson, J. and Hamilton, M.A. (2010). Eagle`s Nest: A Magmatic Ni-silfide deposit in the James Bay lowlands, Ontario, Canada. Society of Economic Geologists Inc, Special Publications, **15**, 539-557.

Munyanyiwa, H. (1999). Geochemical study of the Umkondo dolerites and lavas in the Chimanimani and Chipenge Districts (Eastern Zimbabwe) and their regional implications, Journal of African Earth Sciences, **25(2)**, 349-385.

Naldrett, A.J. (2004). Magmatic Sulfide Deposits: Geology, Geochemistry and Exploration. Springer Verlag, Heidelberg, Berlin.728pp.

Naldrett, A.J. (1999). World-class Ni-Cu-PGE deposits: key factors in their genesis. Mineralium Deposita, **34**,227-240.

Nguuri,T.K.,Gore,J., James,D.E.,Webb,S.J.,Wright,C.,Zengeni.T.G.,Gwavava,O., Snoke,J.A., Kaapvaal Seismic Group. (2001). Crustal structure beneath southern Africa and its implications for the formation and evolution of the Kaapvaal and Zimbabwe cratons, Geophysical research letters, **28 (13)**, 2501-2504.

Oberthür, T., Davis, D.W., Blenkinsop, T.G. and Hohndorf, A. (2002). Precise U-Pb mineral ages, Rb-Sr and Sm-Nd systematics for the Great Dyke, Zimbabwe-constraints on late Archaean events in the Zimbabwe craton and Limpopo belt. Precambrian Research, **113**, 293-305.

Pearce, J.A., Harris, N.B.W. and Tindle, A.G. (1984). Trace element discrimination diagrams for the tectonic interpretation of granitic rocks, Journal of Petrology, **25**, 956-983.

Pirajno, F. and Gonzalez-Alvarez, I. (2013). Re-appraisal of the Epoch nickel sulphide deposit, Filabusi Greenstone Belt, Zimbabwe: A hydrothermal nickel mineral system? Ore Geology Reviews, **52**, 58-65.

Pirajno F, (2000). Mantle plumes, associated intraplate tectono-magmatic processes and ore systems, Episodes, 30 (1).

Pirajno, F. (2000). Ore Deposits and Mantle Plumes, Springer Netherlands, Netherlands, 556pp.

Poli, G.E. and Tommasini, S. (1991). Model for the origin and significance of microgranular enclaves in calc-alkaline granitoids, Petrology, **32(3)**, 657-666.

Prendergast, M.D. (2013). Landscape evolution, regolith formation and Nickel laterite development in the northern part of the Great Dyke, Zimbabwe, South Africa Journal of Geology, **116**, 219-240.

Ranganai, R.T. (2013). Structural and subsurface relationships between the Fort Rixon-Shangani greenstone belt and the Nalatale pluton, Zimbabwe craton as derived from gravity and aeromagnetic data. South Africa Journal of Geology, **116**, 273-296.

Ranganai, R.T. (2012). Gravity and Aeromagnetic Studies of the Filabusi Greenstone Belt, Zimbabwe craton: Regional and Geotectonic Implications. International Journal of Geosciences, **3**, 1048-1064

Ranganai R.T., Kampunzu A.B., Atekwana E.A., Paya B.K., King J.G., Koosimile D.I. and Stettler, E.H. (2002). Gravity Evidence for a larger Limpopo belt in Southern Africa and geodynamic implications. Geophysical Journal International, F9-F14.

Ranganai, R.T., Whaler, K.A. and Ebinger, C.J. (2008). Gravity anomaly patterns in the south –central Zimbabwe Archaean craton and their geological interpretation. Journal of African Earth Sciences, **51**, 257-276.

Roering, C., Van Reenen, D.D., Smit, C.A., Barton Jr, J.M., De Beer, J.H., De Wit, M.J., Stettler, E.H., Van Schalkwyk, J.F., Stevens, G. and Pretorius, S. (1992). Tectonic model for the evolution of the Limpopo Belt. Precambrian Research, **55**, 539-552.

Rogers, J. (2007). Jims Luck prospect. Technical report (unpubl). IAMGOLD BOTSWANA, Francistown, 37pp.

Rollinson, H.R. and Whitehouse, M. (2011). The growth of the Zimbabwe Craton during the late Arcghaean: an ion microprobe U-Pb zircon study. Journal of the Geological Society, **168**, 941-952.

Rollinson, H. and Blenkinsop, T. (1995). The magmatic, metamorphic and tectonic evolution of the Northern Marginal Zone of the Limpopo Belt in Zimbabwe. Journal of the Geological Society, **152**, 65-75.

Rollison, H.R. (1993). Using geochemical data; evaluation, presentation, interpretation. Harlow, Longman Scientific and Technical, United Kingdom, 352pp.

Sandmann, D. and Gutzmer, J. (2014). Nature and distribution in gabbroic units of the Lusatian Block, Saxony, Germany. Z.DE.Geowiss (German j. Geol.), **166**, 35-53.

Saggerson, E.P. and Turner, L.M. (1976). A review of the distribution of metamorphism in the ancient Rhodesian craton. Precambrian Research, **3**, 1-53.

Saumur, B.M., Cruden, A.R., Evans-Lamswood, D. and Lightfoot, P.C. (2015). Wall-Rock Structural Controls on the Genesis of the Voisey's Bay Intrusion and its Ni-Cu-Co Magmatic Sulfide Mineralization (Labrador, Canada), Economic Geology, **110**, 691-711.

Schulz, K.J., Chandler, V.W., Nicholson, S.W., Piatak, N., Seal II, R.R., Woodruff, L.G. and Zientek. (2010). Magmatic Sulfide-Rich Nickel-Copper Deposits Related to Picrite and (or) Tholeiitic Basalt Dike-Sill Complexes: A Preliminary Deposit Model.

Severson, M. (2009). Field, Petrographic and Mineralization Characteristics of Mafic Layered Intrusions, Precambrian Research Centre Professional Workshop, University of Minnesota Duluth, United States of America.

Shackleton, R.M. (1995). Tectonic evolution of greenstone belts. In: Coward, M.P. and Ries, A.C. (Eds.), Early Precambrian Processes. Geological Society Special Publication, **95**, 163-176.

Siegesmund, S., Jelsma, H., Becker, J., Davies, G., Layer, P., Van Dijik, E., Later, L. and Vinyu, M. (2002). Constraints on the timing of granite emplacement, deformation and metamorphism in the Shamva area, Zimbabwe, International Journal Earth Sciences (Geol Rundsch), **19**, 20-34.

Smit, C.A. and Van Reenen, D.D. (2010). Thrust exhumation of the Southern Marginal Zone of the Limpopo Complex in the Neoarchaean: link of distinct high-grade shear zones with DC and IC P-T-t paths, Geophysical Research Abstracts, 12, EGU2010-15590-1, EGU General Assembly.

Smithies, R.H., Champion, D.C. and Cassidy, K.F. (2003). Formation of Earth`s early Archaean continental crust. Precambrian Research, **127**, 89-101.

Snowden, P.A. and Snowden, V.D. (1981). Petrogeochemistry of the late Archaean Granites of the Chinamora Batholith, Zimbabwe. Precambrian Research, **16**, 103-129.

Song, X., Wang, Y. and Chen, L. (2011). Magmatic Ni-Cu-(PGE) deposits in magma plumbing systems: Features, formation and exploration, Geoscience Frontiers, **2(3)**, 375-384.

Taylor, P.N., Kramers, J.D., Moorbath, S., Wilson, J.F., Orpen, J.L. and Martin, A. (1991). Pb/Pb, Sm-Nd and Rb-Sr geochronology in the Archaean Craton of Zimbabwe. Chemical Geology (Isotope Geoscience Section), **87**, 175-196.

Rogers, J.,(2002). Tekwane platinum prospect Botswana. company report (unpubl). Gallery Gold, Francistown, 54pp.

Tikoff, B., Davis, M.R., Teyssier, C., St. Blanquat, M., Harbet, G. and Morgan, S. (2005). Fabric studies within the Cascade Lake shear zone, Sierra Nevada, California. Tectonophysics, **400**, 209-226.

Tingjie, Y., Aibing, L. and Ritzwoller, M. (2008). Crustal and uppermost mantle structure in southern Africa revealed from ambient noise and teleseismic tomography. Geophysical Journal International, 1-14.

Thorne, R., Roberts, S. and Herrington, R. (2012). The formation and evolution of the Bitincke nickel laterite deposit, Albania, Mineralium Deposita, **47**, 933-947.

Tombale, R.A. (1992). The Geology, Geochemistry and Metallogeny of the Tati greenstone belt, northeastern Botswana. PhD. thesis (unpubl), Memorial University of Newfoundland, St John`s, 490pp.

Tornos, F., Galindo C., Casquent, C., Pevida, L.R., Martinez, E., Velasco, F. and Irindo, A. (2006).The Aguablanca Ni-(Cu) sulfide deposit, SW Spain: geologic and geochemical controls and the relationship with a midcrustal layered mafic complex, **41 (8)**, 737-769.

Treloar, P.J. and Blenkinsop, T.G. (1995). Archaean deformation patterns in Zimbabwe: true indicators of Tibetan-style crustal extrusion or not? Geological Society, Special Publications, **95**, 87-107.

Treloar, P.J., Coward, M.P. and Harris, N.B.W. (1992). Himalayan-Tibetan analogies for the evolution of the Zimbabwe Craton and Limpopo Belt. In: D.D. van Reenen, C. Roering, L.D. Ashwal and M.J. de Wit (Editors), The Archaean Limpopo Granulite Belt: Tectonics and Deep Crustal Processes. Precambrian Res., **55**: 571-587.

Tsunogae, T., Miyano, J. and Ridley, J. (1992). Metamorphic P-T profiles from the Zimbabwe craton to the Limpopo Belt, Zimbabwe. Precambrian Reasearch, **55**, (1-4), 259-277.

Tsunogae, T., Nabara, A., Fukuni, T., Mzvanga, W., and Mugumbate, F. (2001). Ultrahigh-temperature metamorphism of the Archaean Limpopo Belt and its thermal effect on the adjacent low-grade Zimbabwe Craton, southern Africa.AGSO Geoscience Australia, Record 2001/37,362-364.

Tsunogae, T., Shimuzu, H., Santosh, M. and Van Reenen. (2010). Mg-rich Staurolite+Sapphirine+Quartz Association as an evidence of high-pressure and ultrahigh-temperature metamorphism in collisional orogens. GeoCanada 2010-Working with the Earth, 3pp.

Treloar, P.J., Coward, M.P. and Harris, N.B.W. (1992). Himalayan-Tibetan analogies for the evolution of the Zimbabwe and Limpopo Belt. Precambrian Research, **55**, 571-587.

Van de Wel, L., Barton, J.M. Jr. and Kinny, P.D. (1998). 1.02 Ga granite magmatism in the Tati–granite greenstone Terrane of Botswana: implications for mineralization and terrane evolution. South African Journal Geology, **101**, 67–72.

Van Geffen, P.W.G. (2005). Geochemistry of the Phoenix Ni-Cu-PGE Deposit Francistown, Botswana: Applications of Remote Sensing in Ni-Cu Exploration & PGE Distribution over Fe-Ni-Cu Sulphide Phases. MSc. thesis (unpubl), Utrecht University, Utrecht, 88pp.

Van Kranedonk, M.J. (1996). Tectonic evolution of the Paleoproterozoic Torngat Orogen: Evidence from pressure-temperature-time-deformation paths in the North River map area, Labrador, Tectonics, **15 (4)**, 843-869.

Van Reenen, D.D., Roering, A., Ashwal, L.D. and De Wit, M.J. (1992). Regional geological setting of the Limpopo Belt. Precambrian Research, **55**, 1-51.

Van Reenen, D.D., Roering, C., Brandl, C., Smit, A.C. and Barton Jr, J.M. (1990). The Granulite-facies rocks of the Limpopo Belt, southern Africa. In: Vielzeuf D. and Vidal Ph. (Ed.), Granulites and Crustal Evolution. 311, NATO ASI Series, 257-289.

Vinyu, M.L., Hanson, R.E., Martin, M.W., Bowrin, S.A., Jelsma, H.A. and Dirks, P.H.G.M. (2001). U-Pb zircon ages from a craton-margin Archaean Orogenic belt in Northern Zimbabwe. Journal of Earth Sciences, **32(1)**, 103-114.

Wiebe, R.A. (1994). Silicic magma chambers as traps for basaltic magmas: the Cardillac Mountain intrusive complex, Mount Desert Island, Maine.The Journal of Geology, 102(4), 423-437.

Wilson, J.F. (1990). A craton and its cracks: some of the behavior of the Zimbabwe block from the late Archaean to the Mesozoic in response to horizontal movements and the significance of its mafic dyke fracture patterns. Journal of African Geology, **10**, 483-501.

Wilson, J.F., Bickle, M.J., Hawkesworth, C.J., Martin, A., Nisbet, E. and Orpen, J.F. (1978). Granite-greenstone terrains of the Rhodesian Archaean craton. Nature, **27 (1)**, 23-27.

Yang, X.M., Gilbert, H.P., Corkery, M.T. and Houlé, M.G. (2011. The Mayville mafic–ultramafic c intrusion in the Neoarchean Bird River greenstone belt, southeastern Manitoba (part of NTS 52L12): preliminary geochemical investigation and implication for PGE-Ni-Cu-(Cr) mineralization; in Report of Activities 2011, Manitoba Innovation, Energy and Mines, Manitoba Geological Survey, p. 127–142.

Zhai, M., Kampunzu, A.B., Modisi, M.P. and Bagai, Z. (2006). Sr and Nd isotope systematic of Francistown plutonic rocks, Botswana: implications for Neoarchaean crustal evolution of Zimbabwe craton. International Journal of Earth Sciences, **95**,355-369.

Zeh, A., Gerdes, A. and Barton Jr, J.M. (2009). Archaen accretion and crustal evolution of the Kalahari craton-the Zircon age and Hf isotope record of granitic rocks from Barberton/Swaziland to the Francistown arc. Journal of Petrology, **00(0)**, 1-34.

Zhou, M. (1994) PGE distribution in 2.7 Ga layered komatiite flows from the Belingwe greenstone belt, Zimbabwe. Chemical Geology, **118**, 155 -172.

Zhou, M. and Kerrich, R. (1992). Morphology and composition of chromite in komatiites from the Belingwe greenstone belt, Zimbabwe. Canadian Mineralogist, **30**, 303-317.

APPENDIX A

Table A1: The foliation data collected during geological mapping in TSMDC.

(i). Phoenix mine shear zone (PMSZC) foliation and lineation data

SHEAR ZONE ID	UNIT	COORDINATES				STRIKE	DIP	DIP DIRECTION
				SOUTH AFRICA GRID				
		UTM_E	UTM_N	X	Y	281	71	189
WS1	Melanogabbro					304	53	204
WS2	Melanogabbro	579738	7654071	2346868	27 -079771	304	86	36
WS3	Melanogabbro	579737	7654095	2346844	27 -079761	306	83	32
WS4	Melanogabbro	579737	7654111	2346827	27 -079766	331	80	59
WS5	Melanogabbro	579742	7654142	2346796	27 -079774	328	83	60
WS6	Melanogabbro	579743	7654177	2346762	27 -079774	315	86	45
WS7	Melanogabbro	579742	7654197	2346741	27 -079773	325	60	151
WS8	Melanogabbro	579741	7654217	2346720	28 -079774	250	62	150
WS9	Melanogabbro	579749	7654318	2346622	27 -079780	252	52	127
WS10	Melanogabbro	577951	7654419	2346524	29 -079774	315	32	200
WS11	Mineralised mesogabbro	577949	7654384	2346555	27 -079773	266	66	175
WS12	Mineralised mesogabbro	579717	7654442	2346495	27 -079750	284	75	31
WS13	Mineralised mesogabbro	579686	7654597	2346346	27 -079718	226	29	132
WS14	Mineralised mesogabbro	579688	7654592	2346197	28 -079750	229	29	157
WS15	Mineralised mesogabbro	579655	7654667	2346272	27 -079701	307	85	55
WS16	Mineralised mesogabbro	579655	7654735	2346205	27 -079691	259	27	152
WS17	Mineralised mesogabbro	579655	7654735	2346205	27 -079691	275	30	185
WS18	Mineralised mesogabbro	579655	7654735	2346205	27 -079691	246	40	156
WS19	Mineralised mesogabbro	579650	7654775	2346164	27 -079681	232	40	142
WS20	Mineralised mesogabbro	579659	7654778	2346130	27 -079677	289	87	199
WS21	Mineralised mesogabbro	579645	7654809	2346129	27 -079677	316	74	226
WS22	Mineralised mesogabbro	579637	7654818	2346124	27 -079667	226	46	136
WS23	Mineralised mesogabbro	579648	7654820	2346117	27 -079676	284	46	14
WS24	Mineralised mesogabbro	579647	7654855	2346083	27 -079679	341	88	71
WS25	Mineralised mesogabbro	579647	7654855	2346083	27 -079679	335	89	65
WS26	Mineralised mesogabbro	579351	7654895	2346044	27 -079382	294	72	24
WS27	Mineralised mesogabbro	579364	7654938	2346000	27 -079395	289	84	19
WS28	Mineralised mesogabbro	579364	7654938	2346000	27 -079395	344	68	74
WS29	Mineralised mesogabbro	579460	7654994	2345944	27 -079494	329	68	59
WS30	Mineralised mesogabbro	579498	7655010	2345925	27 -079530	293	65	23
WS31	porphyritic granodiorite	579946	7654657	2346281	27 -079979	307	86	217
WS32	Mineralised mesogabbro	579368	7654878	2346060	27 -079400	69	62	66
WS33	Mineralised mesogabbro	579368	7654878	2346060	27 -079400	39	44	219
WS34	Mineralised mesogabbro	579371	7654881	2346057	27 -079402	38	66	322

(ii). Selkirk mine shear zone (SMSZ) foliation and lineation data

SHEAR LOCALITY ID	UNIT	UTM COORDINATES		STRIKE	DIP	DIP DIRECTION
SEL 01	Mesogabbro	574911	7642153	59	42	149
SEL 02	Mesogabbro	574903	7642149	66	65	156
SEL 03	Mesogabbro	574896	7642143	75	52	165
SEL 04	Mesogabbro	574894	7642143	49	75	139
SEL 05	Mesogabbro	574953	7642151	51	57	141
SEL 06	Basalt	574970	7642170	76	28	166
SEL 07	Basalt	574971	7642136	78	56	168
SEL 08	Basalt	574974	7642104	74	41	164
SEL 09	Basalt	574969	7642149	80	48	170
SEL 10	Basalt	574994	7642128	75	32	165
SEL 11	Basalt	574957	7642171	88	51	178
SEL 12	Basalt	574957	7642171	88	56	178
SEL 13		574930	7642187	75	46	165

LINEATION

SHEAR LOCALITY ID	UNIT	UTM COORDINATES		TREND	PLUNGE
SEL 04L	Mesogabbro	574894	7642143	234	57
SEL 04 (1)L	Mesogabbro	574900	7642156	209	41
SEL 04 (2)L	Mesogabbro	574901	7642157	203	77
SEL 04 (3)L	Mesogabbro	574901	7642157	184	57
SEL 05L	Basalt	574974	7642104	208	42
SEL 06L	Basalt	574957	7642171	167	81
SEL 07L	Basalt	574969	7642149	200	73

SHEAR LOCALITY ID	UNIT	UTM COORDINATES		TREND	PLUNGE
SEL 04L	Mesogabbro	574894	7642143	234	57
SEL 04 (1)L	Mesogabbro	574900	7642156	209	41
SEL 04 (2)L	Mesogabbro	574901	7642157	203	77
SEL 04 (3)L	Mesogabbro	574901	7642157	184	57
SEL 05L	Basalt	574974	7642104	208	42
SEL 06L	Basalt	574957	7642171	167	81
SEL 07L	Basalt	574969	7642149	200	73

(iii). Rooikoppie deposit shear zone (RDSZ) foliation and lineation data

LOCALITY IDENTITY	UNIT	X	Y	STRIKE	DIP	DIP DIRECTION
RKP_SHRZ 001	Amphibolite	588902	7648273	19	73	109
RKP_SHRZ 002	Amphibolite	588950	7648301	14	82	104
RKP_SHRZ 003	Amphibolite	588910	7648684	15	71	105
RKP_SHRZ 004	Amphibolite	588908	7647410	30	43	120
RKP_SHRZ 005	Amphibolite	588085	7647463	21	85	111
RKP_SHRZ 006	Amphibolite	588011	76498701	34	76	124
RKP_SHRZ 007	Amphibolite	588071	7647933	32	79	122
RKP_SHRZ 008	Amphibolite	587111	7646004	31	86	121
RKP_SHRZ 009	Amphibolite	586211	7644612	26	68	116
RKP_SHRZ 010	Amphibolite	586007	7644078	30	71	120
RKP_SHRZ 011	Amphibolite	587511	7645024	23	83	113
RKP_SHRZ 012	Amphibolite	589071	7645111	23	82	113
RKP_SHRZ 013	Amphibolite	586417	7643518	27	70	117
RKP_SHRZ 014	Amphibolite	586015	7645084	26	72	116
RKP_SHRZ 015	Amphibolite	587101	7645603	29	88	119
RKP_SHRZ 016	Amphibolite	589174	7648053	17	81	107
RKP_SHRZ 017	Amphibolite	589174	7648053	20	69	110
RKP_SHRZ 018	Amphibolite	589174	7648053	28	69	118
RKP_SHRZ 019	Amphibolite	589174	7648053	26	61	116
RKP_SHRZ 020	Amphibolite	588612	7648503	26	71	116
RKP_SHRZ 021	Amphibolite	588645	7647005	24	74	114
RKP_SHRZ 022	Amphibolite	588671	7647521	20	67	110
RKP_SHRZ 023	Amphibolite	588610	7645259	31	76	121
RKP_SHRZ 024	Amphibolite	587012	7646005	27	78	117
RKP_SHRZ 025	Amphibolite	587054	7646005	17	81	107
RKP_SHRZ 026	Amphibolite	587045	7645510	29	53	119
RKP_SHRZ 027	Amphibolite	587003	7645517	22	75	112
RKP_SHRZ 028	Amphibolite	587067	7644098	38	72	128
RKP_SHRZ 029	Amphibolite	587046	7643789	31	71	121
RKP_SHRZ 030	Amphibolite	587034	7643743	33	55	123
RKP_SHRZ 031	Amphibolite	584124	7642210	25	61	115
RKP_SHRZ 032	Amphibolite	583507	7641813	34	61	124
RKP_SHRZ 033	Amphibolite	586005	7645106	32	79	122
RKP_SHRZ 034	Amphibolite	586007	7644523	31	86	121
RKP_SHRZ 035	Amphibolite	586065	7644108	26	68	116
RKP_SHRZ 036	Amphibolite	586099	7643514	30	61	120
RKP_SHRZ 037	Amphibolite	586102	7648052	23	83	113

LOCALITY IDENTITY	UNIT	X	Y	STRIKE	DIP	DIP DIRECTION
RKP_SHRZ 038	Amphibolite	586090	7648067	23	82	113
RKP_SHRZ 039	Amphibolite	586364	7648042	27	70	117
RKP_SHRZ 040	Amphibolite	588164	7647885	28	88	118
RKP_SHRZ 041	Amphibolite	590101	7646212	25	61	115
RKP_SHRZ 042	Amphibolite	588610	7646900	35	79	125
RKP_SHRZ 043	Amphibolite	590021	7646023	31	86	121
RKP_SHRZ 044	Amphibolite	590091	7645903	33	68	123
RKP_SHRZ 045	Amphibolite	588416	7645413	30	71	120
RKP_SHRZ 046	Amphibolite	587014	7644573	11	83	101
RKP_SHRZ 047	Amphibolite	589511	7648007	27	82	117
RKP_SHRZ 048	Amphibolite	589016	7647976	26	70	116
RKP_SHRZ 049	Amphibolite	588126	7643621	29	88	119
RKP_SHRZ 050	Amphibolite	589011	7647511	21	81	111
RKP_SHRZ 051	Amphibolite	589003	7646013	34	86	124
RKP_SHRZ 052	Amphibolite	588986	7646005	29	79	119
RKP_SHRZ 053	Amphibolite	588519	7644511	24	84	114
RKP SHRZ 26	Amphibolite	590021	7646023	31	86	121
RKP SHRZ 27	Amphibolite	590091	7645903	33	68	123
RKP SHRZ 28	Amphibolite	588416	7645413	30	61	120
RKP SHRZ 29	Amphibolite	587014	7644573	35	83	125
RKP SHRZ 30	Amphibolite	589511	7648007	27	82	117
RKP SHRZ 31	Amphibolite	589016	7647976	26	70	116
RKP SHRZ 32	Amphibolite	588126	7643621	36	88	126

Table A2: The list of samples obtained from Phoenix and Selkirk mines and Tekwane deposit, which were selected for normal thin sections and polished thin sections and whole rock geochemistry.

SITE	SAMPLE IDENTITY LABEL	LITHOLOGY
Phoenix mine	W8	Unmineralised melanogabbro
	NW1	Unmineralised melanogabbro
	S10	Mineralised mesogabbro
	N1	Mineralised mesogabbro
	S1	Mineralised leucogabbro
	W3	Porphyritic granodiorite
	W1	Tonalite
	W9	Tonalite
Selkirk mine	SL1A	Leucogabbro
	SL1B	Melanogabbro
	SL04	Mineralised mesogabbro
	SL5	Mineralised mesogabbro
	SL07	Mineralised mesogabbro
	SL09	Leucogabbro
	SL06	Porphyritic granodiorite
	SL08	Porphyritic granodiorite
Tekwane deposit	TEK1	Mineralised mesogabbro
	TEK3	Mineralised mesogabbro
	TEK4	Mineralised mesogabbro
	TEK6	Mineralised mesogabbro
	TEK7	Mineralised melanogabbro
	TEK8	Mineralised melanogabbro
	TEK9	Mineralised melanogabbro
	TEK2	Leucogranodiorite
	TEK5	Quartz diorite

Table A3: The list of samples obtained from Rooikoppie deposit, which were selected for normal thin sections and polished thin sections and for whole rock geochemistry. Samples, R1 and R4 were studied under reflected light to understand the ore petrography of the Rooikoppie deposit.

SITE	SAMPLE IDENTITY LABEL	LITHOLOGY
Rooikoppie deposit	R1	Dolerite
	R2	Massive sulphide
	R4	Dolerite
	R7	Quartz diorite
	R9	Gossan
	R011	Amphibolite
	R11	Mesogabbro
	R 12	Mesogabbro
	P2	Granodiorite
	P3	Basalt
	P4	Dolerite
	P12	Pyroxenitic gabbro
	P14	Leucogranodiorite
	PIN011	Granodiorite
	PIN012	Granodiorite
	PIN013	Granodiorite
	PIN014	Basalt
	PIN015	Granodiorite

APPENDIX B

(i) Phoenix mine drill hole logs

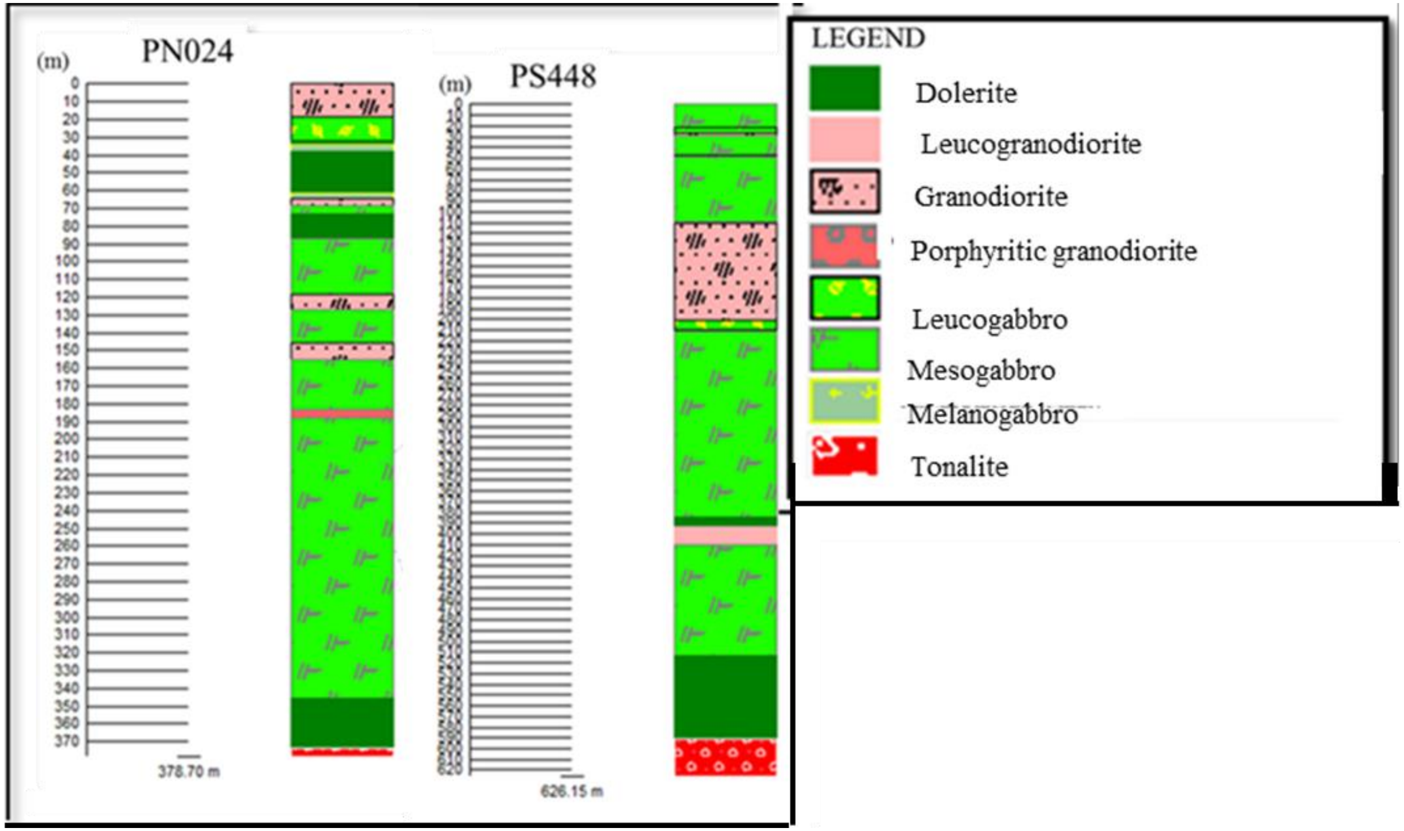

(ii) Selkirk drill hole logs

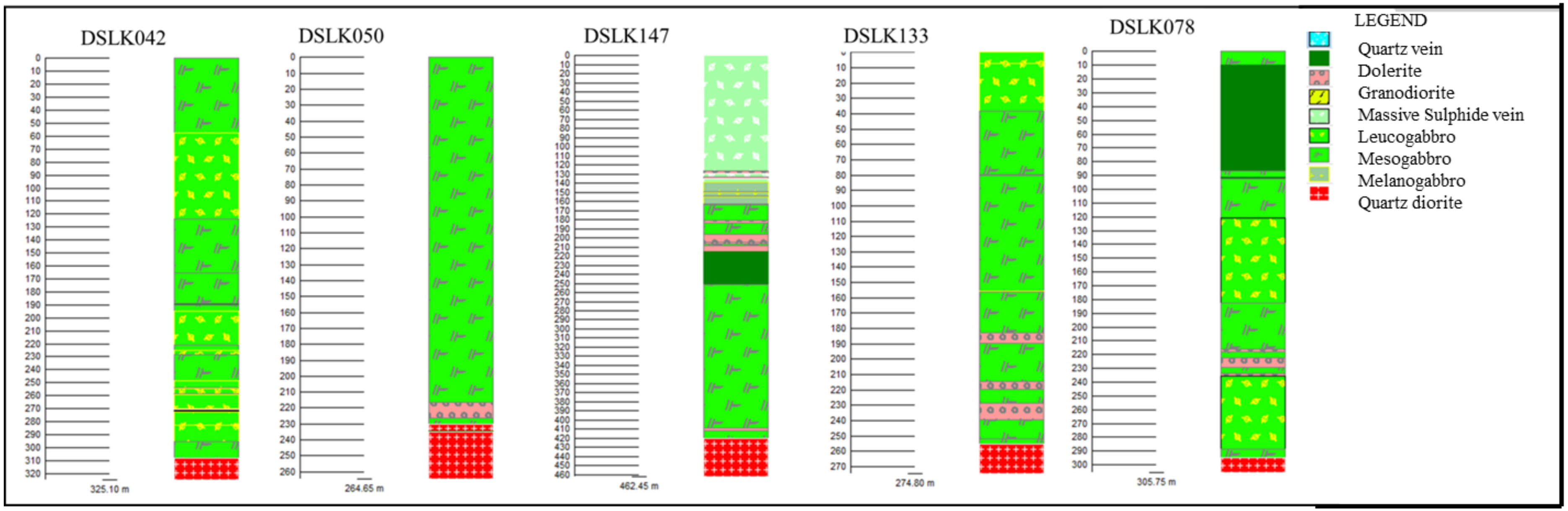

(iii) Rooikoppie deposit drill hole logs

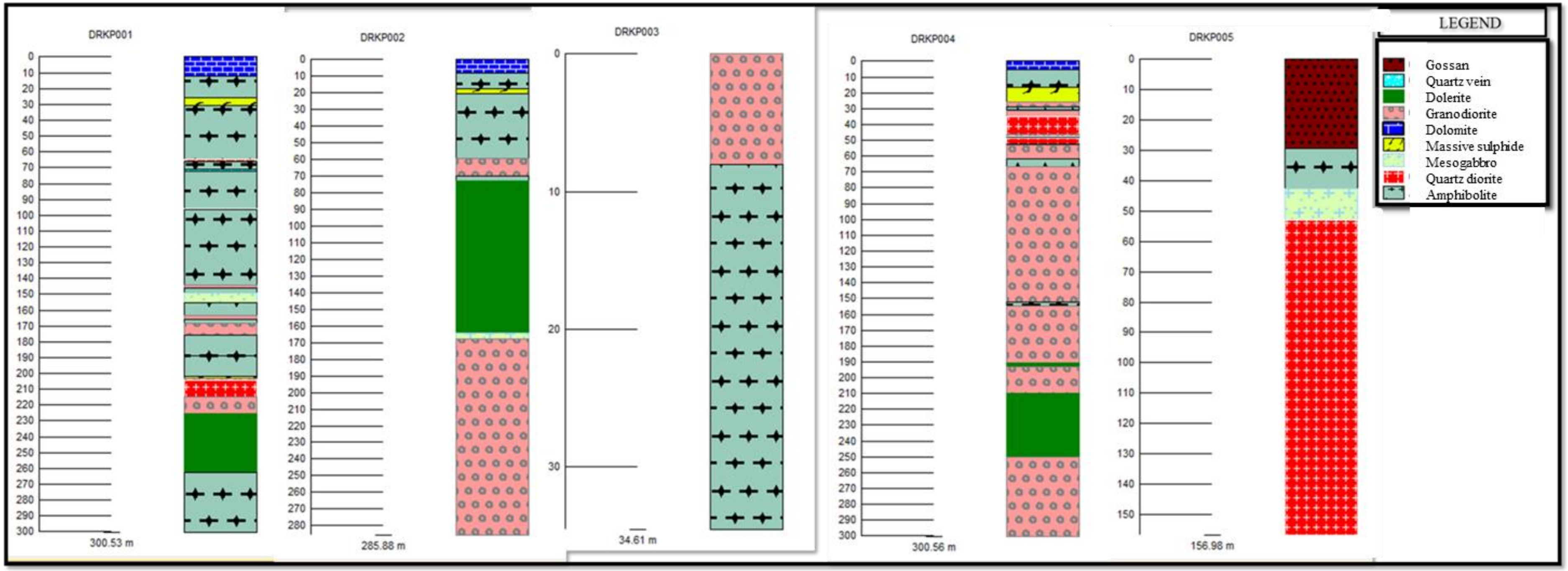

APPENDIX C

(i). Photomicrographs of selected samples obtained from magmatic rocks

SAMPLE NUMBER	LOCATION	ESTIMATED MODAL COMPOSITION	DESCRIPTIONS	UNIT NAME
NW1	PHOENIX MINE PIT UTM 35 K 0579478 (mE), 7654963 (mN)	63% plagioclase, 30 % hornblende, 4% quartz, 3% muscovite	Polysynthetic twinned plagioclase and green-brown hornblende grains exhibit sutured boundaries. Myrmekitic plagioclase occurs sporadically.	Melanogabbro
	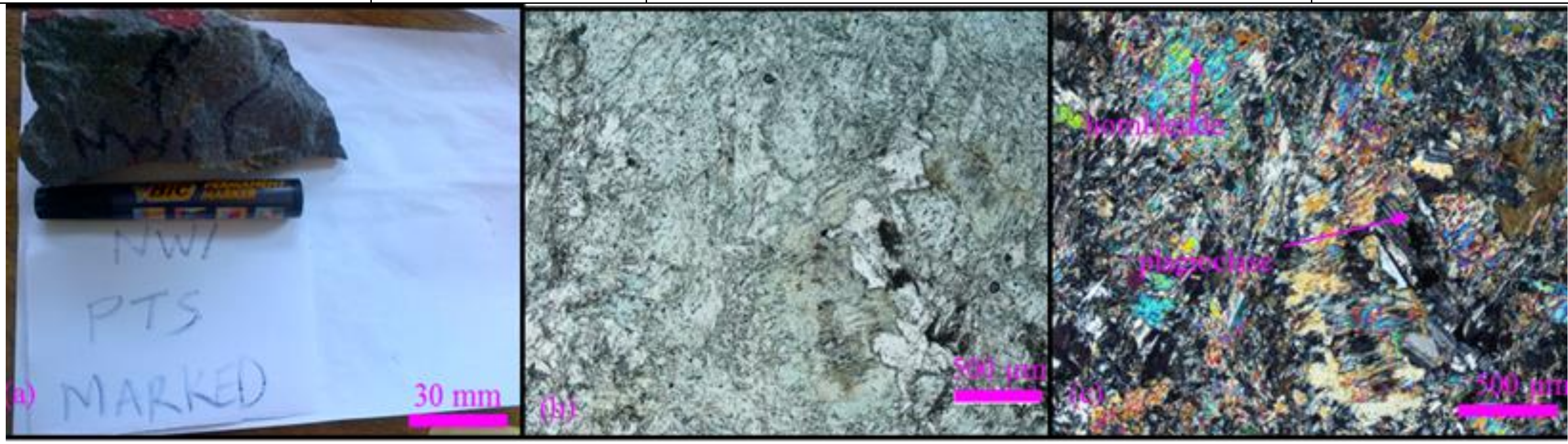			

W8	PHOENIX MINE PIT UTM 35 K 0579716 (mE), 7654055 (mN))	67% plagioclase, 25 % hornblende, 5% quartz, 3% muscovite	Intergranular matrix is dominated by plagioclase (~300 µm) and hornblende (~400 µm). Polysynthetic twinning is common within the unzoned plagioclase. Subhedral quartz grains occurs as fine aggregates along the boundaries of plagioclase and hornblende.	Melanogabbro
	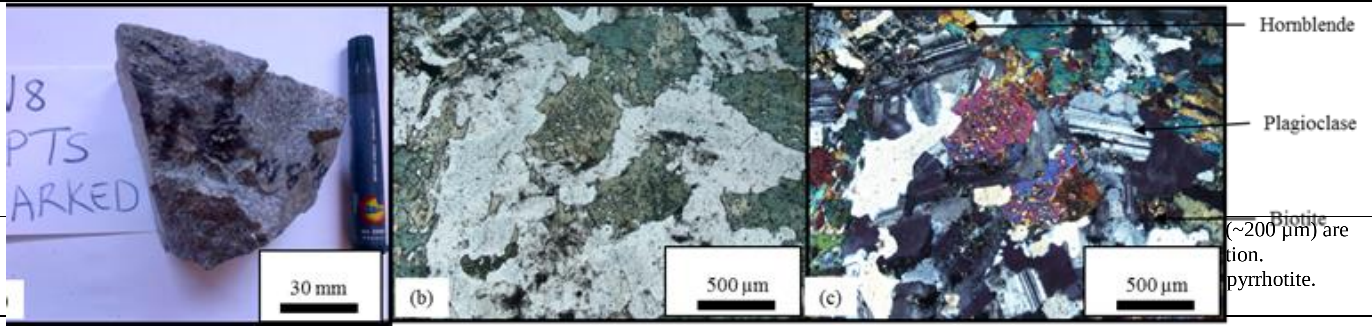			
N1			(~200 µm) are tion. pyrrhotite.	Mesogabbro
	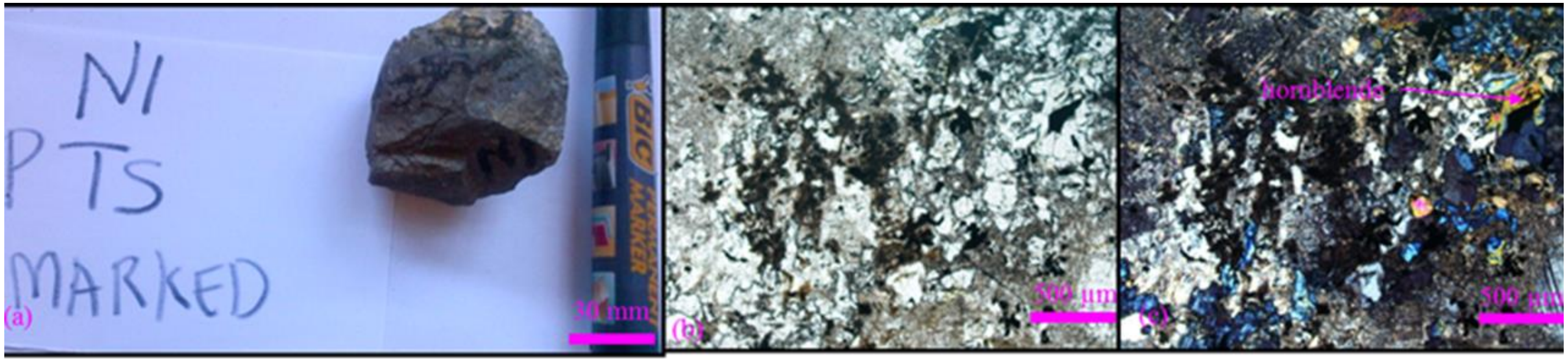			
S1	PHOENIX MINE PIT UTM 35K 0547008 (mE), 7620294(mN)	75% plagioclase, 25 % hornblende, 5% quartz, 5% muscovite	Subhedral plagioclase characterized by polysynthetic twinning occurs dominantly though affected by sericitisation in some zones.. Medium grained hornblende (~400 µm) is surrounded by opaque minerals possibly sulphides and oxides.	Leucogabbro

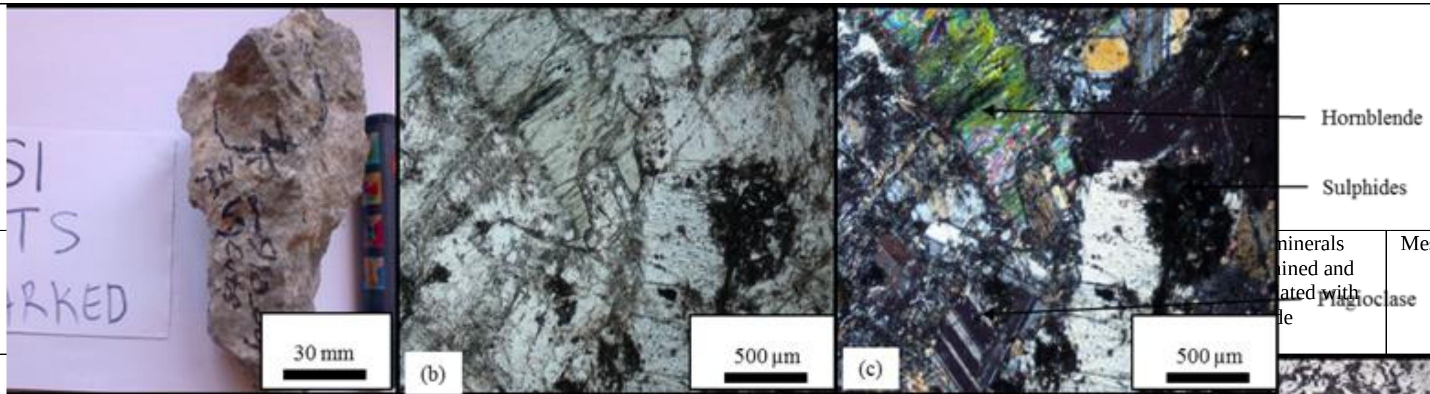

SL5			minerals ined and ated with le	Mesogabbro

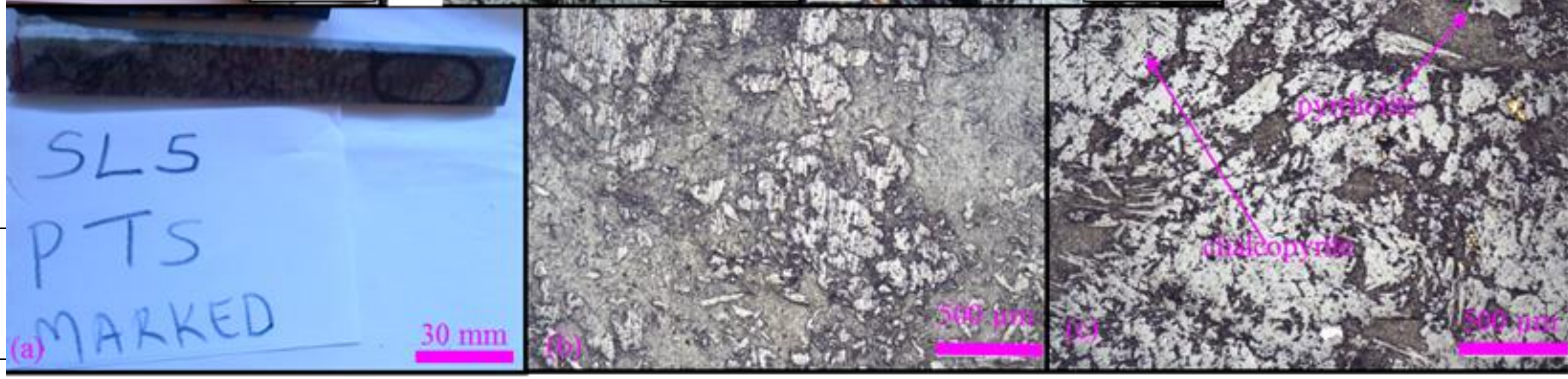

SL1A				
SL1B	SELKIRK MINE BOREHOLE ID: UTM 35K 0574965 (mE), 7642145 (mN)	63% plagioclase, 30 % hornblende, 4% quartz, 3% muscovite	Fibrous and very fine-grained hornblende, biotite and plagioclase (<100 µm) are present as alternate zones throughout. Opaque minerals, possibly sulphides occurs rarely. Small amounts of chlorite and epidote are observed as inclusions within the aggregates of plagioclase and hornblende.	Melanogabbro

SL 09	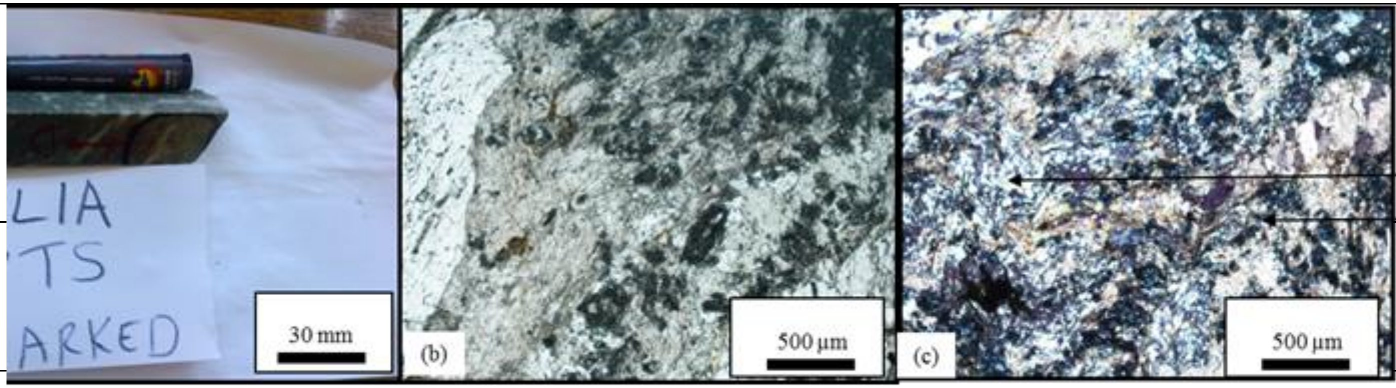			Leucogabbro
	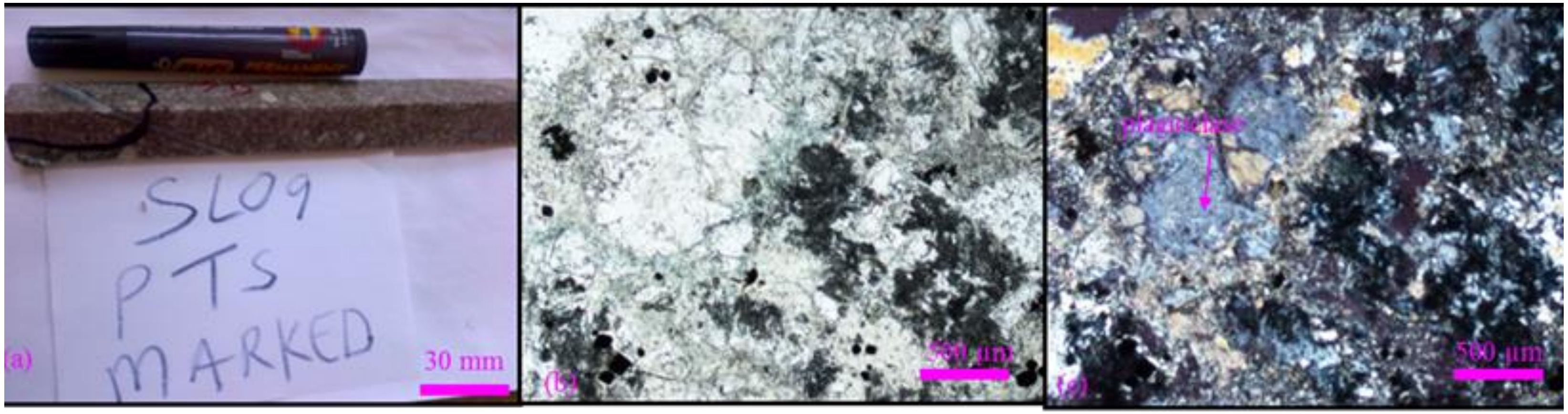			
TEK 1	TEKWANE DEPOSIT BOREHOLE ID: TW27 UTM 35 K 0580910 (mE), 7645590 (mN)	60% plagioclase, 30 % hornblende, 5% quartz, 5% muscovite	Poorly oriented laths of hornblende and plagioclase are very common suggestive of intensive mingling pattern. Opaque minerals occur scattered throughout.	Mesogabbro

	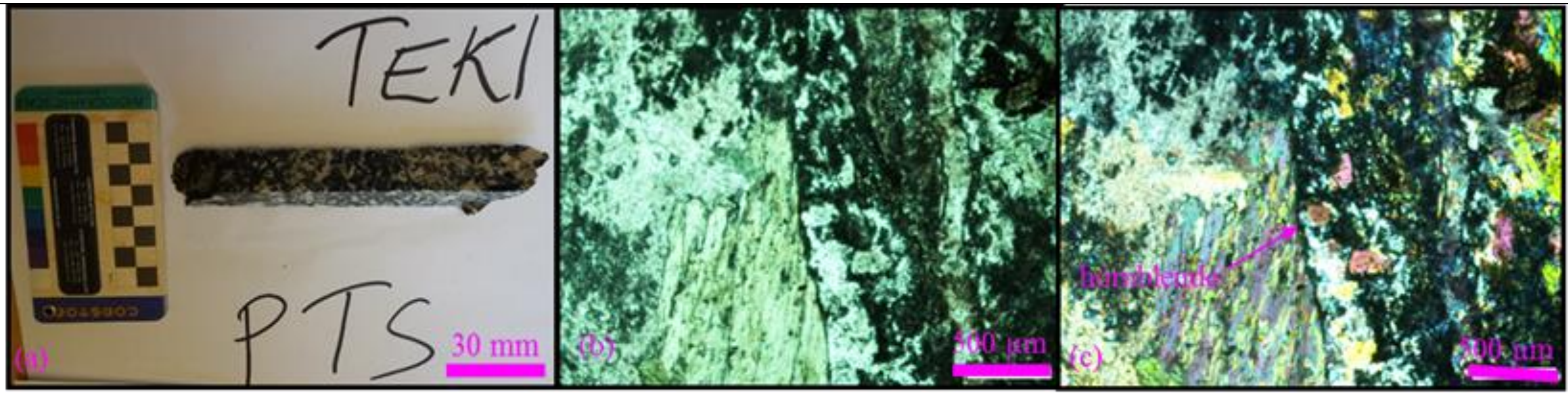			
TEK3	TEKWANE DEPOSIT BOREHOLE ID: TW25 UTM 35K 0580321 (mE), 7643951 (mN)	61% plagioclase, 31 % hornblende, 4% quartz, 4% muscovite	Plagioclase grains (~500 µm) are more abundant than fibrous hornblende grains. Sericite is scattered throughout the plagioclase grains, suggestive of intensive weathering of plagioclase in some zones.	Mesogabbro
	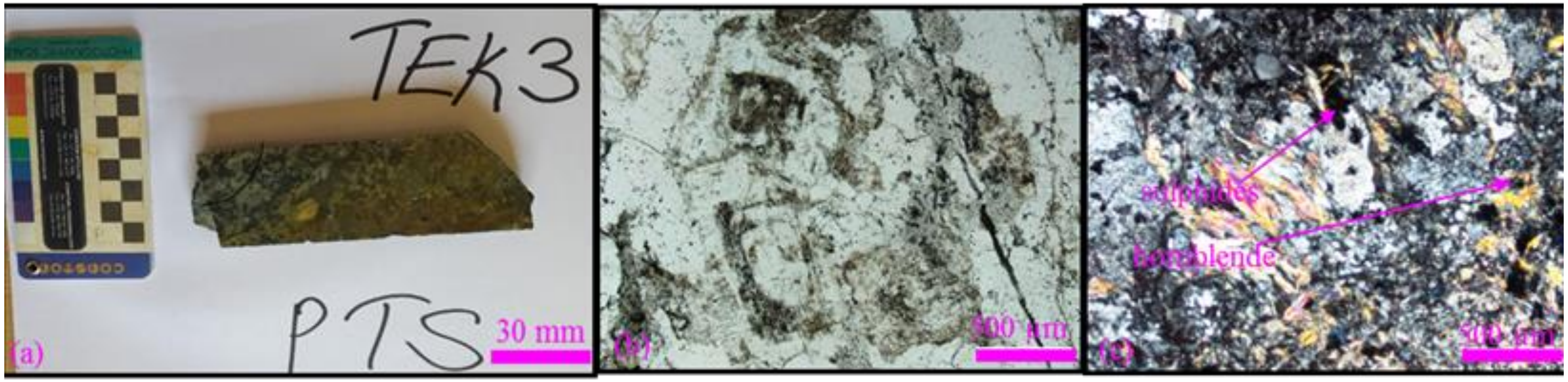			
	TEKWANE DEPOSIT BOREHOLE ID: TW 10	62% plagioclase, 32 % hornblende,	Foliated and very fine-grained hornblende and plagioclase grains occurs with few amounts of opaque minerals, possibly sulphides. No evidence of solid-	Mesogabbro

TE 4	UTM 35 K 0580601 (mE), 7645120 (mN)	4% quartz, 2% muscovite	state deformation and such the foliated pattern of the hornblende and plagioclase could suggestive of magmatic process.	
	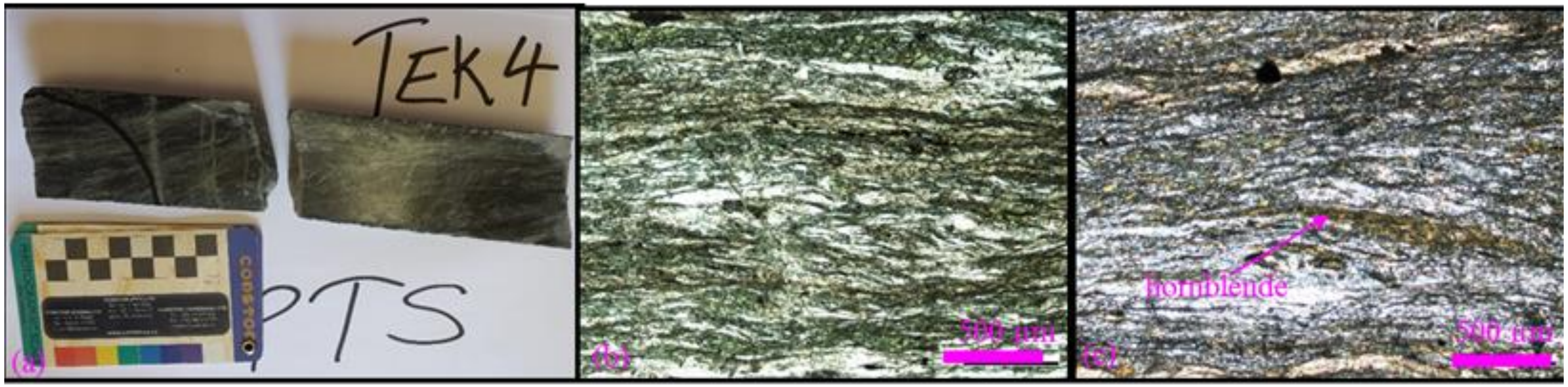			
TEK 7	TEKWANE DEPOSIT BOREHOLE ID: TW07 UTM 35 K 0580451 (mE), 7643963 (mN)	60% plagioclase, 35 % hornblende, 3% quartz, 2% muscovite	Fine grained subophitic matrix of dominant plagioclase and hornblende (~200 µm) interspersed with accessory amounts of quartz and muscovite. Opaque minerals, possibly sulphides occurs interstitial with plagioclase and hornblende.	Mesogabbro

	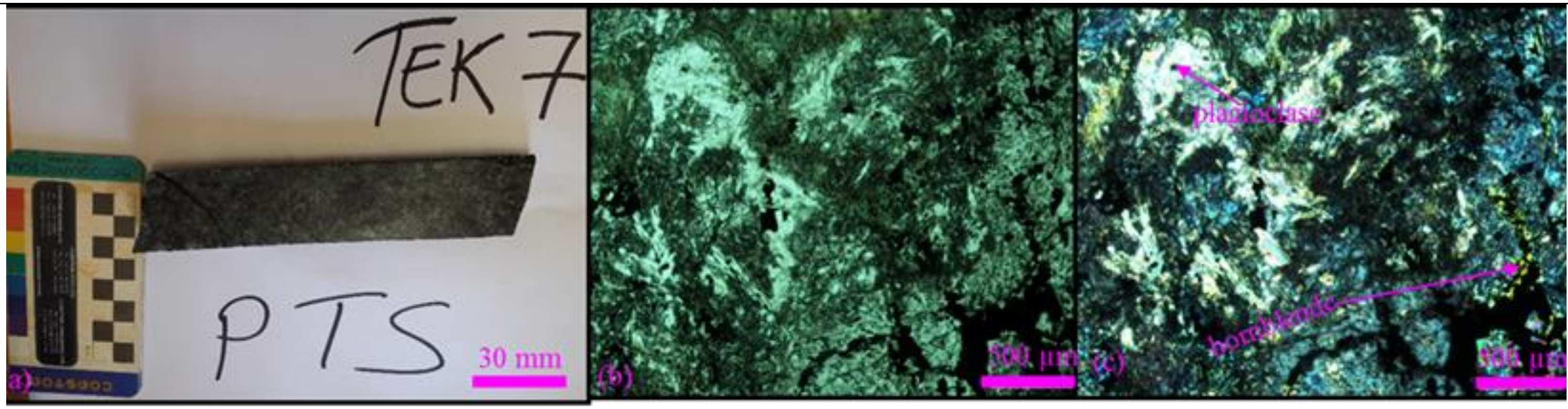			
TEK 8	TEKWANE DEPOSIT BOREHOLE ID: TW29 UTM 35 K 0580110 (mE), 7643280 (mN)	65% plagioclase, 30 % hornblende, 2% quartz, 3% muscovite	Intergranular matrix of medium grained subhedral plagioclase (~500 µm) and hornblende occurs, characterized by sutured boundaries. Opaque minerals occur scattered along the boundaries of the plagioclase and hornblende.	Melanogabbro

	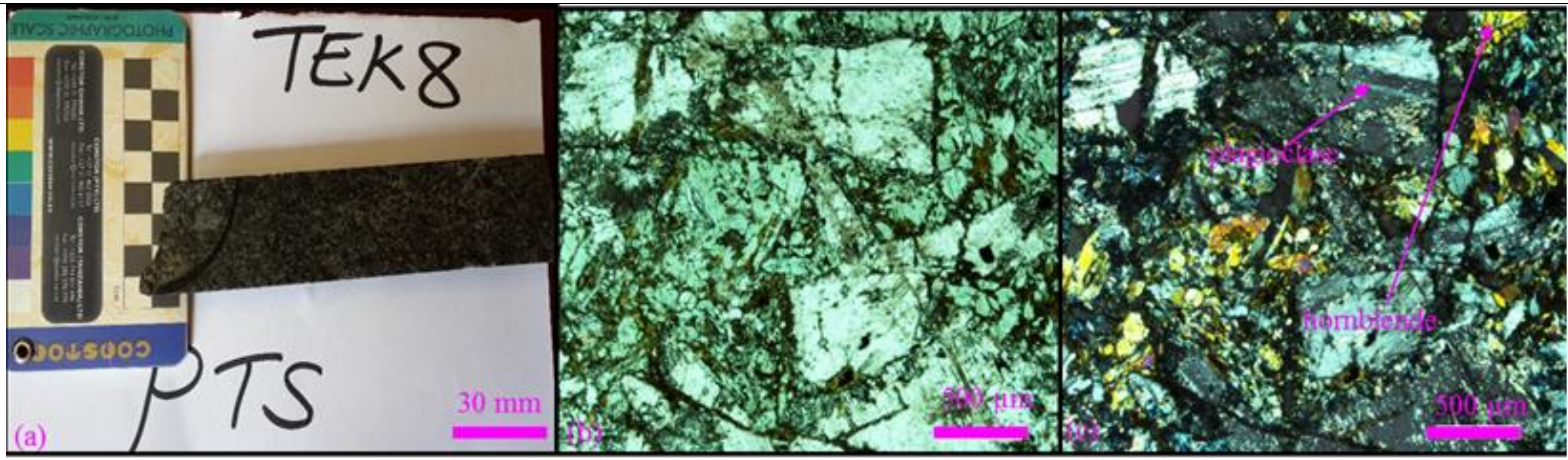			
W3	PHOENIX MINE	30% alkali feldspars, 60% plagioclase, 20% quartz, 3% hornblende, 2% muscovite	Foliated and dominant plagioclase and quartz grains occur surrounded by hornblende throughout suggestive of intense deformation. The recrystallized quartz grains (< 100 µm) show undulose extinction.	Porphyritic granodiorite
	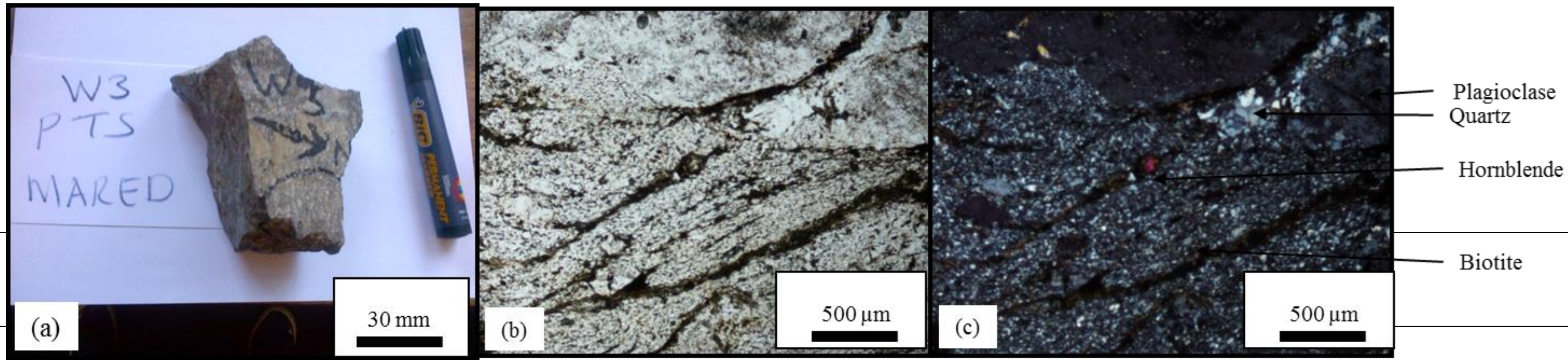			
W1				

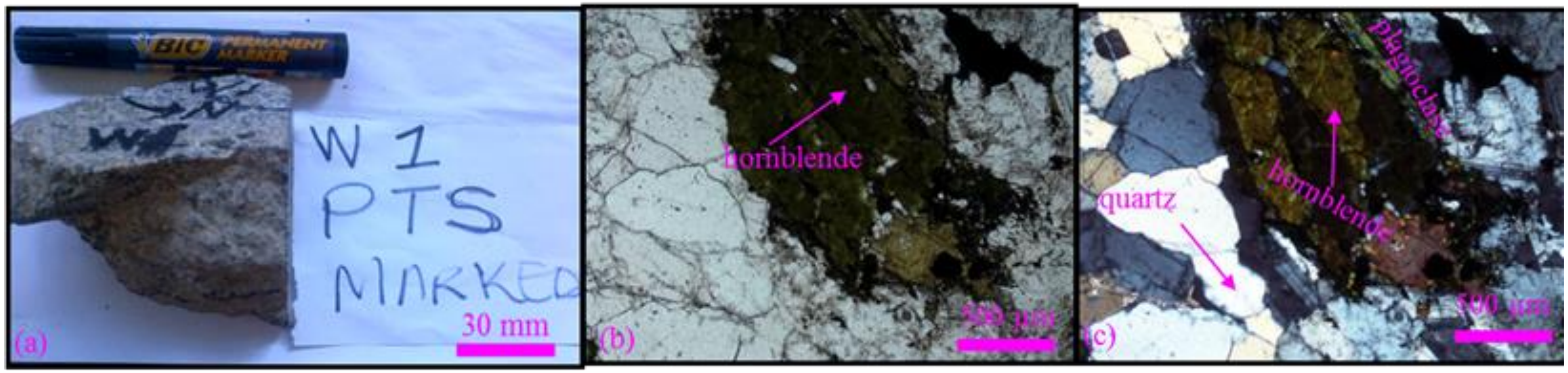

SL 08	SELKIRK MINE	62% plagioclase, 15 % hornblende, 20 % quartz, 3% muscovite	Trachytic textured granodiorite gneiss made up of mineralogy composed of interstitial plagioclase and quartz.	Granodiorite

	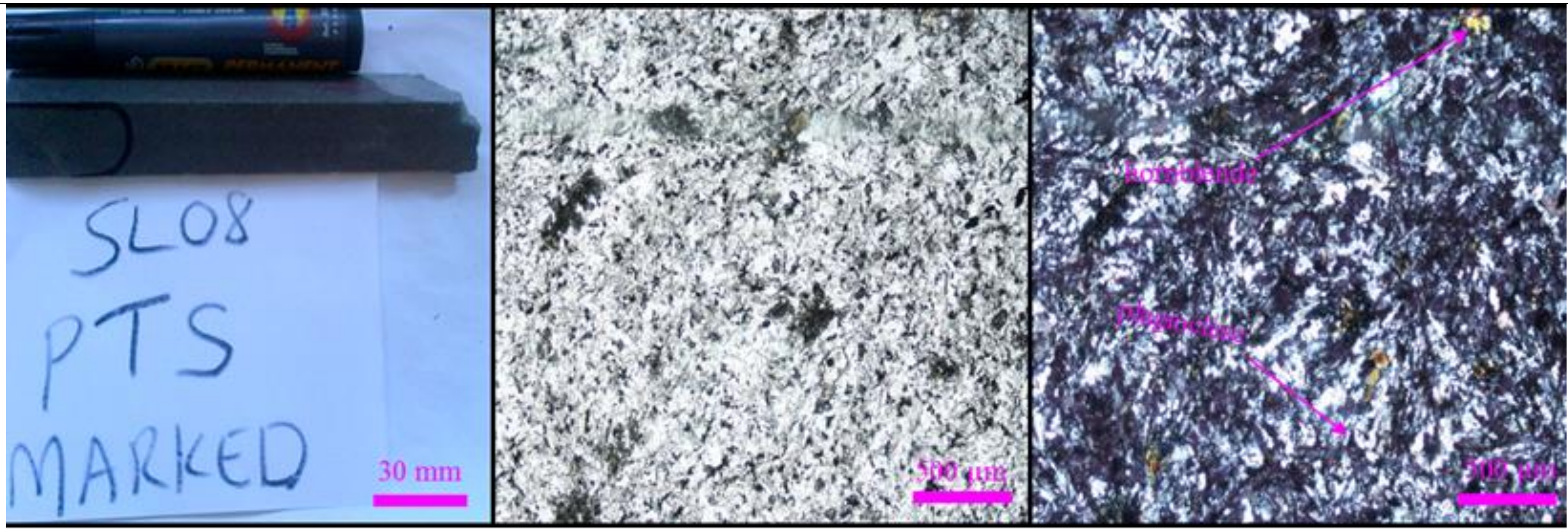			
SL06	SELKIRK MINE	55% plagioclase, 15 % hornblende, 25% quartz, 3% muscovite	Very fine grained (< 500 μm) hornblende and plagioclase are present in trachytic textured granodiorite gneiss.	Granodiorite

	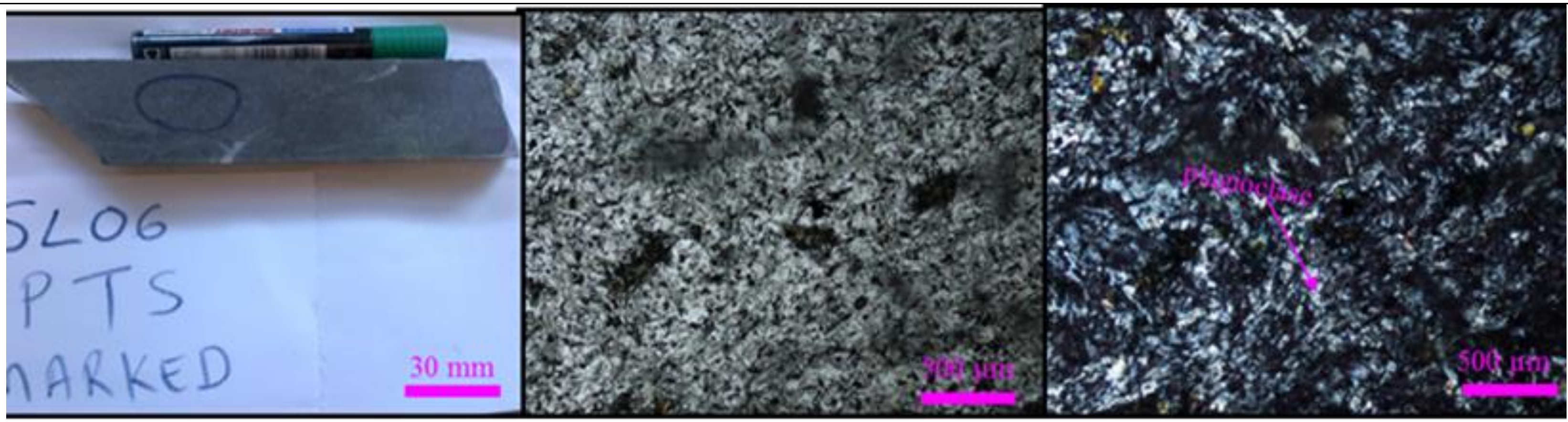 			
TEK 2	TEKWANE DEPOSIT	50% plagioclase, 40 % quartz, 6% hornblende, 4% muscovite	Intergranular matrix of subhderal quartz and plagioclase characterize the leuco-granodiorite. Plagioclase shows zoning suggestive of different rates of cooling during crystallisation. Inclusions of sericite occurs within the plagioclase, which suggests effects of thermal alteration and weathering. Quartz grains show some form of undulose extinction.	Leucogranodiorite

	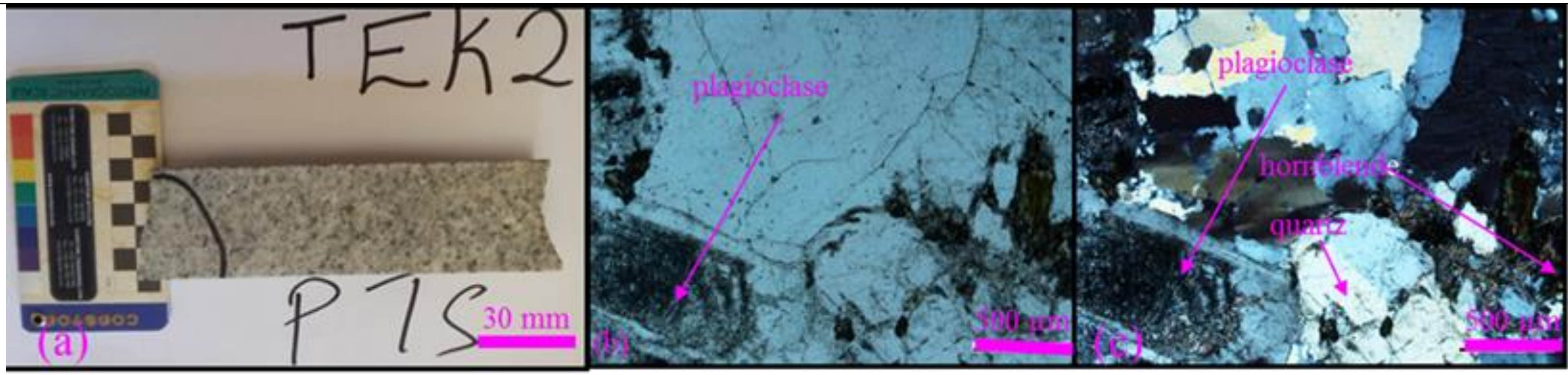			
TEK 5	TEKWANE DEPOSIT	55% plagioclase, 35 % quartz, 8% quartz, 2% muscovite	Subhedral medium grained quartz grains (~800 µm) occurs surrounded by, sericitised and oscillatory zoned plagioclase. Quartz grains exhibit undulatory extinctions. Hornblende grains (~500 µm) are characterised by suture margins. Some plagioclase grains are coarsely sieved with resorption rims.	Leucogranodiorite
	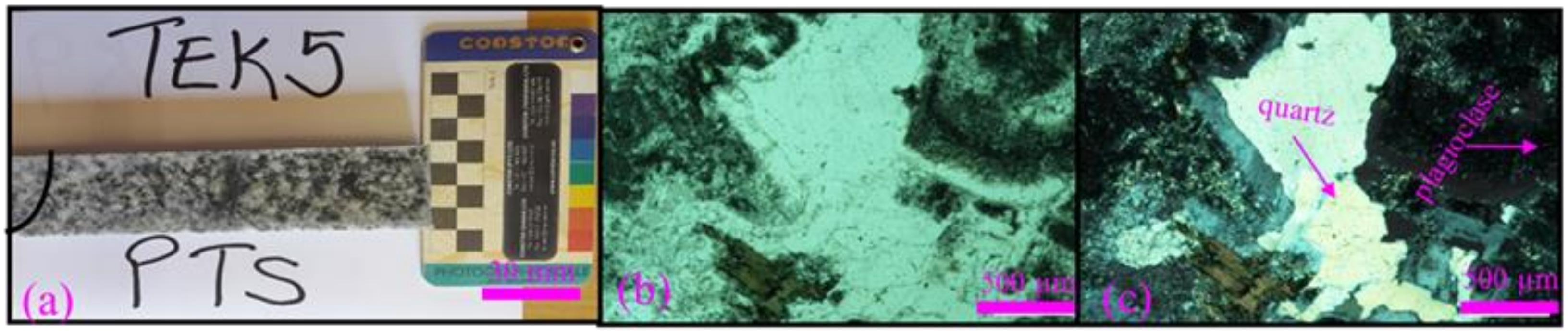			

PIN011	ROOIKOPPIE DEPOSIT	50% plagioclase, 10% alkali feldspars, 10 % hornblende, 27% quartz, 3% muscovite	Coarse grained matrix of quartz, oscillatory zoned plagioclase and hornblende dominate the mineralogy of the leuco-granodiorite. Orthoclase generally shows Carlsbad twinning.	Granodiorite
	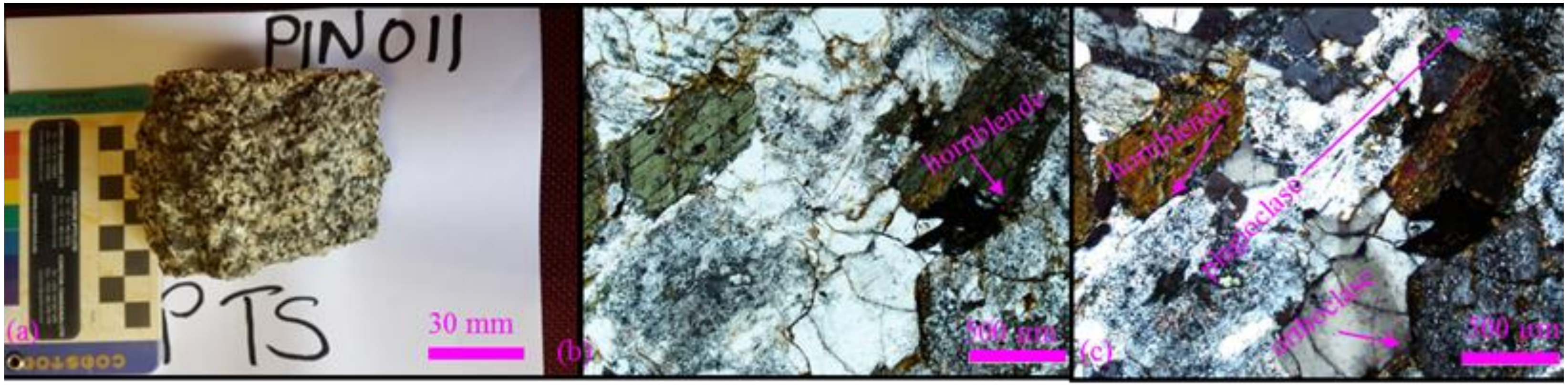			
PIN012	ROOIKOPPIE DEPOSIT	50% plagioclase, 30 % quartz, 18% hornblende, 2% muscovite	Anhedral quartz, hatch twinned microcline, green hornblende and unzoned plagioclase grains occur dominantly characterised by sutures. Sericite is present within the plagioclase suggestive of alteration effects.	Granodiorite
W9	PHOENIX MINE	63% plagioclase, 30 % hornblende, 4% quartz, 3% muscovite	Polycrystalline matrix illustrates medium grained plagioclase, quartz and green-brown hornblende characterised by irregular boundaries. Plagioclase is typical of polysynthetic twinning whereas quartz shows undulatory phases.	Tonalite

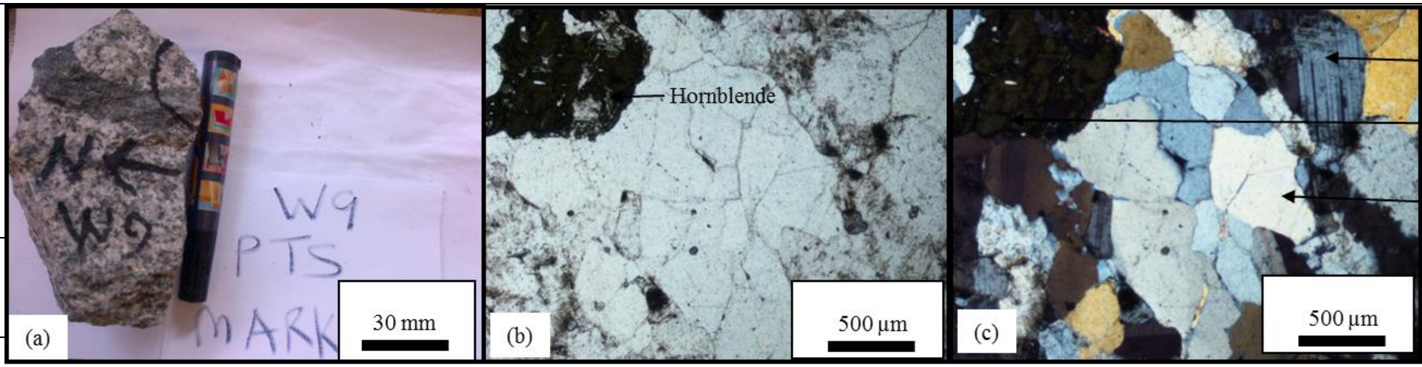

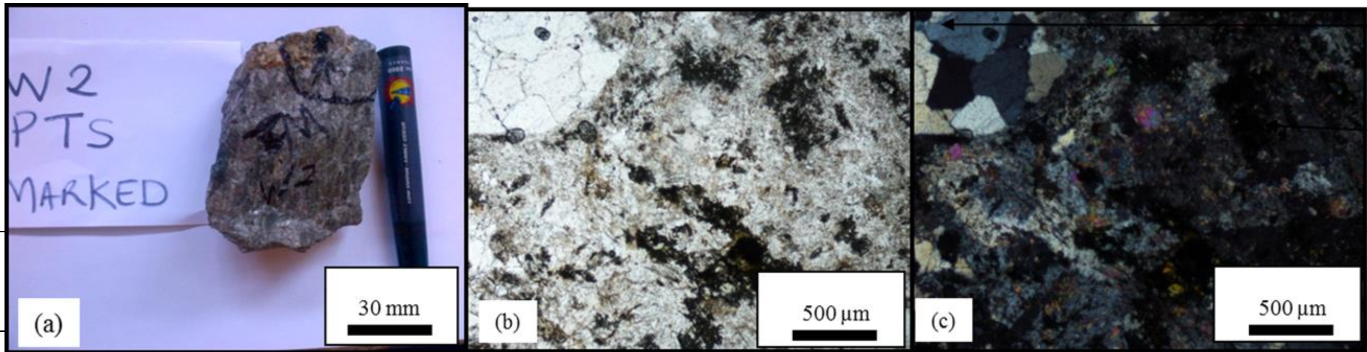

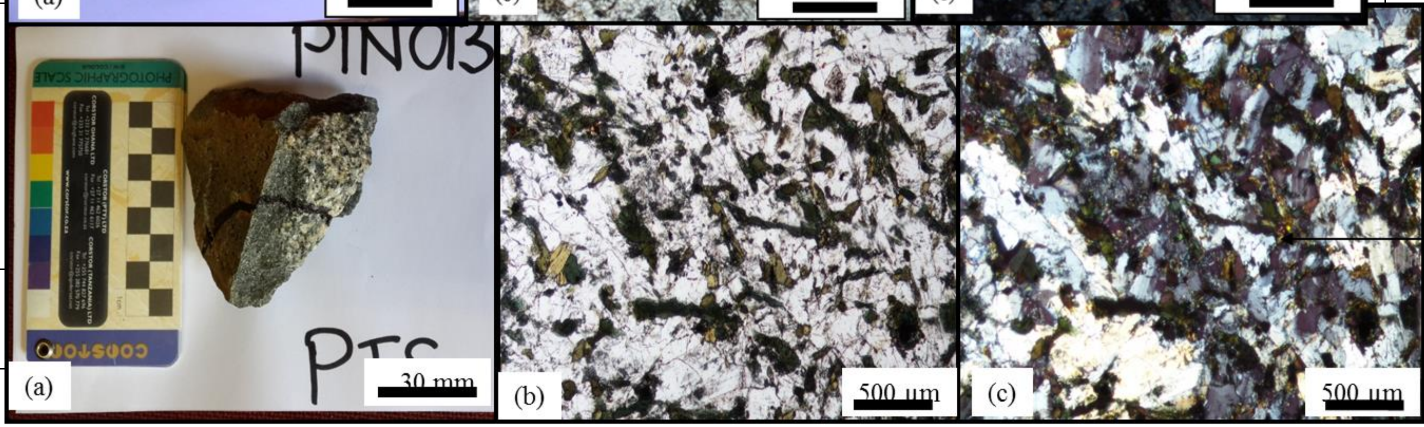

W2		elanogabbro
PIN013		Basalt
PIN014		salt

	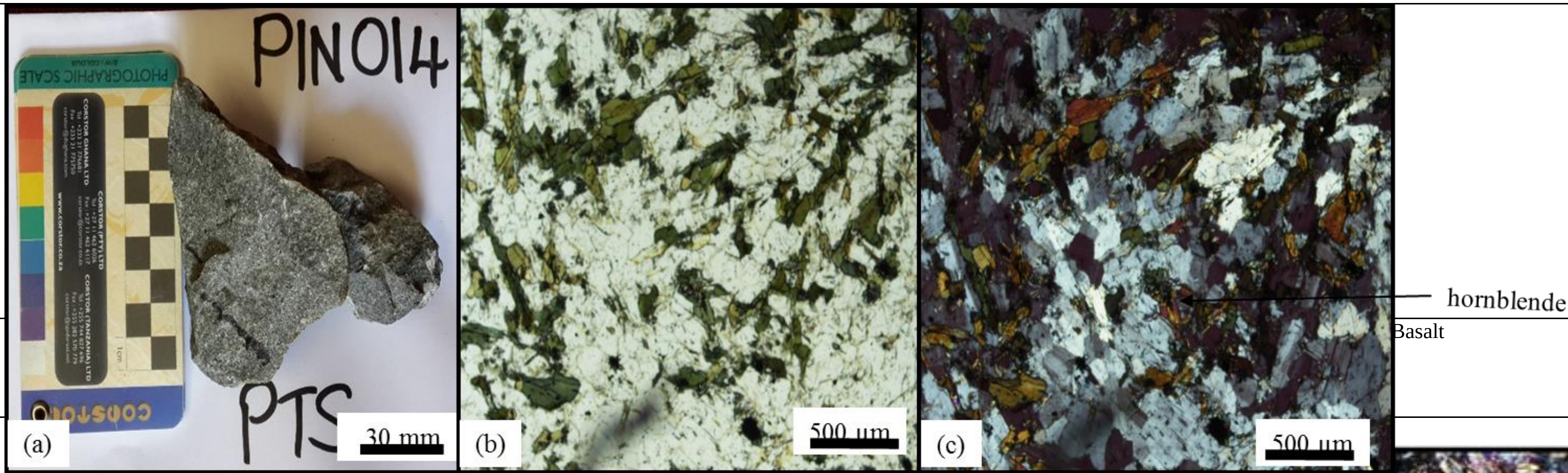			
P3	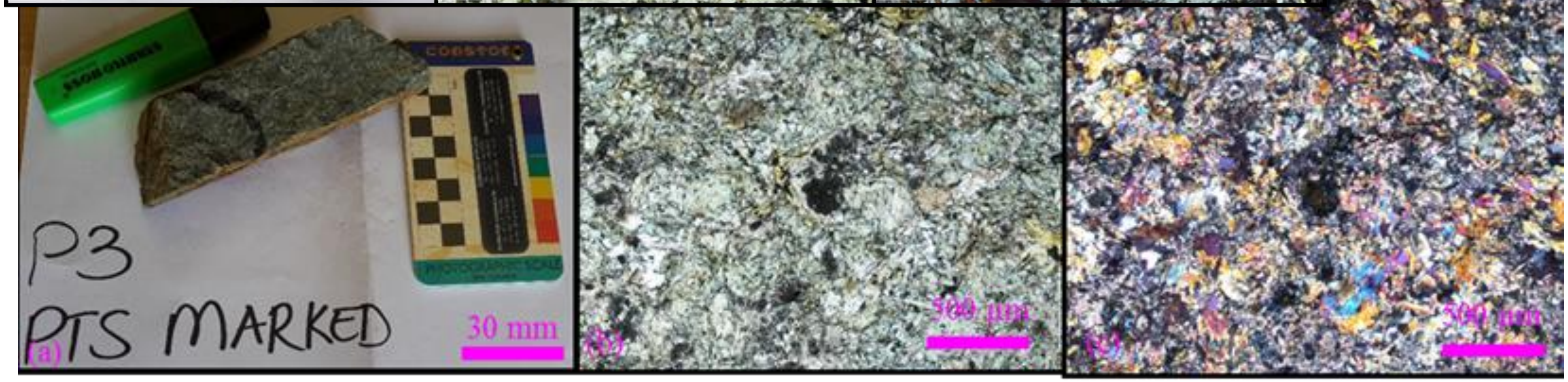			Basalt
R2	ROOIKOPPIE DEPOSIT	63% plagioclase, 30 % hornblende, 4% quartz, 3% muscovite	Polysynthetic twinned laths of plagioclase are surrounded by subhedral clinopyroxene and orthopyroxene. Plagioclase laths exhibit symplectitic textures. Olivine occurs rarely. Opaque minerals occurs sporadically and could represent magnetite.	Dolerite

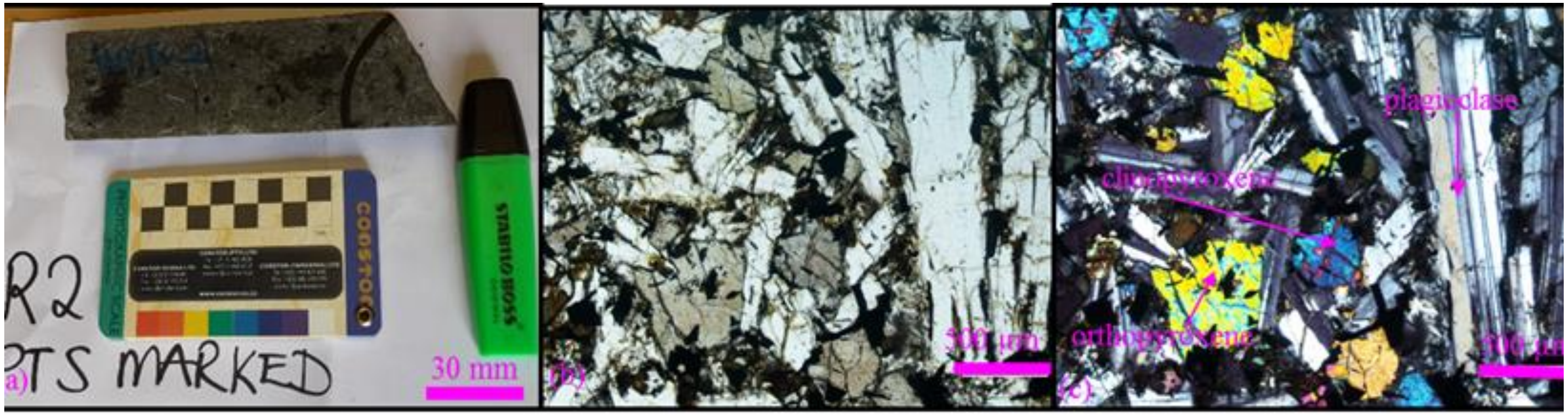

P4	ROOIKOPPIE DEPOSIT	63% plagioclase, 30 % hornblende, 4% quartz, 3% muscovite	Orthopyroxene occurs, surrounded by unzoned plagioclase and hornblende laths. Anhedral olivine grains occurs erratically.	Dolerite

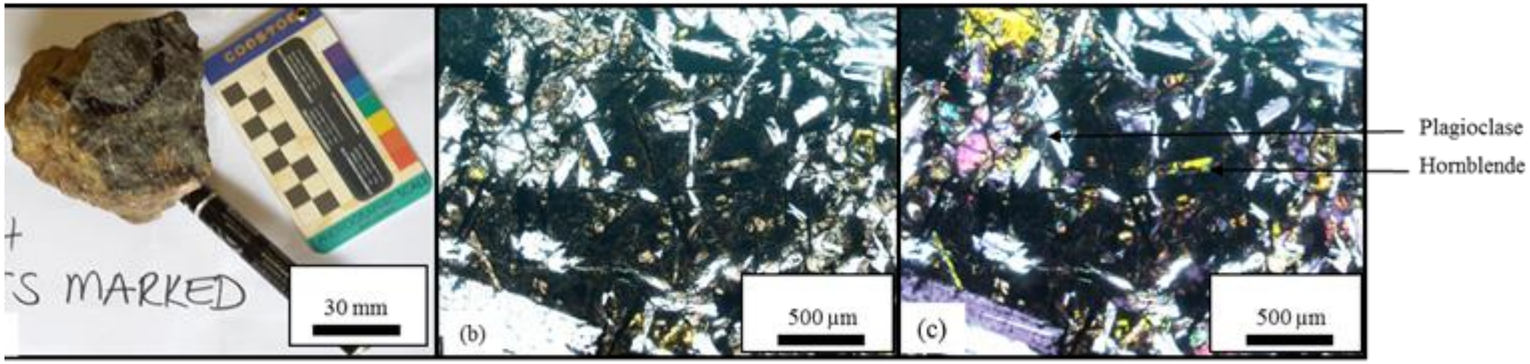

SL07	SELKIRK MINE	63% plagioclase, 30 % hornblende, 4% quartz, 3% muscovite		Contact between meta-mesogabbro and leuco-gabbro.
	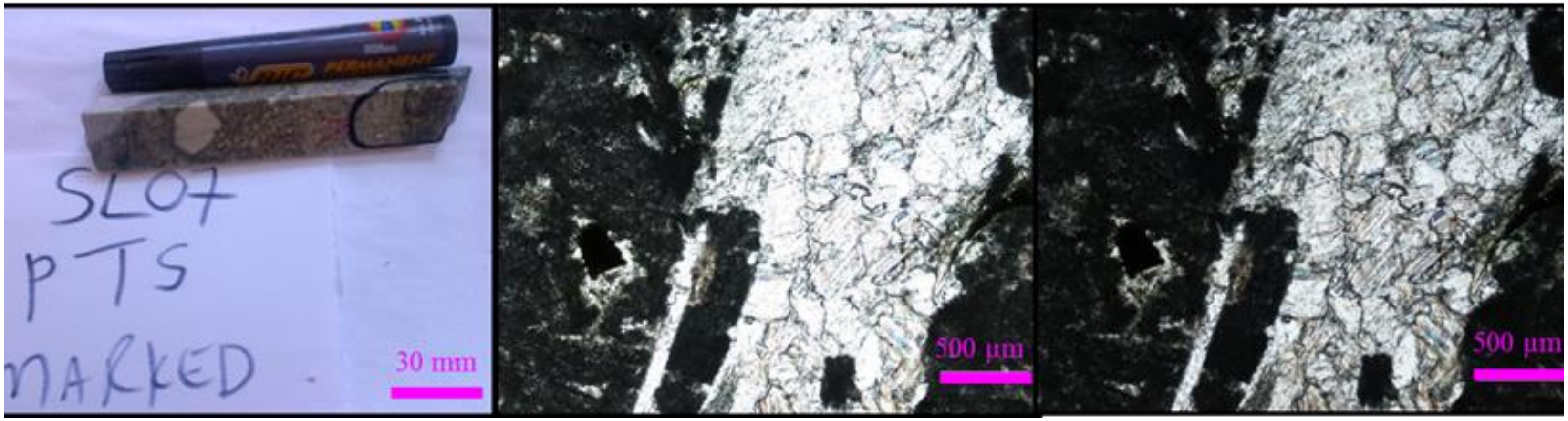			
P2	PHOENIX PIT CUT 9 (NORTH WEST FACE) 960 level	45% plagioclase, 35 % alkali feldspars, 17 % quartz, 3% muscovite		Leucogranodiorite

	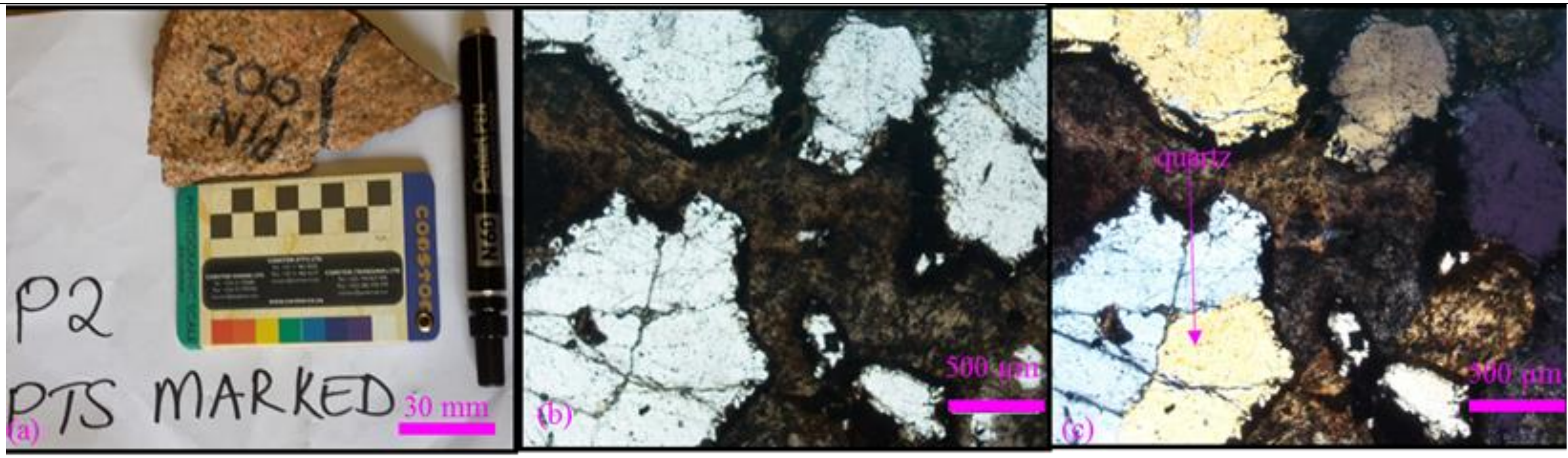200 PIN P2 PTS MARKED 30 mm (a) (b) 500 µm quartz (c) 500 µm